

**A NEW SOLUTION TO AN OLD PROBLEM:  
DESIGNING AN ULTRALOW WEAR POLYMERIC SOLID LUBRICANT  
FOR BEARING APPLICATIONS IN CHALLENGING ENVIRONMENTS**

by

Diana R. Haidar

A dissertation submitted to the Faculty of the University of Delaware  
in partial fulfillment of the requirements for the degree of  
Doctor of Philosophy in Mechanical Engineering.

Spring 2018

© 2018 Diana R. Haidar  
All Rights Reserved

**A NEW SOLUTION TO AN OLD PROBLEM:  
DESIGNING AN ULTRALOW WEAR POLYMERIC SOLID LUBRICANT  
FOR BEARING APPLICATIONS IN CHALLENGING ENVIRONMENTS**

by

Diana R. Haidar

Approved: \_\_\_\_\_  
Ajay K. Prasad, Ph.D.  
Chair of the Department of Mechanical Engineering

Approved: \_\_\_\_\_  
Babatunde A. Ogunnaike, Ph.D.  
Dean of the College of Engineering

Approved: \_\_\_\_\_  
Ann L. Ardis, Ph.D.  
Senior Vice Provost for Graduate and Professional Education

I certify that I have read this dissertation and that in my opinion it meets the academic and professional standard required by the University as a dissertation for the degree of Doctor of Philosophy.

Signed:

---

David L. Burris, Ph.D.  
Professor in charge of dissertation

I certify that I have read this dissertation and that in my opinion it meets the academic and professional standard required by the University as a dissertation for the degree of Doctor of Philosophy.

Signed:

---

Michael H. Santare, Ph.D.  
Member of dissertation committee

I certify that I have read this dissertation and that in my opinion it meets the academic and professional standard required by the University as a dissertation for the degree of Doctor of Philosophy.

Signed:

---

M. Zubaer Hossain, Ph.D.  
Member of dissertation committee

I certify that I have read this dissertation and that in my opinion it meets the academic and professional standard required by the University as a dissertation for the degree of Doctor of Philosophy.

Signed:

---

Thomas H. Epps, III, Ph.D.  
Member of dissertation committee

## **ACKNOWLEDGMENTS**

I am sincerely grateful for all the amazing people in my life that have helped me personally and professionally in times of hardship and happiness.

Upon arriving to the University of Delaware, I sought to pursue my research interests in mechanics of materials and nanotechnology with Prof. David Burris. Even though funds were not available for a new student, I stayed determined, and he accepted my request for a rotation in his Materials Tribology Laboratory. After this initial experience, my interest remained, and he took a risk in accepting me as a member of his group without funding. I thank him for providing me with this opportunity, and the excellent advisement that lead to successfully securing support for my graduate career. Throughout the entire graduate program, he was the mentor I had sought and needed, and for that I cannot thank him enough.

Thanks to the leadership of Prof. David Burris, and support from Prof. Xiachun Li and Prof. Timothy Osswald from my alma mater the University of Wisconsin-Madison, I was awarded financial support of my doctoral degree by the National Science Foundation (Grant No. 124d7394). I thank the UD Department of Mechanical Engineering and National Science Foundation's Graduate Research Fellowship for fully funding my doctoral degree and providing academic freedom for the pursuit of knowledge.

I thank the senior laboratory members Harman Khare, Jiabin Ye, Axel Moore, and Ben Gould for training me as a new lab member and their significant contributions

to this research. I also thank the staff and technicians of the Keck Advanced Microscopy Facility and Advanced Materials Characterization Laboratory for the technical assistance and resources to conduct this research. A big thanks to those in the Mechanical Engineering Office, Letitia Toto, Lisa Katzmire, Ann Connor, Amy Adams, and Prof. Suresh Advani, your friendship, guidance, and aid were invaluable.

To the people of the Design Studio, Prof. Jenni Buckley, Prof. Dustyn Roberts, Scott Nelson, and Steve Beard, you brought me into the fold of makers and engineering educators. This gave me new focus for a career in academia, and for that you have my unending gratitude. In my pursuit of this avenue, my mentors Prof. Jenni Buckley and Prof. Heather Doty were inspirational figures. Their leadership during my participation in the Perry Initiative, conducting engineering outreach to female youth, as well as the Women In Engineering, developing a better academic culture for diverse groups, has given me new heights to reach for.

To the friends I have made during graduate career Raja Ganesh, Shyamala Athaide, Adam Stager, Zach Adams, Anahid Ebrahimi, Nicole Ray, Brian Graham, Noelle Borchardt, Albraa Jaber, Heba Jameel, Ben McNealy, Sophie Le Blanc, Rohit Kakodkar, Sagar Doshi, Sushant Veer, Minyoung Yun, Elahe Ganji, Anagha Kulkarni, Adam Smith, Pavielle Haines, Philip Fugate, Gabriel Man, Dhelma Salzr, Xin Lin, Jing Wang, and many others, I have been so fortunate to have you in my life. Please know that you were my greatest gift from the doctoral program. When I entered graduate school, I expected it all to be about the program, thank you for teaching me it's all about the people. And to my undergrad and high school mentees Erin Rezich, Ryan Tocker, Sophia Marianiello, and Arshia Faghri, thanks for all your hard work and please send me updates occasionally.

I thank my Chart, Haidar, Hartwig, and Endres family members for their unconditional love and never ending support throughout my entire life. You are all more dear to me than words can express, and you truly make my life special. Even though earning this degree has kept us apart more than we would like, I am so grateful that we make the most of our time when we are together. An additional thanks to my parents, you never held me back, always cheered me forward, and gave me the best of you. I am especially grateful to my mother Shirlene Chart, she has been there for me during every step in the journey of life and I never would have made it without her.

Last, but never least, I give thanks to my life partner James Endres. Your continual encouragement and understanding was my greatest support throughout this process. Even with us both earning undergraduate and doctoral degrees, the past ten years together have been the best of my life. I am grateful for the time we have shared, and I cannot wait for more in this new chapter of our lives.

## TABLE OF CONTENTS

LIST OF TABLES .....	x
LIST OF FIGURES .....	xiii
ABSTRACT .....	xxv
Chapter	
1 INTRODUCTION .....	1
1.1 Importance of Tribology in Engineering Applications .....	1
1.2 Overview of Solid Lubrication .....	4
2 POLYMERIC SOLID LUBRICANTS .....	7
2.1 Solid Lubrication in Space Applications .....	7
2.2 Polymers for Tribological Applications .....	10
2.3 Effect of Fillers on the Friction and Wear of Polymers .....	13
2.4 Role of the Transfer Film in the Tribological Performance of Polymer Systems .....	17
2.5 Study of alumina-PTFE Nanocomposites for Space Applications.....	27
2.6 Tribochemistry in the alumina-PTFE System .....	37
2.7 Designing a Polymer System for Space Applications: Motivation for Study .....	45
3 INSTRUMENTATION OF A WEAR TESTING TRIBOMETER WITH HIGH-THROUGHPUT CAPABILITIES .....	48
3.1 Overview .....	48
3.2 Methods and Materials .....	50
3.3 Development of New Equipment .....	52
3.4 Conclusions .....	57
3.5 Recommendations for Future Work .....	58
4 MATERIALS AND METHODS .....	60
4.1 Polymer Composite Preparation .....	60
4.2 Polymer Wear Testing Procedure .....	62
4.3 Polymer Friction Testing Procedure .....	66
4.4 Transfer Film Quality Characterization.....	66
4.5 Transfer Film Thickness Measurements .....	69
4.6 Fourier-Transform Infrared (FTIR) Spectroscopy of Tribological Interfaces .....	71

4.6.1	Spectroscopy of Polymer Running Films .....	71
4.6.2	Spectroscopy of Developed Transfer Films .....	71
5	QUANTITATIVE METRICS OF TRANSFER FILMS AS INDICATORS OF POLYMER WEAR PERFORMANCE.....	72
5.1	Overview .....	72
5.2	Materials and Methods .....	74
5.3	Results and Discussion .....	75
5.4	Conclusions .....	84
5.5	Recommendations for Future Work .....	84
6	PEEK-PTFE ENVIRONMENTAL MOISTURE STUDY .....	85
6.1	Overview .....	85
6.2	Results .....	90
6.3	Discussion.....	114
6.4	Conclusions .....	123
6.5	Recommendations for Future Work .....	126
7	FUTURE DIRECTIONS.....	129
7.1	Dissertation Summary .....	129
7.2	Recommendations for Future Work .....	130
	REFERENCES .....	132
Appendix		
A	DESIGN OF A WEAR TESTING TRIBOMETER WITH HIGH- THROUGHPUT CAPABILITIES .....	144
A.1	Tribometer Assembly .....	144
A.2	Frame Components.....	146
A.3	Flexure Components.....	157
A.4	Reciprocation Components.....	169
A.5	Table Components .....	178
A.6	Carriage Components .....	182
A.7	Pneumatics.....	185
B	DATA FROM PEEK-PTFE ENVIRONMENTAL MOISTURE STUDY ....	187
C	EVALUATION OF TRANSFER FILMS METRICS USING MATLAB CODE .....	194

C.1	Transfer Film Characterization Code .....	194
C.2	Tutorial for Transfer Film Characterization Code .....	206
D	REPRINT PERMISSION LETTERS.....	226

## LIST OF TABLES

Table 3-1	Design metrics with target values for a wear testing tribometer with high-throughput capabilities.....	53
Table 5-1	The dataset of wear rates and transfer film thickness measurements for 10 polymers and polymer composites with a wide range in wear resistance. The metric values are reported as $\pm$ the root sum square of the standard deviations (N=5). Table reproduced with permission from [80].....	81
Table 5-2	The dataset of wear rates, transfer film area fraction, and transfer film free-space length for 10 polymers and polymer composites with a wide range in wear resistance. All metric values are reported as the mean $\pm$ 95% confidence interval (N=5). Table reproduced with permission from [80]. .....	82
Table 6-1	Composites of PEEK filler in PTFE matrix selected to be tested for wear performance when moisture is available or absent in the environment. ....	89
Table 6-2	The complete dataset of wear rates and transfer film topological metrics quantified in this study. The wear test was conducted in a dry nitrogen environment unless indicated by the * symbol as a humid environment. All metric values are reported as the mean $\pm$ 95% confidence interval (N=5).....	101
Table A-1	Bill of materials listing the fabricated parts for the tribometer assembly. ....	144
Table A-2	Bill of materials listing the purchased parts for the tribometer assembly, excluding purchased screws. ....	145
Table B-1	Average surface roughness ( $R_a$ ) of each 304 stainless steel counterface used for wear tests conducted in dry nitrogen environment (<0.05% RH). The roughness value reported for each counterface was measured in 3 regions within the area designated for the polymer sample's wear track to form during testing. Measurements were taken using a Veeco Wyko NT9100 scanning white light interferometer at 5.5x zoom with a viewing window of 0.86 mm x 1.10 mm (N=3). .....	187

Table B-2	Average surface roughness ( $R_a$ ) of each 304 stainless steel counterface used for wear tests conducted in humid air environment (30% RH). The roughness value reported for each counterface was measured in 3 regions within the area designated for the polymer sample's wear track to form during testing. Measurements were taken using a Veeco Wyko NT9100 scanning white light interferometer at 5.5x zoom with a viewing window of 0.86 mm x 1.10 mm (N=3). .....	188
Table B-3	Density ( $\rho$ ) of each polymer sample subject to wear tests conducted in both dry nitrogen environment (<0.05% RH) and humid air environment (30% RH). The density value reported for each counterface was determined by measuring volume using a Starrett outside micrometer and mass using a Mettler Toledo XP105 DeltaRange™ balance (N=1). .....	188
Table B-4	A collection of mass (m) values measured for a ~10 g calibration 'weight' as a function of date using a Mettler Toledo XP105 DeltaRange™ balance. The mass values for this reference object were gathered in the same sessions as mass values for polymer samples, which was conducted each time a wear test was interrupted. Data in this table displays the long-term variability in the mass balance, which could have influenced polymer volume loss and polymer wear rate. The mass reported for each session is an average of 3 measurements (N=3). .....	189
Table B-5	The complete dataset of polymer wear rates and running film FTIR-ATR spectra comparing the peak-to-peak signal intensity of 1650/1150 $\text{cm}^{-1}/\text{cm}^{-1}$ in this study. The wear test was conducted in a dry nitrogen environment unless indicated by the * symbol as a humid environment. All metric values are reported as the mean $\pm$ 95% confidence interval (N=5).....	191
Table B-6	The complete dataset of polymer wear rates and running film FTIR-ATR spectra comparing the peak-to-peak signal intensity of 1490/1150 $\text{cm}^{-1}/\text{cm}^{-1}$ in this study. The wear test was conducted in a dry nitrogen environment unless indicated by the * symbol as a humid environment. All metric values are reported as the mean $\pm$ 95% confidence interval (N=5).....	192

Table B-7	The complete dataset of polymer wear rates and running film FTIR-ATR spectra comparing the peak-to-peak signal intensity of 1280/1150 $\text{cm}^{-1}$ / $\text{cm}^{-1}$ in this study. The wear test was conducted in a dry nitrogen environment unless indicated by the * symbol as a humid environment. All metric values are reported as the mean $\pm$ 95% confidence interval (N=5).....	193
-----------	---	-----

## LIST OF FIGURES

- Figure 1-1 Illustration of the solid lubricant lamellar lattice structures of (a) hexagonal boron nitride, (b) graphite, and (c) molybdenum disulfide. Image created using Avogadro open source GNU GPL software..... 5
- Figure 1-2 Solid lubricant structures illustrated for the (a) face-centered cubic lead and (b) polymer chain of polytetrafluoroethylene. Image created using Avogadro open source GNU GPL software. .... 5
- Figure 2-1 Mechanical systems in space have a variety of parts moving in contact including gimbals, bushings, gyroscopes, momentum wheels, motors, etc. Image courtesy of Prof. W. G. Sawyer at the University of Florida..... 7
- Figure 2-2 The ranges for poor, moderate, and excellent bearing performance as a function of friction coefficient and wear rate. These domains were developed from a survey of traditionally lubricated compatible metals with poor, moderate, or excellent lubrication (black circles) [2]. Using a straight line connecting the three benchmark data points, the transition between regimes can be defined as a perpendicular gradient from the midpoint of poor to moderate as well as midpoint of moderate to excellent. Common polymers in their neat form have a wide range of friction coefficient and wear values, most of which classify as poor performance bearing materials (white circles) [6, 22, 24, 46–50]..... 11
- Figure 2-3 Normalized wear rate plotted against filler loading for microcomposites (a-d) and nanocomposites (e-h) from literature. The normalized wear rate is defined as the composite wear rate ( $k$ ) divided by the unfilled polymer wear rate ( $k_0$ ), hence the normalized wear rate for an unfilled polymer is equal to 1. The variation in wear rate based on filler material is observed between microcomposites a) PTFE- $\text{Al}_2\text{O}_3$  particles [63], b) PTFE- $\text{Al}_2\text{O}_3$  particles [22], c) PTFE-glass fibers [66], d) PTFE-bronze particles [21] and nanocomposites e) PTFE- $\text{Al}_2\text{O}_3$  particles [22], f) PTFE- $\text{Al}_2\text{O}_3$  particles [67], g) PTFE- $\text{Al}_2\text{O}_3$  particles [68], h) PTFE-ZnO particles [20]..... 16

Figure 2-4	<p>In a tribological application, initial sliding places the low surface energy (20-50 mJ/m<sup>2</sup>) polymer composite in direct contact with the high surface energy (~900 mJ/m<sup>2</sup>) steel counterface (left). Due to the disparity in surface energies, debris preferentially formed by the polymer then transfers to the steel. When polymer debris transfers to the counterface it can adhere and build up as a transfer film (right). This low surface energy third body inhibits direct contact and allows the polymer to slide with low friction and long lifetime. ....</p>	18
Figure 2-5	<p>Tribological properties of friction coefficient and wear rate as a function of transfer film quality for PTFE-based composites with various filler materials. Image adapted and reprinted with permission from [5]. ....</p>	20
Figure 2-6	<p>Transfer film wear rate as a function of probe surface energy. The transfer film formed by the alumina-PTFE nanocomposite displayed poor wear resistance against high surface energy probes, moderate wear rates to low surface energy probes, and excellent wear performance to very low surface energy probes that include the parent polymer composite's majority PTFE material. Image adapted and reprinted with permission from [78]. ....</p>	22
Figure 2-7	<p>Current model for a lubricious polymer matrix filled with hard microparticles (left), filled with hard nanoparticles (middle), and unfilled (right). The addition of fillers has a net positive effect on the transfer film and polymer wear rate compared to the neat form, because the unfilled polymer deposits large debris that poorly covers and adheres to the counterface. Yet, neither filler size is optimal. Microparticles arrest crack development, which nanoparticles are too small to achieve, for improved mechanical adhesion of polymer debris to the counterface and more tenacious transfer films. However, microparticles abrade the counterface and remove transfer film requiring more replenishment by polymer debris, whereas nanoparticles gently polish the interface and promote stable film formation. ....</p>	25

Figure 2-8	The bearing performance of several polymer composites (grey circles) as a function of friction coefficient and wear rate [49, 56, 68, 79]. The bearing performance of the respective neat polymer (white circles) can be improved from poor performing to moderate or excellent performing bearing materials by the addition of fillers that supplement the lacking tribological trait of lubricity or wear resistance [6, 22, 24, 46–50]. Domains for bearing performance were developed from a survey of traditionally lubricated compatible metals with poor, moderate, or excellent lubrication (black circles) [2]. Using these survey values, a subdomain of excellent bearing performance is observed to fulfill the demands of aerospace applications. This subdomain, which requires ultralow wear rates ( $k \leq 3 \times 10^{-7} \text{ mm}^3/(\text{Nm})$ ) and moderate friction ( $\mu \leq 0.17$ ), is termed advanced bearing performance. The alumina-PTFE system, tested in ambient conditions, was the first polymeric solid lubricant to display advanced bearing performance [22, 79].	28
Figure 2-9	Profiles of transfer films for nanocomposites of 2.5 vol% 44 nm $\Delta$ : $\Gamma$ -phase alumina in PTFE (left) and 2.5 vol% 80 nm $\alpha$ -phase alumina in PTFE. Image reprinted with permission from [83].	30
Figure 2-10	TEM (Transmission Electron Microscopy) images of alumina filler materials reported as 44 nm $\Delta$ : $\Gamma$ -phase (left) and 80 nm $\alpha$ -phase (right). Image reprinted with permission from [79].	31
Figure 2-11	Wear rate of alumina-PTFE composites as a function of the filler’s particle or agglomeration size. Image adapted and reprinted with permission from [84].	32
Figure 2-12	SEM (Scanning Electron Microscopy) image of alumina sample E from Nanostructured and Amorphous Materials 1015WW shows this filler material to have a micro-scale characteristic size. Image reprinted with permission from [84].	32
Figure 2-13	Three-dimensional X-ray microtomography of an alumina-PTFE composite using filler material alumina sample E from Nanostructured and Amorphous Materials 1015WW. This image was taken of the composite’s side view after wear testing. The top of the image at the wear surface shows an accumulation of alumina in the polymer sliding surface (running film). Image reprinted with permission from [84].	34

Figure 2-14 TEM (Transmission Electron Microscopy) image of an alumina-PTFE composite using filler material alumina sample E from Nanostructured and Amorphous Materials 1015WW. This side view of the polymer composite’s sliding surface (running film) after wear testing shows the accumulated alumina filler to have nano-scale characteristic size. Image reprinted with permission from [84]..... 35

Figure 2-15 NASA’s Materials International Space Station Experiments 7 (MISSE 7) (left), in November 2009 the tribology unit ground-test before launch resulted in alumina-PTFE forming a uniform transfer film (center), and in May 2011 the tribology unit post 325,000,000 miles of testing in space resulted in alumina-PTFE forming a patchy transfer film (right). The tribology unit tested gold, alumina-PTFE bulk, chameleon coating, and commercial MoS<sub>2</sub>/Gold/Sb<sub>2</sub>O<sub>3</sub> (top to bottom). Images courtesy of NASA. .... 36

Figure 2-16 Wear rate of alumina-PTFE nanocomposite in ambient air environment as a function of vacuum pressure. Below a critical pressure the alumina-PTFE showed environmental sensitivity by having 100x less wear resistance than ambient air conditions. Image reprinted with permission from [86]..... 38

Figure 2-17 Transfer films of alumina-PTFE composite formed in ambient air environment without vacuum 760 Torr (top row) and with high vacuum 4x10<sup>-6</sup> Torr (bottom row). In ambient conditions the alumina-PTFE composite had ultralow wear, correlated to forming a good quality transfer film that is brown discolored, thin, and uniform. Testing in high vacuum caused alumina-PTFE to have higher wear rates, relating to its lower quality transfer film. Image adapted and reprinted with permission from [86]..... 38

Figure 2-18 Wear rate of alumina-PTFE composite as a function of relative humidity in the environment. The alumina-PTFE system displayed environmental sensitivity by necessitating humidity for wear resistance in having 100x worse wear rates at the lowest humidity tested (0.6% RH) than in high humidity (69% RH). Image reprinted with permission from [87]. .... 40

- Figure 2-19 Transfer films of alumina-PTFE composite formed in a nitrogen rich environment with high humidity of 69% RH (left) and low humidity of 0.6% RH (right). In the presence of high humidity the alumina-PTFE composite had ultralow wear, correlated to forming a good quality transfer film that was brown discolored, thin, and uniform. The absence of moisture caused alumina-PTFE to have higher wear rates, relating to its lower quality transfer film that is light grey and patchy. Image reprinted with permission from [87]...... 40
- Figure 2-20 FTIR spectrum of the transfer film formed on a steel counterface were taken from an in-situ tribology test of alumina-PTFE composite in ambient conditions. After 1 cycle of sliding debris has not yet built a transfer film and only PTFE signal at 1200 and 1150  $\text{cm}^{-1}$  is present (grey). After 1 million cycles a transfer film has fully formed and carboxylates at 1650 and 1430  $\text{cm}^{-1}$  are present along with the PTFE (black). Spectra were collected using a Nicolet 6700 FTIR spectrometer with Continuum Microscope from ThermoFisher Scientific having a penetration depth of ~1 micron. Image adapted and reprinted with permission from [90]...... 43
- Figure 2-21 FTIR spectra of the alumina-PTFE composite transfer film (left) and running film (right) after wear testing. Transfer film spectra show the carboxylate peaks at 1655 and 1430  $\text{cm}^{-1}$  to be strong for humid (25 °C, 1 pph water), attenuated for humid heated (100 °C, 1 pph water), and absent for dry nitrogen (25 °C, 15 ppm water) environments (left). Running film spectra show these peaks as strong for humid, attenuated for dry nitrogen, and absent for humid heated conditions (right). Spectra of the transfer film (left) were collected using a NanoIR2 AFM-IR from Anasys Instruments having a penetration depth on the order of tens of nanometers. Spectra of the running film (right) were collected using a Nicolet Nexus 670 FTIR with a smart orbit attenuated total reflectance (ATR) accessory having a penetration depth of ~1 micron. Image reprinted with permission from [91]...... 44

Figure 2-22 Current model for a hard metallic filler in lubricous polymer matrix has three requisites for excellent bearing performance 1) micro-scale functionality of filler material in the bulk to arrest crack propagation for fine debris formation and in effect quality transfer film development, 2) nano-scale functionality of filler material at the sliding interface that gently polishes instead of abrades and provides stability of the protective transfer film, 3) polymer debris mechanically degraded by sliding chemically bonds to the counterface to provide the strongest method of transfer film adhesion and minimal replenishment for low polymer wear rates. Fully-dense hard microparticles fail requirement #2 (left), true hard nanoparticles fail requirement #1 (middle), and micro-sized agglomerates of hard nanoparticles fulfill requirement #1&2 (right). ..... 47

Figure 3-1 Illustration of the pin-on-flat tribometer used for testing the friction and wear of heavy-duty bearing materials. Polymer sample pins (6.4 mm x 6.4 mm) are mated to flat 304 stainless steel (38 mm x 25 mm) and undergo linear reciprocating motion. Tests were conducted with a normal force of 250 N (6.3 MPa), sliding speed of 50.8 mm/s, and wear track length of 50.8 mm per cycle. Image adapted and reprinted with permission from [75]. ..... 51

Figure 3-2 Illustration of the pin-on-flat tribometer used for high-throughput wear testing of polymer samples. Each polymer pin (6.4 mm x 6.4 mm) was mated to a 304 stainless steel counterface (38 mm x 25 mm). This custom-made equipment allows six samples, with a wide range of tribological performance, to be tested simultaneously. Wear tests were conducted with a normal force of 250 N (6.3 MPa), sliding speed of 50.8 mm/s, and wear track length of 50.8 mm per cycle. Image reprinted with permission from [93]. ..... 56

Figure 3-3 Picture of the pin-on-flat tribometer with high-throughput wear testing capabilities that was designed, fabricated, prototyped, and implemented over a year and a half. This equipment has facilitated studies investigating broad trends across multiple polymer systems and a single polymer system as a function of several variables, both of which would have been logistically limited otherwise. .... 57

Figure 4-1	SEM image of PTFE Teflon™ 7C resin from DuPont has a micro-scale characteristic size (left). SEM image of PEEK 450PF resin from Victrex has a micro-scale characteristic size (right). Images were collected using a Carl Zeiss STM Auriga® 60 SEM, with SESI (Secondary Electrons or Secondary Ions) detector set to 1 kV and gun set to 3 kV, from the Keck Electron Microscopy Lab at the University of Delaware. ....	61
Figure 4-2	Illustration of a polished steel counterface inspected at the left region, center region, and right region within the area designated for the polymer sample’s wear track to form during testing. Surface roughness was measured at these three locations using a Veeco Wyko NT9100 scanning white light interferometer. The average surface roughness ( $R_a$ ) of each counterface was reported as the average of those three values. ....	63
Figure 4-3	Schematic of the pin-on-flat tribometer with high-throughput capabilities housed in an environmental glovebox. This dry environment contained less than 0.05% RH (<10 ppm water) by using 99.9998% pure dry nitrogen gas with constant closed-cycle recirculation through an activated charcoal purifier. Image adapted and reprinted with permission from [91, 93]. ....	65
Figure 4-4	Example image of an entire wear track (25.4 mm width) developed by linear reciprocating motion of a polymer pin (6.4 mm x 6.4 mm) mated to a flat steel counterface. Representative images of the transfer film formed on the counterface were captured at 5 locations within the central area of the counterface to eliminate reversal effects and collect relevant statistics. Image adapted and reprinted with permission from [77]. ....	67

- Figure 4-5 Example captured image of a polymeric transfer film deposited on a steel counterface was collected using an optical microscope (left). The optical image was converted from RGB color to binary black (transfer film) and white (counterface) using an algorithm for pixel intensity thresholding coded in MATLAB® (middle). Following conversion, a second operation in the same MATLAB® code evaluates area fraction and free-space length. The area fraction is determined by a ratio of black to white pixels. Then, free-space length is found through a process of calculating the most likely number of intersecting black pixels in a randomly placed box of given side length (right). The resulting free-space length value is the side length of the largest box in which the most probable number of intersecting black pixels is zero. Image adapted and reprinted with permission from [77]. ..... 68
- Figure 4-6 Illustration of the method for determining average transfer film thickness using stylus profilometry. (a) Custom equipment with a 3 mm radius HDPE spherical probe was used to collect line scans of the transfer film perpendicular to the sliding direction of the parent polymer. (b) An 8 mm wide scan was made across ~1 mm of counterface, 6.4 mm of wear track, and ~1 mm of counterface. (c) A total of 5 line scans for each transfer film were combined into a 50-bin histogram with a bi-Gaussian fit. Average transfer film thickness was defined as the difference between the two modes. Image adapted and reprinted with permission from [80]...... 70
- Figure 5-1 Volume lost as a function of sliding distance for all polymers and polymer composites (left), which were tested in humid air environment (30% RH). Wear rates for all polymer materials tested (right). Note that all axes were necessarily plotted on a logarithmic scale due to the wide range in wear performance. Image reprinted with permission from [80]. ..... 75
- Figure 5-2 Representative profile line scans (left), original images (center), and converted images (right) of the transfer films for neat polymer (a) PTFE, (b) PPS, (c) epoxy, (d) PEEK, and (e) PET. Polymer materials are organized by descending in order of decreasing wear rate. For each transfer film, a square identifying the mean free-space length is provided to illustrate the relationship between this metric and film appearance. Image adapted and reprinted with permission from [80]. .. 77

Figure 5-3	Representative profile line scans (left), original images (center), and converted images (right) of the transfer films for polymer composites (a) PTFE+5 wt% $\gamma$ -Al <sub>2</sub> O <sub>3</sub> , (b) PEEK+5 wt% $\gamma$ -Al <sub>2</sub> O <sub>3</sub> , (c) PEEK+5 wt% $\alpha$ -Al <sub>2</sub> O <sub>3</sub> , (d) PTFE+5 wt% $\alpha$ -Al <sub>2</sub> O <sub>3</sub> , and (e) PTFE+32 wt% PEEK. For each transfer film, a square identifying the mean free-space length is provided to illustrate the relationship between this metric and film appearance. Image adapted and reprinted with permission from [80].	78
Figure 5-4	For common polymers and polymer composites, with a wide range in wear resistance, the polymer wear rate is plotted as a function of average transfer film thickness (black circles). The mean thickness (dashed line) and standard deviation (grey shaded region) for all data points indicate that overall the polymer wear rate is not a function of thickness. Image adapted and reprinted with permission from [80].	79
Figure 5-5	For common polymers and polymer composites, with a wide range in wear resistance, the polymer wear rate is plotted as a function of average transfer film thickness (black circles). Resulting best-fit trendline (dashed line) and mean variation (grey shaded region) indicate a generally poor fit to polymer wear rates. Image adapted and reprinted with permission from [80].	80
Figure 5-6	For common polymers and polymer composites, with a wide range in wear resistance, the polymer wear rate is plotted as a function of transfer film area fraction (top) and free-space length (bottom). The calculated best-fit trendline (dashed line) and mean variation (grey shaded region) for each morphology metric is plotted. These results indicate area fraction had a moderately good fit and free-space length had the best fit to polymer wear rate. Image adapted and reprinted with permission from [80].	83

Figure 6-1	Proposed model for a soft microparticle filler in lubricious polymer matrix is presented as fulfilling the necessary functions for advanced tribological performance 1) micro-scale filler material is relatively harder than the matrix for bulk crack arrest and fine debris formation needed for quality transfer film development, 2) filler material is soft enough not to abrade the sliding interface and allows stable formation of a protective transfer film, 3) polymer matrix is mechanically degraded by sliding and the filler provides the oxygen and hydrogen elements regardless of environment for strong chemical bonding to the counterface and tenacious transfer film adhesion requiring minimal replenishment for low polymer wear rates. Soft microparticles could satisfy all of the requirements #1, 2, & 3 for a low wear PTFE-based system (right).....	87
Figure 6-2	Wear rates and friction coefficients for PEEK-based composites tested in humid air (black) and dry nitrogen environments (white). From the results, it is observed that PEEK composites generally have lower friction in an environment absent of moisture. Image reprinted with permission from [116]......	89
Figure 6-3	Wear volume as a function of sliding distance for all PEEK-PTFE composites tested in dry N <sub>2</sub> environment (top) and humid air environment (bottom). All samples were tested in dry nitrogen environment (<0.05% RH), unless indicated by the * symbol as a humid air environment (30% RH). Image adapted and reprinted with permission from [93]......	91
Figure 6-4	Wear rate as a function of filler loading for all PEEK-PTFE composites tested in dry N <sub>2</sub> environment (circles) and humid air environment (squares). Uncertainty for weight percent of PEEK filler in PTFE is represented by the work of Burris and Sawyer [48]. Image reprinted with permission from [93]......	93
Figure 6-5	Volume loss (top) and friction coefficient (bottom) as a function of sliding distance for 20 wt% PEEK-PTFE composite tested in dry N <sub>2</sub> and humid air environments. The sample tested in humid air environment is indicated by the * symbol. Top image adapted and reprinted with permission from [93]......	95
Figure 6-6	Representative images of transfer films after test termination for PTFE-based composite filled with PEEK ranging from 5-90 wt% in dry nitrogen environment and 5-50 wt% in humid air environment indicated by the * symbol. Image adapted and reprinted with permission from [93]......	97

Figure 6-7	Polymer wear rate as a function of transfer film area fraction (top) and free-space length (bottom). Expected correlation is predicted by the results of common polymers and polymer composites (white circles), the calculated best-fit trendline (dashed line), and mean variation (grey shaded region) for each morphology metric [80]. The correlation of PEEK-PTFE composites wear rate to area fraction was poor for dry testing conditions (dark grey circles) and moderate for humid testing conditions (light grey squares). For the metric of free-space length in relation to wear rate, the PEEK-PTFE system had moderate correlation across both environmental conditions. Image adapted and reprinted with permission from [80].	100
Figure 6-8	Images of running films after test termination for PTFE-based composite filled with PEEK ranging from 5-90 wt% in dry nitrogen environment, and 5-50 wt% PEEK in humid air environment indicated by the * symbol. Image adapted and reprinted with permission from [93].	103
Figure 6-9	FTIR-ATR spectra of polymer running films after test termination for reference samples of 100% PEEK and 100% PTFE tested in dry N <sub>2</sub> environment (<0.05% RH) and humid air environment indicated by the * symbol (30% RH). Image adapted and reprinted with permission from [93].	106
Figure 6-10	FTIR-ATR spectra of polymer running films after test termination for all PEEK-PTFE composites tested in dry N <sub>2</sub> environment (top) and humid air environment (bottom). All samples were tested in dry nitrogen environment (<0.05% RH), unless indicated by the * symbol as a humid air environment (30% RH). Image adapted and reprinted with permission from [93].	107
Figure 6-11	FTIR-ATR peak ratios displayed the signals of PEEK (1650, 1490, 1280 cm <sup>-1</sup> ) to PTFE (1150 cm <sup>-1</sup> ) for all PEEK-PTFE composite unworn surfaces and running films. Three PEEK peaks were used to observe an overall trend in the ratio of PEEK versus PTFE without misrepresentation from potential new chemistry. Tests were conducted in dry N <sub>2</sub> environment (top) and humid air environment (bottom). Results indicated that 30 wt% PEEK or less in PTFE in both testing conditions show stronger PEEK signals at the sliding interface than bulk material. This trend was exacerbated in higher PEEK loading only for humid testing conditions.	110

- Figure 6-12 FTIR-ATR spectra of polymer running films after test termination for composites of 20 wt% PEEK-PTFE tested in dry and humid environments. These running films were compared to both the unworn 20 wt% PEEK-PTFE and the running film formed in humidity by the alumina-PTFE composite from literature [91]. Image adapted and reprinted with permission from [91, 93]..... 111
- Figure 6-13 FTIR-ATR peak ratios displayed the signals of O-H Stretching ( $3300\text{ cm}^{-1}$  within this region), C=O Stretching ( $1655\text{ cm}^{-1}$  within this region), and C=C Stretching ( $1490\text{ cm}^{-1}$  within this region) to PTFE ( $1150\text{ cm}^{-1}$ ) for 20 wt% PEEK-PTFE running films formed in dry and humid environments. These running films were compared to both the unworn 20 wt% PEEK-PTFE material and the running film formed in humidity by the alumina-PTFE composite from literature [91]. Results indicated PEEK filler does not facilitate tribochemical change of PTFE in environments absent of moisture. Moreover, 20 wt% PEEK-PTFE displayed excellent wear performance without showing any measurable new tribochemistry in both dry and humid conditions. 113
- Figure 6-14 The PEEK-PTFE composite is the first solid lubricant identified to display advanced bearing performance in both humid (brown) and dry (yellow) conditions. The PEEK-PTFE system's 20 wt% composite (triangles) showed advanced bearing performance regardless of environmental moisture, which satisfy the needs of demanding applications that require both moderate friction ( $\mu \leq 0.17$ ) and ultralow wear ( $k \leq 3 \times 10^{-7}\text{ mm}^3/(\text{Nm})$ ). This was a significant improvement over the bearing performance of the alumina-PTFE system (squares), which has advanced bearing performance in humidity but poor performance in dry conditions. For reference, neat polymers often have poor bearing performance (white circles) [6, 22, 24, 46–50] and many polymer composites have moderate bearing performance (grey circles) [49, 56, 68, 79]. This scale was developed from a survey of bearing performance for traditionally lubricated compatible metals with poor, moderate, or excellent lubrication [2].... 125

## ABSTRACT

Solid lubricants are materials capable of providing low friction in bearing applications that prohibit the use of traditional oils and greases due to physical, chemical, thermal, or other environmental challenges. A necessity of these tribological systems is functioning with long lifetimes and high efficiencies with little to no maintenance. Mechanical systems operating in space have the greatest need to adopt advanced performance bearing materials for demanding applications, defined here as displaying ultralow wear ( $k \leq 3 \times 10^{-7} \text{ mm}^3/(\text{Nm})$ ) and moderate friction ( $\mu \leq 0.17$ ). This dissertation proposed to fulfill the need for an advanced performing bearing material in challenging environments by using the body of knowledge gathered on a particular alumina-PTFE composite to improve tribomaterials design.

The current model for alumina-PTFE necessitates a hard filler with multi-scale functionality and an operating environment that supports beneficial tribochemistry. This study proposed to satisfy the current model requirements by replacing alumina with a soft micro-sized filler that also supports tribochemistry in any environment. Several materials could meet these filler requirements, including micro-sized PEEK. A tribology study on PEEK-PTFE composites was implemented to test the proposed model for a relatively soft filler in lubricious matrix to display advanced bearing performance in conditions representing terrestrial and space operating environments.

To conduct the proposed investigation, prior work was necessary to increase sample testing capacity and identify reliable metrics for assessing test results. First, there existed a logistical limitation to the number of ultralow wear polymer materials that could undergo tribology testing in a timely manner. This barrier was overcome by designing, fabricating, prototyping, and implementing a new wear testing tribometer

with high-throughput capabilities. Second, it was necessary to establish a standard for numerically assessing the success or failure of polymer materials in bearing applications. This goal was achieved by studying common polymers and polymer composites, with a wide range in bearing performance, to identify a quantitative metric to reliably predict polymer wear rate. Finally, the equipment and methodologies developed in this dissertation were applied to testing PEEK-PTFE composites for ultralow wear performance in controlled humidity environments.

This study was the first to identify a solid lubricant capable of demonstrating ultralow wear rates ( $k = \sim 8 \times 10^{-8} \text{ mm}^3/(\text{Nm})$ ) and moderate friction ( $\mu = \sim 0.17$ ) in both dry ( $< 0.05\% \text{ RH}$ ) and humid ( $30\% \text{ RH}$ ) conditions. Results from this dissertation have marked PEEK-PTFE as a tribomaterial with high potential for advanced bearing performance in aerospace applications. The outcomes of this investigation have enhanced the understanding of tribological mechanisms driving the success of polymeric solid lubricants, and opened avenues for designing more composites to display advanced bearing performance in challenging environmental conditions.

## Chapter 1

### INTRODUCTION

#### 1.1 Importance of Tribology in Engineering Applications

Tribology is the study of surface interactions between bodies moving in relative motion, particularly the contact mechanics involved in the friction and wear of materials. Nearly all mechanical systems have points of contact between moving parts (e.g. car engines, train axles, satellite gimbals) that require lubrication for long lifetimes and high efficiency. The role of a tribologist is to assess these systems and subsequently select the appropriate lubrication by considering factors such as temperature, sliding speeds, contact force, geometry, and much more. Sufficient lubrication is particularly important as lubricant starvation initiates direct interactions of bodies that are often large, heavy, and metallic. These situations commonly lead to extra maintenance, and if left unchecked can cause catastrophic failure.

The term tribology became ubiquitous after The Jost Report announced in 1966 that Britain had accrued significant financial losses of over 1% of GDP that year to early machinery failure caused by friction and wear [1]. Although this estimate was a significant sum, it is argued that this value should be much larger to account for the detriment to productivity when wear forces machinery down-time for maintenance or replacement. Taking this into consideration, it is estimated that in 1976 the U.S. economy lost 6% of GDP due to the effects of friction and wear [2].

# Chapter 1

## INTRODUCTION

### 1.1 Importance of Tribology in Engineering Applications

Tribology is the study of surface interactions between bodies moving in relative motion, particularly the contact mechanics involved in the friction and wear of materials. Nearly all mechanical systems have points of contact between moving parts (e.g. car engines, train axles, satellite gimbals) that require lubrication for long lifetimes and high efficiency. The role of a tribologist is to assess these systems and subsequently select the appropriate lubrication by considering factors such as temperature, sliding speeds, contact force, geometry, and much more. Sufficient lubrication is particularly important as lubricant starvation initiates direct interactions of bodies that are often large, heavy, and metallic. These situations commonly lead to extra maintenance, and if left unchecked can cause catastrophic failure.

The term tribology became ubiquitous after The Jost Report announced in 1966 that Britain had accrued significant financial losses of over 1% of GDP that year to early machinery failure caused by friction and wear [1]. Although this estimate was a significant sum, it is argued that this value should be much larger to account for the detriment to productivity when wear forces machinery down-time for maintenance or replacement. Taking this into consideration, it is estimated that in 1976 the U.S. economy lost 6% of GDP due to the effects of friction and wear [2].

Friction is the result of surfaces in contact resisting relative motion. Engineers consider it an inefficiency because energy is lost between the force applied and resulting motion of a system. Studies of this interfacial phenomena date back to the work of Leonardo da Vinci. He is credited with defining the metric of friction coefficient ( $\mu$ ), finding friction coefficient to be independent of apparent contact area, and estimating the force resisting motion as directly proportional to applied load [3]. These observations are still relevant to the field of tribology today, as it is currently understood that friction between two bodies arises from the actual points of nano-scale or micro-scale contact rather than the macro-scale apparent area of contact [4, 5]. Surface interactions are investigated by bring at least two materials into contact with a set force and relative velocity, using a specialized piece of equipment termed a tribometer [6]. The value of friction coefficient ( $\mu$ ) can be calculated with the known relationship  $F_{\text{friction}} = \mu * F_{\text{normal}}$  by using the tribometer to measure the force resisting motion ( $F_{\text{friction}}$ ) over the known normal force applied to the contact area ( $F_{\text{normal}}$ ) [2].

The act of rubbing materials in a tribometer typically causes wear of one or both of those bodies. This material loss for the body of interest is characterized as wear rate ( $k$ ), which is defined as the measured volume removed divided by the known sliding distance and the applied normal force with units of  $\text{mm}^3/(\text{Nm})$ . The volume of material lost from a body can be calculated by changes in displacement, but this method is unreliable for materials that uptake or outgas, deform elastically or plastically, creep, or otherwise dimensionally fluctuate, as it inherently causes uncertainties [7]. Many materials are more accurately evaluated by measuring mass loss when the density is known for conversion to volume. The type of wear incurred from the rubbing of materials can commonly be categorized as adhesive, abrasive,

corrosive, or surface fatigue, depending on several conditions including the surface roughness, material hardness, presence of corrosives, temperature, and applied pressure [2, 7].

Engineering applications that necessitate appropriate lubrication to dissuade wear from occurring and to improve efficiency are mechanisms with bearings, which are machine elements that support load and constrain movement to the desired motion. Bearings are usually made of heavy and hard materials, most commonly steel. These machine elements are intended to have lubricants bar the direct contact of surfaces by filling in the space between them, effectively lowering friction and wear rate.

Lubricants date far back into human history. Many centuries before Common Era in Ancient Egypt heavy objects were slid more easily over sand by pouring liquid on the ground in front of a loaded sled [8, 9]. With the subsequent advent of wheeled chariots and carts, axle shafts required lubrication using plant oil, animal fat, or other media [8]. Modern lubrication began with the Petroleum Age, meeting the needs of post Industrial Revolution high quantity and heavy duty manufacturing equipment [9]. Over time, these petrol-based liquid lubricants have been continually improved in formula and additives to satisfy many of industry's most challenging applications [9]. However, there remain applications that preclude the use of liquid lubricants due to physical limitations or environmental constraints, particularly aerospace applications [10]. In these cases, materials commonly known as solid lubricants are implemented to provide the necessary long lifetimes and high efficiency desired for tribological applications [10, 11].

## 1.2 Overview of Solid Lubrication

Solid lubricants are materials in the solid phase that are inherently capable of sliding with low friction. They are considered an alternative to traditional greases and liquid lubricants in bearing applications involving extreme temperatures, high vacuum, radioactivity, and chemical reactivity [12, 13]. Additional benefits of implementing solid lubricants include lower cost, lighter weight, easier maintenance, and higher cleanliness by not requiring the components necessary for liquid lubricants to sustain a continuous flow of clean fluid with plumbing, reservoirs, pumps, filters, seals, and other elements [13, 14].

Among the most common solid lubricants are hexagonal boron nitride (h-BN), graphite (Gr), and molybdenum disulfide ( $\text{MoS}_2$ ) [2, 15]. Their low friction coefficients are attributed to their tightly packed and strongly bonded lamellar lattice structure, illustrated in Figure 1-1. These materials are essentially two-dimensional sheets that easily slide over each other with only weak van der Waals forces to resist their motion and induce friction [2, 15].

Other solid lubricants include films or coatings of soft metals, such as lead, indium, gold, tin, and silver [15]. Most of these metals possess face-centered cubic structures, as depicted for lead in Figure 1-2a. The isotropy of this crystal structure and low material hardness are attributed to the relatively low shear strength that permits easy interior slip of atoms for lubricating abilities [15].

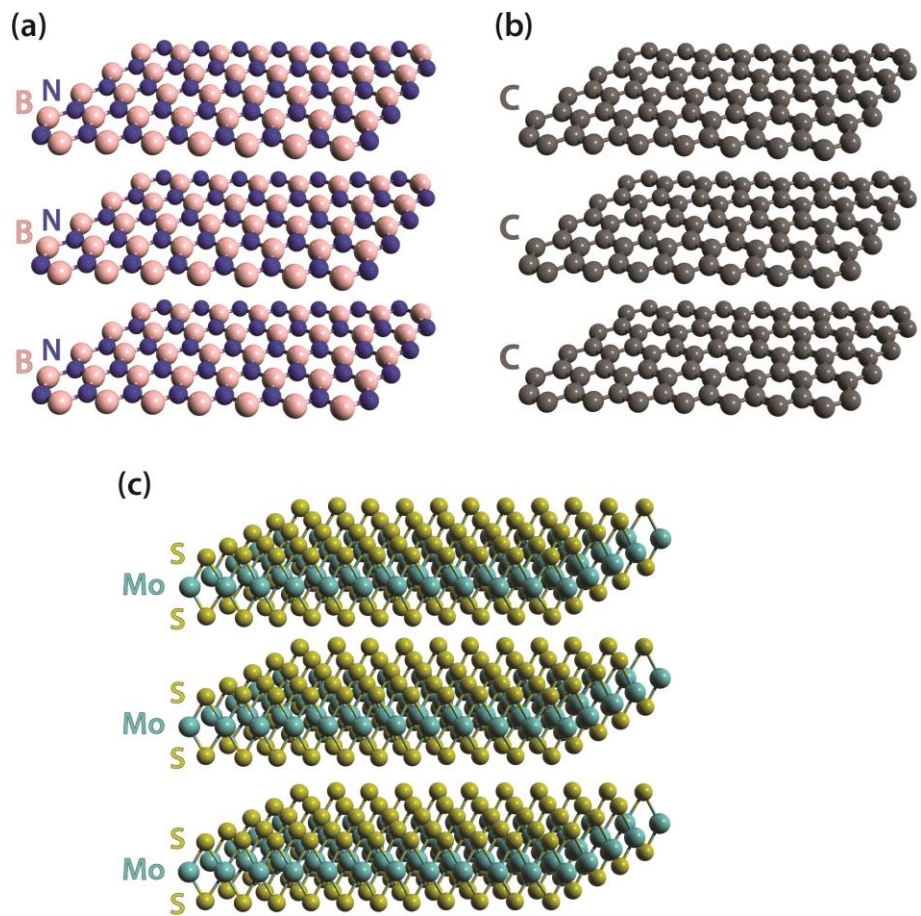


Figure 1-1 Illustration of the solid lubricant lamellar lattice structures of (a) hexagonal boron nitride, (b) graphite, and (c) molybdenum disulfide. Image created using Avogadro open source GNU GPL software.

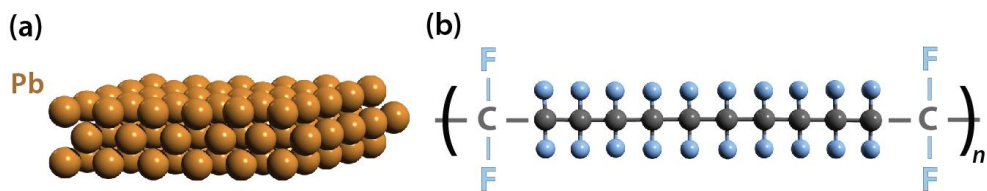


Figure 1-2 Solid lubricant structures illustrated for the (a) face-centered cubic lead and (b) polymer chain of polytetrafluoroethylene. Image created using Avogadro open source GNU GPL software.

Certain polymers are also considered solid lubricants due to their low friction coefficients, including polytetrafluoroethylene (PTFE) and high density polyethylene (HDPE) [2, 15]. These polymers share a similar structure, a backbone of single bonded carbons each with the remaining two of four bonds connected to single atoms, as illustrated for PTFE in Figure 1-2b. The low profile of these tightly-packed chains and very low surface energy accounts for their low shear strength that allows easy slip over other chains or materials for low friction [2, 15–17]. PTFE is a desirable lubricant in sliding conditions due to its low friction, but its wear rate is unacceptably high for bearing applications [18, 19]. The addition of hard fillers is generally successful in improving the wear resistance of this material, occasionally with little to no detriment to the friction coefficient [20–22]. This outcome is attributed to the formation of transfer films, a sacrificial layer of polymer debris built up on the mating surface during sliding [18, 23, 24]. Transfer films are extremely important for the tribological success of polymeric solid lubricants because they protect the soft polymer from directly contacting the hard counterface thereby reducing the interface friction, polymer wear rate, or both [6, 24–26].

## Chapter 2

### POLYMERIC SOLID LUBRICANTS

#### 2.1 Solid Lubrication in Space Applications

Space applications have several mechanical systems with moving parts (e.g. gimbals, bushings, actuators, gyroscopes, momentum wheels, gears, bearings, and motors shown in Figure 2-1) that require lubrication for long lifetimes and high efficiency. In industrial applications, greases and oils are commonly used to lubricate tribological mechanisms. However, traditional lubricants are either undesirable for their complexity (e.g. filters, pipes, pumps, reservoirs) or they are prohibited by the environment from use in extra-terrestrial operations [12–14]. The need for simpler lubricants that can withstand extreme temperature fluctuations ( $-200\text{ }^{\circ}\text{C}$  to  $250\text{ }^{\circ}\text{C}$ ), radiation from high-energy particle bombardment, and ultrahigh vacuum ( $<10^{-7}\text{ Pa}$ ) gave rise to investigating solid lubricants for bearings operating in space [10, 11, 27].

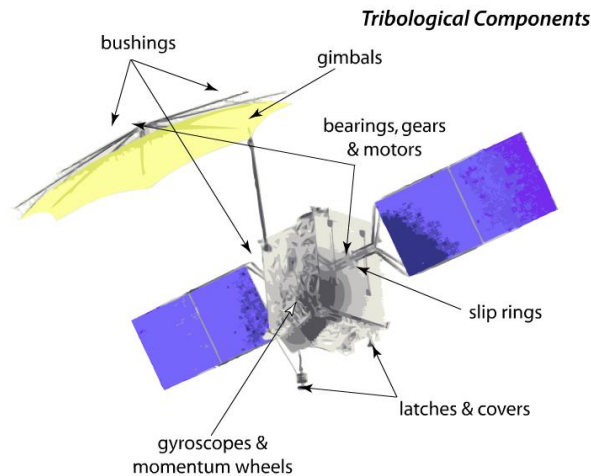


Figure 2-1 Mechanical systems in space have a variety of parts moving in contact including gimbals, bushings, gyroscopes, momentum wheels, motors, etc. Image courtesy of Prof. W. G. Sawyer at the University of Florida.

Solid lubricants are materials in the solid phase (e.g. certain lamellar structures, polymers, and metals) that are capable of sliding with low friction, generally attributed to their low shear strength allowing motion easily [15]. Even though these materials offer a wide range of desirable traits, many have shown their tribological performance to be strongly dependent on operating environment. For instance, graphite (Gr) makes a good lubricant in nitrogen rich environments when water vapor is present at a high level of 50% RH ( $0.1 < \mu < 0.2$ ) [28]. This condition is attributed to the passivation of  $\pi$  electron attraction to neighboring lamellae by the adsorption of water molecules thus reducing hindrance to shear, whereas the general absence of moisture at 100 ppm or presence of other atmospheric contaminants causes the friction coefficient to increase drastically ( $0.2 < \mu < 0.4$ ) [28, 29].

Molybdenum disulfide ( $\text{MoS}_2$ ) is another environmentally dependent solid lubricant. It performs poorly in atmospheric conditions but acts as an excellent lubricant in evacuated environments ( $0.005 < \mu < 0.05$ ), making it the gold standard for lubrication in space applications [27, 29–31]. Even though  $\text{MoS}_2$  has proven an ideal lubricant for extra-terrestrial environment, issues have arisen from its use there. One high-profile example comes from NASA's Galileo spacecraft failing to fully deploy an antenna due to lack of lubrication between multiple ribs of the umbrella-shaped structure. Investigations determined that vibrations from pre-launch ground transportation incited joint rubbing, and this sliding motion damaged the  $\text{MoS}_2$  coating [32, 33]. It is now understood that this early degradation was an outcome of its environmental sensitivity,  $\text{MoS}_2$  is susceptible to water vapor adsorption that greatly increases friction coefficient ( $0.10 < \mu < 0.20$ ) and lowers wear resistance [34, 35]. In effect, the integrity of a  $\text{MoS}_2$  coating can be compromised during required

transportation, storage, testing, and launch in atmospheric conditions prior to entering space, leaving mechanisms to lack sufficient lubrication during operation and to be vulnerable to early failure.

To overcome the environmental sensitivity typical of lamellar solid lubricants, the Air Force Research Lab (AFRL) made efforts to develop ‘chameleon’ coatings that provided lubrication in variable environmental conditions. These chameleon coatings compartmentalize at least two reservoirs of material, one for humid (moist) and the other for dry (moisture absent) environments, thereby expressing favorable tribological traits in either condition [36–39]. These environmentally adaptive lubrication coatings have the benefit of lower friction than MoS<sub>2</sub> in humid air, as well as a relatively low friction coefficient in ultra-high vacuum simulating space.

The mechanisms requiring lubrication to function are of particular concern in space, where they are expected to continually operate for 10-30 years with little to no maintenance [10]. Due to this, wear rate is a significant factor for coatings as they have a limited amount of material to lose before wearing out. Chameleon coatings are generally applied as ~1 micron thick films and display low wear rates of 10<sup>-7</sup> mm<sup>3</sup>/(Nm) [40–43]. Yet, even with low wear rates these coatings have a lifetime of only a few thousand kilometers of sliding before leaving the contact devoid of lubrication and susceptible to failure. In effect, low wear rates are not adequate for extended lifetime of thin coatings. An alternative lubrication method having a combination of low wear rates, low friction, and sufficient bulk material is necessary. In these scenarios, composites of polymeric solid lubricants offer high promise due to their wide range of lubrication performance (friction and wear) and material properties (inertness for environmental insensitivity).

## 2.2 Polymers for Tribological Applications

Polymeric solid lubricants commonly provide lubrication for consumer items including laptop hinges, computer mice, office chairs, cookware, sliding drawers, children's toys, and much more. These materials are utilized in both common and challenging applications when oils or greases are impractical for use in the physical, chemical, thermal, or environmental circumstances [12]. Moreover, solid lubricants can provide the benefits of lower cost, lighter weight, simpler maintenance, ease of manufacture, and higher cleanliness by not requiring the mechanical components necessary for traditional lubricants to function [14].

Polymers are unique from other structural materials like metals because of their low surface energy to hardness ratio, which tends to correlate with reduced adhesion strength for less resistance to sliding that lowers friction and wear [2]. Furthermore, their relatively low elastic modulus to strength ratio implies that adhesive junctions must experience large shear strains to fail and form debris; in effect, polymers can experience shear without forming debris, which also corresponds to lower wear [2]. Although polymers have properties that are related to good tribological traits, their actual performance in load bearing applications is based on friction coefficient and wear rate [6, 7, 44, 45].

According to a broad survey of compatible (not identical) metals in load bearing applications using traditional lubrication methods, friction coefficient and wear rate values are dependent on whether the lubrication is poor ( $0.3$  ,  $1 \times 10^{-4}$   $\text{mm}^3/(\text{Nm})$ ), moderate ( $0.17$  ,  $1 \times 10^{-5}$   $\text{mm}^3/(\text{Nm})$ ), or excellent ( $0.09$  ,  $3 \times 10^{-7}$   $\text{mm}^3/(\text{Nm})$ ) [2]. This benchmark can be used to define bearing performance as a function of both friction coefficient and wear rate [6]. In using a straight line to connect these three points, a complete path from poor to moderate to excellent wear

performance is observed. Along this line, the midpoint between poor and moderate, as well as moderate and excellent, indicates a transition between these domains. These two boundaries are represented by gradients perpendicular to the line connecting all three points. In using these data points as the standard for poor, moderate, and excellent bearing performance, three performance ranges are given in Figure 2-2.

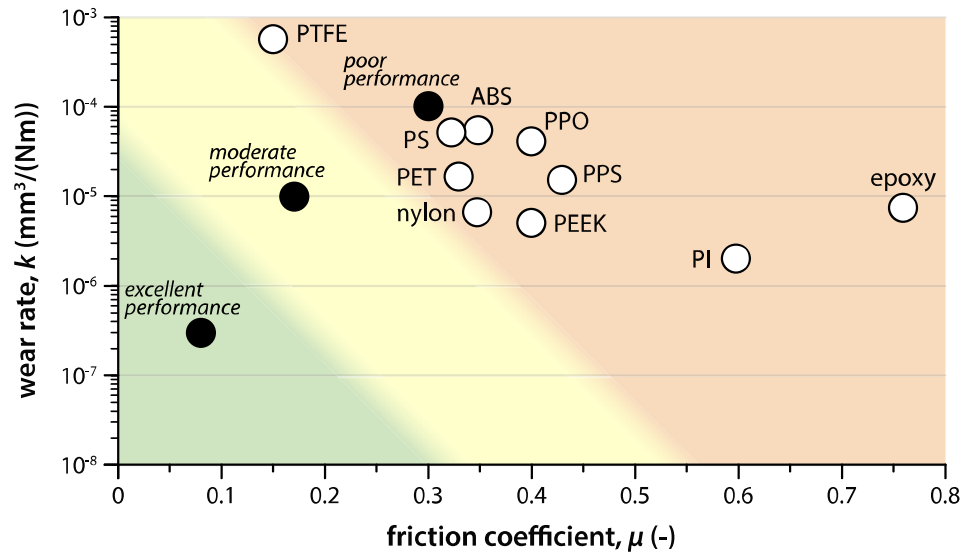


Figure 2-2 The ranges for poor, moderate, and excellent bearing performance as a function of friction coefficient and wear rate. These domains were developed from a survey of traditionally lubricated compatible metals with poor, moderate, or excellent lubrication (black circles) [2]. Using a straight line connecting the three benchmark data points, the transition between regimes can be defined as a perpendicular gradient from the midpoint of poor to moderate as well as midpoint of moderate to excellent. Common polymers in their neat form have a wide range of friction coefficient and wear values, most of which classify as poor performance bearing materials (white circles) [6, 22, 24, 46–50].

By applying this rating system, it is observed that many common polymers are identified as poor performing bearing materials. Due to the balance between friction coefficient and wear rate in quantifying bearing performance, each range can include a broad spectrum of materials. For example, polymer in the poor bearing performance category extend from lower friction coefficient and higher wear polytetrafluoroethylene (PTFE) to mid-range polyamide (nylon) to higher friction coefficient and lower wear polyimide (PI). Since most common polymers in neat form (e.g. acrylonitrile butadiene styrene (ABS), polyetheretherketone (PEEK), polyethylene terephthalate (PET), polyphenylene oxide (PPO), polyphenylene sulfide (PPS), and polystyrene (PS)) do not possess a combination of good lubricity and wear resistance, methods employing the addition of filler materials are used to improve bearing performance [51].

### 2.3 Effect of Fillers on the Friction and Wear of Polymers

Despite the advantages of utilizing polymers over other engineering materials in bearings, polymers often necessitate fillers to sufficiently improve their lubricity and wear resistance for tribological applications [6]. Most approaches to composite design identify the lacking trait of the matrix material and add fillers that have those desired attributes [6, 52]. For soft polymers with low friction (“friction coefficient” values are commonly referred to as “friction” for brevity, unless specified otherwise), hard particles are often added to increase wear resistance. In contrast, hard polymers with low wear rates are typically filled with solid lubricants to decrease friction. These methods aim to strike a balance between friction and wear to formulate a polymeric solid lubricant with good bearing performance [6, 52].

One popular approach to designing polymer composites for tribological applications has relatively harder and more wear resistant polymers filled with lubricating materials. The solid lubricants PTFE, Gr, and MoS<sub>2</sub> are commonly used to lower friction because they reduce the interfacial adhesion for matrix materials such as polyetheretherketone (PEEK) [53, 54], PI [55, 56], or epoxy [49, 57–59] to their mated sliding surface (counterface). This ‘interface modification’ method has the desired effect of decreasing friction coefficient without sacrificing wear resistance, as the wear rate tends to be comparable or improved [52]. Including relatively softer additives has a negative affect on the bulk mechanical properties of strength and hardness [53, 60]. However, the disadvantage of some reduction to mechanical properties from employing this composite design method is generally outweighed by the advantage of these materials becoming moderate bearing performers.

In contrast, the opposite approach is ‘bulk modification’ of a soft and lubricous polymer using micro-scale hard fillers [52]. Neat PTFE is a prime example of a

material that is well known for good lubricity but has unacceptably poor wear resistance, attributed to its continual transfer of large debris to the often higher surface energy metallic counterface [16, 19, 61]. The addition of hard fillers such as glass fibers, bronze, titanium oxide, or aluminum oxide (alumina) to PTFE's soft polymer matrix has improved its wear resistance by up to two orders of magnitude [19, 62–64]. When these large and hard fillers are used, the PTFE polymer debris transferred to the counterface is noticeably smaller. It is hypothesized that these fillers are arresting crack propagation by acting as a physical barrier to deformation within the PTFE bulk [19, 65]. In effect, the polymer is releasing smaller-sized debris from between locations of suspended micro-scale additive into the sliding interface. This method has the benefit of reducing the wear rate by exposing a section of the hard fillers still held in the matrix to the counterface and permits the fillers to support load applied to the bulk composite [19, 64]. In some cases but not all, this method has the detriment of increased friction coefficient by up to 25%, which is minor enough that the polymer composite can be classified as having moderate performance in bearing applications [19, 21, 62–64, 66].

A more recent approach using nano-scale hard fillers to reinforce a polymer with high wear and good lubrication has gained momentum. Again, PTFE is commonly used as the polymer matrix material because of its exceptionally low friction coefficient in sliding applications. An early study on the effects of fillers in PTFE utilized various hard fillers ranging from micron to submicron in size that resulted in the smallest filler having the worst wear performance; this outcome led researchers to hypothesize small hard particles are ineffective at both arresting crack propagation in the bulk polymer and supporting load needed for wear reduction [65].

However, since the study used various fillers, material composition was not held constant as size changed. It was noticed that this lack in control may have led to false assumptions when a subsequent study found nanometer ZnO particles could reduce the wear rate of PTFE by two orders of magnitude [20]. To clarify this disparity in results another study used only alumina fillers of nanometer, submicron, and micrometer sizes, finding that nano-scale particles offered PTFE the best wear resistance [63]. The alumina nanoparticles in PTFE reduced the wear rate by well over three orders of magnitude with only a minor increase in friction coefficient of 20%, placing it within the category of excellent performing bearing materials.

In the interface modification and bulk modification methods presented, micro-scale fillers are utilized to supplement the lacking tribological trait of the polymer and result in successfully developing moderate performance bearing materials [6, 52]. However, the significant improvement in bearing performance observed for nano-scale compared to micro-scale hard fillers in a lubricious polymer matrix indicates a tribological mechanism different from supplementing traits. This observed orders of magnitude reduction in composite wear rate for nano-scale hard fillers compared to similar micro-scale hard fillers is shown in Figure 2-3.

For the excellent performing composites with nano-scale fillers, there were two items of note. First, nano-scale fillers were expected to be too small to disrupt crack propagation for smaller debris formation, but the alumina-PTFE nanocomposite clearly formed fine debris [63, 65]. Second, the abrasion to the metallic counterface commonly caused by micro-scale hard fillers was not present for the PTFE system, potentially due to the gentler polishing action of nano-scale hard fillers [63, 64]. These two outcomes of smaller polymer debris and gentle interface polishing were

associated as beneficial factors contributing towards the tribological performance of polymeric nanocomposites. With polymer debris generally transferring from the low surface energy polymer to the high surface energy counterface, this small debris was observed to accumulate on the counterface without notable mechanical removal by filler abrasion. The formation of this layer, termed the transfer film, results in a third body that inhibits direct interfacial contact of the polymer and counterface. With this protective film in place, the polymer system performs with long-term low friction and high wear resistance.

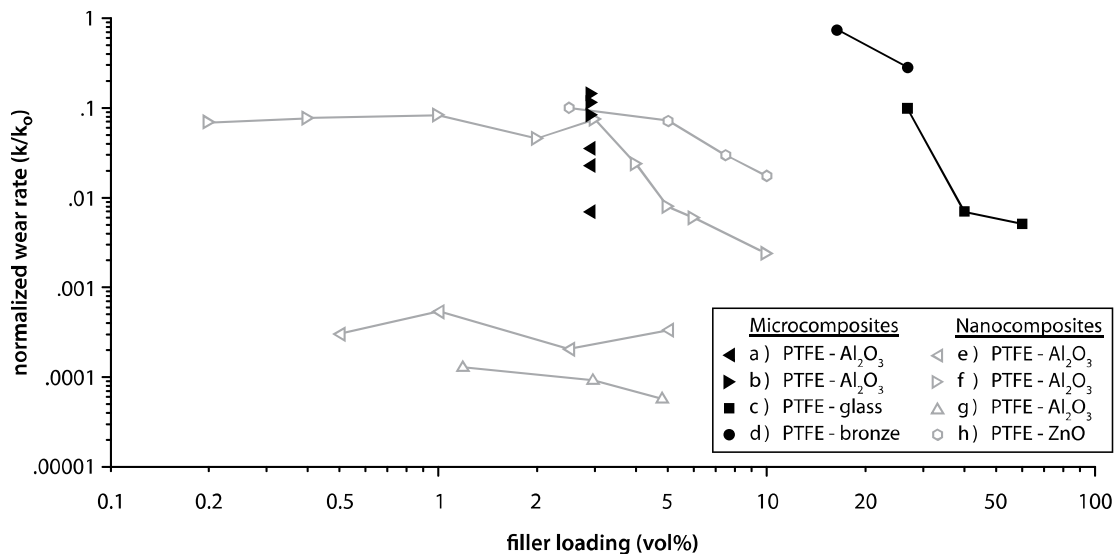


Figure 2-3 Normalized wear rate plotted against filler loading for microcomposites (a-d) and nanocomposites (e-h) from literature. The normalized wear rate is defined as the composite wear rate ( $k$ ) divided by the unfilled polymer wear rate ( $k_0$ ), hence the normalized wear rate for an unfilled polymer is equal to 1. The variation in wear rate based on filler material is observed between *microcomposites* a) PTFE-Al<sub>2</sub>O<sub>3</sub> particles [63], b) PTFE-Al<sub>2</sub>O<sub>3</sub> particles [22], c) PTFE-glass fibers [66], d) PTFE-bronze particles [21] and *nanocomposites* e) PTFE-Al<sub>2</sub>O<sub>3</sub> particles [22], f) PTFE-Al<sub>2</sub>O<sub>3</sub> particles [67], g) PTFE-Al<sub>2</sub>O<sub>3</sub> particles [68], h) PTFE-ZnO particles [20].

## **2.4 Role of the Transfer Film in the Tribological Performance of Polymer Systems**

Certain polymer composites are attractive as solid lubricants for bearing applications that prohibit the use of traditional lubrication methods. Commonly, the polymer is mated to a steel counterface, such pairings include guides, bushings, seals, and valve seats. In these situations, the lower surface energy polymer will preferentially transfer debris to the mating higher surface energy metallic counterface. The polymer composite's success in bearing applications is dependent on its ability to deposit this debris onto the counterface that adheres as a protective layer, termed the transfer film [24]. With the film inhibiting direct contact between the two bodies, the soft polymer is shielded from the hard counterface asperities, as depicted in Figure 2-4. The sliding contact between parent polymer and similarly low surface energy transfer film can greatly reduce future debris formation for lower polymer wear and provide a lower shear sliding interface for low friction, thus improve bearing performance [69].

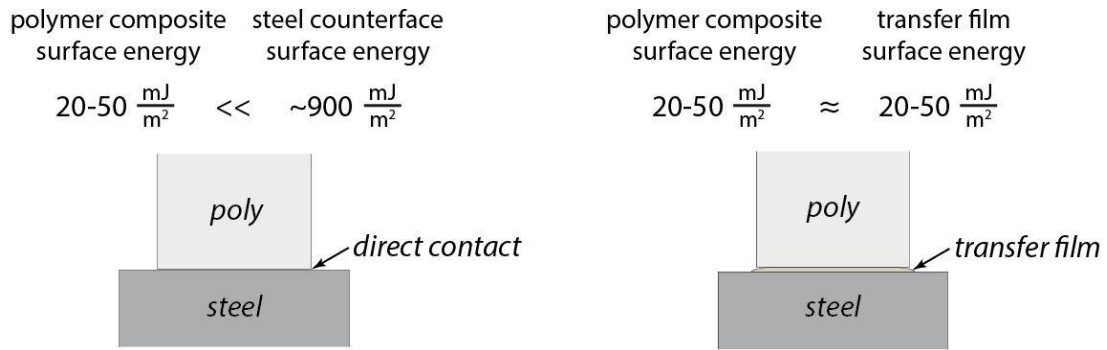


Figure 2-4 In a tribological application, initial sliding places the low surface energy ( $20-50 \text{ mJ/m}^2$ ) polymer composite in direct contact with the high surface energy ( $\sim 900 \text{ mJ/m}^2$ ) steel counterface (left). Due to the disparity in surface energies, debris preferentially formed by the polymer then transfers to the steel. When polymer debris transfers to the counterface it can adhere and build up as a transfer film (right). This low surface energy third body inhibits direct contact and allows the polymer to slide with low friction and long lifetime.

The wear resistance of polymer systems is universally associated with the appearance of their transfer films. In poor performing polymer systems, transfer films are characterized as ‘thick,’ ‘patchy,’ and ‘non-uniform’ [18, 70–74]. Conversely, improved performance corresponds to the transfer film being more ‘thin,’ ‘uniform,’ ‘continuous,’ and ‘coherent’ [18, 70–74]. This range in film quality is observed across various polymer materials and for different composites of the same polymer matrix. Most notable are PTFE-based composites, whose uniquely broad range of wear resistance corresponds to the entire span of film quality, as shown in Figure 2-5. Observations of neat PTFE have identified this system as having an unstable transfer film consisting of thick and wide plate-like debris that are inconsistently scattered across the counterface [16, 19, 61]. This poor transfer film quality offers little to no protection of the polymer from the counterface, which coupled with the continual

removal and replacement of large debris during sliding is attributed to PTFE's unacceptably high wear rate and poor bearing performance [16, 19, 61]. PTFE with micro-scale hard fillers produces finer debris that accumulates on the counterface as a more substantive transfer film than unfilled polymer and corresponds to wear rate improvements of up to 100x for moderate bearing performance [62–64]. Moreover, the moderate performance of composites with micro-scale fillers corresponds to the moderate quality of their respective transfer film, which appear streaky or incoherent from gouges in the direction of sliding motion due to interface abrasion by the large hard fillers [23, 62–64]. Some PTFE composites filled with a nano-scale hard filler of alumina have excellent bearing performance that corresponds to good quality transfer films, for which the films appear thin, uniform, and coherent [63, 75]. For composites with nano-scale fillers, there is no observed interface abrasion that would destabilize transfer film formation or compromise the protective role of the transfer film [20, 63, 72–75].

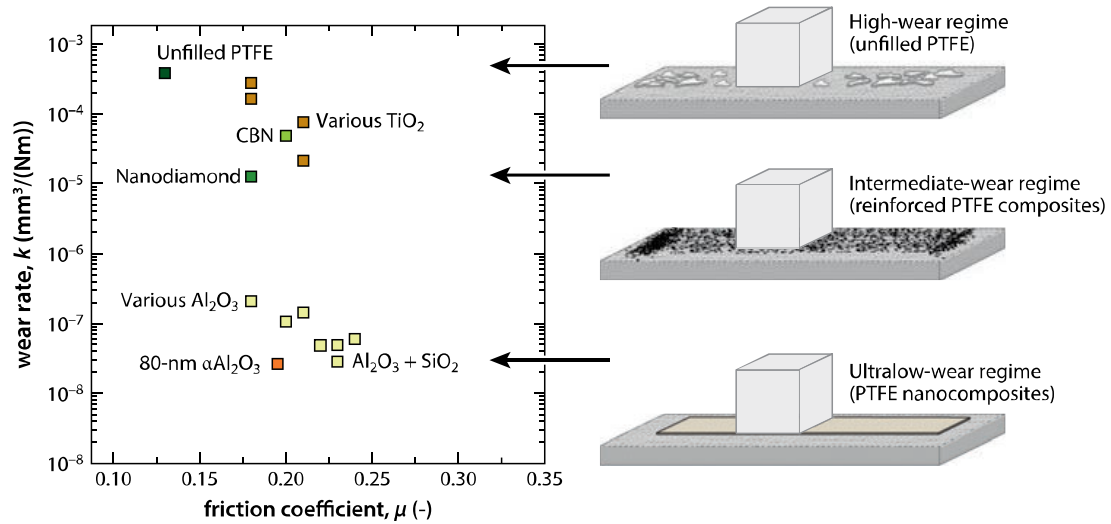


Figure 2-5 Tribological properties of friction coefficient and wear rate as a function of transfer film quality for PTFE-based composites with various filler materials. Image adapted and reprinted with permission from [5].

Although these qualitative descriptions of transfer film appearance reflect the ability of this deposited layer to bar direct contact between the parent polymer and counterface, developing quantitative measures has been a critical need towards identifying which attributes of these films truly affect polymer wear resistance [6]. Due to this need, recent studies have proposed methods for quantitatively characterizing film thickness, coverage, and uniformity [22, 71, 76, 77]. From these studies, the relationship between wear resistance and quantitative transfer film metrics had mixed results, ranging from no correlation to good correlation. Another limitation of these studies is that they only investigated one polymer system each, maintaining the need for a broadly applicable relationship between transfer film metrics and polymer bearing performance.

The ability of transfer films to protect the polymer bulk from directly contacting the counterface and contribute to improved bearing performance is a

function of debris adhesion and tenacity. These films are initially formed by the parent polymer depositing a significant amount of debris onto the counterface. When this debris forms a film that sticks to the counterface, much less debris develops and the system transitions into long-term lower wear [75]. If during every sliding cycle the transfer film was removed and had to be replaced by large amounts of new debris, it would result in unacceptably high wear rates that are observed with neat PTFE [19]. Therefore, the amount of debris formed by the parent polymer to maintain the transfer film is the minimum possible wear rate of the system [19]. This understanding has been supported by measurements of transfer film wear rates, particularly those for a wear resistant alumina-PTFE composite presented in Figure 2-6. In this study, the transfer film wear rate was measured to be nearly 100x more wear resistant than the parent polymer composite itself when worn by probes with very low surface energy, which included a probe of the composite's majority material PTFE [78].

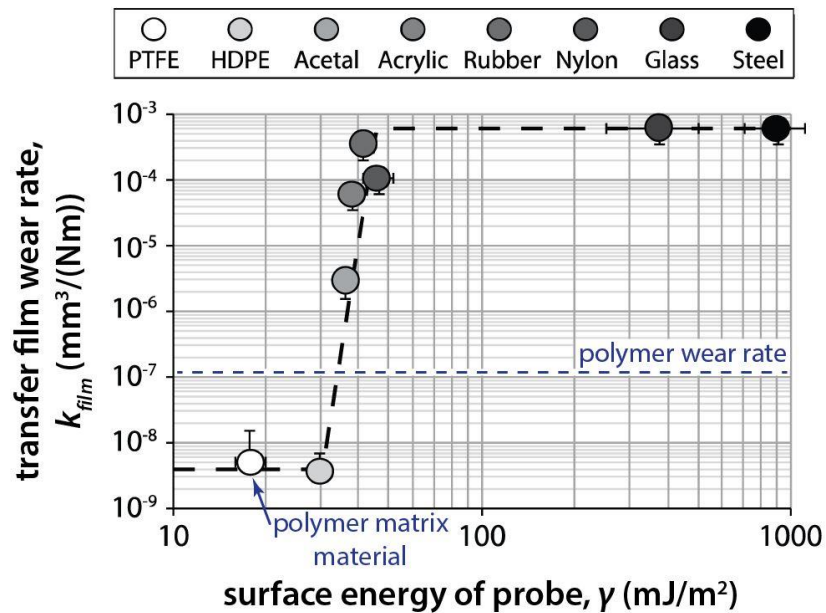


Figure 2-6 Transfer film wear rate as a function of probe surface energy. The transfer film formed by the alumina-PTFE nanocomposite displayed poor wear resistance against high surface energy probes, moderate wear rates to low surface energy probes, and excellent wear performance to very low surface energy probes that include the parent polymer composite's majority PTFE material. Image adapted and reprinted with permission from [78].

Among the most important factors of transfer film formation and preservation, which contributes to its role as a protective barrier improving bearing performance, is the adhesion of debris to the counterface. One proposed mechanism of adhesion is polymer debris mechanically interlocking into the crevices of counterface asperities [18]. This method can occur more readily for small debris for two main reasons. Firstly, smaller debris can fit within the valleys of counterface asperities, which could be nanometers to a micrometer in size depending on the counterface surface roughness [18]. Secondly, small debris lacks sufficient elastic energy to overcome plastic deformation applied during deposition and detach from the counterface from spring-

back [78]. The inability of large debris to mechanically interlock with counterface asperities is exemplified by neat PTFE because it deposits large debris, on the order of tens of micrometers wide by a few micrometers thick, which is physically pushed out of the sliding interface by the polymer parent during the next sliding encounter [16, 19, 61]. Moreover, the improvements to PTFE's bulk wear rate by the addition of fillers corresponds to a significant reduction in debris size [19, 63, 67, 79]. A study of transfer film development for an alumina filled PTFE composite showed fine debris was deposited on the counterface and grew into a quality transfer film [75]. Although mechanical interlocking of debris can support a reduction in polymer wear rate, it is not the strongest method of adhesion [23].

It has been proposed that transfer films are more tenacious for composites than unfilled materials because fillers play a role in the adhesion of polymer debris at the sliding interface. One study that observed filler degradation during sliding suggested the filler itself can provide a link between the polymer debris and metallic counterface for a more strongly bonded transfer film [24]. Alternatively, the filler could be inducing polymer degradation during sliding, which would avail the polymer debris to directly link to the counterface through chemical bonding (tribochemistry) [69]. Either mechanism inducing a tribochemical change would provide the transfer film with a strong method of bonding to the counterface. This can allow the transfer film tenacity needed for lower film wear rates, thus require less maintenance from parent polymer debris and support lower system wear rates.

Transfer films have been recognized as contributing to the wear resistance of the system by impeding direct contact of the low surface energy polymer to high surface energy counterface [24, 69]. Evidence from investigations have indicated that

these films are successful in this role when they have sufficiently high coverage over the counterface, small gaps exposing counterface, and strong adhesion to the counterface [18, 23, 24, 70–74, 77]. In comparison, unfilled polymers like PTFE would have high wear rates attributed to their transfer film consisting of large debris that are inconsistently placed over a minority of the counterface and often replaced during sliding [16, 19, 61]. Incorporating fillers into the polymer bulk generally reduces wear rate, possibly by improving the beneficial traits of the transfer film overall, as illustrated in Figure 2-7. The addition of microparticles benefits the transfer film by arresting internal crack propagation for reduced debris size, which allows improved mechanical adhesion and permits tribochemical bonding of debris to the counterface [23, 24, 69, 78]. However, these hard microparticles are known to abrade the counterface, and in effect the transfer film requires more polymer debris to replenish the film for minimal reductions to polymer wear rate [23, 62–64]. By substituting hard nano-sized fillers, it was hypothesized that only gentle interface polishing would occur, which would allow stable transfer film formation and still avail tribochemical bonding of debris to the counterface [20, 63, 72–75]. A detriment of this filler size is it should be unable to inhibit bulk crack propagation, causing the polymer composite to form large debris with weak mechanical adhesion to the counterface that will result in poor film quality and tenacity for minimally reduced polymer wear rate [65].

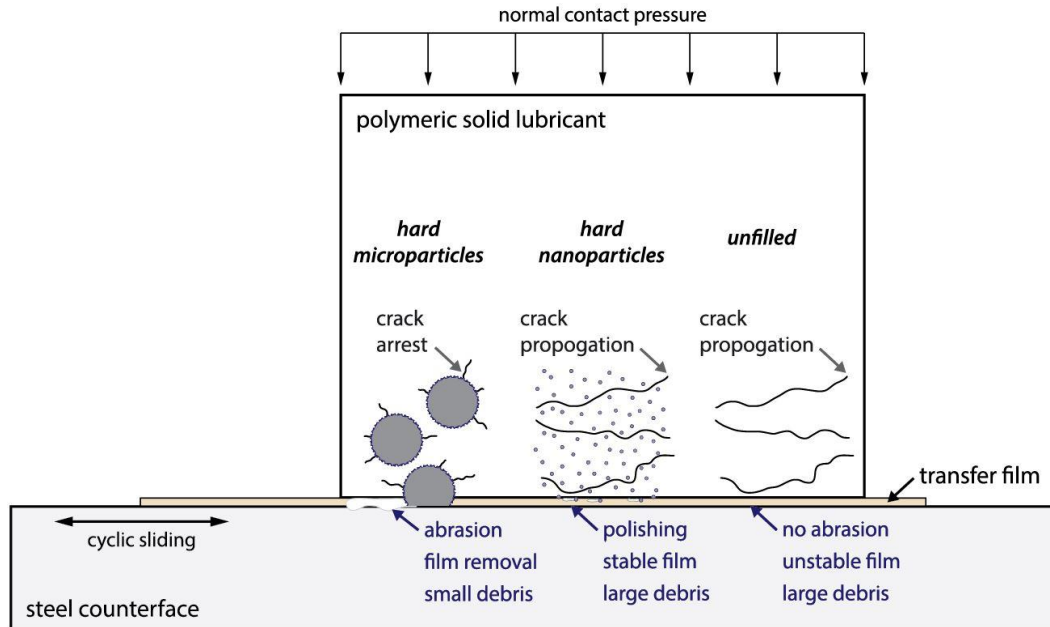


Figure 2-7 Current model for a lubricious polymer matrix filled with hard microparticles (left), filled with hard nanoparticles (middle), and unfilled (right). The addition of fillers has a net positive effect on the transfer film and polymer wear rate compared to the neat form, because the unfilled polymer deposits large debris that poorly covers and adheres to the counterface. Yet, neither filler size is optimal. Microparticles arrest crack development, which nanoparticles are too small to achieve, for improved mechanical adhesion of polymer debris to the counterface and more tenacious transfer films. However, microparticles abrade the counterface and remove transfer film requiring more replenishment by polymer debris, whereas nanoparticles gently polish the interface and promote stable film formation.

Interestingly, a particular composite of alumina nanoparticles in PTFE has appeared to be outside the model of understanding for polymer composites presented in Figure 2-7. Although nanoparticles should be too small for disrupting the crack propagation that leads to finer debris formation, the alumina-PTFE system is observed to produce small-sized debris [63]. Its fine debris particles strongly adhere to the counterface, lasting for thousands of meters in sliding contact [75]. Moreover, the

strong adhesion of polymer debris has led to the transfer film being measured as 100x more wear resistant than the alumina-PTFE polymer when measured by probes of very low surface energy, including a probe of the composite's majority material PTFE [78]. In addition, this transfer film has been observed and measured to have better coverage and uniformity than other PTFE-based composites [5, 80]. Many of these outcomes are shared by composites filled with microparticles, except interface abrasion was not significant for this alumina-PTFE system due to the gentler polishing action of nano-scale hard fillers [63]. Due to this unique combination of fine debris formation, strongly adhered transfer films, and gentle interface polishing, the alumina-PTFE system appeared to have the benefits of both microparticles and nanoparticles without the detriments of either.

In the early 2000s, there was not an explanation for the discrepancy between the filler model and filler function, which permitted the alumina-PTFE composite to have unprecedented ultralow wear rates ( $k \leq 3 \times 10^{-7} \text{ mm}^3/(\text{Nm})$ ). Yet, this did not impede the alumina-PTFE composite from being distinguished from many common polymeric solid lubricants. By generally displaying excellent bearing performance and having well-known inert components, the alumina-PTFE composite was considered the ideal bulk material for bearing applications [81, 82]. Thus, up to this point in time, there was no suggestion that this system required tribochemistry for the well adhered debris and tenacious transfer film contributing to its tribological success [22, 67, 79]. In effect, this alumina-PTFE system had the highest potential for tribological applications in the challenging conditions of an extraterrestrial operating environment, which prompted further investigations to test the applications of alumina-PTFE and elucidate the unique mechanisms of this system.

## 2.5 Study of alumina-PTFE Nanocomposites for Space Applications

Solid lubricants, materials that are inherently capable of sliding with low friction, are utilized when traditional oils or greases are impractical for use due to the physical, chemical, thermal, or environmental conditions [12–14]. In the most extreme situations, notably aerospace applications, machinery is expected to operate in challenging conditions for decades without maintenance [10]. Certain polymer composites offer a high potential to display the combination of long lifetime and high efficiency necessary for these systems to succeed. Yet, in the most demanding bearing applications, even the range of wear rate and friction for excellent performance bearing materials is too wide. For a bearing material to be in service for thousands of kilometers sliding while performing with high efficiency, common requirements for bearings operating in space, only a subdomain of excellent bearing performance is acceptable. Hence, mechanical systems with the most demanding bearing applications are defined here to require a combination of ultralow wear ( $k \leq 3 \times 10^{-7} \text{ mm}^3/(\text{Nm})$ ) and moderate friction ( $\mu \leq 0.17$ ). This subdomain is termed here as advanced bearing performance, and is represented by the bounded region in Figure 2-8.

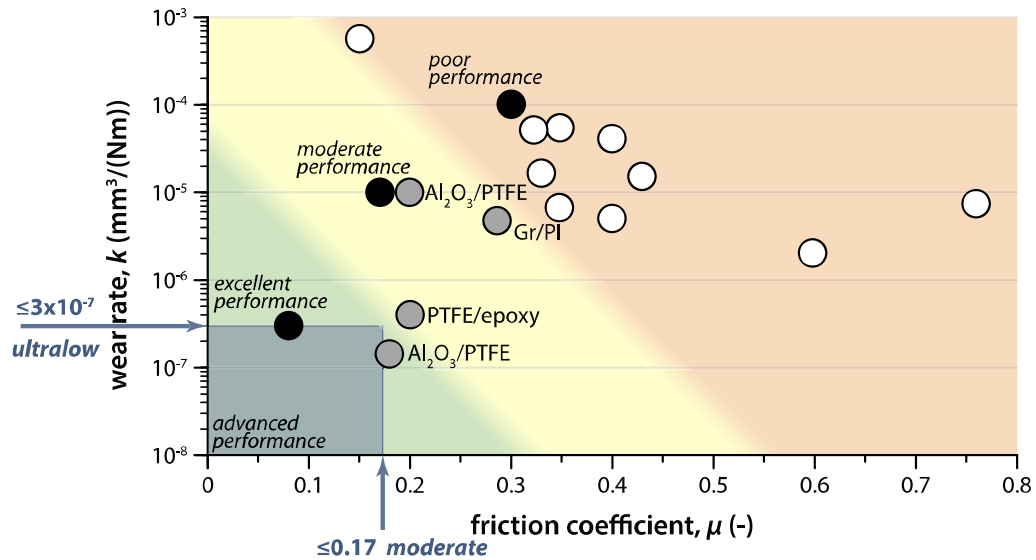


Figure 2-8 The bearing performance of several polymer composites (grey circles) as a function of friction coefficient and wear rate [49, 56, 68, 79]. The bearing performance of the respective neat polymer (white circles) can be improved from poor performing to moderate or excellent performing bearing materials by the addition of fillers that supplement the lacking tribological trait of lubricity or wear resistance [6, 22, 24, 46–50]. Domains for bearing performance were developed from a survey of traditionally lubricated compatible metals with poor, moderate, or excellent lubrication (black circles) [2]. Using these survey values, a subdomain of excellent bearing performance is observed to fulfill the demands of aerospace applications. This subdomain, which requires ultralow wear rates ( $k \leq 3 \times 10^{-7} \text{ mm}^3/(\text{Nm})$ ) and moderate friction ( $\mu \leq 0.17$ ), is termed advanced bearing performance. The alumina-PTFE system, tested in ambient conditions, was the first polymeric solid lubricant to display advanced bearing performance [22, 79].

PTFE is among the most well-known inert solid lubricants, making it an ideal material for variable environments [81, 82]. Although its pure form has unacceptably high wear rates, this issue can be overcome with the addition of fillers [18, 19, 66]. Most notably, adding only 1 wt% alumina nanoparticles to PTFE can reduce the wear rate by 3,000x in ambient conditions, which made this system the first polymeric solid

lubricant identified as an advanced performing bearing material [22, 79]. Due to this, many studies of PTFE-based materials have focused on alumina-PTFE nanocomposites as the most promising bulk tribomaterials for engineering applications in challenging environments [67, 79].

The success of this alumina-PTFE system is surprising because it contradicts the inherent disadvantages of inert polymer nanocomposites in tribological applications. First, a nano-scale filler should be too small for arresting crack propagation in the polymer bulk, understood to be necessary for small debris formation that leads to quality transfer film formation [65]. Second, the inertness of both polymer and filler should prevent chemical bonding, the strongest method for debris to adhere to the counterface and form a tenacious transfer film that is necessary for excellent tribological performance (e.g. van der Waals attraction is orders of magnitude weaker than covalent bonds) [6].

The discrepancy between expected moderate performance and observed excellent performance is reflected in the broad range of actual tribological performance and transfer film quality for various PTFE-based nanocomposites, as shown in Figure 2-5. One study found that two chemically identical alumina fillers of similar reported size, 44 nm  $\Delta$ : $\Gamma$ -phase and 80 nm  $\alpha$ -phase, resulted in  $\sim 10x$  and  $\sim 1,000x$  reduction in the wear rate of PTFE for various filler loadings, respectively [79]. The transfer films formed by composites with 2.5 vol% loading are presented in Figure 2-9, were used to show moderate wear resistance  $k \sim 10^{-5} \text{ mm}^3/(\text{Nm})$  corresponding to a thick and lumpy film versus excellent wear resistance  $k \sim 10^{-7} \text{ mm}^3/(\text{Nm})$  corresponding to a thin and uniform film.

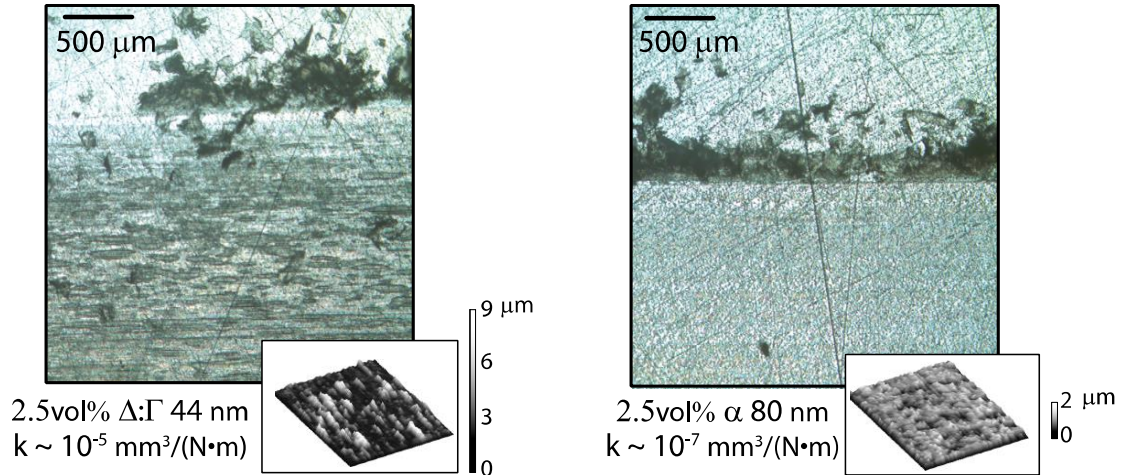


Figure 2-9 Profiles of transfer films for nanocomposites of 2.5 vol% 44 nm  $\Delta:\Gamma$ -phase alumina in PTFE (left) and 2.5 vol% 80 nm  $\alpha$ -phase alumina in PTFE. Image reprinted with permission from [83].

These seemingly identical fillers, having notably different effects on the PTFE nanocomposite wear resistance and transfer film quality, were found to be physically different by an inspection utilizing TEM (Transmission Electron Microscopy) [79]. The images in Figure 2-10 were used to determine the  $\Delta:\Gamma$ -phase alumina had an overall spherical shape of a few hundred nanometers in size and  $\alpha$ -phase alumina had an irregularly shaped with sub-micron or larger size. Thus, the discrepancy between reported and observed geometry for the  $\alpha$ -phase alumina filler was suspected to have benefitted the tribological performance of these PTFE-based composites.

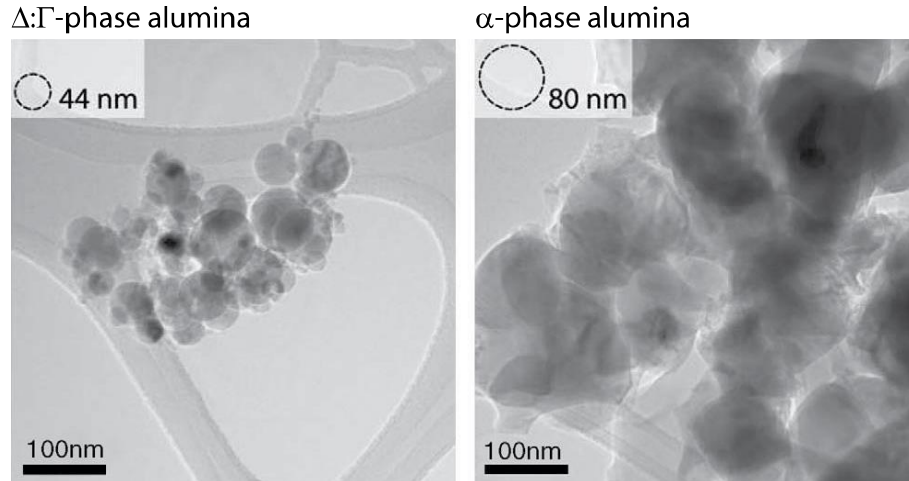


Figure 2-10 TEM (Transmission Electron Microscopy) images of alumina filler materials reported as 44 nm  $\Delta:\Gamma$ -phase (left) and 80 nm  $\alpha$ -phase (right). Image reprinted with permission from [79].

A subsequent investigation evaluated the wear performance of PTFE with various  $\alpha$ -phase alumina fillers [84]. The results shown in Figure 2-11 were used to indicate that the most wear resistant PTFE composite had an alumina filler with the lowest vendor reported particle size of ~40 nm and largest measured particle size of ~4,000 nm using SLS (Static Light Scattering). SEM (Scanning Electron Microscopy) images of this particular alumina material (Nanostructured and Amorphous Materials 1015WW) are displayed in Figure 2-12 and were used to indicate this vendor reported “nanoparticle” has a micro-scale characteristic length. This observation permits support for the particular alumina filler to be sufficiently large enough to arrest crack propagation in the bulk composite. Thus, the micro-scale particle size can account for the composite’s fine debris formation that leads to improved transfer film quality and wear resistance compared to neat PTFE.

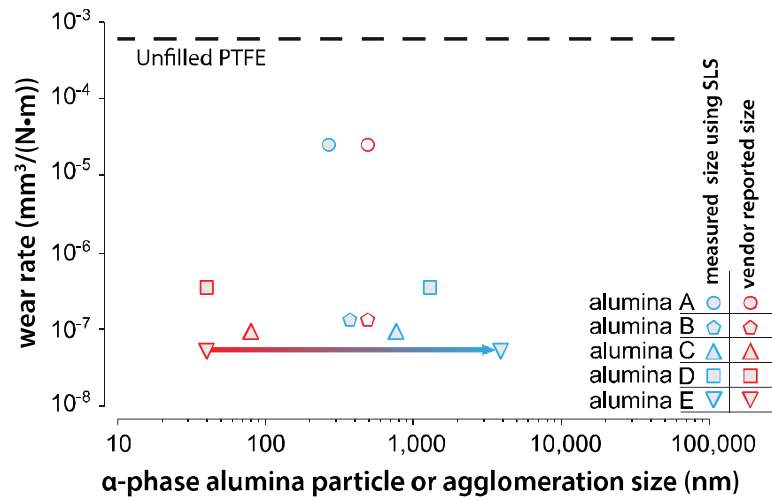


Figure 2-11 Wear rate of alumina-PTFE composites as a function of the filler's particle or agglomeration size. Image adapted and reprinted with permission from [84].

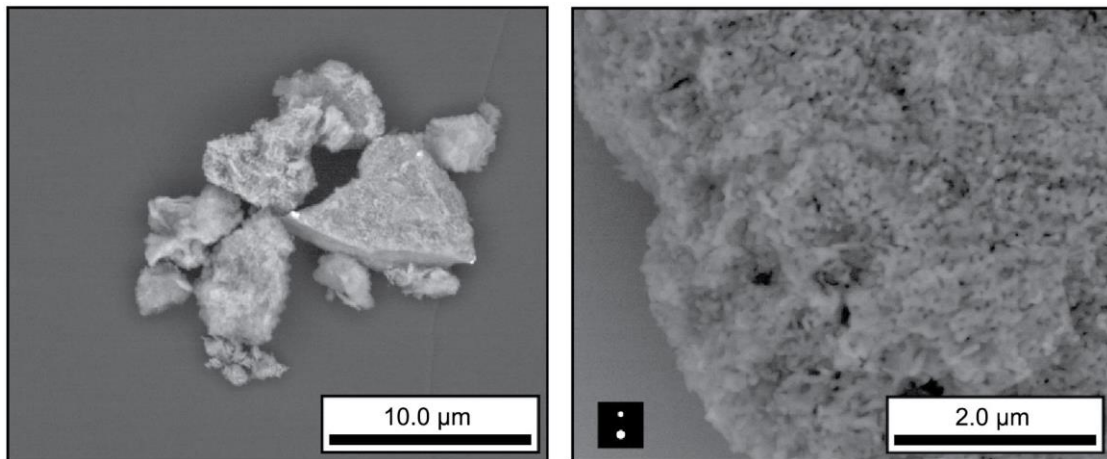


Figure 2-12 SEM (Scanning Electron Microscopy) image of alumina sample E from Nanostructured and Amorphous Materials 1015WW shows this filler material to have a micro-scale characteristic size. Image reprinted with permission from [84].

However, findings from this study did not explain the significant improvement to transfer film quality and wear rate for the particular micro-scale alumina “nanoparticle” over regular alumina microparticles. Thus, the PTFE-based composite using this particular alumina filler was the subject of further inspection. A three-dimensional X-ray microtomography of the alumina-PTFE composite post tribological testing is shown in Figure 2-13 [84]. The resulting image revealed this particular alumina filler was distributed throughout the polymer bulk and accumulated at the polymer sliding surface (running film). TEM images in Figure 2-14 were used to determine the alumina accumulation on the running film was in the form of nano-scale particles, not the micro-sized bodies that were incorporated into the PTFE matrix from Figure 2-12. This result was a major finding, as it clarified this particular filler’s ability to support crack arrest in the polymer bulk without abrading the transfer film or counterface like traditional hard microparticles [64]. In effect, this unique alumina filler provides the beneficial functionality of a microparticle within the polymer bulk and a nanoparticle at the sliding interface, which was used to explain the alumina-PTFE’s improved quality transfer film and polymer wear rate compared to composites using true hard microparticles or nanoparticles [63].

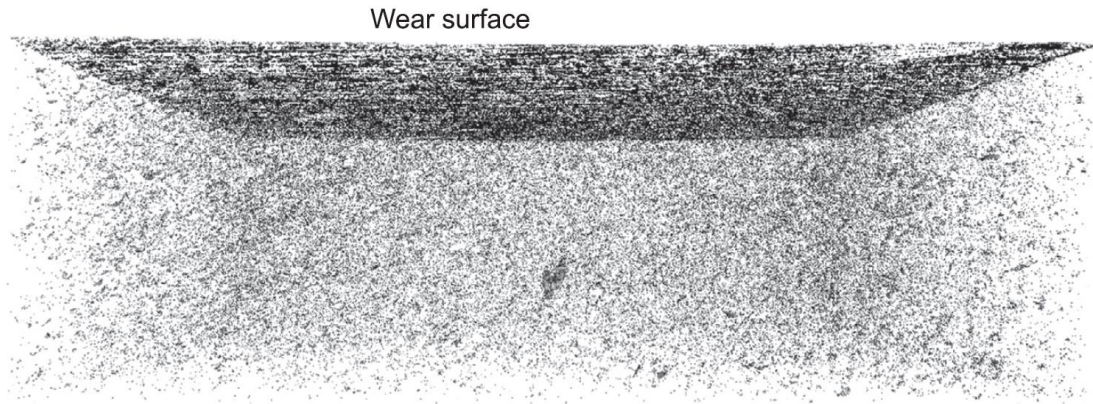


Figure 2-13 Three-dimensional X-ray microtomography of an alumina-PTFE composite using filler material alumina sample E from Nanostructured and Amorphous Materials 1015WW. This image was taken of the composite's side view after wear testing. The top of the image at the wear surface shows an accumulation of alumina in the polymer sliding surface (running film). Image reprinted with permission from [84].

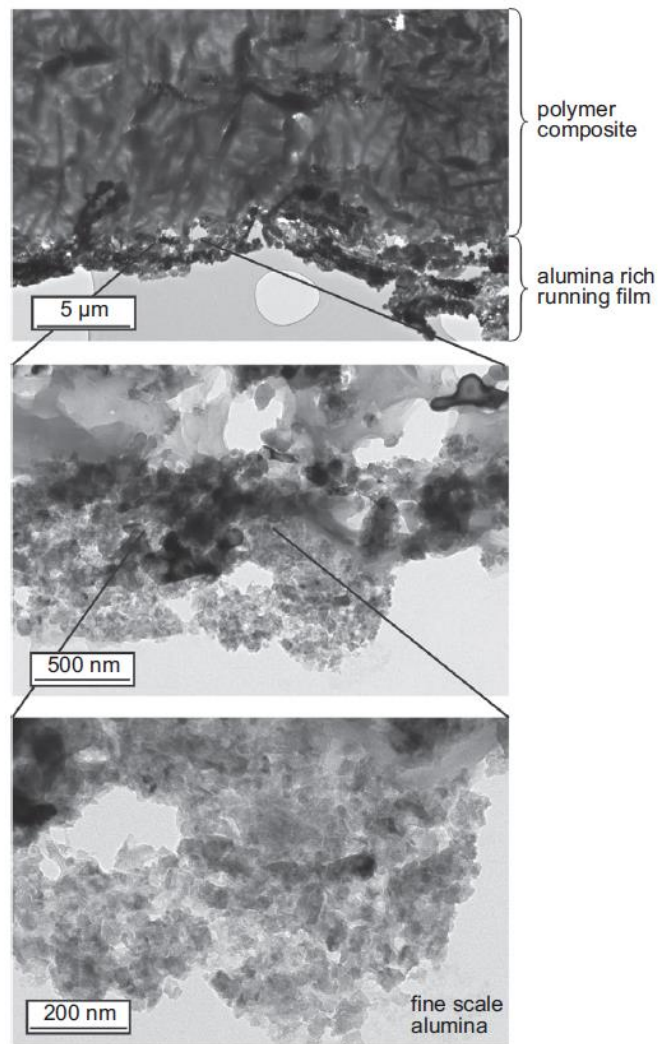


Figure 2-14 TEM (Transmission Electron Microscopy) image of an alumina-PTFE composite using filler material alumina sample E from Nanostructured and Amorphous Materials 1015WW. This side view of the polymer composite's sliding surface (running film) after wear testing shows the accumulated alumina filler to have nano-scale characteristic size. Image reprinted with permission from [84].

The particular alumina-PTFE composite, known for its high wear resistance and quality transfer films, was the most promising inert bulk material for tribological applications in variable environments when it was sent for testing on the International

Space Station. Prior to this, NASA's Materials International Space Station Experiments (MISSE) program had only conducted passive experiments. Through a collaboration between the University of Florida, Air Force Research Lab, and NASA, engineers developed the capabilities for this tribology experiment to become the first active test in the MISSE program [85]. The results of this unprecedented experiment, shown in Figure 2-15, revealed that during ground-testing prior to launch the alumina-PTFE formed a uniform transfer film. However, after 325,000,000 miles of testing in space the alumina-PTFE formed a patchy transfer film. This MISSE 7 tribology experiment refuted the hypothesis that the alumina-PTFE composite consisting of inert materials is insensitive to the operating environment.

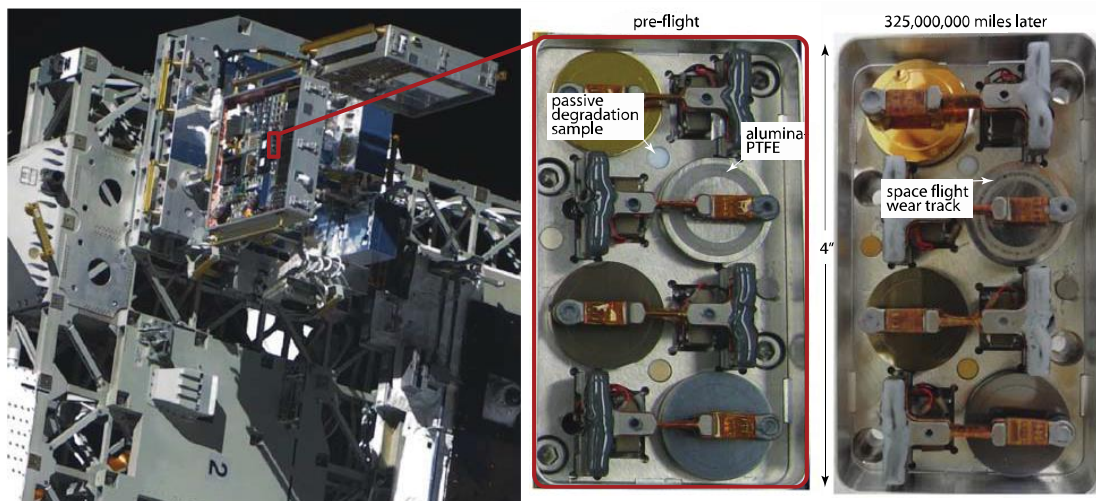


Figure 2-15 NASA's Materials International Space Station Experiments 7 (MISSE 7) (left), in November 2009 the tribology unit ground-test before launch resulted in alumina-PTFE forming a uniform transfer film (center), and in May 2011 the tribology unit post 325,000,000 miles of testing in space resulted in alumina-PTFE forming a patchy transfer film (right). The tribology unit tested gold, alumina-PTFE bulk, chameleon coating, and commercial MoS<sub>2</sub>/Gold/Sb<sub>2</sub>O<sub>3</sub> (top to bottom). Images courtesy of NASA.

## 2.6 Tribochemistry in the alumina-PTFE System

Before being tested on NASA's MISSE 7 program in space, the alumina-PTFE composite was well known for its inert components, high wear resistance, and quality transfer films in standard laboratory conditions. When the results of tribological testing showed that alumina-PTFE had high wear rates and poor quality transfer films in lower Earth orbit, it revealed that the bearing performance this material was dependent on the operating environment. After discovering the environmental sensitivity of this particular alumina-PTFE composite, studies have focused on elucidating the role of chemistry in the tribological success of this system.

One prominent study investigated the wear rate of alumina-PTFE in ambient environment as a function of vacuum pressure [86]. Results in Figure 2-16 were used to show that below a critical vacuum pressure alumina-PTFE experiences an increase in wear rate by two orders of magnitude. Observations of the transfer film quality, assessed by visual inspection and measurement of height from the profile in Figure 2-17, directly correlates worsened wear performance in strong vacuum to lowered film quality. In ambient conditions without vacuum (760 Torr) the alumina-PTFE had ultralow wear rates and formed a good quality transfer film that was red-brown discolored, thin, and uniform. In contrast, within the strongest vacuum pressure tested by this study ( $4 \times 10^{-6}$  Torr) the alumina-PTFE had 100x worse wear rates and formed a poor quality transfer film that was light grey colored and patchy. Although this study corroborated the results of MISSE 7, the alumina-PTFE requires constituents from ambient environment to form a quality transfer film and display ultralow wear rates, it did not isolate the active chemistry necessary for this system's tribological success.

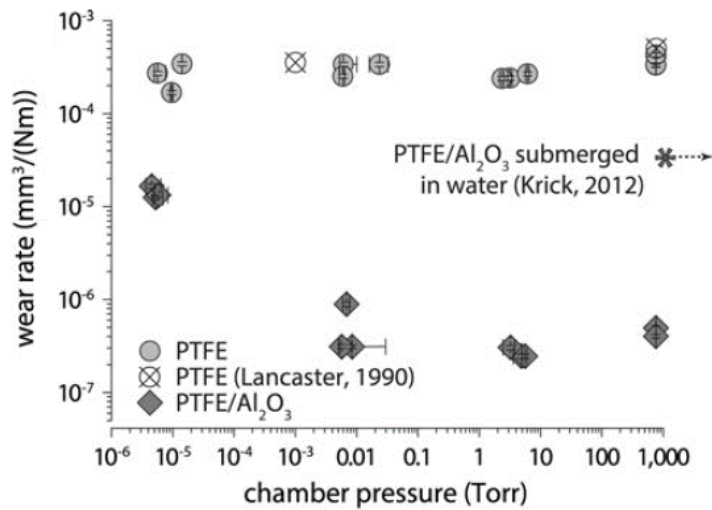


Figure 2-16 Wear rate of alumina-PTFE nanocomposite in ambient air environment as a function of vacuum pressure. Below a critical pressure the alumina-PTFE showed environmental sensitivity by having 100x less wear resistance than ambient air conditions. Image reprinted with permission from [86].

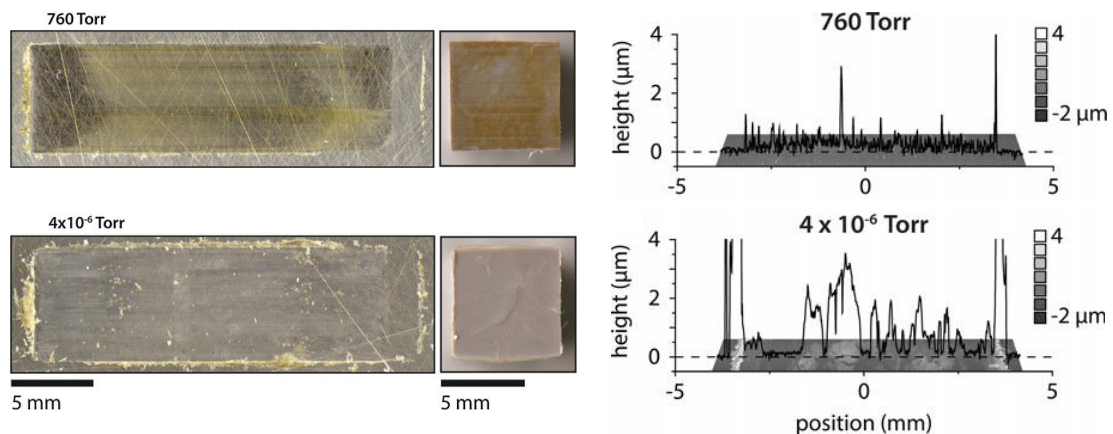


Figure 2-17 Transfer films of alumina-PTFE composite formed in ambient air environment without vacuum 760 Torr (top row) and with high vacuum  $4 \times 10^{-6}$  Torr (bottom row). In ambient conditions the alumina-PTFE composite had ultralow wear, correlated to forming a good quality transfer film that is brown discolored, thin, and uniform. Testing in high vacuum caused alumina-PTFE to have higher wear rates, relating to its lower quality transfer film. Image adapted and reprinted with permission from [86].

Another important study investigated the wear rate of alumina-PTFE as a function of humidity in environment [87]. Results presented in Figure 2-18 were used to clearly show that as environmental humidity increased the alumina-PTFE wear rate decreased. Over the same range in humidity, observations of transfer film quality by visual assessment and profile measurement in Figure 2-19 were used to show that better quality films directly correlated with improved wear performance, which was consistent with findings from literature [18, 70–73]. Similar to results in ambient conditions (760 Torr) presented previously, alumina-PTFE in the nitrogen rich environment with high humidity (69% RH) had ultralow wear rates and developed a good quality transfer film that was red-brown discolored, thin, and uniform. Moreover, the results of alumina-PTFE in ambient high vacuum conditions ( $4 \times 10^{-6}$  Torr) from the previous study were comparable to those from the nitrogen rich environment with low humidity (0.6% RH), as the alumina-PTFE had 100x worsened wear rates and a lower quality transfer film that was light grey and patchy. The nearly identical results of alumina-PTFE wear rate and transfer film quality in atmospheric vacuum and dry nitrogen rich environment indicated that water vapor is the necessary component for this system's beneficial tribochemistry.

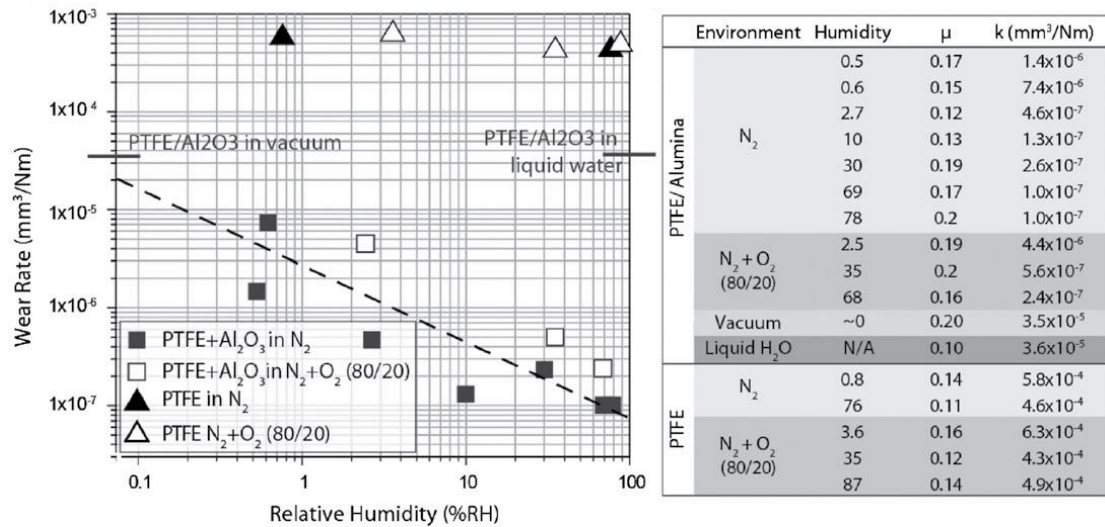


Figure 2-18 Wear rate of alumina-PTFE composite as a function of relative humidity in the environment. The alumina-PTFE system displayed environmental sensitivity by necessitating humidity for wear resistance in having 100x worse wear rates at the lowest humidity tested (0.6% RH) than in high humidity (69% RH). Image reprinted with permission from [87].

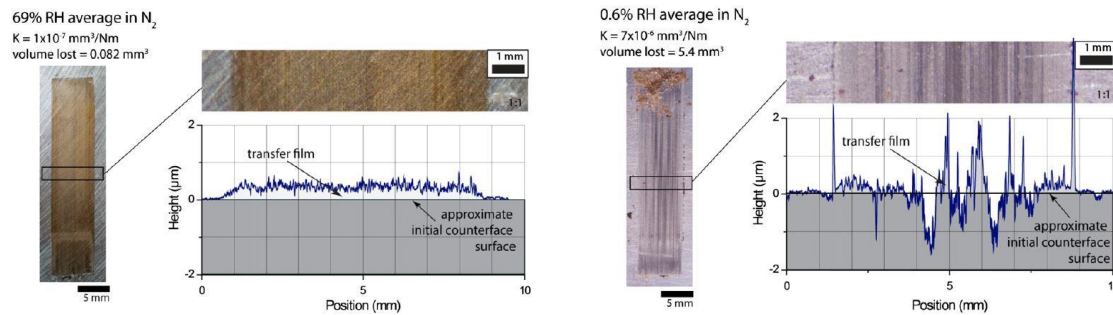


Figure 2-19 Transfer films of alumina-PTFE composite formed in a nitrogen rich environment with high humidity of 69% RH (left) and low humidity of 0.6% RH (right). In the presence of high humidity the alumina-PTFE composite had ultralow wear, correlated to forming a good quality transfer film that was brown discolored, thin, and uniform. The absence of moisture caused alumina-PTFE to have higher wear rates, relating to its lower quality transfer film that is light grey and patchy. Image reprinted with permission from [87].

Although it has been known that degradation of the polymer or filler can initiate chemical bonding of polymer debris to the counterface for a tenacious transfer film, this method for high wear resistance was not considered for the alumina-PTFE system's inert materials until it was observed that environmental moisture was necessary for excellent tribological performance [24, 69, 86, 87]. Following this realization, one study proposed that the bonds of a PTFE chain could be broken during sliding, react with water vapor in environment, and result in the PTFE having carbonyl end groups that strongly bond to the metallic counterface [88]. A subsequent study used theoretical calculations to confirm that when a section of PTFE chain is exposed to the interface and has sufficient contact with the counterface, van der Waals interactions will cause high enough shear stress to induce chain scission of this polymer's carbon backbone during sliding and expose a radical carbon for chemical reaction [89]. This study also proposed a set of chemical reactions in an environment with water vapor available that lead a broken PTFE chain to form carboxylic acid end groups, then chelate as carboxylate salts to the metallic alumina filler and steel counterface within the sliding interface.

Support for carboxylates contributing to the alumina-PTFE system's debris adhesion and transfer film formation comes from studies utilizing Fourier-transform infrared (FTIR) spectroscopy. One study collected FTIR chemical spectra of the transfer film at multiple points throughout a tribology test, in which a polymer pin slid against a flat steel counterface [90]. At the initiation of the tribology test, when the transfer film had not stabilized yet because polymer debris is large and temporary, only the chemical spectrum for PTFE was present [75, 90]. However, after a sufficient distance of sliding has been met to fully form a good quality transfer film,

made up of fine and persistent debris, new chemistry appeared in the spectrum. Two of these new peaks at 1650 and 1430  $\text{cm}^{-1}$  were identified as a significant amount of carboxylate along with the previous PTFE material having peaks at 1200 and 1150  $\text{cm}^{-1}$ , as shown in Figure 2-20. Another study using FTIR spectra probed the importance of humidity available at the sliding interface during tribology testing [91]. A wear test of the alumina-PTFE system was conducted in ambient conditions while heating the sliding interface to drive off water vapor and also in a dry  $\text{N}_2$  environment to exempt water vapor [91]. Both low and absent moisture experiments resulted in higher wear rates than ambient conditions. The low and absent moisture conditions also had a notably attenuated carboxylate signal at the polymer running film and counterface transfer film, shown in Figure 2-21. These two FTIR studies confirmed the necessity of the alumina-PTFE system to have water vapor available for tribochemistry in order to form a good quality and strongly adherent transfer film that supports ultralow wear rates.

Another outcome of these FTIR studies was the observation of ultralow wear rate performance corresponding to a significant signal strength of carboxylates compared to PTFE at the sliding interface, by using a probe depth of tens of nanometers to  $\sim 1$  micron [90, 91]. Such a high level of carboxylate signal implies both sliding surfaces were well-covered by broken PTFE chains with carboxylate end groups. On the counterface, this signal is accounted for by the accumulation of polymer debris undergoing tribochemical change and forming a transfer film. On the polymer pin surface, PTFE chains are entwined with only sections of many chains exposed to the sliding interface and those PTFE chains known to align in the direction of sliding due to the linear reciprocated sliding motion of the tribology test [16, 92].

This orientation could improve contact between sections of PTFE chains and counterface enough to induce the breaking of PTFE chains all over the polymer pin surface. Hence, potentially accounting for the observed proliferation of PTFE chains breaking and undergoing tribochemical change on the running surface of the polymer that correspond to the strong signal of carboxylates gathered by FTIR techniques. This scenario also could account for the observations from literature that show the running film has the same discoloration as the transfer film, when humidity is available in the environment and the alumina-PTFE system performs with ultralow wear rates [68, 86, 91].

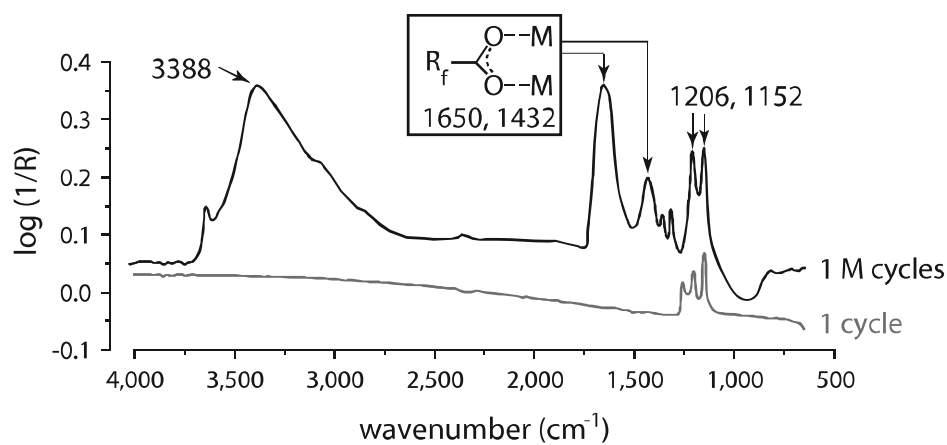


Figure 2-20 FTIR spectrum of the transfer film formed on a steel counterface were taken from an *in-situ* tribology test of alumina-PTFE composite in ambient conditions. After 1 cycle of sliding debris has not yet built a transfer film and only PTFE signal at 1200 and 1150  $\text{cm}^{-1}$  is present (grey). After 1 million cycles a transfer film has fully formed and carboxylates at 1650 and 1430  $\text{cm}^{-1}$  are present along with the PTFE (black). Spectra were collected using a Nicolet 6700 FTIR spectrometer with Continuum Microscope from ThermoFisher Scientific having a penetration depth of  $\sim 1$  micron. Image adapted and reprinted with permission from [90].

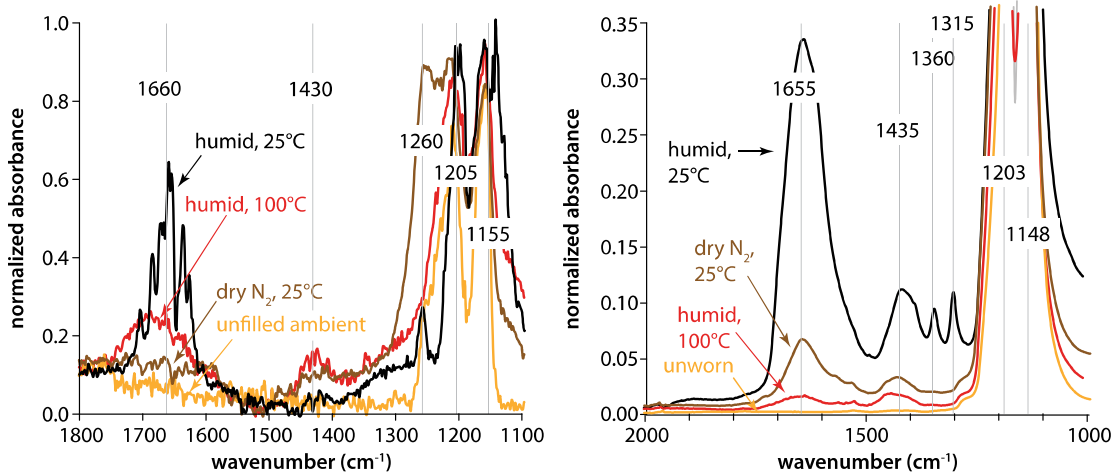


Figure 2-21 FTIR spectra of the alumina-PTFE composite transfer film (left) and running film (right) after wear testing. Transfer film spectra show the carboxylate peaks at 1655 and 1430  $\text{cm}^{-1}$  to be strong for humid (25 °C, 1 pph water), attenuated for humid heated (100 °C, 1 pph water), and absent for dry nitrogen (25 °C, 15 ppm water) environments (left). Running film spectra show these peaks as strong for humid, attenuated for dry nitrogen, and absent for humid heated conditions (right). Spectra of the transfer film (left) were collected using a NanoIR2 AFM-IR from Anasys Instruments having a penetration depth on the order of tens of nanometers. Spectra of the running film (right) were collected using a Nicolet Nexus 670 FTIR with a smart orbit attenuated total reflectance (ATR) accessory having a penetration depth of  $\sim 1$  micron. Image reprinted with permission from [91].

## 2.7 Designing a Polymer System for Space Applications: Motivation for Study

Despite decades of research aimed at developing polymer composites for long lifetime and high efficiency in a range of extreme environments, there remains a need in the aerospace industry for a solid lubricant with advanced performance in bearing applications. Previously, a particular alumina-PTFE composite, with inert components that displayed the necessary ultralow wear ( $k \leq 3 \times 10^{-7} \text{ mm}^3/(\text{Nm})$ ) and moderate friction ( $\mu \leq 0.17$ ), offered promise to change the status quo. This tribomaterial's advanced bearing performance has been attributed to its ability to form a good quality and strongly adherent transfer film that supports ultralow wear rates and low shear sliding. After an unprecedented effort to run an active tribology test on the ISS, results showed this system performed poorly in space. The unexpected environmental sensitivity of this alumina-PTFE system prompted new investigations, which revealed this system's success is dependent on having sufficient moisture available for beneficial tribochemistry. Although the alumina-PTFE composite is not itself a solution to the persisting problem, there are applications for the large body of knowledge gathered from probing its interrelated physical and chemical wear reduction mechanisms.

This project was proposed to fulfill the needs of aerospace bearing applications by using the alumina-PTFE model as a reference for improving tribomaterials design. The current filler theory for a hard (e.g. metal or ceramic) filler in lubricious polymer matrix is depicted in Figure 2-22. The alumina-PTFE model requires the filler to have multi-scale functionality and the initiation of beneficial tribochemistry in an environment with water vapor and oxygen available. This study proposes to replace multi-scale functional alumina with a relatively soft filler material that also supports tribochemistry regardless of environmental conditions. Specifically, a micro-sized

filler material, much softer than steel but harder than PTFE, could replace multi-scale functional alumina by being sufficiently large to arrest crack propagation in the PTFE matrix and non-abrasive to the sliding interface. In addition, the filler can be selected to contain the elements oxygen and hydrogen to supplement necessary components for broken PTFE chains to undergo the tribochemical change of forming carboxyl end groups in environments starved of moisture or oxygen. Several materials could satisfy these filler requirements, including micro-sized PEEK. A tribology study on PEEK-PTFE composites was conducted to test the proposed model for a relatively soft filler in lubricious matrix capable of displaying advanced bearing performance in conditions that simulate both pre-launch activities on the ground and long-term functionality in space applications.

To conduct this project, prior work was needed to increase sample testing capacity and improve results assessment. First, it was necessary to develop a high-throughput tribometer to be capable of testing multiple tribomaterials simultaneously for ultralow wear rates [93]; thus, reducing the duration of testing to months rather than years with a traditional tribometer that tests only one sample at a time [22, 75]. Second, identifying a quantitative metric to correlate wear performance with transfer film quality was required to assess the success or failure of polymer materials in bearing applications. Recent studies have proposed methods to quantitatively characterize the metrics of film thickness, film coverage, and uniformity in correlation to wear rate for singular polymer systems, but no general correlations across different polymer systems [22, 71, 76, 77]. Therefore, an investigation into the relationship between wear resistance and quantitative transfer film metrics was conducted on a wide range of polymer materials to identify a broadly applicable relationship between

transfer film metrics and polymer bearing performance [80]. Finally, the developed experimental equipment and identified assessment metrics were utilized in a study aimed to test the proposed model for designing polymer composites with advanced bearing performance in challenging environmental conditions.

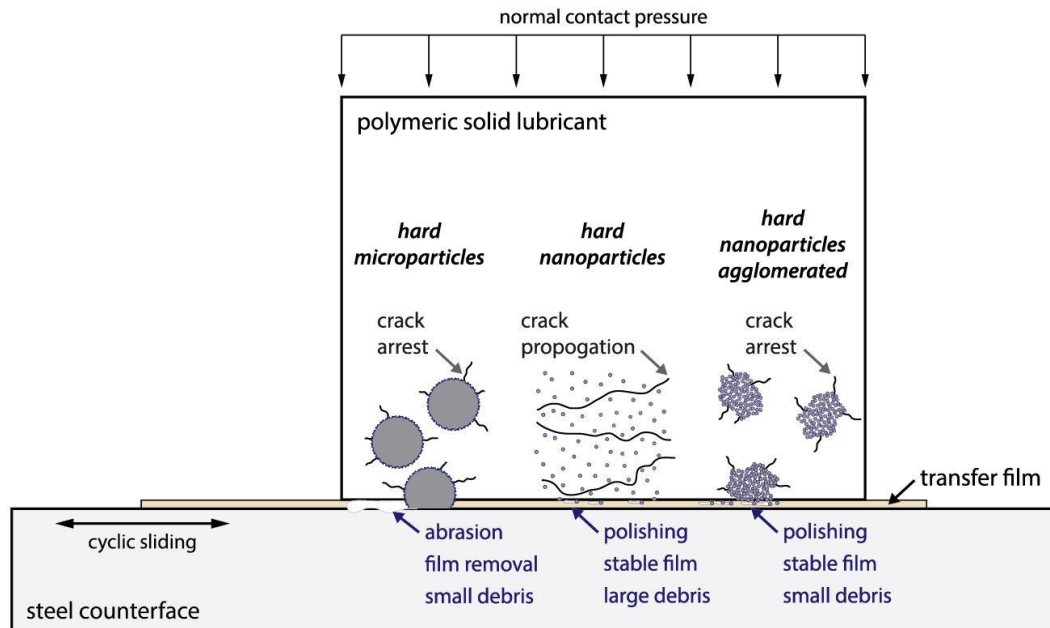


Figure 2-22 Current model for a hard metallic filler in lubricious polymer matrix has three requisites for excellent bearing performance 1) micro-scale functionality of filler material in the bulk to arrest crack propagation for fine debris formation and in effect quality transfer film development, 2) nano-scale functionality of filler material at the sliding interface that gently polishes instead of abrades and provides stability of the protective transfer film, 3) polymer debris mechanically degraded by sliding chemically bonds to the counterface to provide the strongest method of transfer film adhesion and minimal replenishment for low polymer wear rates. Fully-dense hard microparticles fail requirement #2 (left), true hard nanoparticles fail requirement #1 (middle), and micro-sized agglomerates of hard nanoparticles fulfill requirement #1&2 (right).

## Chapter 3

### INSTRUMENTATION OF A WEAR TESTING TRIBOMETER WITH HIGH-THROUGHPUT CAPABILITIES

#### 3.1 Overview

Bearings are essential machine components in engineering applications that range from light-duty laptop hinges to heavy-duty engine crankpins. Mechanical systems with demanding tribological applications are found in all environments including land, ocean, air, and space [94, 95]. Machinery in these conditions, such as automobile engines, wind turbines, steam turbines, electric generators, momentum wheels, and gearboxes, often experience heavy-duty loading by carrying pressures of  $10^5$  Pa to upwards of  $10^7$  Pa [10, 94, 95]. The capability of a bearing material to endure these conditions is tested using a tribometer, which brings materials into contact by applying a normal force and then induces relative sliding motion [6]. The surface interactions of those bodies typically cause measurable wear and friction that can be used to determine bearing lifetime and efficiency, respectively [2, 6].

Traditionally, tribometers have been designed to test the bearing performance of one sample at a time [80, 93]. For most studies, including those on polymer systems, these tribometers are satisfactory for investigating the bearing performance of a few sample materials [68, 77, 84, 96]. However, studies investigating broad trends across multiple polymer systems, or a single polymer system as a function of several variables, would be logistically limited in the number of samples capable of being tested in a timely manner. To exemplify this limitation, it would take 2 years to complete an investigation of 12 polymer samples displaying ultralow wear performance ( $k = 2 \times 10^{-7} \leq 3 \times 10^{-7} \text{ mm}^3/(\text{Nm})$ ) that were tested individually until each incurred  $10 \text{ mm}^3$  of volume loss, a common condition for test termination that is

employed to directly compare results of disparate samples [80, 93]. Due to this physical limit, investigations of polymer tribomaterials by several research groups have necessitated years of work to complete one study [48, 84, 91, 97]. Such a restriction has been a significant hindrance to the breadth and depth of studies capable of being run.

To overcome the barrier to conducting broad tribology studies, a high-throughput tribometer was developed to be capable of wear testing multiple polymer tribomaterials materials simultaneously. This new equipment was developed by designing, fabricating, prototyping, and implementing a new tribometer that can test six individual samples simultaneously. Having the ability to test polymer materials for ultralow wear rates in a timely manner, over the duration of months rather than multiple years, avails investigations aimed at improving fundamental knowledge of tribology and discovering new materials for demanding bearing applications.

### 3.2 Methods and Materials

Testing the bearing performance of polymer materials is often accomplished by using a tribometer that is functionally similar to that depicted in Figure 3-1 and reported in literature [22, 75, 86]. Polymer pins with a testing surface of 6.4 mm x 6.4 mm are compressed against a larger flat steel surface 38 mm x 25 mm to represent the usual polymer to metal pairing of bearings including guides, bushings, seals, and valve seats. Through the constant application of 250 N of normal force, tribology testing of the polymer sample against a steel counterface is conducted at pressure of 6.3 MPa to simulate heavy-duty bearing applications [94, 95].

Tribometers offer tribology testing of materials with a variety of geometries, with pin-on-flat, pin-on-disk, and block-on-ring among the most commonly used [7]. The pin-on-flat geometry is employed here because it provides consistent contact between the sample pin and flat counterface throughout testing. In contrast, a pin-on-disk test will always have some variability in contact due to imperfect alignment of the sample pin's sliding surface to the rotating disk. Furthermore, a block-on-ring test has the sample block undergo a change in contact area and thus contact pressure during sliding due to volume loss of the sample block.

The relative sliding motion of the pin-on-flat tribometer is commonly induced by linear reciprocation of the flat counterface while the polymer pin is held stationary [22, 75, 86]. A wear track length of 25.4 mm (50.8 mm/cycle) is often selected because it is long enough to produce a constant velocity zone in the central region of sliding [77]. Although tribometers can be built to run a wide variety of speeds, polymer materials are often tested at 50.8 mm/s. This selected speed is low enough to minimize frictional heat generation and allow sufficient time for cooling of heat that is generated, avoiding significant increases in temperature at the sliding interface that

change tribological performance [13, 98–100]. Since heat generation during sliding is a function of speed, testing with low sliding speeds ( $<100$  mm/s) causes the sliding interface temperature to rise only a few degrees Celsius above the environment temperature ( $\sim 25$  °C) [101, 102]. By setting up tribology tests to have a minimal temperature increase during sliding, the results of many different bearing materials can be directly compared.

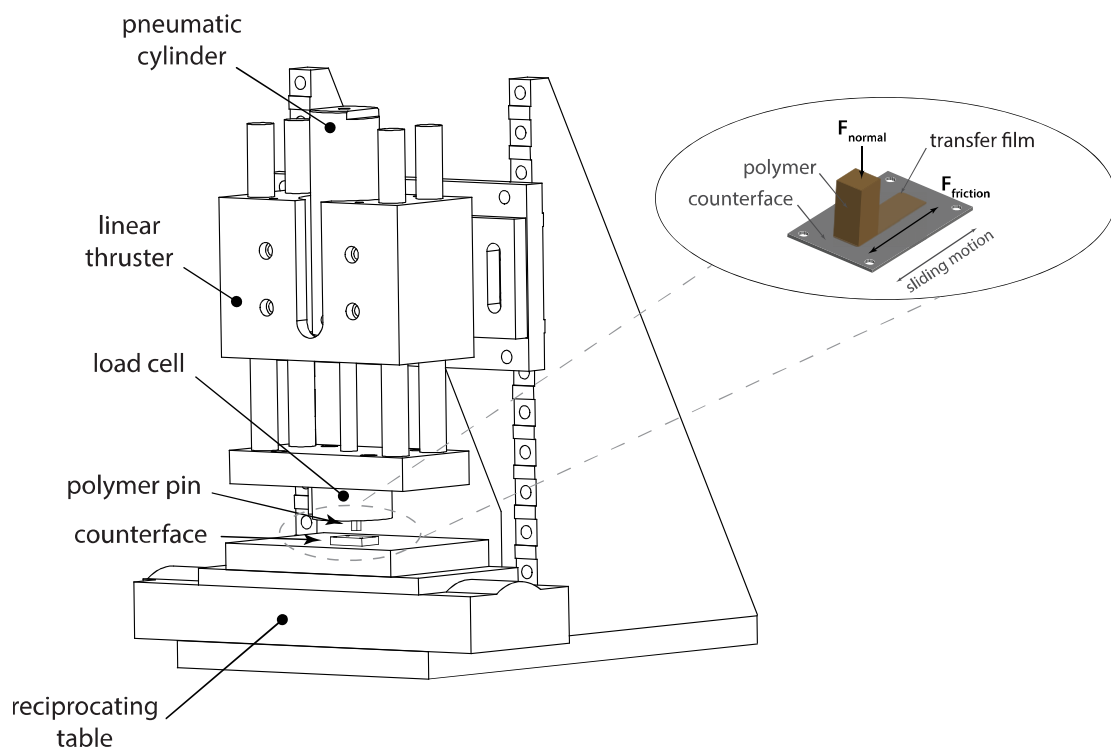


Figure 3-1 Illustration of the pin-on-flat tribometer used for testing the friction and wear of heavy-duty bearing materials. Polymer sample pins (6.4 mm x 6.4 mm) are mated to flat 304 stainless steel (38 mm x 25 mm) and undergo linear reciprocating motion. Tests were conducted with a normal force of 250 N (6.3 MPa), sliding speed of 50.8 mm/s, and wear track length of 50.8 mm per cycle. Image adapted and reprinted with permission from [75].

### **3.3 Development of New Equipment**

To overcome the limitations to the scope of studies from single-sample tribometers, a wear testing tribometer with high-throughput capabilities was designed by D.R. Haidar, R. Ganesh, M. Wessel, and M. Dick under the advisement of Prof. D.L. Burris in 2015. The following design considerations for this new tribometer, as well as the bill of materials and engineering drawings in Appendix A, were a product of this collaborative team.

At the beginning of the design process, the metrics listed in Table 3-1 were defined. Included in these considerations was the necessity to have minimal footprint, so that the tribometer would fit on an average laboratory countertop and in an OMNI-LAB environmental chamber from Vacuum Atmospheres Co. It was also desired to build this equipment as a pin-on-flat tribometer with the standard experimental settings, 6.3 MPa contact pressure (250 N normal force) for each stationary polymer pin against a flat counterface moving at 50.8 mm/s on the linear table, as the mid-range of the machine's capabilities. In order to meet these design metrics, it was necessary to replace the large 150 mm wide linear thruster traditionally used to hold one polymer pin stationary against a moving flat counterface during testing. The compact alternative chosen was a double-leaf flexure, which measured less than 50 mm wide and permitted a total of six samples to be tested in the width of 150 mm. The final metrics to meet were easy functionality for the user and low cost for a typical academic laboratory to afford building this machine.

Table 3-1 Design metrics with target values for a wear testing tribometer with high-throughput capabilities.

Metrics	Target Value	
	Minimal Footprint	$\leq 600 \times 500$
Rectangular Polymer Sample Geometry	Boolean	—
Control Contact Pressure (Normal Force)	1-20	MPa
Measure Contact Pressure (Normal Force)	Boolean	—
Control Sliding Speed	1-100	mm/s
Measure Sliding Speed	Boolean	—
Sample Holder Resists Deflection from Friction Force	$\leq 50$	$\mu\text{m}$
Sample Holder Applies Insignificant Force to Sample	$\leq 1\%$	N/N
Frame Resists Deflection from Normal Force	$\leq 200$	$\mu\text{m}$
User Functionality		
# Tools to Insert/Remove Sample	$\leq 3$	—
Ease of Insert/Remove Sample	$\leq 30$	sec
Cost for Bill of Materials	$\leq \$3,000$	USD

The overall design of this tribometer was divided into the main categories of frame, flexure, reciprocation, table, carriage, and pneumatic components. The three areas that were most significant to reliable tribological testing were the frame, flexure, and reciprocation. These sets of components were critical to the tribometer holding each polymer pin in contact with its flat counterface during relative sliding to incur friction and wear at each sliding interface.

The structure of the entire pin-on-flat tribometer was dependent on a frame that could hold six sample pins in flush contact with their paired flat counterface using 250 N of force normal (6.3 MPa pressure) each for a total of 1500 N. This frame, shown in Figure 3-2, consisted of a horizontal Piston Plate as the top, two vertical Moment Supports on the sides, and a horizontal Base Plate at the bottom. Upon the application of this 1500 N total force normal to the plane of interfacial contact, there was an equal and opposite reaction in the c-shaped frame. These four 25.4 mm thick 6061-T6

aluminum frame components were analyzed to confirm that after loading each deflected  $\sim 100\ \mu\text{m}$ , satisfying the specification for  $200\ \mu\text{m}$  or less deflection.

The ability of the sample and counterface to maintain flush surface contact during tribology testing was brought about by using double-leaf flexures in the sample holders. These flexure components were designed to resist deflection from friction force in the direction of sliding and permit deflection from polymer pin volume loss in the direction normal to the sliding interface. This was achieved by using two sheets of 1075 spring steel for the double-leaf flexures, which had significant material width in the direction of friction force and thin material thickness in the direction of normal force. As the pneumatic cylinder pressed each polymer pin in contact with its counterface during testing, wear and friction occurred at the sliding interface. The vast majority of this volumetric wear became incurred by the polymer sample, and resulted in deflection of the sample holder as the sample height was reduced in the direction of applied normal force. Most often, *in-situ* mass measurements will be taken throughout an experiment to track wear rate of the polymer sample. Each time the tribometer was set up to continue a test, the double-leaf flexure deflection was reset to essentially zero. Assuming interruptions occurred at a relatively low frequency, when the polymer specimen had  $1\ \text{mm}^3$  of volume loss of the  $10\ \text{mm}^3$  total per usual experiment, the force of deflection for 1.27 mm thick steel sheets in a double-leaf flexure would be less than the specified 1% of the applied normal force thus less than 0.004% error in wear rate calculations. This result was manually checked during testing by the compression load cell positioned between the pneumatic cylinder's piston and polymer pin, which was used to set the applied normal force to 250 N before test initiation and monitor normal force during testing. Further analysis

of the sample holder components confirmed that deflection from a friction force for 24.5 mm wide steel sheets in a double-leaf flexure can be conservatively estimated as ~10  $\mu\text{m}$ , which was below the specification for 50  $\mu\text{m}$  or less deflection.

While the polymer pins were held relatively stationary by the sample holders, the flat counterfaces were required to slide at 50.8 mm/s in linear reciprocal motion. To conduct six simultaneous experiments with this tribometer, the motor was required to be capable of overcoming a conservatively estimated 750 N of friction force ( $F_{\text{friction}} = 6 * F_{\text{normal}} * \mu = 6 * 250 \text{ N} * 0.5$ ). A NEMA 34 stepper motor was selected for this tribometer as capable of applying enough torque to overcome the resistance to sliding from friction. The rotational motion of this motor shaft was converted to linear motion of the reciprocating table via a ball bearing and lead screw. Calculations were employed to determine the lead screw required a root diameter of at least  $\text{Ø}17 \text{ mm}$  to avoid early failure by buckling or fatigue from experimental conditions. The lead screw and ball bearing were purchased as a reciprocating table unit with model number 2RB16I0N0450-100N002A0B00 from Thompson Linear Motion. For further details on the engineering work conducted to design of this new wear testing tribometer with high-throughput capabilities see Appendix A.

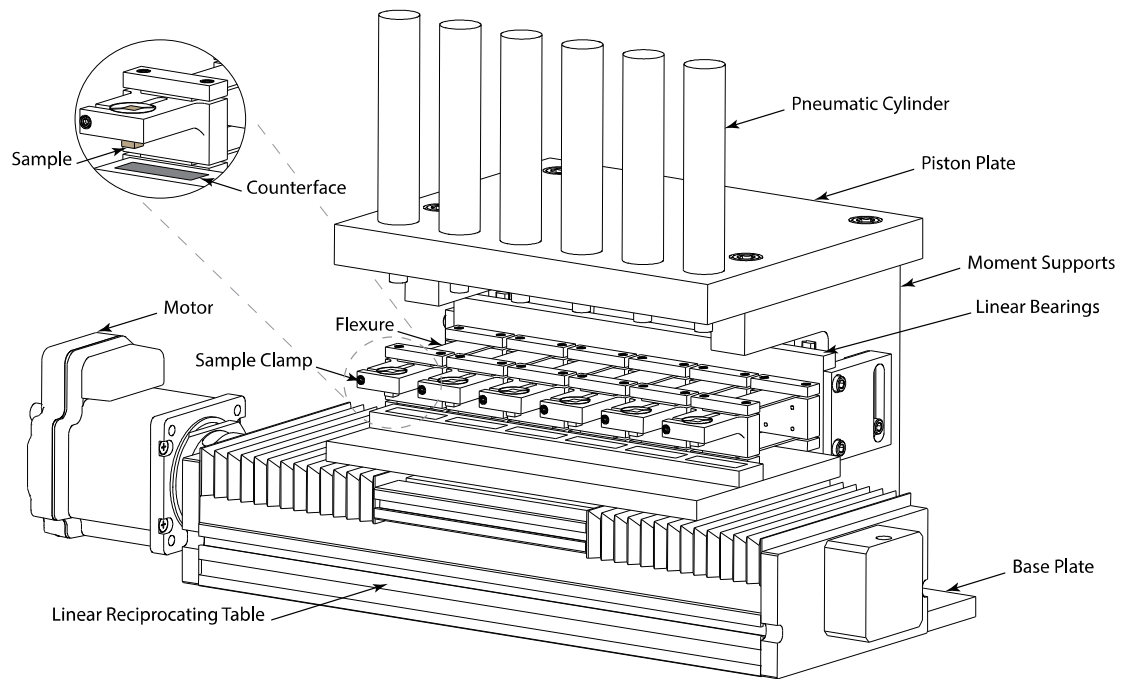


Figure 3-2 Illustration of the pin-on-flat tribometer used for high-throughput wear testing of polymer samples. Each polymer pin (6.4 mm x 6.4 mm) was mated to a 304 stainless steel counterface (38 mm x 25 mm). This custom-made equipment allows six samples, with a wide range of tribological performance, to be tested simultaneously. Wear tests were conducted with a normal force of 250 N (6.3 MPa), sliding speed of 50.8 mm/s, and wear track length of 50.8 mm per cycle. Image reprinted with permission from [93].

### 3.4 Conclusions

The initial design for a custom pin-on-flat tribometer with high-throughput capabilities was followed by fabrication, prototyping, and implementation over the consecutive year by the lead designer D.R. Haidar with the assistance of N. Garabedian and B. Bell. The result was a functioning tribometer capable of wear testing six samples simultaneously for heavy-duty bearing applications, which is shown in Figure 3-3. Thanks to the thorough work of the engineering teams, this specialized equipment has been used to facilitate new investigations by the Materials Tribology Lab of the University of Delaware <http://research.me.udel.edu/~dlburris/>

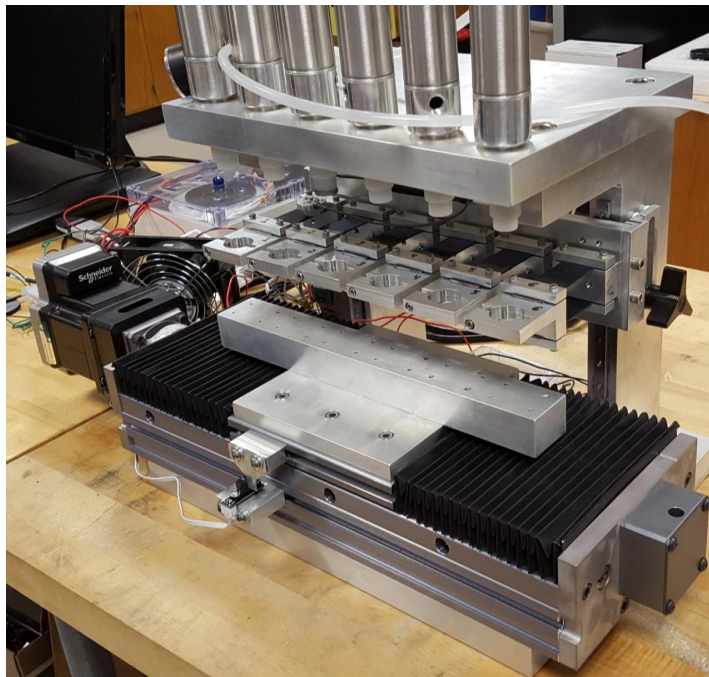


Figure 3-3 Picture of the pin-on-flat tribometer with high-throughput wear testing capabilities that was designed, fabricated, prototyped, and implemented over a year and a half. This equipment has facilitated studies investigating broad trends across multiple polymer systems and a single polymer system as a function of several variables, both of which would have been logistically limited otherwise.

### **3.5 Recommendations for Future Work**

Design is an iterative process, and the first version should always be used to inform future work. The pin-on-flat tribometer with high-throughput capabilities succeeded at the goal of wear testing six individual samples simultaneously, but further improvements can be made. For example, this tribometer was enabled to collect normal force values throughout testing, but without the functionality to collect friction force the friction coefficient cannot not be calculated. By adding this capability, both metrics of bearing performance could be measured concurrently. To achieve this aim, some recommendations are offered here for consideration:

**High Expense & High Quality** – The guaranteed way to collect friction force is to purchase a load cell with this capability. If money were a low priority, six total xyz compression load cells can be purchased for a few thousand dollars each. A v-clamp can be attached to each load cell, in which the polymer pin is mounted during testing. This load cell would be used to simultaneously capture the two perpendicular loads of normal force and friction force for calculating friction coefficient throughout testing.

**Moderate Expense & Moderate Quality** – The mid-range method for collecting friction force would require time and funds to design, fabricate, and implement a second set of double-leaf flexures. In addition to the pre-existing six polymer sample double-leaf flexures, the six new double-leaf flexures would be built for mounting the counterfaces. These six new double-leaf flexures can be oriented so that their two spacers are in the plane of the counterface (horizontal) and leaves are on the right and left of the counterface (vertical). One spacer will be bolted to the linear table (bottom) and the other will have the counterface mounted to it (top). In this setup, friction force experienced by each polymer-counterface pair is collected by a strain gauge purchased for ~\$150 and mounted to the counterface's double-leaf flexure. The mounting

orientation for each of the six strain gauges is in the direction of normal force. The mounting location, which will be on only one of the two leaves per counterface double-leaf flexure, is centered on the leaf face with the largest surface area. For this setup, strain gauge resolution is based on leaf deflection, which can be controlled by the leaf thickness in the direction of friction force. It is necessary to decide an amount of counterface translation deemed acceptable and calibrate force applied to leaf deflection for conversion to friction force during testing. To calculate the friction coefficient for an entire experiment, acquisition of both friction force and normal force are necessary throughout testing. Collection of normal force can be conducted with a button-style compression load cell purchased for ~\$500. This single-axis load cell would be located between a sample and pneumatic screw tip, which was the method implemented in the current high-throughput tribometer. To avoid over-spending, instead of buying six total load cells for the six polymer-counterface pairs, one load cell can collect a single value of normal force that is assumed to be the same for all pairs. This assumption can be made when the pneumatic cylinders have identical bore size and their air flow is connected in parallel.

## Chapter 4

### MATERIALS AND METHODS

#### 4.1 Polymer Composite Preparation

The PEEK-PTFE composites investigated by this study were fabricated in the same manner as previous work [80, 91] and analogous to materials tested in literature [48, 89, 90, 103]. PEEK and PTFE polymers utilized for sample fabrication were in powder form. The PTFE used was Teflon™ 7C resin (~30 μm reported diameter particles) from DuPont. The PEEK employed was 450PF resin (~10 μm reported diameter particles) from Victrex. Actual powder sizes were observed to be tens of micrometers in characteristic size by inspection using a Carl Zeiss STM Auriga® 60 SEM (Scanning Electron Microscopy) with SESI detector (Secondary Electrons or Secondary Ions) set to 1 kV and gun set to 3 kV, as shown in Figure 4-1.

These polymer powders were individually massed as 0, 5, 10, 20, 30, 40, 50, 60, 70, 90, and 100% by weight PEEK in PTFE composites, totaling to 6 g of material per sample. Materials were combined as one part of the powders to two parts of anhydrous ethanol by volume. Mixing was conducted with an OMNI International Sonic Ruptor 400 having an ultrasonic horn set to apply 460 W power for 2 s out of every 3 s over 5 min in total. Post mixing, this wet powder mixture was dried at 100 °C with a hot plate under rough vacuum. The dried powder ensemble was cold compacted in a 13 mm diameter cylindrical mold using 100 MPa of pressure for 1 h before being removed from the mold. This compacted part was set in a nitrogen backfilled Thermolyne 47900 furnace to be heated by ramping up to 365 °C in 3 h, holding at 365 °C for 10 h, and ramping down to 50 °C in 3 h.

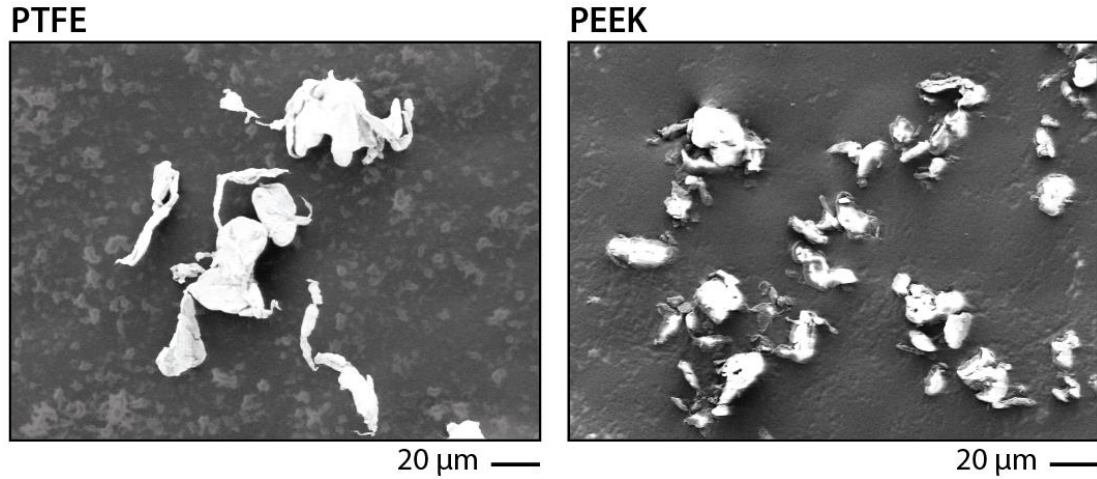


Figure 4-1 SEM image of PTFE Teflon™ 7C resin from DuPont has a micro-scale characteristic size (left). SEM image of PEEK 450PF resin from Victrex has a micro-scale characteristic size (right). Images were collected using a Carl Zeiss STM Auriga® 60 SEM, with SESI (Secondary Electrons or Secondary Ions) detector set to 1 kV and gun set to 3 kV, from the Keck Electron Microscopy Lab at the University of Delaware.

## 4.2 Polymer Wear Testing Procedure

Prior to testing, a flat counterface of 304 stainless steel was prepared for each polymer sample. These 38 mm x 25 mm coupons were polished by hand using Buehler CarbiMet silicon carbide abrasive paper on a grinding wheel with a constant stream of tap water. Polishing started with 320 grit (P400) paper to remove any pre-existing marks on the coupon surface. For each grit paper number, the orientation of the coupon with respect to the grinding wheel was held constant. Upon each change in grit paper approaching more fine polishing (400, 600, and 800 grit), the coupon was rotated 90° to have the same surface undergo polishing with the new polishing lines perpendicular to those from the previous grit paper. The polishing conducted for each of these grit papers was considered complete when all lines from the prior grit paper were replaced by lines from the current grit paper. When the coupon had all 600 grit polishing lines removed by the 800 grit paper, the coupon was turned at various angles to impart more randomly oriented polishing lines. For the final two grit papers (1000 and 1200 grit), the coupon was only polished while turning at various angles to impart more randomly oriented polishing lines. After the completion of 1200 grit (P2500) abrasive paper polishing, the coupon was lapped with Buehler ~1 micron diamond suspension on a synthetic polishing pad for 10 min. Finally, the coupon was cleaned with acetone from Fisher Scientific and a KimWipe cloth. The resulting counterface roughness of each coupon was measured in 3 regions within the area designated for the polymer sample's wear track to form during testing, as illustrated by Figure 4-2. These measurements were taken using a Veeco Wyko NT9100 scanning white light interferometer at 5.5x zoom with a viewing window of 0.86 mm x 1.10 mm. The counterface roughness of each coupon was reported as the average of those 3 values, which are listed in Appendix B. This polishing procedure resulted in counterfaces

with  $23 \text{ nm} \pm 7 \text{ nm}$  average surface roughness ( $R_a$ ), which provided uniform backgrounds that would later facilitate the inspection of transfer films.

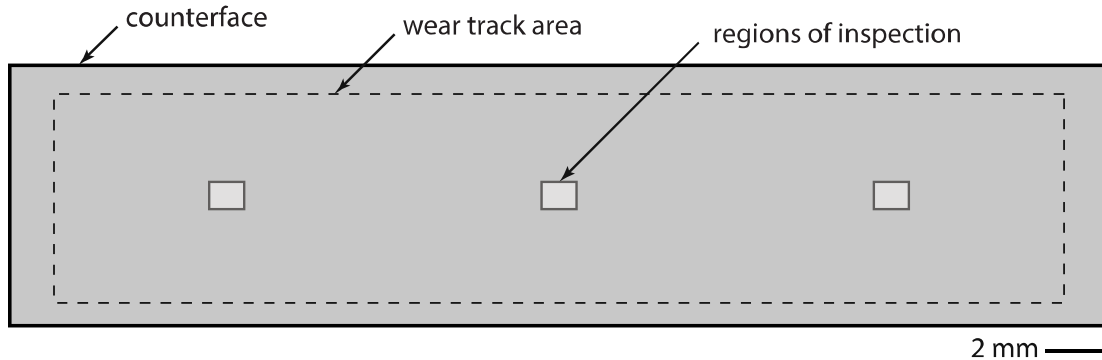


Figure 4-2 Illustration of a polished steel counterface inspected at the left region, center region, and right region within the area designated for the polymer sample's wear track to form during testing. Surface roughness was measured at these three locations using a Veeco Wyko NT9100 scanning white light interferometer. The average surface roughness ( $R_a$ ) of each counterface was reported as the average of those three values.

Before test initiation, polymer samples were machined into rectangular pins having a 6.4 mm x 6.4 mm test surface. The volume of each polymer pin was determined by measuring the 3 exterior dimensions with a Starrett outside micrometer, having an uncertainty of  $\pm 0.05 \text{ mm}$ . Immediately after, the mass was measured using a Mettler Toledo XP105 DeltaRange™ mass balance with an uncertainty of  $\pm 0.05 \text{ mg}$ . With these values, the density for each polymer sample was determined through a calculation of mass divided by volume. The resulting density value of each polymer sample is reported in Appendix B.

Each polymer pin was prepared for testing by mounting it in the linear reciprocating tribometer to have its sliding surface pre-conditioned with 50 N of

normal force (1.2 MPa pressure) against Buehler CarbiMet 600 grit (P1200) silicon carbide abrasive paper over 3 reciprocation cycles of 50.8 mm per cycle. This procedure removed machining marks from the polymer surface and aligned the sliding surfaces. Following this step, compressed dry air was used to remove any debris from the polymer interface. Then, the starting mass of each composite sample was collected and saved as a reference for changes in mass during testing. The polymer pin with known starting mass and flat counterface with known surface roughness were installed in the tribometer in preparation for test initiation.

Wear tests were conducted on the linear reciprocating pin-on-flat tribometer depicted in Figure 3-2. This high-throughput rig was custom designed, fabricated, prototyped, and implemented over the length of a year and a half to facilitate this dissertation. By testing six samples simultaneously, wear experiments that would have spanned multiple years in duration without interruption could instead run in a few months. This high-throughput tribometer is functionally comparable to those previously reported in literature by running linear reciprocating pin-on-flat experiments at a normal force of 250 N (6.3 MPa), sliding speed of 50.8 mm/s, and track length of 50.8 mm per cycle [22, 75, 86].

Wear test were conducted at  $\sim 25$  °C in both humid and dry environment. Testing within humid environment occurred in ambient laboratory conditions of  $\sim 30\%$  RH. Dry environment tests were conducted in a closed glovebox using an OMNI-LAB environmental chamber from Vacuum Atmospheres Co., as illustrated in Figure 4-3. This dry environment contained less than 0.05% RH ( $<10$  ppm water) by using 99.9998% pure dry N<sub>2</sub> gas with constant closed-cycle recirculation through an activated charcoal purifier, consistent with previous work [91]. Tests were interrupted

periodically to measure mass loss of the pin with a Mettler Toledo XP105 DeltaRange™ mass balance. The measurements for total mass change (starting mass minus *in-situ* mass) divided by density, resulted in monitoring the *in-situ* volume loss throughout each experiment [104]. Test interruptions occurred often enough to capture run-in, transition, and steady-state phases of the polymer samples [75]. Polymer samples were tested until either the total sliding distance reached 50 km or the accrued volume lost reached 10 mm<sup>3</sup>. The steady-state wear rate ( $k$  mm<sup>3</sup>/(Nm)) and uncertainty for each composite was determined using the analysis method from literature [104].

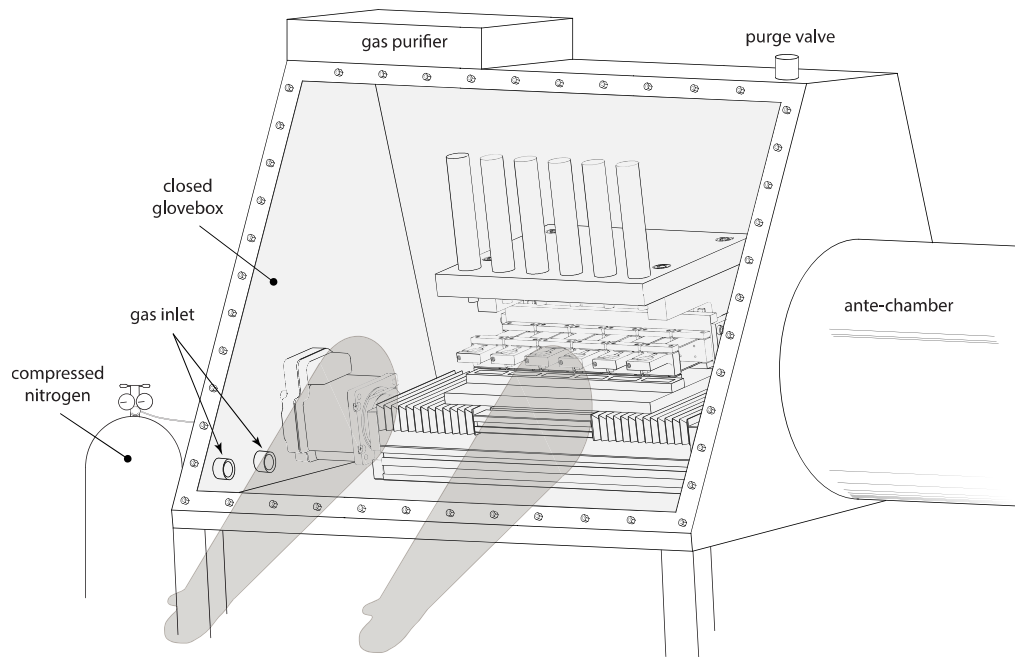


Figure 4-3 Schematic of the pin-on-flat tribometer with high-throughput capabilities housed in an environmental glovebox. This dry environment contained less than 0.05% RH (<10 ppm water) by using 99.9998% pure dry nitrogen gas with constant closed-cycle recirculation through an activated charcoal purifier. Image adapted and reprinted with permission from [91, 93].

### **4.3 Polymer Friction Testing Procedure**

Friction tests were conducted on the linear reciprocating pin-on-flat tribometer depicted in Figure 3-1, which is functionally equivalent to the wear testing tribometer. For consistency, prior to test initiation the polymer composites underwent machining and surface preparation procedures identical to the wear experiments. Moreover, these friction tests were conducted with identical settings of normal force of 250 N (6.3 MPa), sliding speed of 50.8 mm/s, and wear track length of 50.8 mm per cycle. For this tribometer, instantaneous friction force and normal force was collected with a multi-axis load cell during testing, which permitted monitoring of friction coefficient throughout the experiment. Friction coefficient was reported as the average equilibrium value for friction coefficient in the steady-state phase of the polymer sample [75].

### **4.4 Transfer Film Quality Characterization**

An exemplary transfer film developed by the linear reciprocating wear test of a polymer pin mated to a flat steel counterface is shown in Figure 4-4. Following the termination of each wear test in this study, transfer films developed by composite samples had image collection, processing, and analysis conducted in the same manner as previous work [80]. This inspection of each polymeric transfer film occurred within the middle 50% of the wear track to eliminate reversal effects from reciprocal motion and obtain relevant statistics for film attributes [77]. Transfer film images were collected within this central area at the center and four corners, as depicted by Figure 4-4.

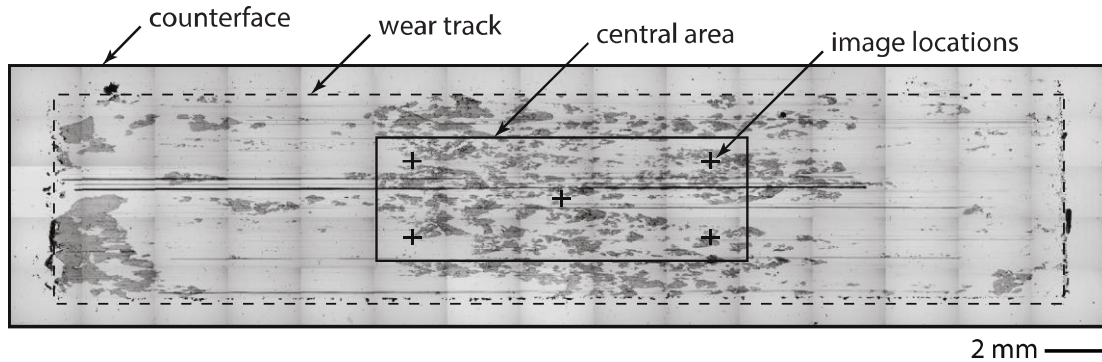


Figure 4-4 Example image of an entire wear track (25.4 mm width) developed by linear reciprocating motion of a polymer pin (6.4 mm x 6.4 mm) mated to a flat steel counterface. Representative images of the transfer film formed on the counterface were captured at 5 locations within the central area of the counterface to eliminate reversal effects and collect relevant statistics. Image adapted and reprinted with permission from [77].

These representative images of the transfer film were captured using a Nikon Instruments MM-400/S optical microscope with Nikon Instruments Digital Sight DS-Fi1 camera. All images were collected using identical light intensity and exposure time for direct comparison of transfer films made by different polymer composites. The images were collected in RGB color, then converted to binary black (transfer film) and white (counterface) using an algorithm for pixel intensity thresholding coded in MATLAB®. Once an image consisted of only black and white pixels, it was in proper form for analysis of transfer film attributes. This study considered two metrics of film morphology, the total percentage of area covering the counterface (area fraction) and the average size of gaps in the film exposing counterface (free-space length). Using a second operation in the same MATLAB® code, area fraction ( $X$  (-)) and free-space length ( $L_f$  ( $\mu\text{m}$ )) were evaluated. These operations are shown in Figure 4-5. The value of area fraction was determined first, by conducting a ratio of black to

white pixels. Then, the free-space length was found through a process of calculating the most likely number of intersecting black pixels in a randomly placed box of given side length. The resulting free-space length value is the side length of the largest box in which the most probable number of intersecting black pixels is zero. The script for this custom MATLAB® code and the directions for its use are presented in Appendix C. To download a copy of this MATLAB® code and user's manual visit the Materials Tribology Lab website at <http://research.me.udel.edu/~dlburris/publicationsOther.html>

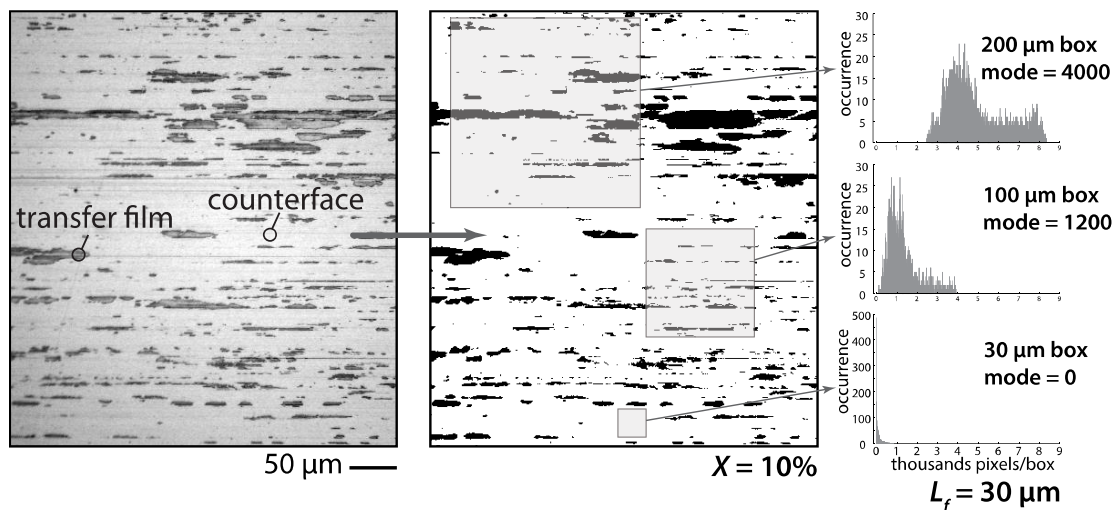


Figure 4-5 Example captured image of a polymeric transfer film deposited on a steel counterface was collected using an optical microscope (left). The optical image was converted from RGB color to binary black (transfer film) and white (counterface) using an algorithm for pixel intensity thresholding coded in MATLAB® (middle). Following conversion, a second operation in the same MATLAB® code evaluates area fraction and free-space length. The area fraction is determined by a ratio of black to white pixels. Then, free-space length is found through a process of calculating the most likely number of intersecting black pixels in a randomly placed box of given side length (right). The resulting free-space length value is the side length of the largest box in which the most probable number of intersecting black pixels is zero. Image adapted and reprinted with permission from [77].

## 4.5 Transfer Film Thickness Measurements

Measurements of transfer film thickness were conducted using the custom equipment shown in Figure 4-6a. Line scans were collected with 1-D stylus profilometry using a HDPE probe with large radius of 3 mm mounted on a 0.15 mN/ $\mu\text{m}$  cantilever. Before measurement, the counterface was leveled to  $0 \pm 1 \mu\text{m}$  per mm of travel parallel to the narrowest dimension of the transfer film (6.4 mm). The xy-stage was moved to locate the probe  $\sim 1$  mm from the edge of the transfer film, and then the z-stage was set to initially apply a nominal contact force of 4 mN. Next, the z-stage was fixed, and then the reciprocating xy-stage translated uniaxially in the x-direction at a speed of 0.3 mm/s. The deflections of the probe as a function of x-axis translation were tracked with a calibrated displacement sensor ( $100 \pm 0.014 \mu\text{m}$ ).

For each transfer film, 5 line scans were taken in the x-direction, which was perpendicular to the sliding direction of the parent polymer. Each of these 8 mm wide scans were made across  $\sim 1$  mm of counterface, 6.4 mm of wear track, and  $\sim 1$  mm of counterface as depicted in Figure 4-6b. The y-axis locations of these scans were selected to be the very center of the wear track defined as 0 mm,  $\pm 3$  mm, and  $\pm 6$  mm to eliminate reversal effects from reciprocal motion [77].

Each collected line scan was individually tilt-corrected to the  $\sim 1$  mm of bare counterface on either side of the wear track. From these measurements, film thickness was calculated using a method defined by literature [76]. In using this method, all five individually tilt-corrected line scans from one transfer film were combined into a single 50-bin histogram, which was fit with a bi-Gaussian function as shown in Figure 4-6c. The difference between the two modes of this distribution was reported as the average transfer film thickness ( $t_{ave}$  ( $\mu\text{m}$ )), for which the uncertainty was the root sum square of the standard deviations.

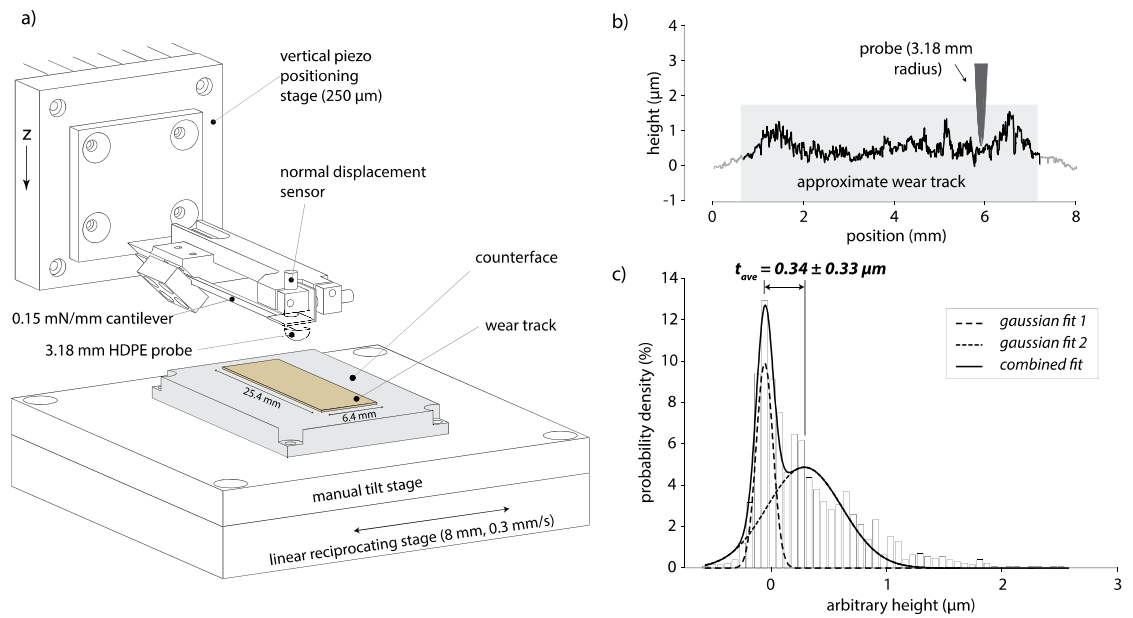


Figure 4-6 Illustration of the method for determining average transfer film thickness using stylus profilometry. (a) Custom equipment with a 3 mm radius HDPE spherical probe was used to collect line scans of the transfer film perpendicular to the sliding direction of the parent polymer. (b) An 8 mm wide scan was made across ~1 mm of counterface, 6.4 mm of wear track, and ~1 mm of counterface. (c) A total of 5 line scans for each transfer film were combined into a 50-bin histogram with a bi-Gaussian fit. Average transfer film thickness was defined as the difference between the two modes. Image adapted and reprinted with permission from [80].

## 4.6 Fourier-Transform Infrared (FTIR) Spectroscopy of Tribological Interfaces

### 4.6.1 Spectroscopy of Polymer Running Films

The infrared spectra of each sample's unworn bulk material before testing and running films after test termination were collected using a Bruker Tensor 27 FTIR spectrometer with a smart orbit attenuated total reflectance (ATR) accessory. Prior to every spectra collection, the diamond ATR crystal was mechanically cleaned by the shearing motion of a cotton swab with acetone to remove any transferred material and then wiped further with a dry KimWipe cloth. The spectra were captured by placing polymer surface of interest in contact with the diamond window. The collected spectrum consisted of 64 scans coaveraged at  $2\text{ cm}^{-1}$  spectral resolution. The method for conducting these measurements was identical to previous work [91].

### 4.6.2 Spectroscopy of Developed Transfer Films

The IR spectra of each sample's developed transfer films after test termination were collected using a NanoIR2 AFM-IR from Anasys Instruments. This equipment combines the nano-scale accuracy of an atomic force microscope (AFM) and IR spectroscopy to collect localized chemical spectra. Prior to spectra collection, the AFM was used in contact mode to map the height (nm) and deflection (V) of a  $40\text{ }\mu\text{m}$  x  $20\text{ }\mu\text{m}$  area at the center of the transfer film, which was oriented perpendicular and parallel to the direction of sliding, respectively. At least five total spectra were captured at high, middle, and low locations of the profile. The collected spectrum consisted of 256 scans coaveraged at  $4\text{ cm}^{-1}$  spectral resolution using a power level of 14.04%, polarization of  $0^\circ$ , frequency center of 200 kHz, and frequency window of 50 kHz. This method of measurement were identical to previous work [91].

## Chapter 5

### QUANTITATIVE METRICS OF TRANSFER FILMS AS INDICATORS OF POLYMER WEAR PERFORMANCE

#### 5.1 Overview

For decades, the wear resistance of polymer systems has been associated with the appearance of their transfer films. In poor performing polymer systems, transfer films are often described as ‘thick,’ ‘patchy,’ and ‘non-uniform’ [18, 70–74]. Conversely, the improved performance of a polymer by the addition of fillers corresponds to the transfer films being more ‘thin,’ ‘uniform,’ ‘continuous,’ and ‘coherent’ [18, 70–74]. This overall trend in appearance does reflect the role of the transfer film in barring direct contact between the parent polymer and counterface. However, it was still necessary to develop quantitative methods of assessing transfer film quality in order to identify the attributes of these films influencing polymer wear resistance [6]. Recent studies have endeavored to define, quantify, and correlate the attributes of transfer films to wear resistance of polymers or polymer composites [22, 71, 76, 77]. An outcome of these studies was the initial investigation of transfer film thickness, coverage, and uniformity in relation to polymer wear rate.

Investigations into transfer film thickness have measured the height of films built up on the counterface using profilometers. For one study, the thickness of transfer films formed by differently manufactured PEEK samples were measured using a scanning white light interferometer and determined to have no correlation to polymer wear rate [105]. In another study, AFM stylus profilometry was used to measure the thickness of films deposited by alumina-PTFE composites on counterfaces with variable roughness, which resulted in a strong correlation of thickness to composite wear rate [22]. Both of these studies investigated polymer

wear rate as a function of film thickness for a singular polymer system and resulted in opposite conclusions; thus, further exploration of a wider range of materials was necessary to assess the strength of this relationship.

A consequence of transfer films being built up from a collection of polymer debris particles is they do not provide perfectly uniform coverage; even transfer films formed by polymer composites with ultralow wear rates leave small gaps exposing the counterface [75]. As a result, the morphology of a transfer film has been characterized by both the total percentage of area covering the counterface (area fraction,  $X$  (-)) and the average size of gaps in the film exposing counterface (free-space length,  $L_f$  ( $\mu\text{m}$ )) [71, 106]. One study of polyethylene terephthalate (PET) composites measured transfer film area fraction as a function of composite wear rate for variable alumina nanoparticle filler loading, finding moderate correlation of coverage to polymer wear rate [71]. In another study, both metrics of area fraction and free-space length were measured for films formed by alumina-PTFE at different stages of the tribology test, finding composite wear rate to be poorly correlated to area fraction and strongly correlated to free-space length [106]. Again, discrepancies are prominent between results from two separate studies of singular polymer systems. The outcome of these mixed results is a significant need for an investigation of all three transfer film metrics to be assessed for a variety of polymers in order to identify broadly existing trends between film quality and polymer wear rate.

## 5.2 Materials and Methods

The following study investigating the wear rates of 10 polymers and polymer composites as a function of transfer film thickness, coverage, and uniformity is mainly based on the peer-reviewed article from Haidar *et al.* 2017 [80]. The materials selected for study were chosen to represent common polymers and span a wide range of bearing performance [6, 22, 24, 46–49]. All polymers and polymer composites were fabricated for this study (see Ch. 3 Methods and Materials for details), with the exception of purchased PET from Ensinger's TECAPET® product line and PPS (polyphenylene sulfide) from from Quadrant's Techtron® product line. The alumina filler materials used from Nanostructured & Amorphous Materials Inc. were  $\alpha$ -Al<sub>2</sub>O<sub>3</sub> (reported diameter 27-43 nm but a recent study revealed this powder consists primarily of micro-scale agglomerates of nanoparticles [84]) and  $\gamma$ -Al<sub>2</sub>O<sub>3</sub> (reported diameter of ~44 nm is consistent with findings from literature [79]).

For each polymer material, standard pin-on-flat tribological testing (Ch. 3) was conducted in humid air conditions (30% RH) until either 12 mm<sup>3</sup> of volume lost was incurred or 10 km of sliding distance was met. After test termination, the transfer film metrics of thickness was measured using stylus profilometry, whereas area fraction and free-space length were calculated using a custom MATLAB® code (see Appendix C for details) to process film images gathered with either optical microscopy or scanning electron microscopy (Ch. 3).

### 5.3 Results and Discussion

The results of wear testing for all polymers and polymer composites are shown in Figure 5-1. The wear resistance of these polymer materials spanned more than four orders of magnitude, with unfilled PTFE ( $k= 6 \times 10^{-4} \text{ mm}^3/(\text{Nm})$ ) and PTFE+32 wt% PEEK ( $k= 4 \times 10^{-8} \text{ mm}^3/(\text{Nm})$ ) observed at the extremes of wear performance. After test termination, the transfer films formed by each polymer material were characterized by the three quantitative metrics of film thickness, area fraction, and free-space length.

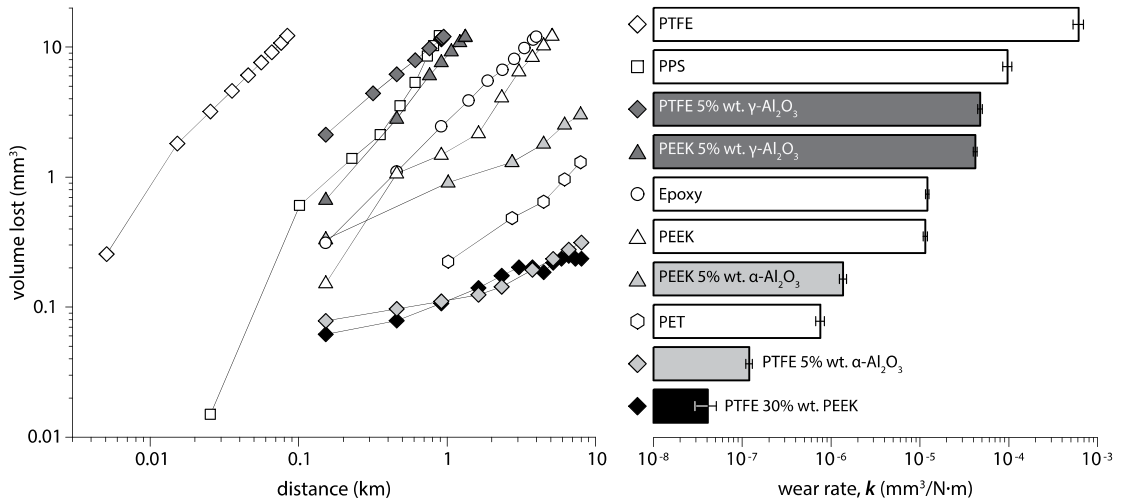


Figure 5-1 Volume lost as a function of sliding distance for all polymers and polymer composites (left), which were tested in humid air environment (30% RH). Wear rates for all polymer materials tested (right). Note that all axes were necessarily plotted on a logarithmic scale due to the wide range in wear performance. Image reprinted with permission from [80].

For all neat polymer materials tested, a representative transfer film height profile, original image, and converted image are shown in Figure 5-2 and organized by descending in order of decreasing wear rate. The representative line scans and average thickness measurements of these transfer films varied widely from thick and patchy by PTFE to thin and patchy by epoxy to thin and streaky by PEEK. In a similar fashion, original images of the neat polymer transfer films appeared distinct in transfer film shape, size, and uniformity. It was noticed that the transfer films of the two highest wear rate polymers were majority uncovered, whereas the two lowest wear rate polymers were half covered. However, this trend was compromised by the nearly equivalent wear rates of epoxy and PEEK having nearly zero coverage and half coverage, respectively. The results of wear performance and transfer film appearance are generally consistent with observations from literature [16, 19, 46, 49, 61, 71–73, 107, 108].

Representative transfer film profiles and images formed by all polymer composites tested are displayed in Figure 5-3. From the representative line scans and average thickness, it is observed that the transfer films formed by polymer composites range broadly from thick and non-uniform by PTFE+5 wt%  $\gamma$ -Al<sub>2</sub>O<sub>3</sub> to thin and non-uniform by PEEK+5 wt%  $\gamma$ -Al<sub>2</sub>O<sub>3</sub> to thin and uniform by PTFE+5 wt%  $\alpha$ -Al<sub>2</sub>O<sub>3</sub>. The original images of polymer composite transfer films also display wide range in appearance from lumpy PTFE+5 wt%  $\gamma$ -Al<sub>2</sub>O<sub>3</sub> to streaky PEEK+5 wt%  $\alpha$ -Al<sub>2</sub>O<sub>3</sub> to uniform PTFE+5 wt%  $\alpha$ -Al<sub>2</sub>O<sub>3</sub>. Similarly to the neat polymers, transfer films formed by polymer composites with the two highest wear rates were majority uncovered and two lowest wear rates were majority covered. These observations are consistent with literature [20, 22, 46, 48, 72, 73, 109].

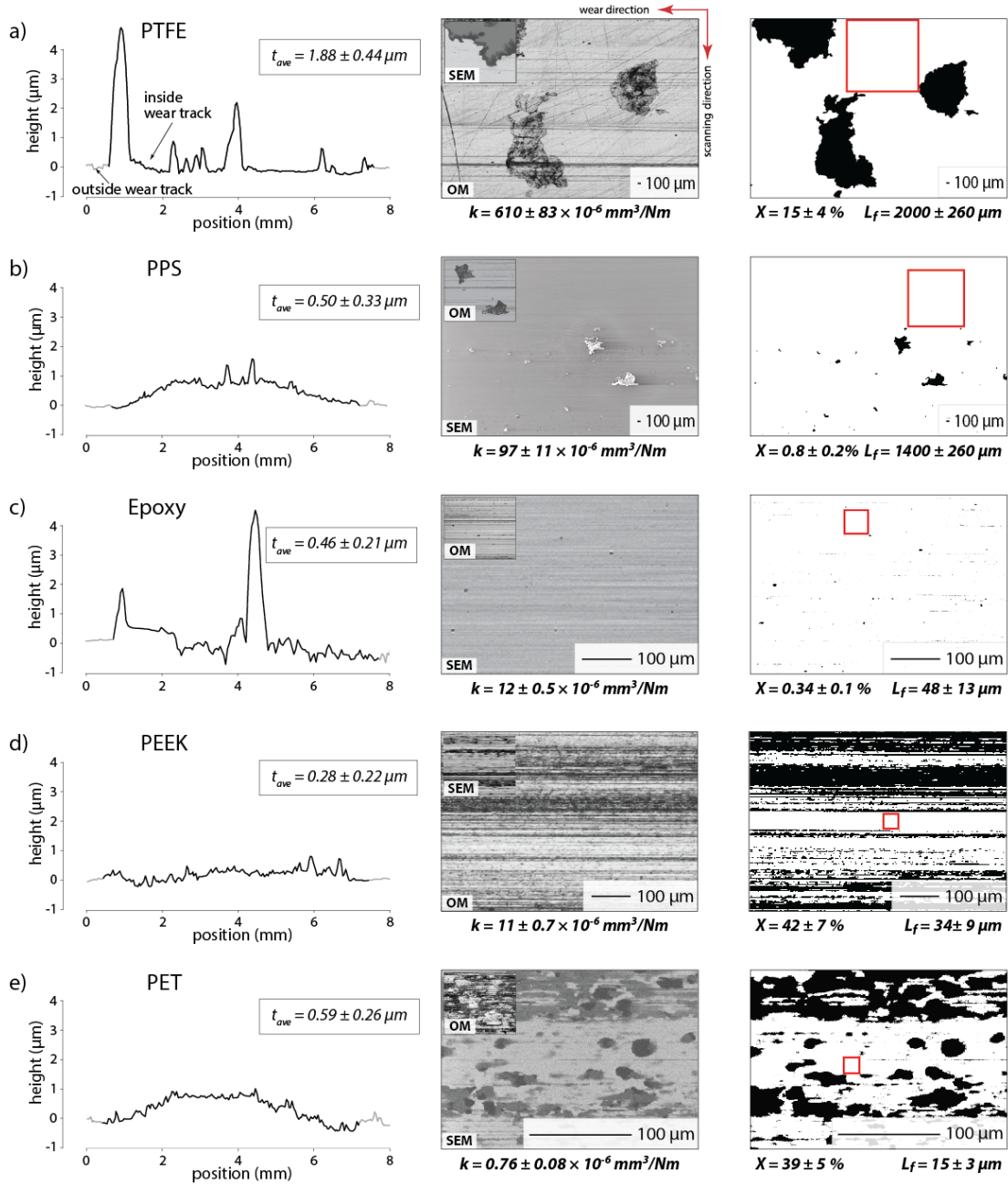


Figure 5-2 Representative profile line scans (left), original images (center), and converted images (right) of the transfer films for neat polymer (a) PTFE, (b) PPS, (c) epoxy, (d) PEEK, and (e) PET. Polymer materials are organized by descending in order of decreasing wear rate. For each transfer film, a square identifying the mean free-space length is provided to illustrate the relationship between this metric and film appearance. Image adapted and reprinted with permission from [80].

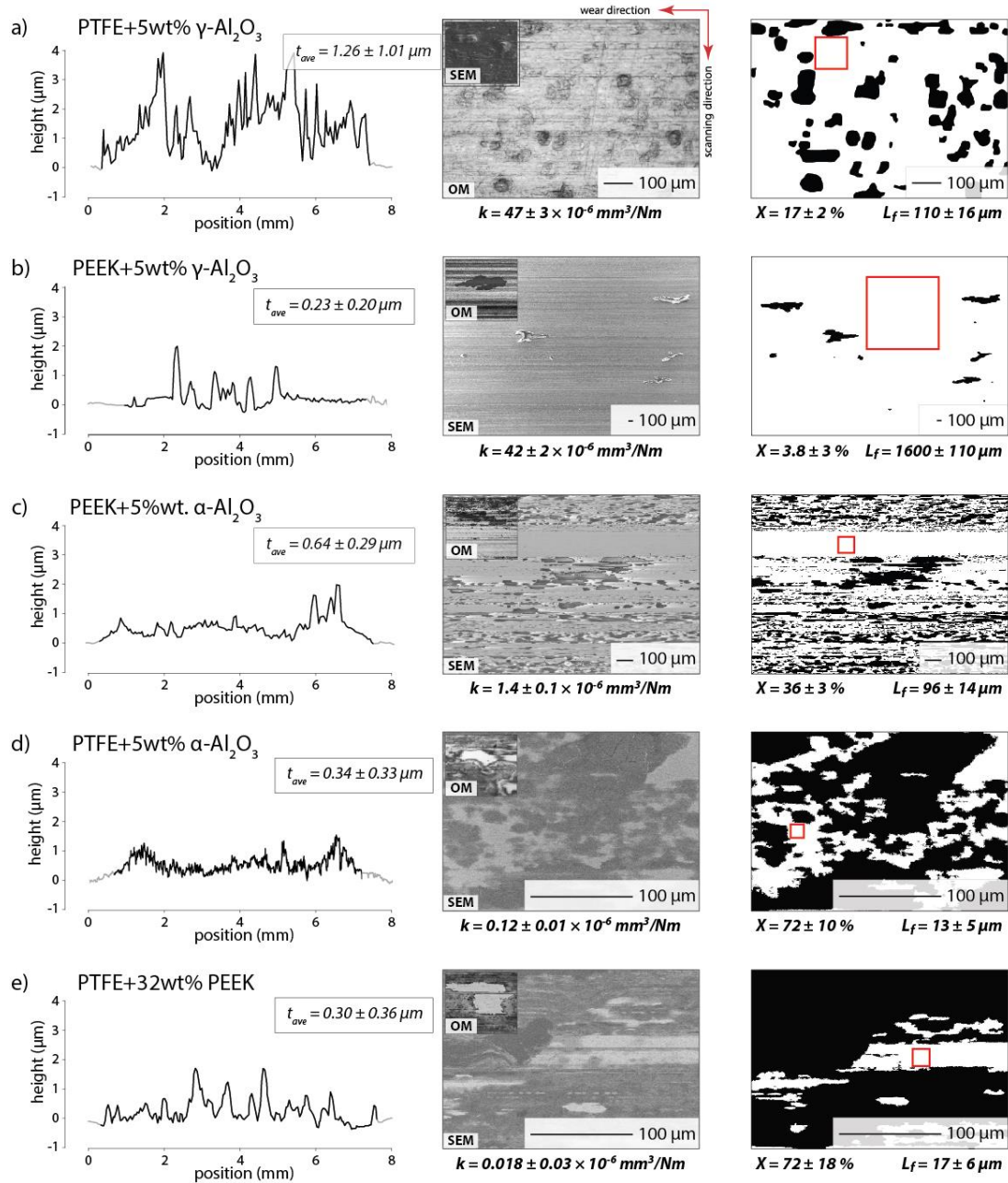


Figure 5-3 Representative profile line scans (left), original images (center), and converted images (right) of the transfer films for polymer composites (a) PTFE+5 wt%  $\gamma\text{-Al}_2\text{O}_3$ , (b) PEEK+5 wt%  $\gamma\text{-Al}_2\text{O}_3$ , (c) PEEK+5 wt%  $\alpha\text{-Al}_2\text{O}_3$ , (d) PTFE+5 wt%  $\alpha\text{-Al}_2\text{O}_3$ , and (e) PTFE+32 wt% PEEK. For each transfer film, a square identifying the mean free-space length is provided to illustrate the relationship between this metric and film appearance. Image adapted and reprinted with permission from [80].

For all polymers and polymer composites tested, the polymer pin wear rate was plotted as a function of transfer film thickness in Figure 5-4 from the results listed in Table 5-1. It was expected that a decrease in polymer wear rate would correspond to a decrease in film thickness, because improved bearing performance is strongly related to the formation of fine debris that accumulates and adheres to the counterface [23, 63, 69, 75, 78]. However, there did not appear to be a correlation between wear rate and film thickness. Visually, the data points were collected in a column centered at 0.65  $\mu\text{m}$  with standard deviation from 0.12  $\mu\text{m}$  to 1.18  $\mu\text{m}$ , as shown in Figure 5-4. Hence, there is a strong indication that polymer wear rate is not a function of transfer film thickness.

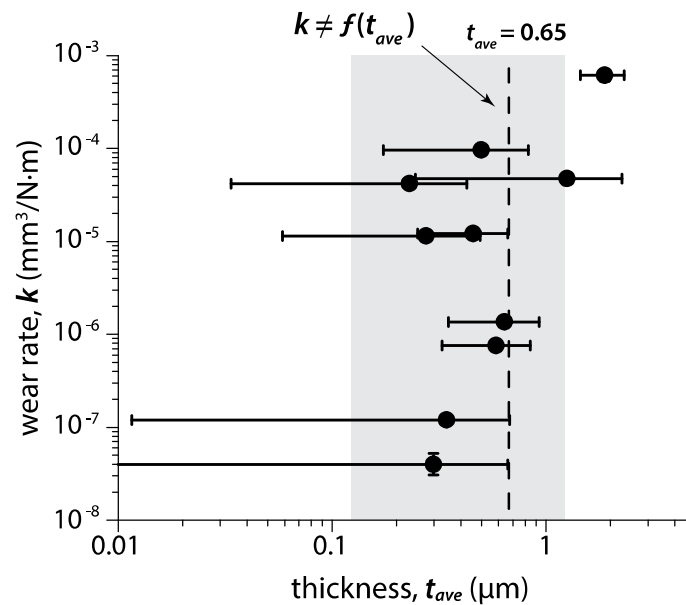


Figure 5-4 For common polymers and polymer composites, with a wide range in wear resistance, the polymer wear rate is plotted as a function of average transfer film thickness (black circles). The mean thickness (dashed line) and standard deviation (grey shaded region) for all data points indicate that overall the polymer wear rate is not a function of thickness. Image adapted and reprinted with permission from [80].

Despite the lack of a direct relationship between thickness and wear rate, having a numerical trend strength of wear rate to thickness was necessary to establish a comparison of wear rate to the other metrics area fraction and free-space length. By setting wear rate as a function of film thickness, it was found that exponential, linear, logarithmic, and power trends each had  $R^2 \approx 0.5$ . Although these had equivalently poor correlation for wear rate as a function of film thickness, the power trend's straight line was most similar to the column from Figure 5-4. The power trend was used to indicate an overall poor correlation between wear rate and thickness by its high mean variation of  $\sim 15x$  from the best-fit trendline, shown in Figure 5-5. As a result, film thickness was determined to be a poor indicator of polymer wear rate.

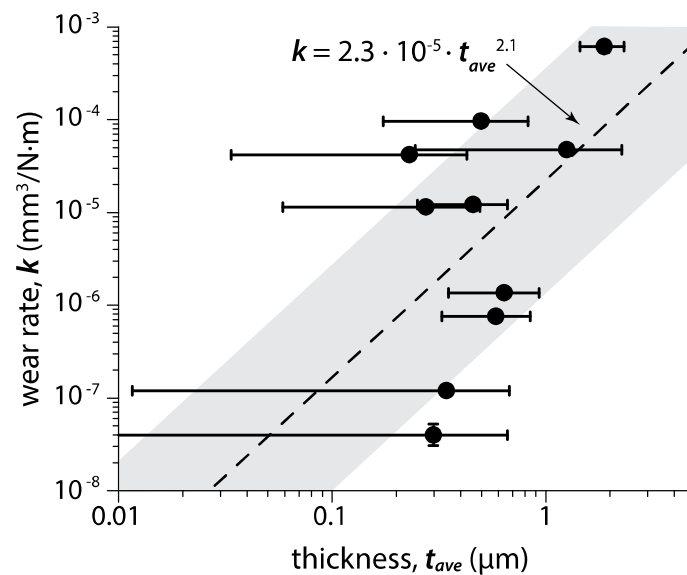


Figure 5-5 For common polymers and polymer composites, with a wide range in wear resistance, the polymer wear rate is plotted as a function of average transfer film thickness (black circles). Resulting best-fit trendline (dashed line) and mean variation (grey shaded region) indicate a generally poor fit to polymer wear rates. Image adapted and reprinted with permission from [80].

Table 5-1 The dataset of wear rates and transfer film thickness measurements for 10 polymers and polymer composites with a wide range in wear resistance. The metric values are reported as  $\pm$  the root sum square of the standard deviations (N=5). Table reproduced with permission from [80].

<b>Material</b>	<b>Wear Rate, <math>k</math> (<math>10^{-6} \text{ mm}^3/(\text{Nm})</math>)</b>	<b>Average Film Thickness, <math>t_{avg}</math> (<math>\mu\text{m}</math>)</b>
PTFE	$610 \pm 83$	$1.9 \pm 0.4$
PPS	$97 \pm 11$	$0.5 \pm 0.3$
PTFE+5 wt% $\gamma$ -Al <sub>2</sub> O <sub>3</sub>	$47 \pm 3$	$1.3 \pm 1.0$
PEEK+5 wt% $\gamma$ -Al <sub>2</sub> O <sub>3</sub>	$42 \pm 2$	$0.2 \pm 0.2$
Epoxy	$12 \pm 0.5$	$0.5 \pm 0.2$
PEEK	$11 \pm 0.7$	$0.3 \pm 0.2$
PEEK+5 wt% $\alpha$ -Al <sub>2</sub> O <sub>3</sub>	$1.4 \pm 0.1$	$0.6 \pm 0.3$
PET	$0.76 \pm 0.09$	$0.6 \pm 0.3$
PTFE+5 wt% $\alpha$ -Al <sub>2</sub> O <sub>3</sub>	$0.12 \pm 0.01$	$0.3 \pm 0.3$
PTFE+32 wt% PEEK	$0.04 \pm 0.01$	$0.3 \pm 0.4$

The metrics of area fraction and free-space length were measured in order to evaluate the impact of transfer film coverage and uniformity on polymer wear resistance, respectively. The polymer wear rate as a function of area fraction and free-space length is presented as a plot in Figure 5-6 using the data is listed in Table 5-2. From multiple observations in literature noting improved bearing performance to correlate with increased coherence and coverage of transfer films, it was expected that an increase in area fraction would correlate to a decrease in polymer wear rate [18, 70, 71, 73, 74]. This outcome is supported by a fairly low mean variation of  $\sim 6x$  from the best-fit trendline.

The metric of free-space length is particularly related to coherence and uniformity. This metric was originally developed to measure the average size of areas within the transfer film region exposing counterface, which were proposed to predict the debris size to fill that gap and in effect polymer wear rate [77]. The polymer wear rate as a function of free-space length had the lowest mean variation of ~4x from the best-fit trendline. This result suggested that smaller sized adhesive zones, here smaller sized domains of exposed counterface within the wear track, directly relates to less polymer wear loss and improved wear resistance.

Table 5-2 The dataset of wear rates, transfer film area fraction, and transfer film free-space length for 10 polymers and polymer composites with a wide range in wear resistance. All metric values are reported as the mean  $\pm$  95% confidence interval (N=5). Table reproduced with permission from [80].

<b>Material</b>	<b>Wear Rate, <math>k</math> (<math>10^{-6}</math> mm<sup>3</sup>/(Nm))</b>	<b>Area Fraction, <math>X</math> (%)</b>	<b>Free-Space Length, <math>L_f</math> (<math>\mu</math>m)</b>
PTFE	610 $\pm$ 83	15 $\pm$ 4	2000 $\pm$ 260
PPS	97 $\pm$ 11	0.8 $\pm$ 0.2	1400 $\pm$ 260
PTFE+5 wt% $\gamma$ -Al <sub>2</sub> O <sub>3</sub>	47 $\pm$ 3	17 $\pm$ 2	110 $\pm$ 16
PEEK+5 wt% $\gamma$ -Al <sub>2</sub> O <sub>3</sub>	42 $\pm$ 2	4 $\pm$ 3	1600 $\pm$ 110
Epoxy	12 $\pm$ 0.5	0.3 $\pm$ 0.1	48 $\pm$ 13
PEEK	11 $\pm$ 0.7	42 $\pm$ 7	34 $\pm$ 9
PEEK+5 wt% $\alpha$ -Al <sub>2</sub> O <sub>3</sub>	1.4 $\pm$ 0.1	36 $\pm$ 3	96 $\pm$ 14
PET	0.76 $\pm$ 0.09	39 $\pm$ 5	15 $\pm$ 3
PTFE+5 wt% $\alpha$ -Al <sub>2</sub> O <sub>3</sub>	0.12 $\pm$ 0.01	72 $\pm$ 10	13 $\pm$ 5
PTFE+32 wt% PEEK	0.04 $\pm$ 0.01	72 $\pm$ 18	17 $\pm$ 6

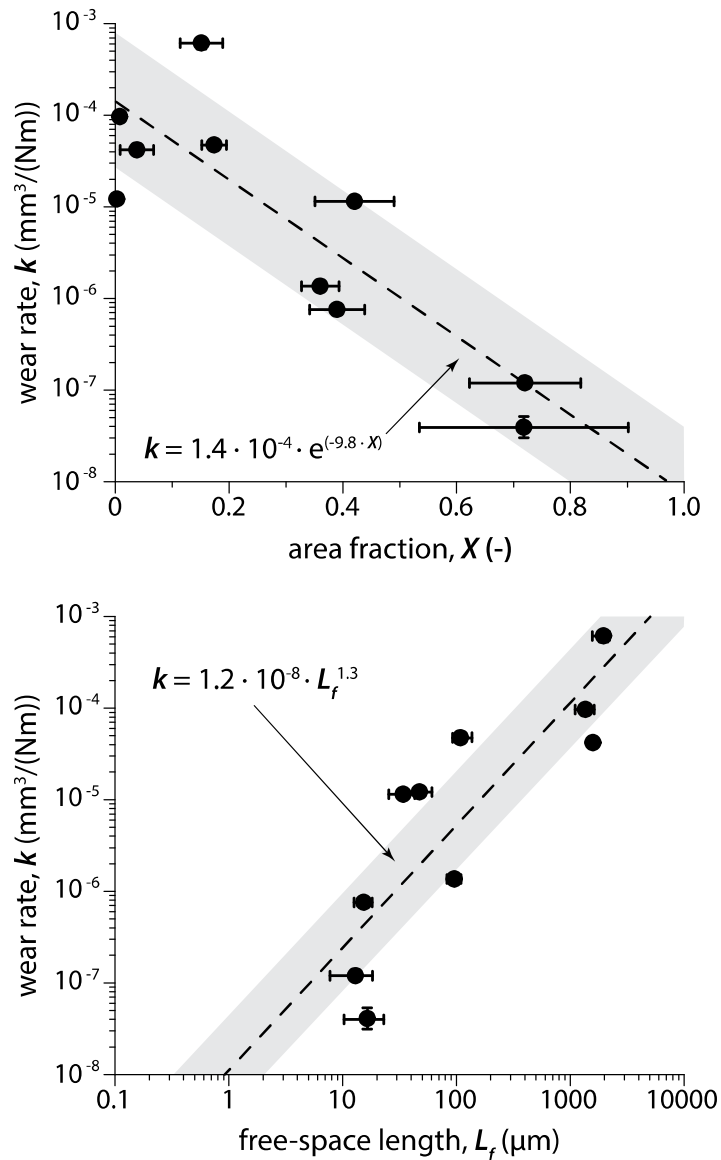


Figure 5-6 For common polymers and polymer composites, with a wide range in wear resistance, the polymer wear rate is plotted as a function of transfer film area fraction (top) and free-space length (bottom). The calculated best-fit trendline (dashed line) and mean variation (grey shaded region) for each morphology metric is plotted. These results indicate area fraction had a moderately good fit and free-space length had the best fit to polymer wear rate. Image adapted and reprinted with permission from [80].

## **5.4 Conclusions**

To investigate a generally applicable relationship between polymer wear rate and transfer film quality, 10 polymer and polymer composite systems with wear performance spanning over four orders of magnitude were studied. The transfer films formed by each polymer material were quantitatively characterized by the metrics of film thickness, area fraction, and free-space length. An assessment of polymer wear rate as a function of each film metric individually revealed a correlation strength of poor for thickness, good for area fraction, and best for free-space length. As a result, free-space length was determined to be the best independent indicator of polymer wear performance.

## **5.5 Recommendations for Future Work**

This study made an effort to assess transfer film metrics for 10 different polymers and polymer composites with a broad range in bearing performance in order to observe generally applicable trends. However, it has yet to be determined how robust these metrics are for the many polymer materials not tested by this study. Future investigations of different polymer systems such as acrylonitrile butadiene styrene (ABS), polyamide (nylon), polyimide (PI), polyphenylene oxide (PPO), and polystyrene (PS) will be necessary to assess whether area fraction and free-space length offer relevant information on polymer wear rates universally. It is expected that high area fraction ( $X \geq 60\%$ ) and low free-space length ( $L_f \leq 10 \mu\text{m}$ ) will correlate to ultralow wear rate. To confirm this trend, it is recommended that all future studies include a data table of polymer wear rate with respective area fraction and free-space length values, which will provide the necessary information to verify the significance and usefulness of these metrics.

## Chapter 6

### PEEK-PTFE ENVIRONMENTAL MOISTURE STUDY

#### 6.1 Overview

Over the past two decades, the alumina-PTFE system has been the subject of study to elucidate the mechanisms enabling its advanced performance as a bearing material. Investigations by at least four independent research groups have resulted in the current filler theory for a hard (e.g. metal or ceramic) filler in lubricous polymer matrix [63, 75, 84, 88, 89]. For this system, three main mechanisms contribute to its tribological success 1) micro-scale functionality of the filler material in the bulk arrests crack propagation for fine debris formation – small debris is necessary for quality transfer film development [18, 19, 24, 65], 2) nano-scale functionality of the filler material at the sliding interface for gentle polishing – avoiding abrasion at the interface provides stability for a protective transfer film to develop and removes less film thus requiring less replenishment by polymer debris for lower polymer wear [63, 64], 3) degraded polymer debris chemically bonding to the counterface is the strongest method of transfer film adhesion – less transfer film maintenance by polymer debris permits lower polymer wear [23, 78]. The necessity for all three of these factors has been shown by the tribological failure of chemically identical alumina in PTFE when the filler material is a fully-dense microparticle, the filler material is a true nanoparticle, or moisture is absent from environment [63, 79, 84, 89, 91].

Due to the large body of knowledge gathered from probing the alumina-PTFE system, results from studies on this particular polymer have fundamentally enhanced our understanding of tribology [5, 78, 89, 96]. An application of such knowledge, with the potential for broad impacts, is using this system as a model for improving

tribomaterials design. This study aims to inform composite material selection by replacing the multi-scale functional alumina with an alternative filler material capable of 1) arresting PTFE matrix crack propagation, 2) avoiding abrasion of the transfer film, and 3) forming a tenacious transfer film without constituents from the environment. Here, it is hypothesized that a micro-sized filler material, much softer than steel but harder than PTFE, will be sufficiently large and hard enough to arrest crack propagation in the PTFE matrix without being abrasive to the sliding interface. Note, many polymers meet the specifications of being much softer than steel but harder than PTFE. However, only a few polymers have similarly high melting temperatures to PTFE ( $T_m > 300^\circ\text{C}$ ), which is necessary for bearing materials to function in conditions with extreme temperatures. Here, it is also hypothesized that that the soft micro-sized filler material in PTFE can be selected to contain the elements oxygen and hydrogen to supplement necessary components for broken PTFE chains to undergo the tribochemical change of forming carboxyl end groups in moisture starved environments. This proposed model for a polymer composite that will display advanced bearing performance in challenging environmental conditions is depicted in Figure 6-1.

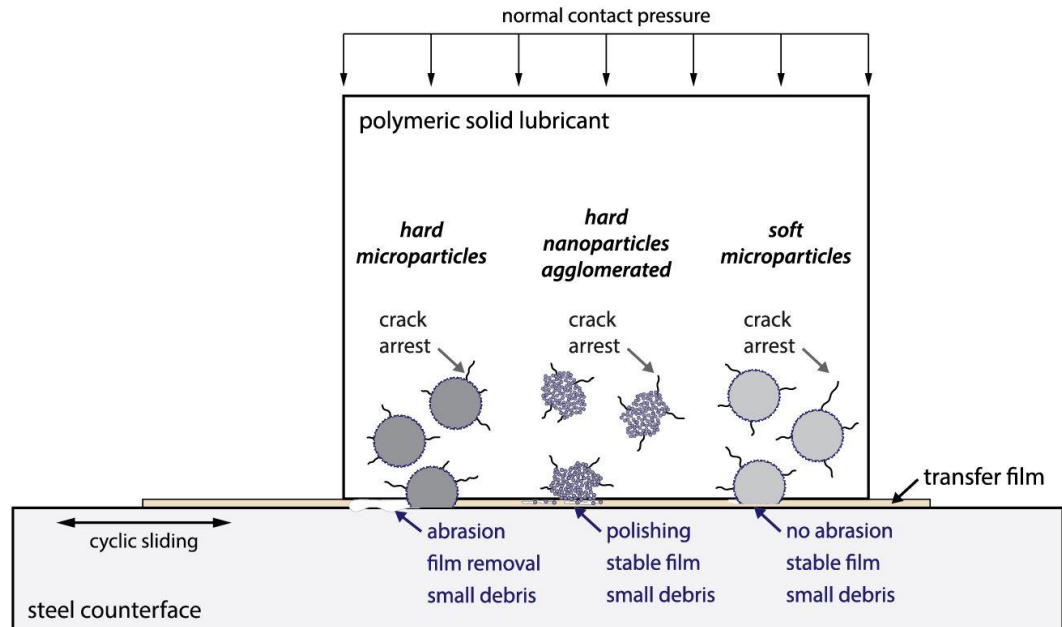


Figure 6-1 Proposed model for a soft microparticle filler in lubricious polymer matrix is presented as fulfilling the necessary functions for advanced tribological performance 1) micro-scale filler material is relatively harder than the matrix for bulk crack arrest and fine debris formation needed for quality transfer film development, 2) filler material is soft enough not to abrade the sliding interface and allows stable formation of a protective transfer film, 3) polymer matrix is mechanically degraded by sliding and the filler provides the oxygen and hydrogen elements regardless of environment for strong chemical bonding to the counterface and tenacious transfer film adhesion requiring minimal replenishment for low polymer wear rates. Soft microparticles could satisfy all of the requirements #1, 2, & 3 for a low wear PTFE-based system (right).

In this study, PEEK-PTFE composites were selected to test the proposed model of tribomaterials consisting of relatively soft filler in PTFE for bearing applications in the aerospace industry. PEEK was chosen as the filler material in PTFE for several reasons. First, the penetration hardness ( $p \approx 3\sigma_y$  N/m) of PEEK (~300 MPa) is higher than PTFE (~30 MPa) by a factor of 10, which suggested that PEEK could be sufficiently hard to arrest PTFE matrix crack propagation even though its hardness value is much lower than the steel counterface (~1300 MPa) [2, 110–112]. Second, the surface energy of PEEK (~35 mJ/m<sup>2</sup>) is much lower than steel (~900 mJ/m<sup>2</sup>) and only slightly higher than PTFE (~18 mJ/m<sup>2</sup>) [2, 78, 113–115]. Thus, unlike true microparticles of alumina (~600 mJ/m<sup>2</sup>), PEEK was not expected to cause any abrasion to the steel counterface nor significant abrasion to the polymer transfer film [2, 78, 113–115]. Third, PEEK chains contain oxygen and hydrogen elements, which upon degradation could provide broken PTFE with the necessary components for tribochemistry to induce carboxyl end group formation in dry conditions. This chemical change has been identified as the mechanism permitting advanced bearing performance for alumina-PTFE in humid conditions [89–91]. Fourth, it has been known that neat PEEK and several PEEK-based composites display improved friction and wear in conditions absent of moisture, as shown in Figure 6-2 [116]. Fifth, PEEK ( $T_m > 300^\circ\text{C}$ ) has a similarly high melting temperature to PTFE, which makes it desirable for extreme temperature conditions. In sum, the alumina-PTFE model has been applied to selecting micro-scale PEEK as the filler material for PTFE. It was expected that results would show an optimal ratio of PEEK to PTFE among the composites listed in Table 6-1, which would perform with ultralow wear ( $k \leq 3 \times 10^{-7}$  mm<sup>3</sup>/(Nm)) and moderate friction ( $\mu \leq 0.17$ ) for advanced bearing performance.

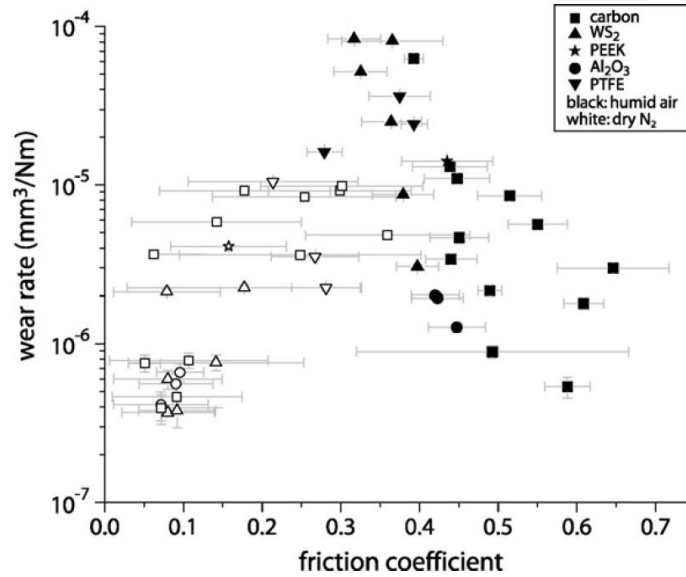


Figure 6-2 Wear rates and friction coefficients for PEEK-based composites tested in humid air (black) and dry nitrogen environments (white). From the results, it is observed that PEEK composites generally have lower friction in an environment absent of moisture. Image reprinted with permission from [116].

Table 6-1 Composites of PEEK filler in PTFE matrix selected to be tested for wear performance when moisture is available or absent in the environment.

PEEK Filler (wt%)	PTFE Matrix (wt%)	Composite Description
0	100	Reference Material
5	95	Low Filler Loading
10	90	
20	80	
30	70	
40	60	
50	50	
⋮	⋮	High Filler Loading
100	0	Reference Material

## 6.2 Results

The results of volume loss for all PEEK-PTFE composites in this study were plotted as a function of sliding distance during testing in Figure 6-3. As expected, the unfilled PTFE wore to  $10 \text{ mm}^3$  in as little as 0.1 km of sliding in both a dry  $\text{N}_2$  environment ( $<0.05\% \text{ RH}$ ) and humid air environment (30% RH). Neat PEEK also met test termination from  $10 \text{ mm}^3$  of volume loss regardless of environmental humidity, though its inherent 100x better wear resistance than neat PTFE allowed it reach nearly 10 km of total distance in both conditions. Similarly, composites with high weight percentage of PEEK in PTFE, tested only in dry conditions, incurred  $10 \text{ mm}^3$  of volume loss before reaching the experiment termination point at 50 km. Tests in both environments found the composites with the lowest total volumetric wear to be gathered in a narrow stretch between 1 and  $3 \text{ mm}^3$ . Interestingly, the composites within this concentrated range of volume loss depended slightly on the testing environment, in dry conditions 5-40 wt% and in humidity 20-50 wt% PEEK in PTFE, having multiple cubic millimeters less volumetric wear for only 5-10 wt% change in filler loading.

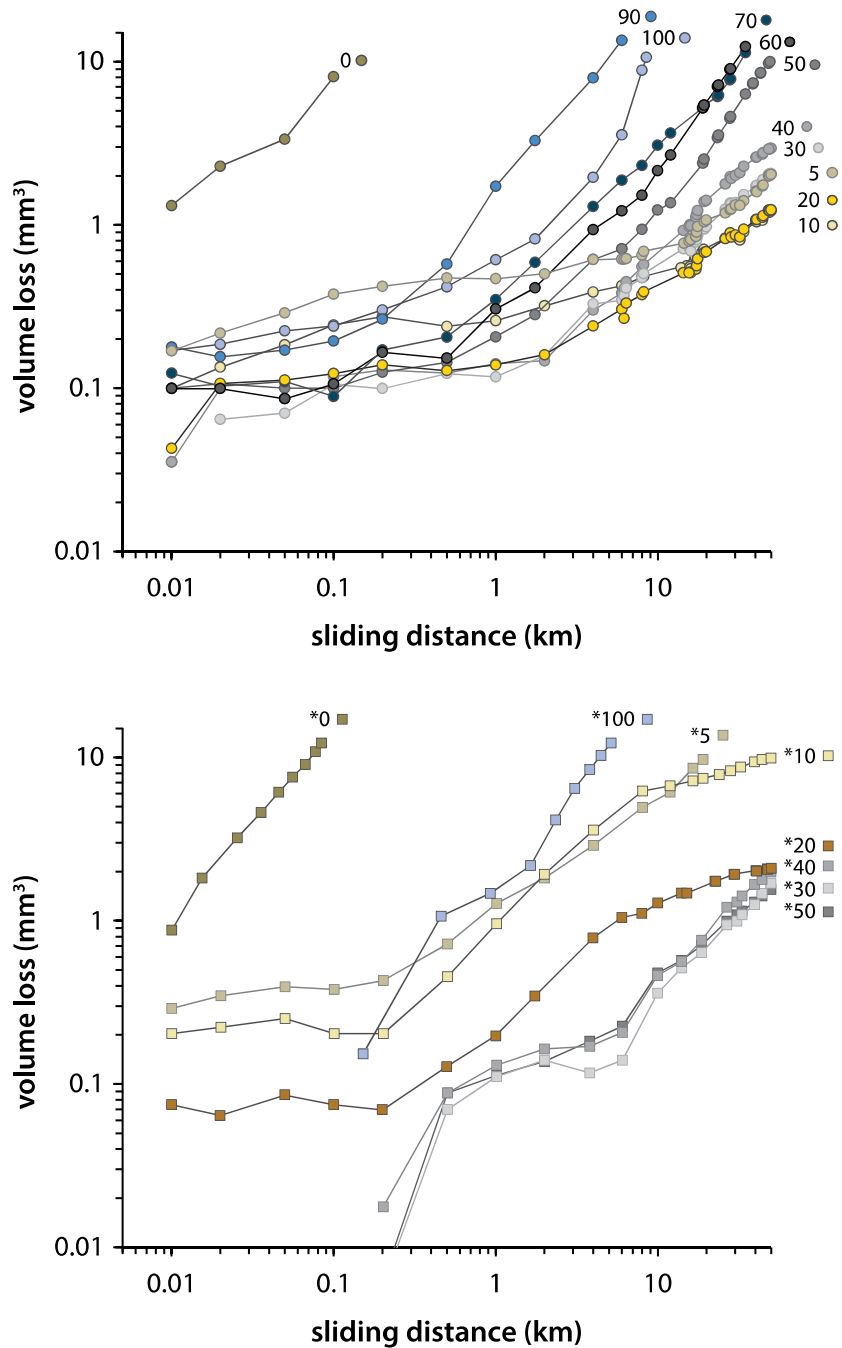


Figure 6-3 Wear volume as a function of sliding distance for all PEEK-PTFE composites tested in dry N<sub>2</sub> environment (top) and humid air environment (bottom). All samples were tested in dry nitrogen environment (<0.05% RH), unless indicated by the \* symbol as a humid air environment (30% RH). Image adapted and reprinted with permission from [93].

Wear rate as a function of PEEK filler in PTFE was plotted in Figure 6-4. Regardless of environmental humidity, the wear rate of neat PTFE and neat PEEK were  $k = \sim 5 \times 10^{-4} \text{ mm}^3/(\text{Nm})$  and  $k = \sim 9 \times 10^{-6} \text{ mm}^3/(\text{Nm})$ , respectively, both of which were consistent with results from literature [29, 116]. The composites' wear rates show a remarkable effect from adding even small amounts of PEEK to PTFE. In dry conditions, as little as 5 wt% filler allowed the composite to perform with nearly 3,000x more wear resistance than PTFE and 100x more wear resistance than PEEK. Composites tested in humid environment had equally impressive improvements to wear resistance, though they required at least 20 wt% filler. In both environments, significant reductions to wear rate were observed for multiple filler loadings of PEEK in PTFE. Moreover, even the highest wearing composites only approached the wear rates of neat PTFE for lower filler and neat PEEK for higher filler loading. Interestingly, this shows a synergistic effect of combined PTFE and PEEK generally having significantly lower wear rates than either PTFE or PEEK alone.

Ultralow wear rates ( $k \leq 3 \times 10^{-7} \text{ mm}^3/(\text{Nm})$ ) were achieved in dry conditions for 5-40 wt% and in humidity for 20-50 wt% of filler, the same compositions as those having the lowest total volumetric material loss. Regardless of environment, stepping further away from these high performing filler ranges had a generally monotonic trend of worsening the wear rate. Within the overlap of these two beneficial filler loading ranges, one composition stands out as having particularly low wear rates in either testing condition. The 20 wt% PEEK in PTFE composite displayed the best overall wear resistance by having a wear rate of  $k = \sim 8 \times 10^{-8} \text{ mm}^3/(\text{Nm})$  in both dry and humid environments.

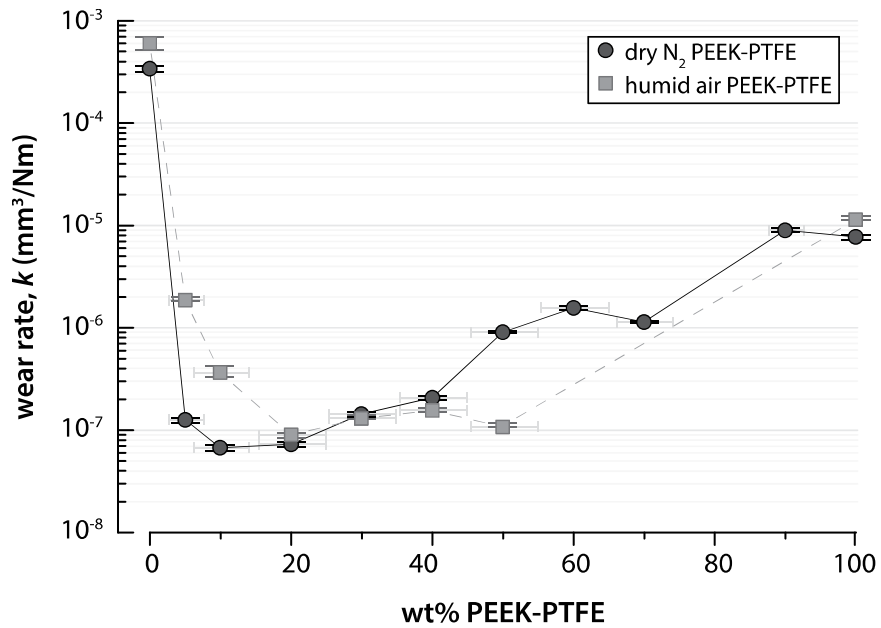


Figure 6-4 Wear rate as a function of filler loading for all PEEK-PTFE composites tested in dry N<sub>2</sub> environment (circles) and humid air environment (squares). Uncertainty for weight percent of PEEK filler in PTFE is represented by the work of Burris and Sawyer [48]. Image reprinted with permission from [93].

The most wear resistant composite across both environments was subject to further investigations of tribological performance, shown in Figure 6-5. The 20 wt% PEEK in PTFE composite had values for friction coefficient collected as a function of sliding distance until test termination at 50 km. Although the wear rates and total volume loss were nearly identical for 20 wt% PEEK-PTFE in the two testing conditions, the friction was noticeably different.

The steady-state friction was nearly identical between dry and humid environments, evaluated as  $\sim 0.18$  and  $\sim 0.17$  respectively, by an average of equilibrated data after the spike caused by interruption. Similarly, neat PTFE had equivalent friction in both dry and humid conditions, though slightly lower at  $\sim 0.15$  from literature [22, 29]. In contrast, the friction coefficient of neat PEEK was dependent on environmental moisture. In humidity PEEK had a friction coefficient of  $\sim 0.4$ , but in an environment devoid of moisture it drastically improved to  $\sim 0.15$  from literature [48, 116]. Although the wear rate of PEEK was not sensitive to environmental moisture, variable friction of PEEK depending on these conditions is remarkably similar to  $\text{MoS}_2$ , which has been shown to be susceptible to water vapor adsorption that greatly increases friction coefficient [34, 35]. A similar water vapor absorption could be involved in the chemistry of PEEK and therefore in the PEEK-PTFE composites, causing the friction from dry nitrogen wear test interruptions to spike higher after mass data collection in humid conditions and return to testing in dry nitrogen environment.

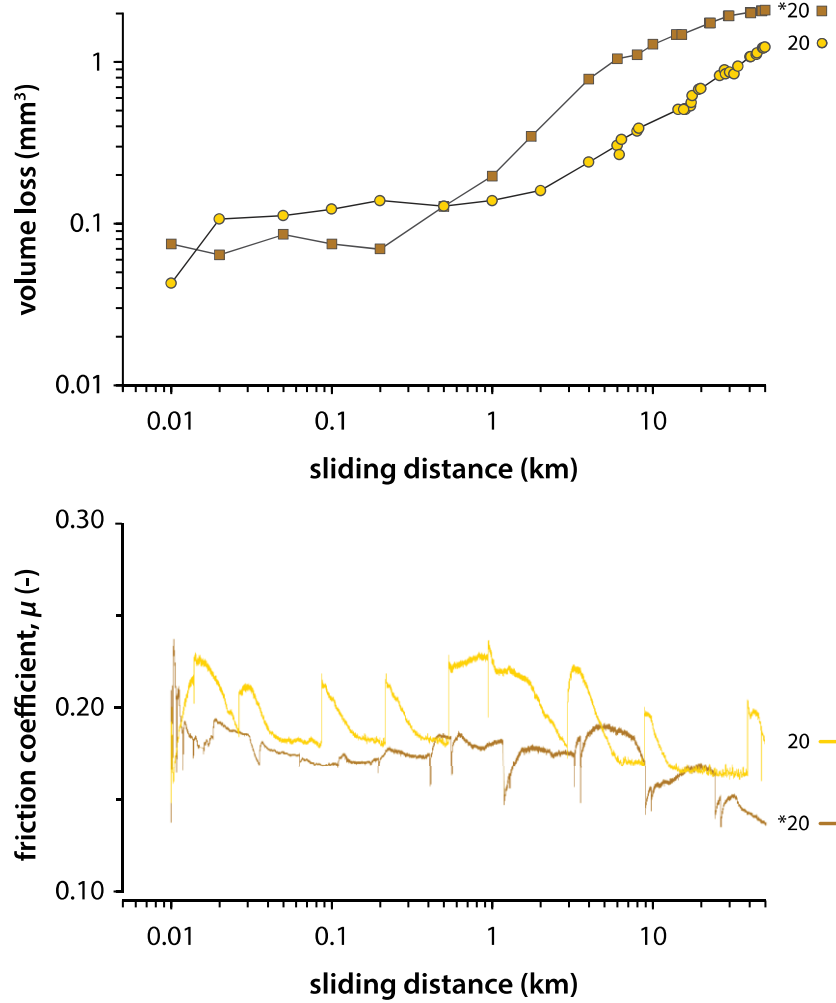


Figure 6-5 Volume loss (top) and friction coefficient (bottom) as a function of sliding distance for 20 wt% PEEK-PTFE composite tested in dry N<sub>2</sub> and humid air environments. The sample tested in humid air environment is indicated by the \* symbol. Top image adapted and reprinted with permission from [93].

An optical image of the transfer film for each PEEK-PTFE composite after test termination is shown in Figure 6-6. For the samples tested in dry conditions, 10 wt% and 20 wt% PEEK filler in PTFE had the most similar transfer films; they appeared visually identical in film coherence, coverage, and distribution. Although the 5 wt% composite appeared lighter than 10 wt% and 20 wt%, all three transfer films had orientation traits often observed from a film drawing formation process [16]. For composites of 30 wt% or more filler, as filler loading increased the transfer film tended to consist of larger sized debris that was deposited more irregularly. This became clearly noticeable for 50 wt% and 60 wt% composites, which had significantly more exposed counterface but still fine debris. The samples with 70 wt% and 90 wt% filler, having significantly larger debris deposited irregularly in streaked regions, were the pinnacle of qualitatively poor quality transfer films observed out of all the composites.

Among the most interesting observations of transfer film quality is the marked difference between those formed in dry nitrogen and humid air. In particular, the transfer films of 20-40 wt% filled composites appeared completely different, despite nearly identical wear rates. The transfer films developed in humid environment were relatively more thick and coherent than their counterparts from dry conditions. Yet, there were still notable variations in film quality amongst those formed in humid air. Qualitatively, the 20 wt% PEEK-PTFE composite formed in humid air had the best quality transfer film and is visually indistinguishable from the well-studied transfer film of ultralow wear alumina-PTFE [75, 77]. Compared to this standard, in humid conditions the lower filled composites were progressively more patchy and higher filled composites had more streaks of exposed counterface or thick debris.

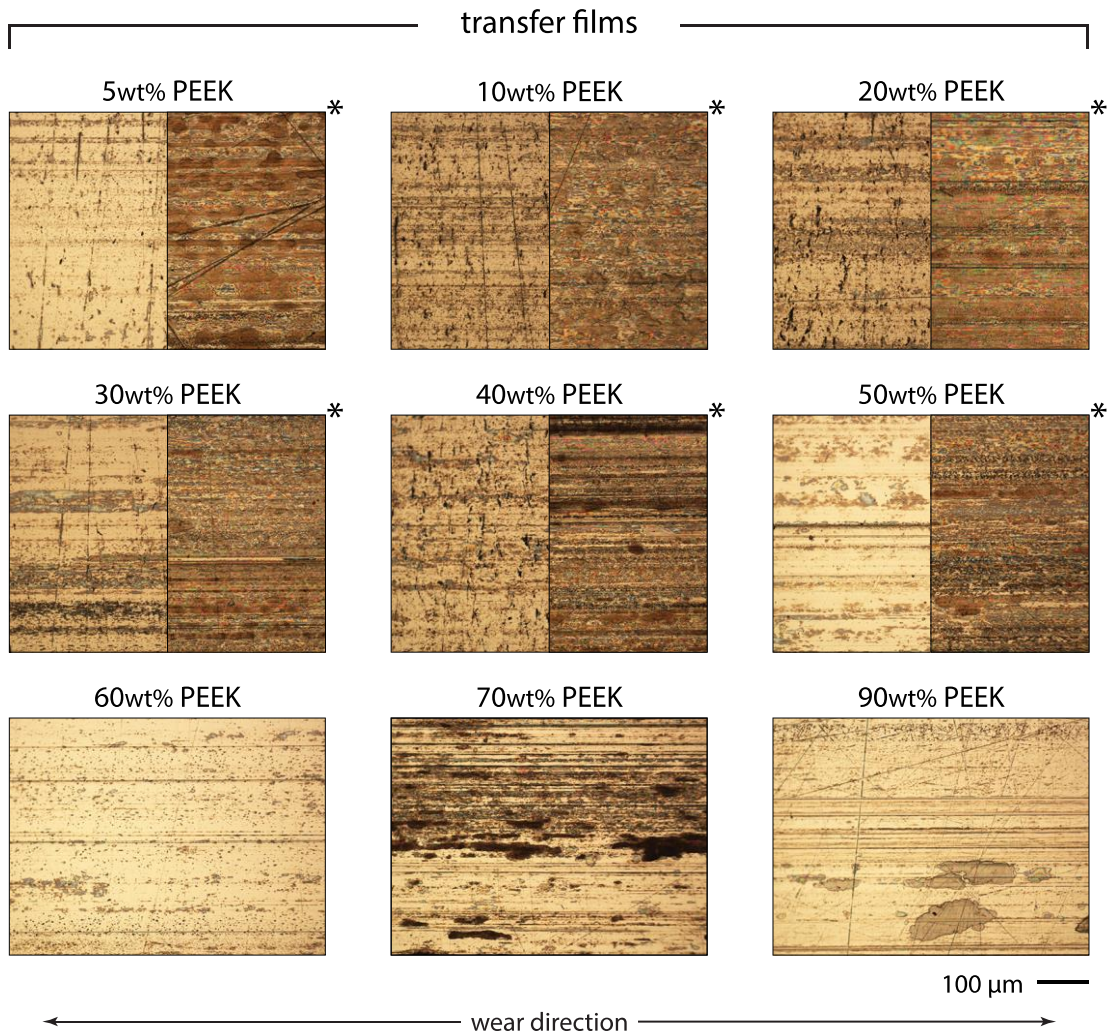


Figure 6-6 Representative images of transfer films after test termination for PTFE-based composite filled with PEEK ranging from 5-90 wt% in dry nitrogen environment and 5-50 wt% in humid air environment indicated by the \* symbol. Image adapted and reprinted with permission from [93].

Although qualitative assessment of transfer films has been practiced for decades, reliable methods for a quantitative analysis have recently become available [18, 70–74, 80]. In particular, a study conducted on common polymers and polymer composites, with a wide range in bearing performance, identified polymer wear rate as having a correlation strength of poor for thickness, good for area fraction, and best for free-space length [80]. Due to the poor reliability of predicting polymer wear rate with film thickness, it was not a metric employed by this study. For all samples in this study, the transfer films were measured for the two metrics of area covering the counterface (area fraction,  $X$  (-)) and the average size of gaps in the film exposing the counterface (free-space length,  $L_f$  ( $\mu\text{m}$ )) [71, 106]. The results for polymer wear rate as a function of each of these metrics were plotted in Figure 6-7 and listed in Table 6-2. Regarding area fraction, it was expected to observe increased coverage corresponding to decreased wear rate, because reduced interfacial contact should lessen debris formation [80]. Counter to expectation, the compilation of all PEEK-PTFE composite data for wear rate vs. area fraction were widely scattered. However, separating the results by testing environment reveals this scatter was due to the superposition of two independent trends. First, it was observed that films formed in dry nitrogen environment have relatively low values for area fraction, which were grouped in a column-like formation from approximately 10-40% coverage of the counterface. Second, the films developed in humid air environment were observed to correlate increased area fraction to decreased polymer wear rate, though there is some grouping of data points above 60% coverage and below  $3 \times 10^{-7} \text{ mm}^3/(\text{Nm})$  wear rate. Whereas the results of area fraction were strongly dependent on testing environment, the metric of free-space length appeared to have one general trend for the entire

dataset. It was expected that as the free-space length decreased, hence the size of adhesive zones that dominate polymer debris size and volume loss were reduced, there would be a corresponding decrease in wear rate. Overall, there was a trend of improved wear rate for smaller free-space length in the transfer film. It is also noteworthy that the results of free-space length values indicated even moderate wear resistance polymers formed films with relatively low free-space length, and much of the data was collected in a column from about 10-25  $\mu\text{m}$ .

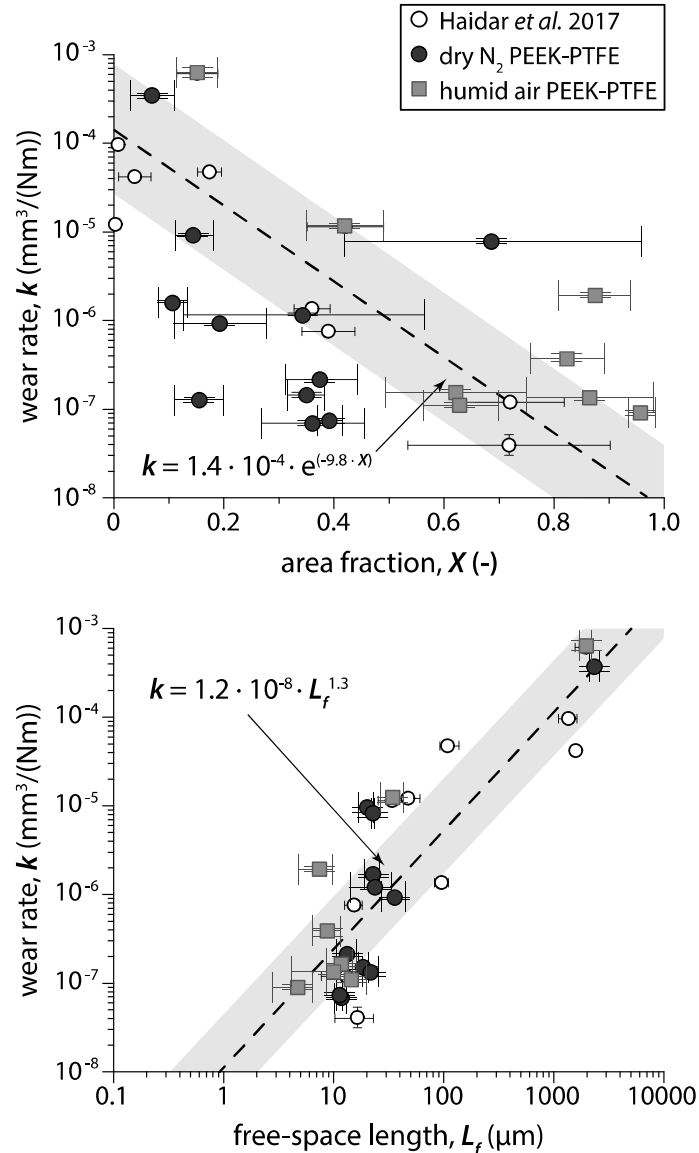


Figure 6-7 Polymer wear rate as a function of transfer film area fraction (top) and free-space length (bottom). Expected correlation is predicted by the results of common polymers and polymer composites (white circles), the calculated best-fit trendline (dashed line), and mean variation (grey shaded region) for each morphology metric [80]. The correlation of PEEK-PTFE composites wear rate to area fraction was poor for dry testing conditions (dark grey circles) and moderate for humid testing conditions (light grey squares). For the metric of free-space length in relation to wear rate, the PEEK-PTFE system had moderate correlation across both environmental conditions. Image adapted and reprinted with permission from [80].

Table 6-2 The complete dataset of wear rates and transfer film topological metrics quantified in this study. The wear test was conducted in a dry nitrogen environment unless indicated by the \* symbol as a humid environment. All metric values are reported as the mean  $\pm$  95% confidence interval (N=5).

<b>material</b>	<b>wear rate, <math>k</math> (<math>10^{-6}</math> mm<sup>3</sup>/(Nm))</b>	<b>area fraction, <math>X</math> (%)</b>	<b>free-space length, <math>L_f</math> (<math>\mu</math>m)</b>
100 wt% PTFE	340 $\pm$ 21	7 $\pm$ 4	2300 $\pm$ 230
* 100 wt% PTFE	610 $\pm$ 83	15 $\pm$ 4	2000 $\pm$ 260
5 wt% PEEK-PTFE	0.13 $\pm$ 0.007	16 $\pm$ 5	21 $\pm$ 4
* 5 wt% PEEK-PTFE	1.9 $\pm$ 0.07	87 $\pm$ 7	7 $\pm$ 2
10 wt% PEEK-PTFE	0.068 $\pm$ 0.005	36 $\pm$ 9	11 $\pm$ 2
* 10 wt% PEEK-PTFE	0.37 $\pm$ 0.04	82 $\pm$ 7	9 $\pm$ 2
20 wt% PEEK-PTFE	0.073 $\pm$ 0.005	39 $\pm$ 2	11 $\pm$ 1
* 20 wt% PEEK-PTFE	0.089 $\pm$ 0.006	96 $\pm$ 2	5 $\pm$ 2
30 wt% PEEK-PTFE	0.14 $\pm$ 0.008	35 $\pm$ 3	19 $\pm$ 2
* 30 wt% PEEK-PTFE	0.13 $\pm$ 0.005	86 $\pm$ 11	10 $\pm$ 6
40 wt% PEEK-PTFE	0.21 $\pm$ 0.011	38 $\pm$ 6	13 $\pm$ 3
* 40 wt% PEEK-PTFE	0.16 $\pm$ 0.007	62 $\pm$ 13	12 $\pm$ 3
50 wt% PEEK-PTFE	0.91 $\pm$ 0.027	20 $\pm$ 8	36 $\pm$ 9
* 50 wt% PEEK-PTFE	0.11 $\pm$ 0.006	63 $\pm$ 7	14 $\pm$ 5
60 wt% PEEK-PTFE	1.6 $\pm$ 0.06	11 $\pm$ 3	22 $\pm$ 4
70 wt% PEEK-PTFE	1.1 $\pm$ 0.03	35 $\pm$ 22	24 $\pm$ 9
90 wt% PEEK-PTFE	9.0 $\pm$ 0.41	15 $\pm$ 4	20 $\pm$ 3
100 wt% PEEK	7.8 $\pm$ 0.44	69 $\pm$ 27	22 $\pm$ 20
* 100 wt% PEEK	11 $\pm$ 0.7	42 $\pm$ 7	34 $\pm$ 9

The optical image of each PEEK-PTFE composite sliding surface following test termination is shown in Figure 6-8. Although transfer films are generally assessed with high magnification, a requisite of measuring the metric of free-space length that is on the order of a few microns for many advanced performance bearing systems, running films are commonly viewed for macroscopic traits [68, 77, 80, 86, 91]. In dry nitrogen environment, the running films for 10 wt% and 20 wt% filler were nearly identical in having a large patch of red-brown discoloration covering a third of the surface. The composites of 5 wt% and 30 wt% produced running films with this same discoloration, though for 5 wt% it was a light haze across the surface and for 30 wt% it only covered localized areas of 100-300  $\mu\text{m}$  in size. Composites with 40 wt% or more filler did not show signs of the red-brown discoloration, though they did occasionally show dark brown streaks oriented in the direction of sliding.

The polymer sliding surfaces produced in humid air were fairly similar to those from dry conditions. However, only the 20 wt% filled sample in humid conditions expressed a red-brown discoloration in the running film, and the morphology was streaky across the entire surface instead of localized. All other composites had no significant surface discoloration, only the lightest brown streaks in the direction of sliding were occasionally observed.

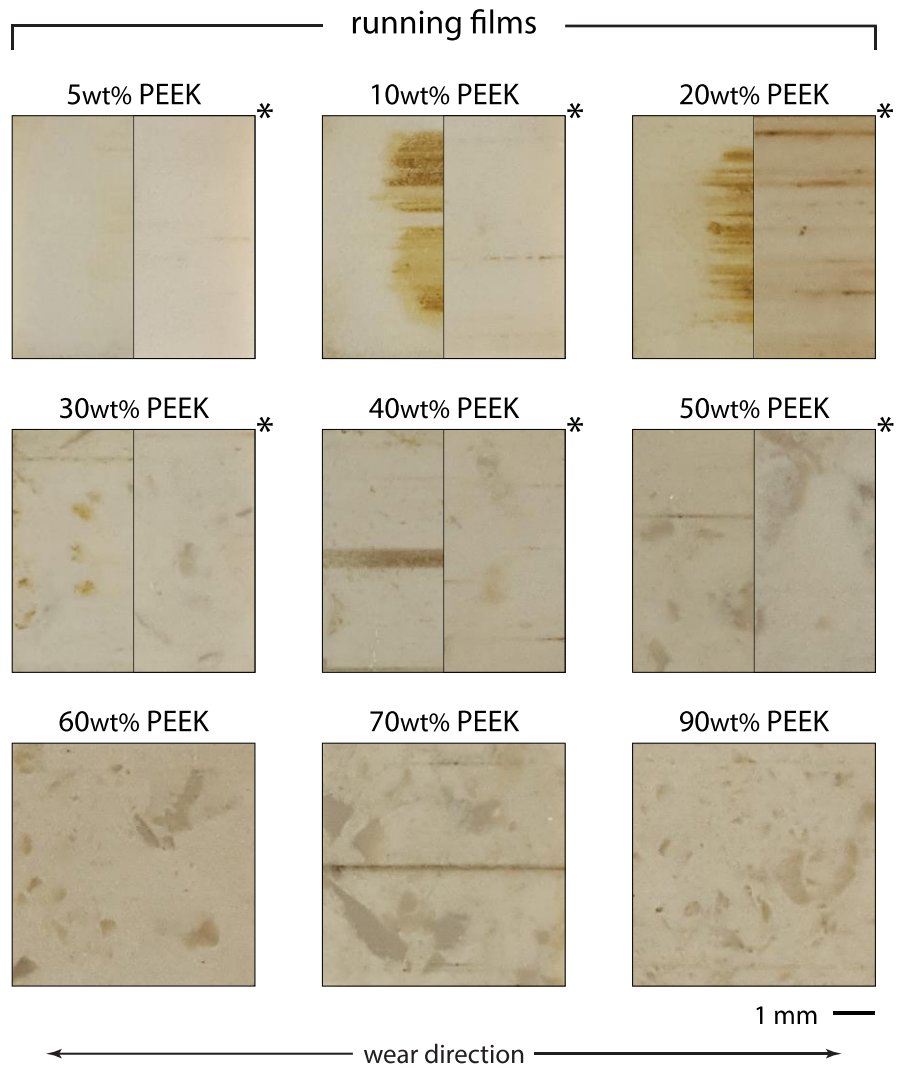


Figure 6-8 Images of running films after test termination for PTFE-based composite filled with PEEK ranging from 5-90 wt% in dry nitrogen environment, and 5-50 wt% PEEK in humid air environment indicated by the \* symbol. Image adapted and reprinted with permission from [93].

After wear testing, the chemical spectrum of each polymer's sliding surface was acquired using a Fourier-transform infrared (FTIR) spectrometer with a smart orbit attenuated total reflectance (ATR) accessory. In order to overlay the chemical spectra of composites with varying quantities of PEEK and PTFE on the same plot, each spectrum was normalized individually. In this context, normalization requires one or more FTIR-ATR peaks to sum to 1. The chemical spectrum of neat PTFE had two large peaks at 1200 and 1150  $\text{cm}^{-1}$ . For the global maximum of neat PTFE to equal to 1 after normalization, the highest intensity peak 1150  $\text{cm}^{-1}$  was selected to be part of the normalization process. In contrast to the simplicity of the PTFE spectrum, neat PEEK had nearly a dozen peaks to choose from between 1,800 and 1,000  $\text{cm}^{-1}$  with about four having notably higher intensity than the rest (1490, 1220, 1190, and 1160  $\text{cm}^{-1}$ ). Although any of these peaks with strong signal strength would have been adequate, 1490  $\text{cm}^{-1}$  was selected to be part of the normalization process specifically because this peak is not shared by PTFE nor alumina-PTFE after tribochemistry and thus would not confound the results.

The outcome of a normalization process that sums the intensities of the peaks at 1490 and 1150  $\text{cm}^{-1}$  to 1 is shown in Figure 6-9. For neat PTFE, the intensity of  $\sim 0$  at 1490  $\text{cm}^{-1}$  results in an intensity of  $\sim 1$  at 1150  $\text{cm}^{-1}$ . For the more complex PEEK spectrum, the intensities at 1490 and 1150  $\text{cm}^{-1}$  are nearly equal. Therefore, the spectrum of neat PEEK has the intensity of approximately 0.5 at 1490  $\text{cm}^{-1}$  and 0.5 at 1150  $\text{cm}^{-1}$ . By normalizing absorbance with the method presented, the FTIR-ATR chemical spectra of composite with any ratio of PEEK to PTFE can be viewed together without arbitrarily inflating or deflating the signal intensities.

The chemical spectra of the running surfaces developed by the reference materials 100% PEEK and 100% PTFE in both environmental conditions are presented in Figure 6-9. The clear overlap of spectra from both environments suggests neither neat polymer material undergoes tribochemical change.

The running films developed by all PEEK-PTFE composites in both dry nitrogen environment and humid air environment are shown in Figure 6-10. A general trend is observed that as PEEK filler loading in PTFE increases incrementally by 10 wt%, each of these composite spectra appear less like PTFE ( $\sim 0$  absorbance above  $1200\text{ cm}^{-1}$ ) and look more like PEEK (5 peaks form above  $1200\text{ cm}^{-1}$  including those at  $1650$  and  $1280\text{ cm}^{-1}$  with an absorbance approaching  $\sim 0.2$ ).

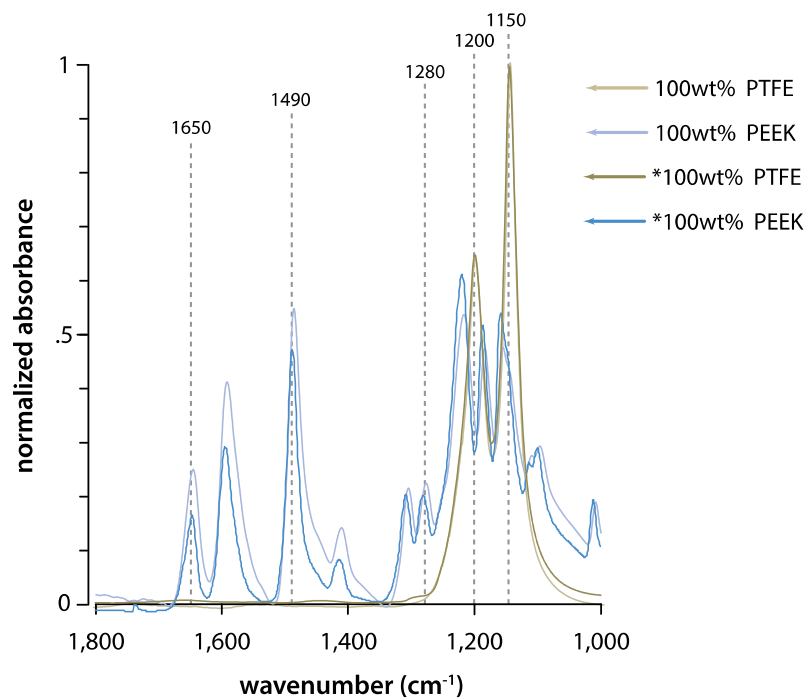


Figure 6-9 FTIR-ATR spectra of polymer running films after test termination for reference samples of 100% PEEK and 100% PTFE tested in dry N<sub>2</sub> environment (<0.05% RH) and humid air environment indicated by the \* symbol (30% RH). Image adapted and reprinted with permission from [93].

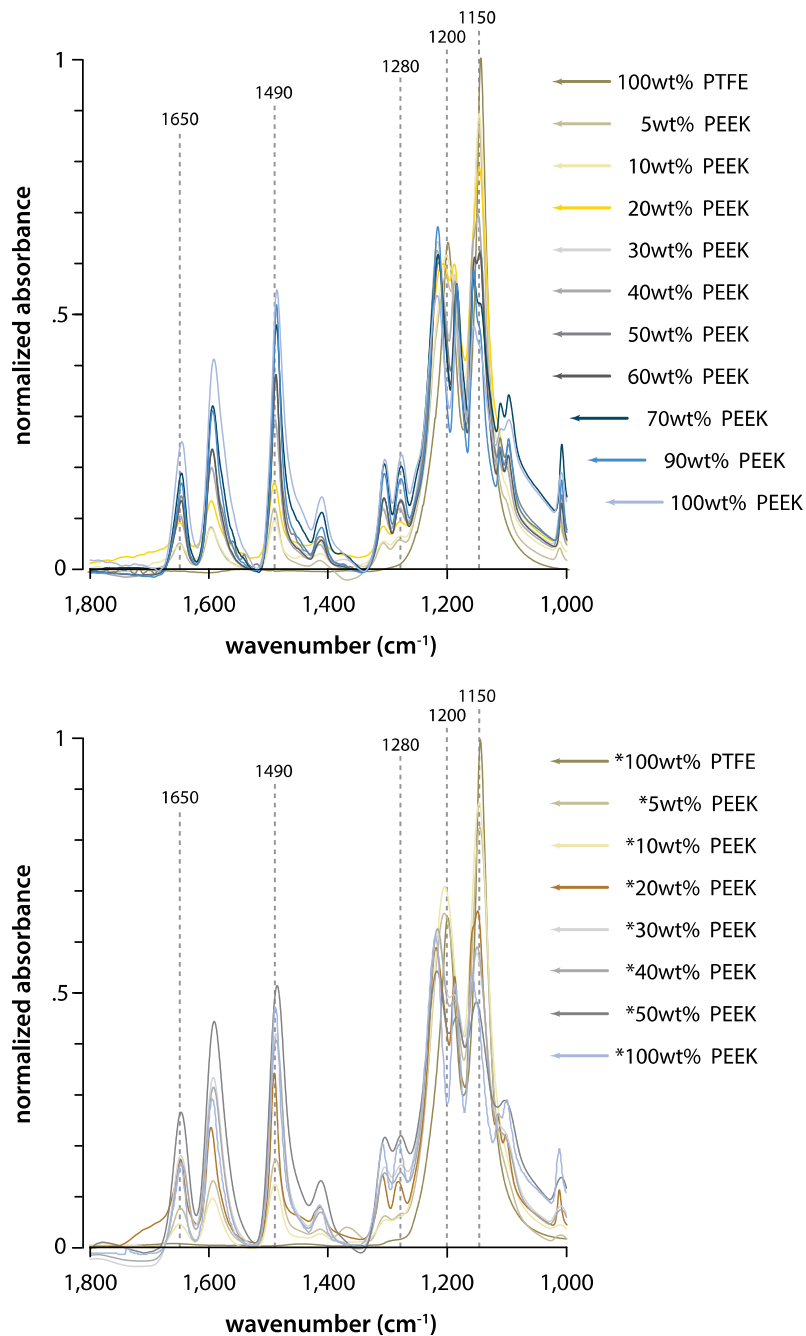


Figure 6-10 FTIR-ATR spectra of polymer running films after test termination for all PEEK-PTFE composites tested in dry N<sub>2</sub> environment (top) and humid air environment (bottom). All samples were tested in dry nitrogen environment (<0.05% RH), unless indicated by the \* symbol as a humid air environment (30% RH). Image adapted and reprinted with permission from [93].

Although the PEEK-PTFE composite running films each possessed a unique FTIR-ATR spectrum, they were all directly comparable by the ratio of peak-to-peak signal strengths. Using the three PEEK peaks of 1650, 1490, and 1280  $\text{cm}^{-1}$  to the peak at 1150  $\text{cm}^{-1}$  with PTFE influence, variations in chemical composition of PEEK-PTFE unworn material versus polymer sliding surface in both environments are shown in Figure 6-11. By comparing changes in three PEEK peaks, an overall trend was observable in the ratio of PEEK to PTFE without misrepresentation from potentially new chemistry.

With regards to the unworn material, it was expected that increasing PEEK filler loading would directly result in increasing signal intensity for all three PEEK peaks of 1650, 1490, and 1280  $\text{cm}^{-1}$  compared to the peak at 1150  $\text{cm}^{-1}$  with PTFE influence. This expected result was found, as there was a monotonic trend for all three ratios increasing as content of PEEK in PTFE of unworn material increased, though individually the 1650/1150  $\text{cm}^{-1}/\text{cm}^{-1}$  had some irregularity in the trend whereas 1490/1150 and 1280/1150  $\text{cm}^{-1}/\text{cm}^{-1}$  were more robust. By further inspecting the visual representation of ratios in Figure 6-11, or reviewing the data listed in Appendix B, it was noticed that 40 wt% PEEK-PTFE unworn was a clear outlier. This result could have been due to the 40 wt% sample having a less uniform filler-matrix distribution at the surface than other samples measured.

For composites with a high filler loading of 50 wt% PEEK or more in PTFE, tested only in dry environment, results were used to indicate that the PEEK signal at the sliding surface was approximately equal to or slightly less than the unworn material. However, a different pattern was observed for composites with a lower filler loading of 30 wt% PEEK or less in PTFE. Whether moisture was present or absent,

composites with 30 wt% or less PEEK-PTFE had a much stronger PEEK signal present at the sliding surface after testing than the unworn bulk material. This observation was surprising, since there was less PEEK material available in the least filled composites. The significance of this trend was reflected by the PEEK signal at the sliding surface being stronger than the PEEK signal in the unworn PEEK-PTFE material by an average of 3x for  $1650/1150\text{ cm}^{-1}/\text{cm}^{-1}$ , 3x for  $1490/1150\text{ cm}^{-1}/\text{cm}^{-1}$ , and 2x for  $1280/1150\text{ cm}^{-1}/\text{cm}^{-1}$ , which were calculated using values listed in Appendix B.

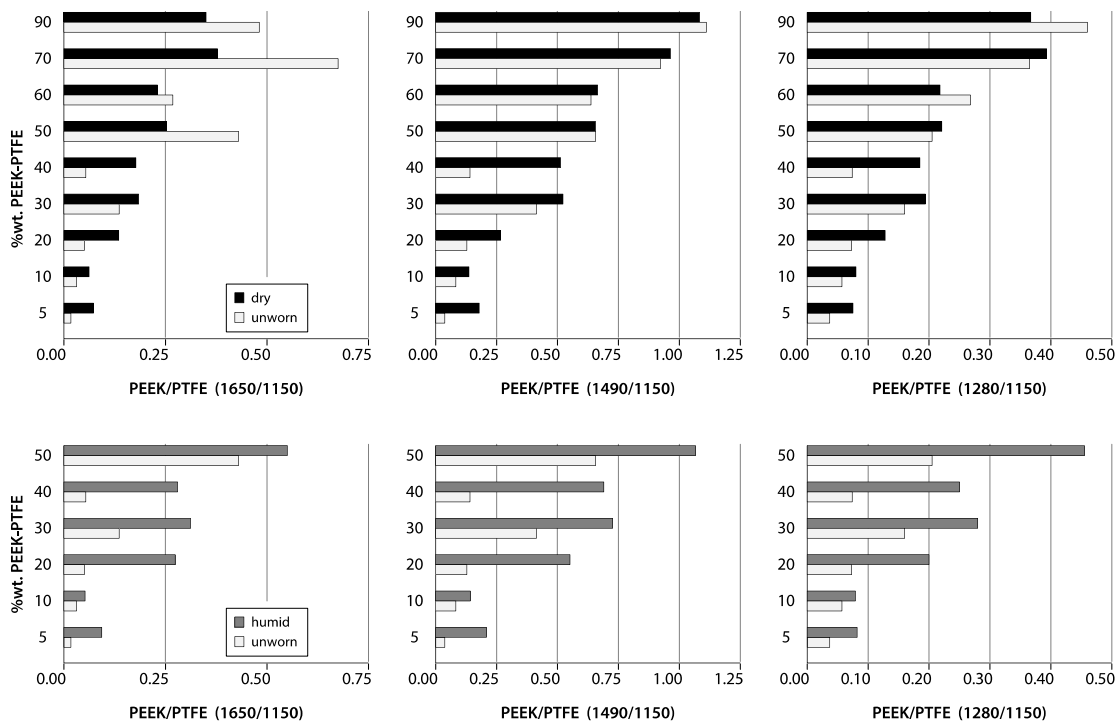


Figure 6-11 FTIR-ATR peak ratios displayed the signals of PEEK (1650, 1490, 1280  $\text{cm}^{-1}$ ) to PTFE (1150  $\text{cm}^{-1}$ ) for all PEEK-PTFE composite unworn surfaces and running films. Three PEEK peaks were used to observe an overall trend in the ratio of PEEK versus PTFE without misrepresentation from potential new chemistry. Tests were conducted in dry  $\text{N}_2$  environment (top) and humid air environment (bottom). Results indicated that 30 wt% PEEK or less in PTFE in both testing conditions show stronger PEEK signals at the sliding interface than bulk material. This trend was exacerbated in higher PEEK loading only for humid testing conditions.

The FTIR spectrum of the polymer sliding surface from the best tribological performer across both environments, 20 wt% PEEK-PTFE composite, is shown in Figure 6-12. The similarities between the 20 wt% PEEK-PTFE composite tested in dry and humid environment were observable throughout the chemical spectrum. The running films developed in both testing environments displayed the same variation from unworn material, which included a slight lifting around the 3300  $\text{cm}^{-1}$  peak, significant broadening plus signal increase around the 1650  $\text{cm}^{-1}$  peak, and significant signal increase at the 1490  $\text{cm}^{-1}$  peak.

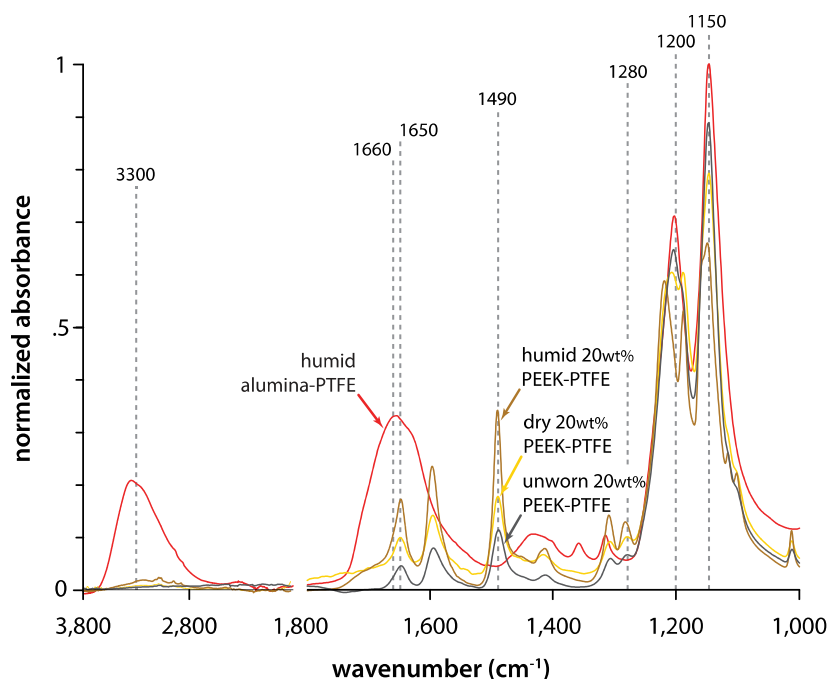


Figure 6-12 FTIR-ATR spectra of polymer running films after test termination for composites of 20 wt% PEEK-PTFE tested in dry and humid environments. These running films were compared to both the unworn 20 wt% PEEK-PTFE and the running film formed in humidity by the alumina-PTFE composite from literature [91]. Image adapted and reprinted with permission from [91, 93].

For the well-known alumina-PTFE composite from literature, also shown in Figure 6-12, chemical change at the sliding interface from testing in humid air environment was attributed to the formation of carboxylic acid on ends of PTFE fibrils [84, 89–91]. In these studies, tribochemistry was identified by the growth of significantly strong and broad peaks, including those around 3300 and 1660  $\text{cm}^{-1}$ . Due to the similar wavenumbers involved in the chemical spectra of running films from 20 wt% PEEK-PTFE and alumina-PTFE, visual identification was not adequate for comparing chemistry involved in these two tribomaterials.

A comparison of 20 wt% PEEK-PTFE and alumina-PTFE running films was made using ratios of peak-to-peak signals at the wavelengths of interest identified above and shown in Figure 6-13. At the 3300  $\text{cm}^{-1}$  peak within the O-H stretching region [117], a strong signal for alumina-PTFE attributed to carboxylic acid was observed, whereas the PEEK-PTFE running film spectra showed low values similar to unworn alumina-PTFE lacking tribochemistry [84, 89–91, 93]. Hence, the slight lifting around the 3300  $\text{cm}^{-1}$  peak for 20 wt% PEEK-PTFE running films in both environments was not a significant indicator of new chemistry in the PEEK-PTFE system. For the alumina-PTFE peak at 1660  $\text{cm}^{-1}$  and PEEK peak at 1650  $\text{cm}^{-1}$  within the C=O stretching region and averaged as 1655  $\text{cm}^{-1}$  [117, 118], both alumina-PTFE and PEEK-PTFE running films displayed a significant signal in this area compared to their unworn reference [84, 89–91, 93]. Due to neat PEEK sharing a neighboring signal at 1650  $\text{cm}^{-1}$  peak [93, 118], this area of interest cannot be used to solely support nor discredit chemical similarities between the running films of alumina-PTFE and PEEK-PTFE. At the 1490  $\text{cm}^{-1}$  in the C=C region [117, 118], a strong signal was present for the PEEK-PTFE running film compared to unworn reference, whereas the

alumina-PTFE running film has a false signal due to a raise between its peaks at 1660 and 1430  $\text{cm}^{-1}$ . Due to neat PEEK sharing a signal at 1490  $\text{cm}^{-1}$  peak [93, 118], this area of interest supports the increased presence of PEEK on the running film compared to the unworn reference material. Based on the comparison of chemical spectra from FTIR, the 20 wt% PEEK-PTFE system had more notable differences than similarities with the tribochemistry behind the success of alumina-PTFE.

In sum, the results did not support the hypothesis that oxygen and hydrogen from PEEK filler facilitates tribochemical change of PTFE to form carboxyl end groups in environments absent of moisture. Notably, 20 wt% PEEK-PTFE composites were indicated as being capable of excellent wear performance without showing any measurable tribochemical change in both dry and humid conditions.

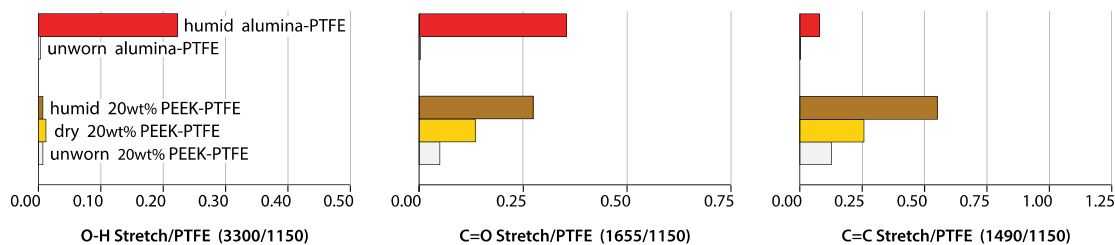


Figure 6-13 FTIR-ATR peak ratios displayed the signals of O-H Stretching ( $3300 \text{ cm}^{-1}$  within this region), C=O Stretching ( $1655 \text{ cm}^{-1}$  within this region), and C=C Stretching ( $1490 \text{ cm}^{-1}$  within this region) to PTFE ( $1150 \text{ cm}^{-1}$ ) for 20 wt% PEEK-PTFE running films formed in dry and humid environments. These running films were compared to both the unworn 20 wt% PEEK-PTFE material and the running film formed in humidity by the alumina-PTFE composite from literature [91]. Results indicated PEEK filler does not facilitate tribochemical change of PTFE in environments absent of moisture. Moreover, 20 wt% PEEK-PTFE displayed excellent wear performance without showing any measurable new tribochemistry in both dry and humid conditions.

### 6.3 Discussion

Solid lubricants are often utilized in bearing applications that prohibit the use of traditional oils and greases due to physical, chemical, thermal, or other environmental challenges. For mechanical systems in demanding applications, most notably the extreme conditions of space, these bearing materials necessitate a combination of moderate friction ( $\mu \leq 0.17$ ) and ultralow wear ( $k \leq 3 \times 10^{-7}$  mm<sup>3</sup>/(Nm)). Although several solid lubricants meet this level of advanced bearing performance (e.g. MoS<sub>2</sub> coatings, chameleon coatings, and alumina-PTFE bulk polymer composite) in a specific environment, none maintains this performance for many thousands of kilometers in sliding contact over the entire range in environmental conditions from terrestrial pre-launch activities through operation in space [29, 35, 40–43, 86, 87, 91]. These requirements preclude coatings due to their limited volume loss before lubricant starvation, and elevates the implementation of bulk polymeric solid lubricants. For the alumina-PTFE system, a dependence on moisture available in the operating environment for ultralow wear rates inhibits its application in dry environments (e.g. the vacuum of space). Although the alumina-PTFE system is not itself a solution to the persistent need of a solid lubricant with long lifetime and high efficiency for the aerospace industry, the large body of knowledge available from this well-studied system permits its use as model for improved tribomaterials design.

This study proposed to fulfill the three requirements of advanced bearing performance for a lubricious polymer matrix reinforced by a hard (e.g. metal or ceramic) filler material by instead utilizing a relatively soft micro-sized filler. Here, it was hypothesized that micro-sized PEEK in a PTFE matrix would 1) be sufficiently large to arrest matrix crack propagation, 2) be non-abrasive to the sliding interface, and 3) provide the elements of oxygen and hydrogen to support beneficial

tribochemical change for advanced bearing performance during wear testing in dry nitrogen (<0.05% RH) and humid air (30% RH) environments.

Previous studies on composites of PEEK-PTFE have shown a wide range in tribological results from moderate to advanced bearing performance in humid air environment [48, 53, 119–121]. Although the outcomes vary between studies, they all agreed that these composites have orders of magnitude lower wear rate than neat PTFE and 50-70% reductions in friction coefficient compared to neat PEEK. These notable improvements have been attributed to the superposition of each polymer's traits, the more wear resistant PEEK and lubricious PTFE. However, this does not explain the apparent synergistic effect of PEEK-PTFE composites, for which the combination has displayed better wear resistance than PEEK and lower friction than PTFE.

This synergistic effect, previously recognized for PEEK-PTFE composites in humid testing conditions, was also observed in this study for several PEEK-PTFE composites in both humid and dry testing environments. Results of this investigation showed 20-50 wt% PEEK in PTFE composites in humid air conditions and 5-40 wt% PEEK-PTFE composites in dry nitrogen testing environment displayed ultralow wear rates ( $k \leq 3 \times 10^{-7} \text{ mm}^3/(\text{Nm})$ ) and minimal material loss (1-3  $\text{mm}^3$ ) after thousands of kilometers sliding. This was an extraordinary outcome has labeled PEEK-PTFE materials as the first known ultralow wear rate solid lubricant, in addition to the first polymeric solid lubricant, to display tribological insensitivity to environmental moisture.

Although the 20 wt% PEEK-PTFE was noticeable for having the lowest wear rates across testing environments, all three filler loadings of 20, 30, and 40 wt% had

nearly identical ultralow wear resistance in both environmental conditions. Due to the similarity in their wear resistance, it was remarkable that the same composite compositions present significantly different looking transfer films between dry and humid conditions. A visual comparison of films from these composites revealed that those formed in humid conditions all appear relatively more coherent and uniform than those from dry environment. The appearance of better quality of films developed in humidity compared to dry conditions caused their equivalent wear rates to be a noticeable deviation from expectations. To best compare the traits of these transfer films, a quantitative analysis of the area fraction (percentage of the counterface's contact area covered by film) and free-space length (average size of gaps in the film exposing the counterface) were used.

According to the trends from literature, it was generally expected that polymers with ultralow wear rates ( $k \leq 3 \times 10^{-7} \text{ mm}^3/(\text{Nm})$ ) would have high area fraction ( $X \geq 60\%$ ) and low free-space length ( $L_f \leq 10 \text{ }\mu\text{m}$ ) [80]. The results for area fraction reveal the presence of two trends, which were dependent on environmental testing conditions. For transfer films formed in humid environment, the predicted trend of ultralow wear rate polymers forming films with area fraction values above 60% was observed. Counter to expectation, the transfer films developed in dry environment had low values of area fraction in the range of approximately 10-40%, even for those formed by ultralow wear rate composites. Unlike area fraction, the results for free-space length generally followed the one expected trend regardless of testing environment. It was observed that the transfer films formed by ultralow wear rate polymers had values of free-space length equal to or less than 21  $\mu\text{m}$  in dry conditions and 14  $\mu\text{m}$  in humid conditions. These outcomes indicated that free-space

length, but not area fraction, fulfilled the expectation of a transfer film metric suitable for universal correlation to polymer wear rate.

Notable outliers from the previously predicted correlation between transfer film metrics and wear rate was the transfer films were 70, 90, and 100% PEEK in PTFE. These majority PEEK-based composites and neat PEEK material generally had higher area fraction and lower free-space length values than expected for the moderate performance of the parent polymer [80]. In particular, the majority PEEK samples performed with moderate wear rates despite being capable of forming transfer films with the free-space length values expected necessary for supporting ultralow wear rates. This outcome could indicate the PEEK material in PEEK-PTFE composites has an important role in the development of quality transfer films.

In this study, composites with a majority PTFE and minority PEEK displaying ultralow wear have shown similar sliding interface conditions to alumina-PTFE. Regardless of moisture availability in the testing environment, the images of these PEEK-PTFE transfer films deposited on steel counterfaces showed an absence of large debris particles, which has indicated successful arrest of crack development by filler in the bulk for the alumina-PTFE system [63, 65]. In addition, none of the PEEK-PTFE composites showed signs of abrasion to the counterface, as predicted for soft fillers with true micro-size due to the much lower hardness of PEEK compared to alumina [2, 110–112]. Furthermore, the ultralow wear PEEK-PTFE composites had transfer films that did not indicate the parent polymer preferentially removing transfer film, as expected for PEEK and PTFE due to their much lower surface energy compared to steel [2, 78, 113–115]. These observations indicated that PEEK-PTFE composites had stable interface conditions for quality transfer film development that generally lead to

ultralow wear rates [18, 19, 24, 65]. In effect, the first two hypotheses of this study were supported – a requisite for ultralow wear of a PTFE-based composite is having a filler material that is sufficiently hard to arrest crack propagation in the bulk but is non-abrasive to the sliding interface. This outcome revealed that ultralow wear rates of PTFE composites can be achieved by the incorporation of either a hard filler material with multi-scale functionality or a soft micro-sized filler that is both much softer than steel and harder than PTFE.

In the current model for alumina-PTFE, a requirement for a tenacious transfer film to form is having moisture available in environment for tribochemistry to strongly bond the PTFE debris to the counterface [23, 78]. Since the amount of debris formed by the parent polymer to maintain the transfer film is the minimum possible wear rate of the system, it is necessary for the transfer film to tenaciously adhere and resist removal to minimize the polymer wear rate [19, 23, 24, 78]. For the model proposed by this study, incorporating a relatively soft filler in lubricious matrix, the requirement of tribochemistry was expected for the PEEK-PTFE system to perform with ultralow wear.

For this study, the selection of a micro-sized polymer filler material was primarily based on the molecular structure including both oxygen and hydrogen atoms. With this setup, it was possible to test whether degraded filler could provide the necessary elements for tribochemistry of PTFE in environments absent of moisture. The polymer selected to fulfill this role was PEEK due to its high melting temperature compared to other polymers, moderate wear resistance, and lower friction coefficient in dry environment than humid air [48, 116]. The wear testing PEEK-PTFE composites in dry nitrogen environment (<0.05% RH) compared to humid air

(30% RH) showed a difference in results for moisture available and moisture starved conditions.

In this study, the 20 wt% PEEK-PTFE composite had the lowest wear rate of all composites tested in humid air conditions. By selecting this material for comparison to the alumina-PTFE system in humid conditions, significant similarities were noticed at the sliding interfaces. For these two systems, the transfer films were visually indistinguishable and running films possess a similar red-brown discoloration. In the alumina-PTFE system, the onset of these traits was attributed to mechanically broken PTFE fibrils forming carboxylates that chemically bond to the metallic counterface for a tenaciously adhered transfer film [84, 89, 90]. To determine whether carboxylate formation was present at the sliding interface of 20 wt% PEEK-PTFE composite, generating these shared visual traits and contributing to tribological success, chemical analysis was necessary.

Chemistry was investigated using FTIR-ATR spectroscopy of the running films. For 20 wt% PEEK-PTFE, the spectrum was collected from unworn material and the running film after test termination for comparison to the alumina-PTFE composite from literature [91]. To examine these spectra, three ratios of peak-to-peak signal intensities were used. From the results, it was determined that the characteristic strong signal at  $3300\text{ cm}^{-1}$  (within the O-H Stretching region) for alumina-PTFE's carboxylic acid has no significant presence in the PEEK-PTFE spectra [91, 117, 118]. In addition, the most notable signal change for 20 wt% PEEK-PTFE from unworn to worn surface was a 4x increase at  $1490\text{ cm}^{-1}$  (within the C=C Stretching region), which was absent in the alumina-PTFE system and attributed to PEEK material originating from the PEEK-PTFE composite bulk [91, 117, 118]. Contrary to

expectation, these results have indicated an absence of perfluorinated carboxylic acid in the PEEK-PTFE system. This outcome indicated that the third hypothesis of this study was not supported – the PEEK-PTFE system studied appeared capable of developing transfer films that promoted advanced bearing performance without measurable new chemistry. Instead, spectra was used to indicate that PEEK from the bulk composite accumulated at the sliding interface. This PEEK accumulation was credited with permitting the PEEK-PTFE composite to form a transfer film with sufficiently strong bonds between polymer debris and the metallic counterface for supporting ultralow wear rates.

Although the results of chemical analysis did not support the tribochemical change of degraded PTFE, they can provide insight into the mechanism driving the formation of sufficiently protective transfer films for ultralow wear of PEEK-PTFE composites. An analysis was conducted on the change to the 1490/1150  $\text{cm}^{-1}/\text{cm}^{-1}$  peak-to-peak ratio before and after wear testing in humid environment. The results showed the PEEK-PTFE composite running film had an increased PEEK signal of 3x relative to unworn material, regardless of polymer wear rate. This significant increase in PEEK signal for composites that are minority PEEK material indicated an accumulation of PEEK at the sliding interface. This accumulation could be explained by a recent study of transfer films formed by PEEK-PTFE composites, in which density functional theory was used to simulate PTFE and PEEK adsorption to a metallic counterface [122]. Molecules of chemically stable fluorocarbon  $\text{C}_5\text{F}_{12}$ , diphenyl ether  $\text{O}(\text{C}_6\text{H}_5)_2$ , and benzophenone  $\text{CO}(\text{C}_6\text{H}_5)_2$  were each subject to simulation with an aluminum atom (fluorine or oxygen atom positioned closest to aluminum atom), resulting in adsorption energies of negative 50, 250, and 285 kJ/mol,

respectively. Due to PTFE's inherent inertness [81, 82], it was found that PEEK derivatives were over 5x more likely to adsorb to the metallic surface [122]. To compare, the alumina-PTFE system's tenacious transfer film can be attributed to ionic bonds of Fe-O 409 kJ/mol and/or covalent bonds of C-O and C-C 350 kJ/mol bond dissociation energy [123, 124]. Thus, it is reasonable for the PEEK component of PEEK-PTFE composites, with an adsorption energy of nearly 300 kJ/mol, to form a transfer film strongly adhered to the counterface during sliding contact and support ultralow polymer wear rates. This argument was upheld by the PEEK-PTFE system generally showing an accumulation of PEEK on the running film for majority PTFE composites and an overall absence of perfluorinated carboxylic acid regardless of environmental moisture. In effect, the PEEK-PTFE system developed transfer films that support advanced bearing performance without new chemistry to improve bonding polymer debris to the metallic counterface.

The 20 wt% PEEK-PTFE composite, the material with the best wear resistance across both environments, displayed a wear rate of  $k = \sim 8 \times 10^{-8} \text{ mm}^3/(\text{Nm})$ . This result marked 20 wt% PEEK-PTFE as 100x more wear resistant than PEEK and 4,000x more wear resistant than PTFE. Moreover, the friction coefficient of this composite was relatively insensitive to environmental moisture. For 20 wt% PEEK-PTFE, the steady-state friction coefficient in both environments was slightly higher than neat PTFE regardless of moisture and higher than neat PEEK in environment devoid of moisture by 20%. Notably, the friction of 20 wt% PEEK-PTFE was 65% improved over neat PEEK in ambient conditions. The combination of moderate friction and ultralow wear marked 20% PEEK-PTFE as the first known solid lubricant, in addition to polymeric solid lubricant, to display advanced bearing performance in environments

with variable moisture. Thus, using the alumina-PTFE system as a model for improved tribomaterial design successfully identified the 20 wt% PEEK-PTFE composite as the first material to meet the demanding tribological applications of the aerospace industry.

## 6.4 Conclusions

This study aimed to employ the current filler theory for a hard (e.g. metal or ceramic) filler in lubricious polymer matrix in improving tribomaterials design. Here, it was hypothesized that the three requirements for the alumina-PTFE system to produce ultralow wear rates could be satisfied for a composite consisting of a relatively soft micro-sized PEEK filler in lubricious PTFE matrix. For a hard filler material, it is necessary for micro-scale reinforcement in the bulk to arrest crack propagation and nano-scale polishing at the interface to avoid abrasion for the development of a quality transfer film. In this study, an analysis of PEEK-PTFE transfer film quality found area fraction to be unreliable metric in relation to wear rate. However, the metric of free-space length was determined to have good correlation between film quality and wear rate for PEEK-PTFE composites, confirming that ultralow wear composites had low values of free-space length ( $L_f \leq 10 \mu\text{m}$ ). These composites did not present large debris particles, signs of abrasion to the counterface, nor indicate the parent polymer preferentially removed transfer film. This outcome indicated that a soft micro-sized filler material, much softer than steel but harder than PTFE, successfully fulfilled the first two requirements of arresting matrix crack propagation and being non-abrasive to the sliding interface. In effect, multi-scale functionality of the filler is not a requirement of ultralow wear. Instead, it is necessary to produce transfer films with low free-space length and high tenacity, as consistent with transfer films formed from fine debris and stable interface sliding.

The third requirement of the current filler model for a hard filler in lubricious polymer matrix is beneficial tribochemistry that chemically bonds polymer debris to the counterface. Since the degradation of polymer bonds has been attributed to the shear forces during sliding, it was expected that the PEEK-PTFE composites with

ultralow wear rates would undergo tribochemical change. However, it was observed that PEEK-PTFE composites displayed advanced bearing performance without the appearance of new chemistry, regardless of environmental moisture. Instead of new chemistry forming covalent bonds between degraded polymer debris and steel counterface, spectra analysis supports the accumulation of PEEK on the steel counterface. Other studies proposing that PEEK adsorption is strong enough to form a tenacious transfer film is supported by this investigation's resulting ultralow wear rate PEEK-PTFE composites, since the wear rate of the transfer film is the lower limit wear rate of the system. Therefore, new chemistry is not a requirement of producing transfer films with the protective qualities and long lifetime necessary to support an ultralow wear system.

The current filler theory for ultralow wear polymer composites was developed by the breadth of literature on alumina-PTFE system. In testing the application of this model in informing the design of future tribomaterials, a soft micro-sized filler in lubricious polymer matrix was investigated for comparison. The PEEK-PTFE system investigated displayed ultralow wear rates without special filler functionality nor the influence of new chemistry. Therefore, this study has been the first to identify a bulk solid lubricant with advanced bearing performance in challenging conditions and variable environments, as indicated by Figure 6-14. Specifically, the PEEK-PTFE system possesses the potential for long lifetime and high efficiency in the bearing applications of terrestrial and space operations.

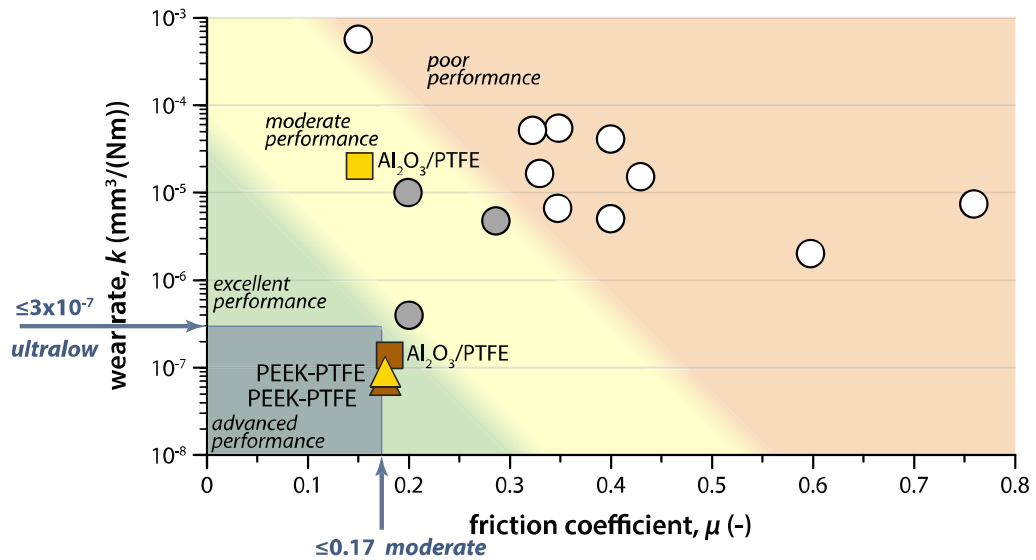


Figure 6-14 The PEEK-PTFE composite is the first solid lubricant identified to display advanced bearing performance in both humid (brown) and dry (yellow) conditions. The PEEK-PTFE system's 20 wt% composite (triangles) showed advanced bearing performance regardless of environmental moisture, which satisfy the needs of demanding applications that require both moderate friction ( $\mu \leq 0.17$ ) and ultralow wear ( $k \leq 3 \times 10^{-7} \text{ mm}^3/(\text{Nm})$ ). This was a significant improvement over the bearing performance of the alumina-PTFE system (squares), which has advanced bearing performance in humidity but poor performance in dry conditions. For reference, neat polymers often have poor bearing performance (white circles) [6, 22, 24, 46–50] and many polymer composites have moderate bearing performance (grey circles) [49, 56, 68, 79]. This scale was developed from a survey of bearing performance for traditionally lubricated compatible metals with poor, moderate, or excellent lubrication [2].

## 6.5 Recommendations for Future Work

This study investigated PEEK-PTFE composites using humid air (30% RH) and dry N<sub>2</sub> (<0.05% RH) environments to simulate conditions for terrestrial and space bearing applications. A relatively inert nitrogen gas was used to mimic space's absence of reactive elements and molecules, filled a large environmental chamber at positive pressure. This setup had the dual benefit of impeding the flow of ambient air contaminants into the chamber and fitting the current high-throughput tribometer within the chamber, which resulted in efficiently running a wide range of PEEK-PTFE composite materials in a controlled environment. An outcome of this study was identifying PEEK-PTFE as the solid lubricant with the highest potential for advanced bearing performance in the aerospace industry. To further test the bearing performance of these materials for space applications, a tribology study should be conducted on PEEK-PTFE composites in vacuo. By using a modified version of the high-throughput tribometer, or a similar equipment that simultaneously collects normal force and friction force, the bearing performance metric of friction coefficient can be calculated throughout testing. Some recommendations for conducting this study are offered here for consideration:

Tribometer Functionalities – In general, tribological experiments on polymeric materials in vacuo run continuously from test start through test termination [86, 125, 126]. For experiments under vacuum, wear rate is calculated from the total volume loss of the polymer sample, as opposed to being closely monitored with *in-situ* measurements. Although experiments in vacuo do not necessitate pausing and restarting for data collection, the tribometer within a vacuum chamber can easily be programmed to mimic similar periodic pauses without otherwise disrupting the tribology test. In this study, it was observed that each time the test was continued

following an *in-situ* mass measurement, the friction coefficient for a 20 wt% PEEK-PTFE composites spiked up in dry nitrogen conditions and dropped down in humid air conditions, eventually returning to a consistent equilibrium value. It is expected that a PEEK-PTFE composite undergoing testing within a vacuum chamber will also experience spikes in friction coefficient upon re-initiating sliding. Observing the presence or absence of this trait could provide more information into the behavior at the interface in relation to operating environment. Moreover, such an investigation would be best informed by collecting temperature values throughout testing, as temperature has been found to affect both the wear rate and friction coefficient of polymers and polymer composites [127, 128]. Similar to other studies, temperature data can be collected with a thermocouple attached to each counterface [91].

Sample Selection – It is recommended to run experiments with PEEK-PTFE composites already identified as having ultralow wear performance in humid air and dry nitrogen. With this criterion, the composites of interest are identified as 10, 20, 30, and 40 wt% PEEK in PTFE. Due to 20 wt% PEEK-PTFE displaying the lowest wear rate in both humid and dry environment, this sample has the highest priority for completing tribological tests in vacuo.

Vacuum Pressure – Each set of experiments should be completed at a single vacuum pressure. Information from literature on alumina-PTFE tribology in vacuo has indicated that ultralow wear rates are observed at vacuum pressures of  $10^3$  to  $10^{-3}$  Torr, and wear rates increase dramatically between vacuum pressures of  $10^{-3}$  and  $10^{-5}$  Torr [86]. Although further studies on alumina-PTFE may focus on changes in wear rate as a function of vacuum pressures between  $10^{-3}$  and  $10^{-5}$  Torr, a study on PEEK-PTFE in vacuo primarily requires comparable results between no vacuum and strong

vacuum conditions. It is recommended to conduct initial tests at vacuum pressures of  $10^3$  (reference to atmospheric pressure) and  $10^{-5}$  Torr (sufficiently significant vacuum to inhibit alumina-PTFE tribochemistry), in order to compare the differences in wear rate, friction coefficient, area fraction, free-space length, and interface chemistry between no vacuum and strong vacuum conditions. The expected outcome for the recommended laboratory study is PEEK-PTFE composites will display advanced bearing performance in both no vacuum and strong vacuum, and this tribomaterial should be further investigated through field testing by tribology researchers collaborating with members of the aerospace industry.

## Chapter 7

### FUTURE DIRECTIONS

#### 7.1 Dissertation Summary

This dissertation aimed to fulfill the needs of the aerospace industry by designing a polymer composite for advanced bearing performance in challenging environmental conditions. By employing the body of knowledge for a particular alumina-PTFE composite, a model was developed for tribological success of a hard filler in lubricious polymer matrix. For alumina-PTFE, advanced bearing performance was dependent on a hard filler having multi-scale functionality and an operating environment that supports beneficial tribochemistry. This study proposed to satisfy the current model requirements by replacing alumina with a relatively soft micro-sized filler that also supports tribochemistry in any environment. To test this alternate model, a tribology study on PEEK-PTFE composites was conducted. The results of this study identified the first solid lubricant to demonstrate advanced bearing performance in dry and humid conditions. The outcomes of this study indicated that advanced bearing performance was achievable without filler multi-scale functionality nor the development of new chemistry. The apparent success of this project suggests the potential to design more polymeric solid lubricant composites for demanding bearing applications.

## 7.2 Recommendations for Future Work

In this dissertation, an alternate model was proposed for a relatively soft micro-sized filler in lubricious PTFE matrix to display advanced bearing performance in challenging environments. Unlike the restrictions to filler selection in the alumina-PTFE model, for which a particular alumina material could satisfy the requirement of being a hard filler with multi-scale functionality, this project claimed many polymers could meet the two filler specifications for the alternate model. The first suggested requirement for this micro-sized filler was being much softer than steel but harder than PTFE, in order to have sufficient size and hardness to arrest crack propagation in the PTFE matrix without abrading the sliding interface. The second suggested requirement of the micro-sized filler was containing the elements oxygen and hydrogen to support beneficial tribochemistry in any environment. Although this study appeared to succeed by using PEEK to satisfy these filler requirements, further investigations are recommended to identify other successful filler materials and improve the understanding of the tribological mechanisms driving the success of polymer-PTFE composites.

It is recommended to conduct a tribology study on the bearing performance of PTFE-based composites with various micro-sized polymer filler materials. Selecting a wide range of polymers would permit observing the impact of the filler's traits, such as mechanical properties, surface energy, and material chemistry, on composite bearing performance. A study testing filler selection should employ some common polymers, which could include polyamide (nylon), polyimide (PI), polyethylene terephthalate (PET), polyethylene (PE), polyphenylene sulfide (PPS), and polystyrene (PS). Although different sample compositions can be studied, priority should be given to testing 20 wt% micro-sized polymer filler in PTFE composites and 100 wt%

polymer reference samples in humid air conditions. Each pair of polymer-PTFE composites and polymer references samples should have data collected for friction coefficient and wear rate throughout the experiment to assess bearing performance. Following testing, it is important to evaluate the transfer film metrics of area fraction and free-space length. Finally, FTIR spectroscopy should be utilized to compare chemical signals for the worn sliding interface and unworn bulk material.

The expected result for the recommended study is identifying some of the 20 wt% micro-sized polymer filler in PTFE composites as advanced bearing performers in humid air conditions. It is predicted that these tribologically successful polymer-PTFE composites will have similar findings as this study of PEEK-PTFE composites. The anticipated similarities include a synergistic effect of combined polymer and PTFE having better tribological performance than either polymer or PTFE alone. For these polymer-PTFE composites, advanced bearing performance is expected to be achieved without detecting new chemistry and with an apparent accumulation of polymer filler material at the sliding interface. In particular, it is expected that the wear rate for these 20 wt% polymer-PTFE composites will be best predicted by the free-space length of their 100 wt% polymer reference sample. The recommended study should test whether the synergistic effect of polymer-PTFE is a function of two separate roles being played by minority polymer filler, depositing a high quality and tenaciously adherent transfer film, and majority PTFE matrix, supporting low friction coefficient with low shear sliding and minimal transfer film removal with very low surface energy. Whether or not the outcomes of polymer-PTFE match those of PEEK-PTFE, the recommended investigation will enhance the understanding of tribological mechanisms driving the success of polymeric solid lubricant composites.

## REFERENCES

1. Jost, H.P.: The Introduction of a New Technology, Report from the Committee on Tribology. Her Majesty's Stationary Office, London (1966)
2. Rabinowicz, E.: Friction and Wear of Materials. Wiley-Interscience, New York (1995)
3. Pitenis, A.A., Dowson, D., Gregory Sawyer, W.: Leonardo da Vinci's Friction Experiments: An Old Story Acknowledged and Repeated. *Tribol. Lett.* 56, 509–515 (2014). doi:10.1007/s11249-014-0428-7
4. Bowden, F.P., Tabor, D.: The Area of Contact between Stationary and between Moving Surfaces. *Proc. R. Soc. Math. Phys. Eng. Sci.* 169, 391–413 (1939). doi:10.1098/rspa.1939.0005
5. Sawyer, W.G., Argibay, N., Burris, D.L., Krick, B.A.: Mechanistic Studies in Friction and Wear of Bulk Materials. *Annu. Rev. Mater. Res.* 44, 395–427 (2014). doi:10.1146/annurev-matsci-070813-113533
6. Burris, D.L., Boesl, B., Bourne, G.R., Sawyer, W.G.: Polymeric Nanocomposites for Tribological Applications. *Macromol. Mater. Eng.* 292, 387–402 (2007). doi:10.1002/mame.200600416
7. Axén, N., Hogmark, S., Jacobson, S.: Friction and Wear Measurement Techniques. In: *Modern Tribology Handbook, Two Volume Set*. CRC Press (2000)
8. Williams, J.A.: *Engineering tribology*. Cambridge University Press, New York (2005)
9. Mang, T., Bobzin, K., Bartels, T.: *Industrial tribology: tribosystems, friction, wear and surface engineering, lubrication*. Wiley-VCH, Weinheim (2011)
10. Fusaro, R.L.: Lubrication of space systems. *Lubr. Eng.* 51, 182–194 (1995)
11. Hilton, M.R., Fleischauer, P.D.: Applications of solid lubricant films in spacecraft. *Surf. Coat. Technol.* 54–55, 435–441 (1992). doi:10.1016/S0257-8972(07)80062-4
12. Lancaster, J.K.: Polymer-based bearing materials—The role of fillers and fibre reinforcement in wear. *Wear.* 22, 412–413 (1972). doi:10.1016/0043-1648(72)90402-4

13. Burris, D.L., Santos, K., Lewis, S.L., Liu, X., Perry, S.S., Blanchet, T.A., Schadler, L.S., Sawyer, W.G.: Polytetrafluoroethylene matrix nanocomposites for tribological applications. In: *Tribology and Interface Engineering Series*. pp. 403–438. Elsevier (2008)
14. Stachowiak, G.W., Batchelor, A.W.: *Engineering tribology*. Butterworth-Heinemann, Boston (2001)
15. Wang, Q.J.: *Encyclopedia of tribology*. Springer, New York (2013)
16. Pooley, C.M., Tabor, D.: Friction and Molecular Structure: The Behaviour of Some Thermoplastics. *Proc. R. Soc. Math. Phys. Eng. Sci.* 329, 251–274 (1972). doi:10.1098/rspa.1972.0112
17. Pooley, C.M., Tabor, D.: Transfer of PTFE and Related Polymers in a Sliding Experiment. *Nat. Phys. Sci.* 237, 88–90 (1972). doi:10.1038/physci237088a0
18. Bahadur, S., Tabor, D.: The wear of filled polytetrafluoroethylene. *Wear.* 98, 1–13 (1984). doi:10.1016/0043-1648(84)90213-8
19. Blanchet, T.A., Kennedy, F.E.: Sliding wear mechanism of polytetrafluoroethylene (PTFE) and PTFE composites. *Wear.* 153, 229–243 (1992). doi:10.1016/0043-1648(92)90271-9
20. Li, F., Hu, K., Li, J., Zhao, B.: The friction and wear characteristics of nanometer ZnO filled polytetrafluoroethylene. *Wear.* 249, 877–882 (2001). doi:10.1016/S0043-1648(01)00816-X
21. Unal, H., Kurtulus, E., Mimaroglu, A., Aydin, M.: Tribological Performance of PTFE Bronze Filled Composites under Wide Range of Application Conditions. *J. Reinf. Plast. Compos.* 29, 2184–2191 (2010). doi:10.1177/0731684409345617
22. Burris, D.L., Sawyer, W.G.: Tribological Sensitivity of PTFE/Alumina Nanocomposites to a Range of Traditional Surface Finishes. *Tribol. Trans.* 48, 147–153 (2005). doi:10.1080/05698190590923842
23. Bahadur, S., Gong, D., Anderegg, J.W.: The role of copper compounds as fillers in transfer film formation and wear of nylon. *Wear.* 154, 207–223 (1992). doi:10.1016/0043-1648(92)90155-2
24. Bahadur, S., Gong, D.: The action of fillers in the modification of the tribological behavior of polymers. *Wear.* 158, 41–59 (1992). doi:10.1016/0043-1648(92)90029-8

25. Bahadur, S.: The development of transfer layers and their role in polymer tribology. *Wear.* 245, 92–99 (2000). doi:10.1016/S0043-1648(00)00469-5
26. Ye, J., Burris, D., Xie, T.: A Review of Transfer Films and Their Role in Ultra-Low-Wear Sliding of Polymers. *Lubricants.* 4, 4 (2016). doi:10.3390/lubricants4010004
27. Miyoshi, K.: Solid lubrication fundamentals and applications. Marcel Dekker, New York (2001)
28. Yen, B.K.: Influence of water vapor and oxygen on the tribology of carbon materials with sp<sup>2</sup> valence configuration. *Wear.* 192, 208–215 (1996). doi:10.1016/0043-1648(95)06807-4
29. Lancaster, J.K.: A review of the influence of environmental humidity and water on friction, lubrication and wear. *Tribol. Int.* 23, 371–389 (1990). doi:10.1016/0301-679X(90)90053-R
30. Donnet, C., Le Mogne, T., Martin, J.M.: Superlow friction of oxygen-free MoS<sub>2</sub> coatings in ultrahigh vacuum. *Surf. Coat. Technol.* 62, 406–411 (1993). doi:10.1016/0257-8972(93)90275-S
31. Colas, G., Saulot, A., Regis, E., Berthier, Y.: Investigation of crystalline and amorphous MoS<sub>2</sub> based coatings: Towards developing new coatings for space applications. *Wear.* 330–331, 448–460 (2015). doi:10.1016/j.wear.2015.01.011
32. Johnson, M.R.: The Galileo high gain antenna deployment anomaly. Presented at the 28th Aerospace Mechanisms Symposium May 1 (1994)
33. Miyoshi, K.: Aerospace mechanisms and tribology technology. *Tribol. Int.* 32, 673–685 (1999). doi:10.1016/S0301-679X(99)00092-4
34. Donnet, C., Martin, J.M., Le Mogne, T., Belin, M.: Super-low friction of MoS<sub>2</sub> coatings in various environments. *Tribol. Int.* 29, 123–128 (1996). doi:10.1016/0301-679X(95)00094-K
35. Khare, H.S.: The coupled effects of environmental composition, temperature and contact size-scale on the tribology of molybdenum disulfide, <http://search.proquest.com.udel.idm.oclc.org/pqdtlocal1006271/docview/1564752823/abstract/70EE67C96AA4422APQ/1>, (2014)
36. Voevodin, A.A., Fitz, T.A., Hu, J.J., Zabinski, J.S.: Nanocomposite tribological coatings with “chameleon” surface adaptation. *J. Vac. Sci. Technol. Vac. Surf. Films.* 20, 1434–1444 (2002). doi:10.1116/1.1487875

37. Voevodin, A., Zabinski, J.: Nanocomposite and nanostructured tribological materials for space applications. *Compos. Sci. Technol.* (2005). doi:10.1016/j.compscitech.2004.10.008
38. Voevodin, A.A., Zabinski, J.S.: Smart Nanocomposite Coatings with Chameleon Surface Adaptation in Tribological Applications. In: Voevodin, A.A., Shtansky, D.V., Levashov, E.A., and Moore, J.J. (eds.) *Nanostructured Thin Films and Nanodispersion Strengthened Coatings*. pp. 1–8. Kluwer Academic Publishers, Dordrecht (2004)
39. Muratore, C., Voevodin, A.A.: Chameleon Coatings: Adaptive Surfaces to Reduce Friction and Wear in Extreme Environments. *Annu. Rev. Mater. Res.* 39, 297–324 (2009). doi:10.1146/annurev-matsci-082908-145259
40. Baker, C.C., Hu, J.J., Voevodin, A.A.: Preparation of Al<sub>2</sub>O<sub>3</sub>/DLC/Au/MoS<sub>2</sub> chameleon coatings for space and ambient environments. *Surf. Coat. Technol.* 201, 4224–4229 (2006). doi:10.1016/j.surfcoat.2006.08.067
41. Baker, C.C., Chromik, R.R., Wahl, K.J., Hu, J.J., Voevodin, A.A.: Preparation of chameleon coatings for space and ambient environments. *Thin Solid Films.* 515, 6737–6743 (2007). doi:10.1016/j.tsf.2007.02.005
42. Dominguez-Meister, S., Cristina Rojas, T., Brizuela, M., Carlos Sanchez-Lopez, J.: Solid lubricant behavior of MoS<sub>2</sub> and WSe<sub>2</sub>-based nanocomposite coatings. *Sci. Technol. Adv. Mater.* 18, (2017). doi:10.1080/14686996.2016.1275784
43. Ren, S., Li, H., Cui, M., Wang, L., Pu, J.: Functional regulation of Pb-Ti/MoS<sub>2</sub> composite coatings for environmentally adaptive solid lubrication. *Appl. Surf. Sci.* 401, 362–372 (2017). doi:10.1016/j.apsusc.2017.01.054
44. Friedrich, K., Lu, Z., Hager, A.M.: Recent advances in polymer composites' tribology. *Wear.* 190, 139–144 (1995). doi:10.1016/0043-1648(96)80012-3
45. Zhang, S.W.: State-of-the-art of polymer tribology. *Tribol. Int.* 31, 49–60 (1998). doi:10.1016/S0301-679X(98)00007-3
46. Bahadur, S., Sunkara, C.: Effect of transfer film structure, composition and bonding on the tribological behavior of polyphenylene sulfide filled with nano particles of TiO<sub>2</sub>, ZnO, CuO and SiC. *Wear.* 258, 1411–1421 (2005). doi:10.1016/j.wear.2004.08.009

47. Bhimaraj, P., Burris, D.L., Action, J., Sawyer, W.G., Toney, C.G., Siegel, R.W., Schadler, L.S.: Effect of matrix morphology on the wear and friction behavior of alumina nanoparticle/poly(ethylene) terephthalate composites. *Wear*. 258, 1437–1443 (2005). doi:10.1016/j.wear.2004.09.077
48. Burris, D.L., Sawyer, W.G.: A low friction and ultra low wear rate PEEK/PTFE composite. *Wear*. 261, 410–418 (2006). doi:10.1016/j.wear.2005.12.016
49. McCook, N.L., Boesl, B., Burris, D.L., Sawyer, W.G.: Epoxy, ZnO, and PTFE nanocomposite: friction and wear optimization. *Tribol. Lett.* 22, 253–257 (2006). doi:10.1007/s11249-006-9089-5
50. Wang, S., Ge, S., Zhang, D.: Comparison of tribological behavior of nylon composites filled with zinc oxide particles and whiskers. *Wear*. 266, 248–254 (2009). doi:10.1016/j.wear.2008.06.019
51. Friedrich, K., Lu, Z., Häger, A.M.: Overview on polymer composites for friction and wear application. *Theor. Appl. Fract. Mech.* 19, 1–11 (1993). doi:10.1016/0167-8442(93)90029-B
52. Briscoe, B.J., Sinha, S.K.: Tribological applications of polymers and their composites: Past, present and future prospects. In: *Tribology and Interface Engineering Series*. pp. 1–14. Elsevier (2008)
53. Bijwe, J., Sen, S., Ghosh, A.: Influence of PTFE content in PEEK–PTFE blends on mechanical properties and tribo-performance in various wear modes. *Wear*. 258, 1536–1542 (2005). doi:10.1016/j.wear.2004.10.008
54. Burris, D.L., Sawyer, W.G.: Tribological behavior of PEEK components with compositionally graded PEEK/PTFE surfaces. *Wear*. 262, 220–224 (2007). doi:10.1016/j.wear.2006.03.045
55. Zheng, F., Wang, Q., Wang, T.: Effects of Aramid Fiber and Polytetrafluoroethylene on the Mechanical and Tribological Properties of Polyimide Composites in a Vacuum. *J. Macromol. Sci. Part B*. 54, 927–937 (2015). doi:10.1080/00222348.2015.1035611
56. Theiler, G., Gradt, T.: Tribological characteristics of polyimide composites in hydrogen environment. *Tribol. Int.* 92, 162–171 (2015). doi:10.1016/j.triboint.2015.06.001

57. Zhang, Z., Breidt, C., Chang, L., Hauptert, F., Friedrich, K.: Enhancement of the wear resistance of epoxy: short carbon fibre, graphite, PTFE and nano-TiO<sub>2</sub>. *Compos. Part Appl. Sci. Manuf.* 35, 1385–1392 (2004). doi:10.1016/j.compositesa.2004.05.005
58. Chang, L., Zhang, Z., Ye, L., Friedrich, K.: Tribological properties of epoxy nanocomposites: III. Characteristics of transfer films. *Wear.* 262, 699–706 (2007). doi:10.1016/j.wear.2006.08.002
59. Li, X., Gao, Y., Xing, J., Wang, Y., Fang, L.: Wear reduction mechanism of graphite and MoS<sub>2</sub> in epoxy composites. *Wear.* 257, 279–283 (2004). doi:10.1016/j.wear.2003.12.012
60. Zhang, Z., Breidt, C., Chang, L., Friedrich, K.: Wear of PEEK composites related to their mechanical performances. *Tribol. Int.* 37, 271–277 (2004). doi:10.1016/j.triboint.2003.09.005
61. Makinson, K.R., Tabor, D.: The Friction and Transfer of Polytetrafluoroethylene. *Proc. R. Soc. Math. Phys. Eng. Sci.* 281, 49–61 (1964). doi:10.1098/rspa.1964.0168
62. Shi, Y.J., Feng, X., Wang, H.Y., Liu, C., Lu, X.H.: Effects of filler crystal structure and shape on the tribological properties of PTFE composites. *Tribol. Int.* 40, 1195–1203 (2007). doi:10.1016/j.triboint.2006.12.006
63. McElwain, S.E., Blanchet, T.A., Schadler, L.S., Sawyer, W.G.: Effect of Particle Size on the Wear Resistance of Alumina-Filled PTFE Micro- and Nanocomposites. *Tribol. Trans.* 51, 247–253 (2008). doi:10.1080/10402000701730494
64. Lancaster, J.K.: The effect of carbon fibre reinforcement on the friction and wear of polymers. *J. Phys. Appl. Phys.* 1, 549–559 (1968). doi:10.1088/0022-3727/1/5/303
65. Tanaka, K., Kawakami, S.: Effect of various fillers on the friction and wear of polytetrafluoroethylene-based composites. *Wear.* 79, 221–234 (1982). doi:10.1016/0043-1648(82)90170-3
66. Khedkar, J., Negulescu, I., Meletis, E.I.: Sliding wear behavior of PTFE composites. *Wear.* 252, 361–369 (2002). doi:10.1016/S0043-1648(01)00859-6
67. Sawyer, W.G., Freudenberg, K.D., Bhimaraj, P., Schadler, L.S.: A study on the friction and wear behavior of PTFE filled with alumina nanoparticles. *Wear.* 254, 573–580 (2003). doi:10.1016/S0043-1648(03)00252-7

68. Krick, B.A., Ewin, J.J., McCumiskey, E.J.: Tribofilm Formation and Run-In Behavior in Ultra-Low-Wearing Polytetrafluoroethylene (PTFE) and Alumina Nanocomposites. *Tribol. Trans.* 57, 1058–1065 (2014). doi:10.1080/10402004.2014.933934
69. Briscoe, B.: Wear of polymers: an essay on fundamental aspects. *Tribol. Int.* 14, 231–243 (1981). doi:10.1016/0301-679X(81)90050-5
70. Schwartz, C.J., Bahadur, S.: Studies on the tribological behavior and transfer film–counterface bond strength for polyphenylene sulfide filled with nanoscale alumina particles. *Wear.* 237, 261–273 (2000). doi:10.1016/S0043-1648(99)00345-2
71. Bhimaraj, P., Burris, D., Sawyer, W.G., Toney, C.G., Siegel, R.W., Schadler, L.S.: Tribological investigation of the effects of particle size, loading and crystallinity on poly(ethylene) terephthalate nanocomposites. *Wear.* 264, 632–637 (2008). doi:10.1016/j.wear.2007.05.009
72. Wang, Q., Xue, Q., Liu, H., Shen, W., Xu, J.: The effect of particle size of nanometer ZrO<sub>2</sub> on the tribological behaviour of PEEK. *Wear.* 198, 216–219 (1996). doi:10.1016/0043-1648(96)07201-8
73. Wang, Q.-H., Xu, J., Shen, W., Xue, Q.: The effect of nanometer SiC filler on the tribological behavior of PEEK. *Wear.* 209, 316–321 (1997). doi:10.1016/S0043-1648(97)00015-X
74. Wang, Q., Xue, Q., Shen, W.: The friction and wear properties of nanometre SiO<sub>2</sub> filled polyetheretherketone. *Tribol. Int.* 30, 193–197 (1997). doi:10.1016/S0301-679X(96)00042-4
75. Ye, J., Khare, H.S., Burris, D.L.: Transfer film evolution and its role in promoting ultra-low wear of a PTFE nanocomposite. *Wear.* 297, 1095–1102 (2013). doi:10.1016/j.wear.2012.12.002
76. Laux, K.A., Schwartz, C.J.: Influence of linear reciprocating and multi-directional sliding on PEEK wear performance and transfer film formation. *Wear.* 301, 727–734 (2013). doi:10.1016/j.wear.2012.12.004
77. Ye, J., Khare, H.S., Burris, D.L.: Quantitative characterization of solid lubricant transfer film quality. *Wear.* 316, 133–143 (2014). doi:10.1016/j.wear.2014.04.017

78. Ye, J., Moore, A.C., Burris, D.L.: Transfer Film Tenacity: A Case Study Using Ultra-Low-Wear Alumina–PTFE. *Tribol. Lett.* 59, (2015). doi:10.1007/s11249-015-0576-4
79. Burris, D.L., Sawyer, W.G.: Improved wear resistance in alumina-PTFE nanocomposites with irregular shaped nanoparticles. *Wear.* 260, 915–918 (2006)
80. Haidar, D.R., Ye, J., Moore, A.C., Burris, D.L.: Assessing quantitative metrics of transfer film quality as indicators of polymer wear performance. *Wear.* 380–381, 78–85 (2017). doi:10.1016/j.wear.2017.03.012
81. Renfrew, M.M., Lewis, E.E.: Polytetrafluoroethylene. Heat Resistant, Chemically Inert Plastic. *Ind. Eng. Chem.* 38, 870–877 (1946). doi:10.1021/ie50441a009
82. Hanford, W.E., Joyce, R.M.: Polytetrafluoroethylene. *J. Am. Chem. Soc.* 68, 2082–2085 (1946). doi:10.1021/ja01214a062
83. Ye, J., Haidar, D.R., Burris, D.L.: Transfer Film Properties and their Role in Polymer Wear. In: Sinha, S.K. (ed.) *The Handbook of Polymer Tribology*. Imperial College Press, Distributed by World Scientific (2017)
84. Krick, B.A., Pitenis, A.A., Harris, K.L., Junk, C.P., Sawyer, W.G., Brown, S.C., Rosenfeld, H.D., Kasprzak, D.J., Johnson, R.S., Chan, C.D., Blackman, G.S.: Ultralow wear fluoropolymer composites: Nanoscale functionality from microscale fillers. *Tribol. Int.* 95, 245–255 (2016). doi:10.1016/j.triboint.2015.10.002
85. Krick, B.A., Sawyer, W.G.: Space Tribometers: Design for Exposed Experiments on Orbit. *Tribol. Lett.* 41, 303–311 (2011). doi:10.1007/s11249-010-9689-y
86. Pitenis, A.A., Ewin, J.J., Harris, K.L., Sawyer, W.G., Krick, B.A.: In Vacuo Tribological Behavior of Polytetrafluoroethylene (PTFE) and Alumina Nanocomposites: The Importance of Water for Ultralow Wear. *Tribol. Lett.* 53, 189–197 (2014). doi:10.1007/s11249-013-0256-1
87. Krick, B.A., Ewin, J.J., Blackman, G.S., Junk, C.P., Gregory Sawyer, W.: Environmental dependence of ultra-low wear behavior of polytetrafluoroethylene (PTFE) and alumina composites suggests tribochemical mechanisms. *Tribol. Int.* 51, 42–46 (2012). doi:10.1016/j.triboint.2012.02.015

88. Onodera, T., Kawasaki, K., Nakakawaji, T., Higuchi, Y., Ozawa, N., Kurihara, K., Kubo, M.: Effect of Tribochemical Reaction on Transfer-Film Formation by Poly(tetrafluoroethylene). *J. Phys. Chem. C*. 118, 11820–11826 (2014). doi:10.1021/jp503331e
89. Harris, K.L., Pitenis, A.A., Sawyer, W.G., Krick, B.A., Blackman, G.S., Kasprzak, D.J., Junk, C.P.: PTFE Tribology and the Role of Mechanochemistry in the Development of Protective Surface Films. *Macromolecules*. 48, 3739–3745 (2015). doi:10.1021/acs.macromol.5b00452
90. Pitenis, A.A., Harris, K.L., Junk, C.P., Blackman, G.S., Sawyer, W.G., Krick, B.A.: Ultralow Wear PTFE and Alumina Composites: It is All About Tribochemistry. *Tribol. Lett.* 57, (2015). doi:10.1007/s11249-014-0445-6
91. Khare, H.S., Moore, A.C., Haidar, D.R., Gong, L., Ye, J., Rabolt, J.F., Burris, D.L.: Interrelated Effects of Temperature and Environment on Wear and Tribochemistry of an Ultralow Wear PTFE Composite. *J. Phys. Chem. C*. 119, 16518–16527 (2015). doi:10.1021/acs.jpcc.5b00947
92. Jang, I., Burris, D.L., Dickrell, P.L., Barry, P.R., Santos, C., Perry, S.S., Phillpot, S.R., Sinnott, S.B., Sawyer, W.G.: Sliding orientation effects on the tribological properties of polytetrafluoroethylene. *J. Appl. Phys.* 102, 123509 (2007). doi:10.1063/1.2821743
93. Haidar, D.R., Alam, K.I., Burris, D.L.: Tribological Insensitivity of an Ultralow-Wear Poly(etheretherketone)–Polytetrafluoroethylene Polymer Blend to Changes in Environmental Moisture. *J. Phys. Chem. C*. 122, 5518–5524 (2018). doi:10.1021/acs.jpcc.7b12487
94. Battle, J.R.: *The Handbook of Industrial Oil Engineering*. J.B. Lippincott, Philadelphia, PA (1920)
95. Nino, E., Nino, T.: *Industrial Lubrication*. REX Bookstore, Inc., Sampaloc, Manila, Philippines (1997)
96. Harris, K.L., Curry, J.F., Pitenis, A.A., Rowe, K.G., Sidebottom, M.A., Sawyer, W.G., Krick, B.A.: Wear Debris Mobility, Aligned Surface Roughness, and the Low Wear Behavior of Filled Polytetrafluoroethylene. *Tribol. Lett.* 60, (2015). doi:10.1007/s11249-015-0581-7
97. Blanchet, T.A., Kandanur, S.S., Schadler, L.S.: Coupled Effect of Filler Content and Countersurface Roughness on PTFE Nanocomposite Wear Resistance. *Tribol. Lett.* 40, 11–21 (2010). doi:10.1007/s11249-009-9519-2

98. Tanaka, K., Uchiyama, Y., Toyooka, S.: The mechanism of wear of polytetrafluoroethylene. *Wear*. 23, 153–172 (1973). doi:10.1016/0043-1648(73)90081-1
99. Lancaster, J.K.: FRICTION AND WEAR. In: *Polymer Science, A Materials Science Handbook*. pp. 959–1046. Elsevier (1972)
100. Friedrich, K., Karger-Kocsis, J., Lu, Z.: Effects of steel counterface roughness and temperature on the friction and wear of PE(E)K composites under dry sliding conditions. *Wear*. 148, 235–247 (1991). doi:10.1016/0043-1648(91)90287-5
101. Kennedy, F.: Frictional Heating and Contact Temperatures. In: *Modern Tribology Handbook, Two Volume Set*. CRC Press (2000)
102. Laux, K.A., Jean-Fulcrand, A., Sue, H.J., Bremner, T., Wong, J.S.S.: The influence of surface properties on sliding contact temperature and friction for polyetheretherketone (PEEK). *Polymer*. 103, 397–404 (2016). doi:10.1016/j.polymer.2016.09.064
103. Urueña, J.M., Pitenis, A.A., Harris, K.L., Sawyer, W.G.: Evolution and Wear of Fluoropolymer Transfer Films. *Tribol. Lett.* 57, (2015). doi:10.1007/s11249-014-0453-6
104. Burris, D.L., Sawyer, W.G.: Measurement Uncertainties in Wear Rates. *Tribol. Lett.* 36, 81–87 (2009). doi:10.1007/s11249-009-9477-8
105. Laux, K.A., Schwartz, C.J.: Effects of contact pressure, molecular weight, and supplier on the wear behavior and transfer film of polyetheretherketone (PEEK). *Wear*. 297, 919–925 (2013). doi:10.1016/j.wear.2012.11.013
106. Ye, J.: Characterizing PTFE transfer film properties to elucidate transfer film's role in ultra-low wear sliding of polymer nanocomposites, <http://search.proquest.com.udel.idm.oclc.org/pqdtlocal1006271/docview/1661456515/abstract/265CDA0452DF4D23PQ/1>, (2014)
107. Zhang, G., Sebastian, R., Burkhart, T., Friedrich, K.: Role of monodispersed nanoparticles on the tribological behavior of conventional epoxy composites filled with carbon fibers and graphite lubricants. *Wear*. 292–293, 176–187 (2012). doi:10.1016/j.wear.2012.05.012
108. Zhao, Q., Bahadur, S.: A study of the modification of the friction and wear behavior of polyphenylene sulfide by particulate Ag<sub>2</sub>S and PbTe fillers. *Wear*. 217, 62–72 (1998). doi:10.1016/S0043-1648(98)00155-0

109. Goyal, R.K., Tiwari, A.N., Negi, Y.S.: High performance nanocomposites for tribological applications: Preparation and characterization. *Mater. Sci. Eng. A.* 486, 602–610 (2008). doi:10.1016/j.msea.2007.09.047
110. *Metals Handbook: Properties and Selection of Metals.* Metals Park, Novelty, OH (1961)
111. DuPont: Properties Handbook Teflon PTFE: fluoropolymer resin, [http://www.rjchase.com/ptfe\\_handbook.pdf](http://www.rjchase.com/ptfe_handbook.pdf), (1996)
112. Victrex PEEK Materials Properties Guide, <https://www.victrex.com/en/victrex-peek>
113. Comyn, J., Mascia, L., Xiao, G., Parker, B.M.: Corona-discharge treatment of polyetheretherketone (PEEK) for adhesive bonding. *Int. J. Adhes. Adhes.* 16, 301–304 (1996). doi:10.1016/S0143-7496(96)00010-3
114. Ha, S.-W., Hauert, R., Ernst, K.-H., Wintermantel, E.: Surface analysis of chemically-etched and plasma-treated polyetheretherketone (PEEK) for biomedical applications. *Surf. Coat. Technol.* 96, 293–299 (1997). doi:10.1016/S0257-8972(97)00179-5
115. Cognard, P. ed: *Handbook of adhesives and sealants.* Elsevier, Amsterdam ; Boston, Mass (2006)
116. McCook, N.L., Hamilton, M.A., Burris, D.L., Sawyer, W.G.: Tribological results of PEEK nanocomposites in dry sliding against 440C in various gas environments. *Wear.* 262, 1511–1515 (2007). doi:10.1016/j.wear.2007.01.036
117. Skoog, D.A., Holler, F.J., Crouch, S.R.: *Principles of Instrumental Analysis.* Cengage Learning (2017)
118. Díez-Pascual, A.M., Xu, C., Luque, R.: Development and characterization of novel poly(ether ether ketone)/ZnO bionanocomposites. *J. Mater. Chem. B.* 2, 3065–3078 (2014). doi:10.1039/c3tb21800g
119. Briscoe, B.J., Lin Heng Yao, Stolarski, T.A.: The friction and wear of poly(tetrafluoroethylene)-poly (etheretherketone) composites: An initial appraisal of the optimum composition. *Wear.* 108, 357–374 (1986). doi:10.1016/0043-1648(86)90013-X
120. Lu, Z.P., Friedrich, K.: On sliding friction and wear of PEEK and its composites. *Wear.* 181–183, 624–631 (1995). doi:10.1016/0043-1648(95)90178-7

121. Hufenbach, W., Kunze, K., Bijwe, J.: Sliding wear behaviour of PEEK-PTFE blends. *J. Synth. Lubr.* 20, 227–240 (2003). doi:10.1002/jsl.3000200305
122. Onodera, T., Nunoshige, J., Kawasaki, K., Adachi, K., Kurihara, K., Kubo, M.: Structure and Function of Transfer Film Formed from PTFE/PEEK Polymer Blend. *J. Phys. Chem. C.* 121, 14589–14596 (2017). doi:10.1021/acs.jpcc.7b02860
123. Dean, J.A.: *Lange's Handbook of Chemistry*. McGraw-Hill (1992)
124. Cottrell, T.L.: *The Strengths of Chemical Bonds*. Butterworths Scientific Publications (1958)
125. Theiler, G., Gradt, T.: Friction and wear of PEEK composites in vacuum environment. *Wear.* 269, 278–284 (2010). doi:10.1016/j.wear.2010.04.007
126. Theiler, G., Gradt, T.: Environmental effects on the sliding behaviour of PEEK composites. *Wear.* 368–369, 278–286 (2016). doi:10.1016/j.wear.2016.09.019
127. Theiler, G., Gradt, T.: Influence of the temperature on the tribological behaviour of PEEK composites in vacuum environment. *J. Phys. Conf. Ser.* 100, 072040 (2008). doi:10.1088/1742-6596/100/7/072040
128. Wang, Q., Zheng, F., Wang, T.: Tribological properties of polymers PI, PTFE and PEEK at cryogenic temperature in vacuum. *Cryogenics.* 75, 19–25 (2016). doi:10.1016/j.cryogenics.2016.01.001

## Appendix A

### **DESIGN OF A WEAR TESTING TRIBOMETER WITH HIGH-THROUGHPUT CAPABILITIES**

#### **A.1 Tribometer Assembly**

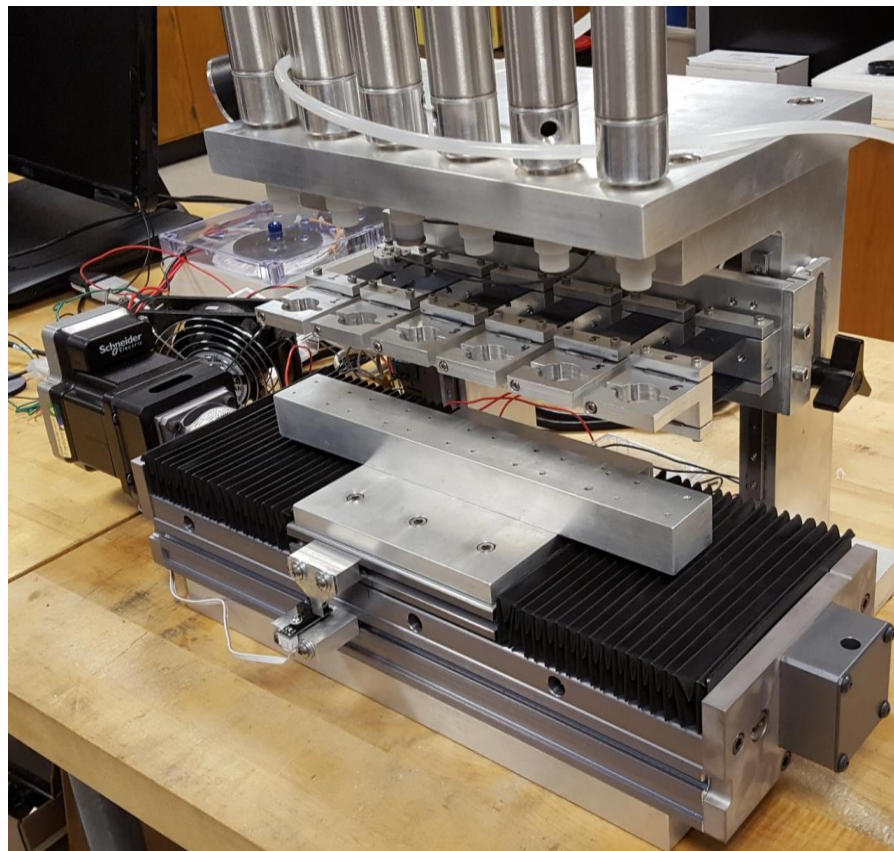
The PTC Creo 2.0® software used in this work was provided as a free student edition by PTC under the license number BK390206EDSTUDENTUNICL, which was usable on a student-owned computer. The technical drawings listed in the bill of materials include all fabricated parts for the tribometer assembly. These parts were designed, fabricated, prototyped, and implemented from 2015-2016 by D.R. Haidar, R. Ganesh, M. Wessel, M. Dick, N. Garabedian, and B. Bell. For this tribometer assembly, all parts were fabricated in the Student Machine Shop run by the Mechanical Engineering Department at the University of Delaware.

Table A-1 Bill of materials listing the fabricated parts for the tribometer assembly.

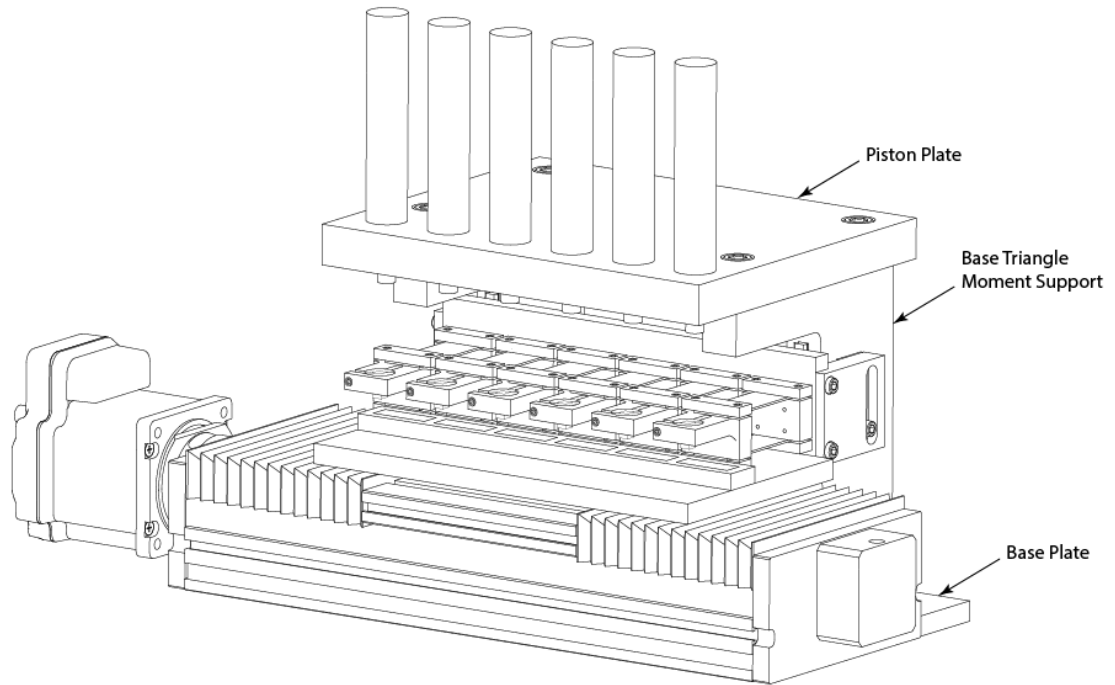
<b>Designation</b>	<b>Part Name</b>	<b>Material</b>	<b>Quantity</b>
Frame	Base Plate	Aluminum	1
Frame	Base Triangle Moment Supports	Aluminum	2
Frame	Piston Plate	Aluminum	1
Flexure	Flexure Clamps	Aluminum	24
Flexure	Flexure Clamps Middle 1	Aluminum	6
Flexure	Flexure Clamps Middle 2	Aluminum	6
Flexure	Flexure Sheet	Spring Steel	12
Flexure	Sample Clamp 1	Aluminum	6
Flexure	Sample Clamp 2	Aluminum	6
Table	Table Bot Connect Nuts	Aluminum	6
Table	Table Bottom Connector	Aluminum	1
Table	Table Top Connector	Aluminum	1
Carriage	Back Base For Flexures	Aluminum	1
Carriage	Clamp Vertical Stage	Aluminum	2
Pneumatics	Pneumatic Screw Tip	HDPE	6

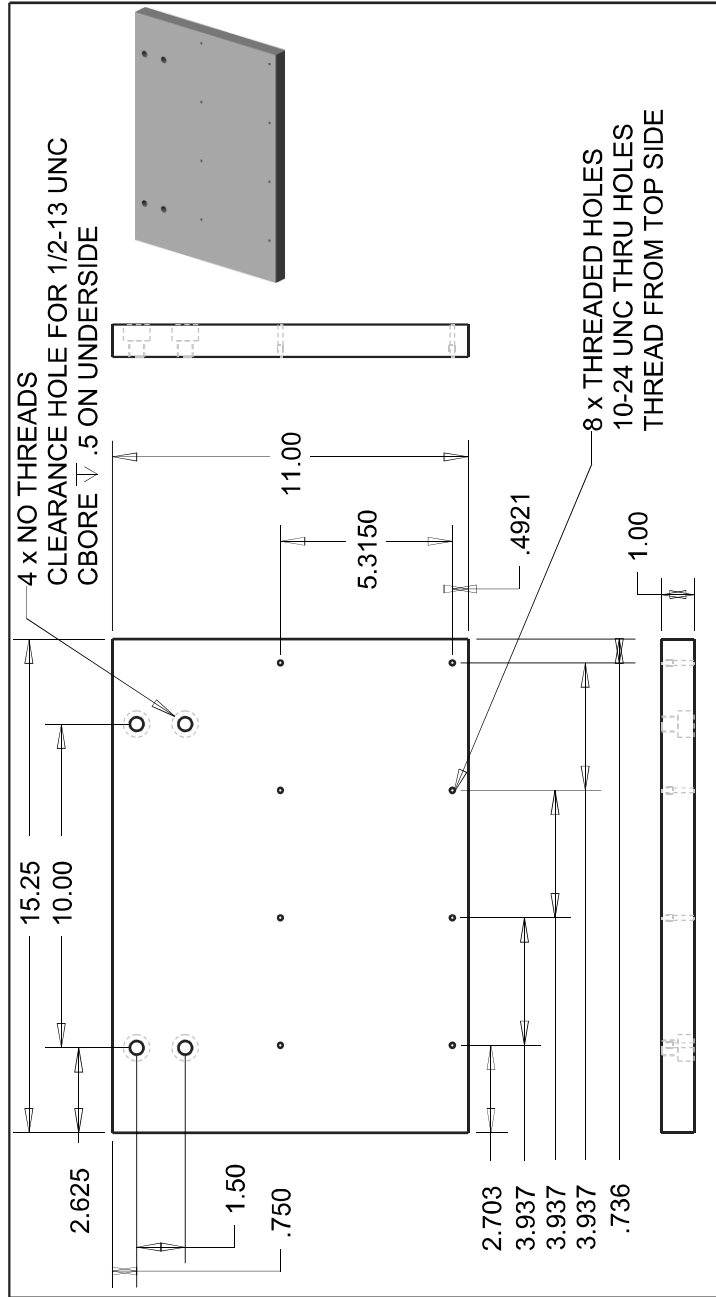
Table A-2 Bill of materials listing the purchased parts for the tribometer assembly, excluding purchased screws.

Designation	Part Name	Company	Model	Quantity
Reciprocation	Reciprocating Table	Thompson Linear Motion	2RB16I0N0450-100N002A0B00	1
Reciprocation	Stepper Motor	Schneider Electric	Lexium MDrive NEMA34	1
Reciprocation	Connector Cable	Industrial Automation Supply	USB-RS422/485 Converter	1
Flexures	Load Cell	Transducer Techniques	SLB-100	1
Pneumatics	Pneumatic Cylinder	Bimba Manufacturing	122-D	6

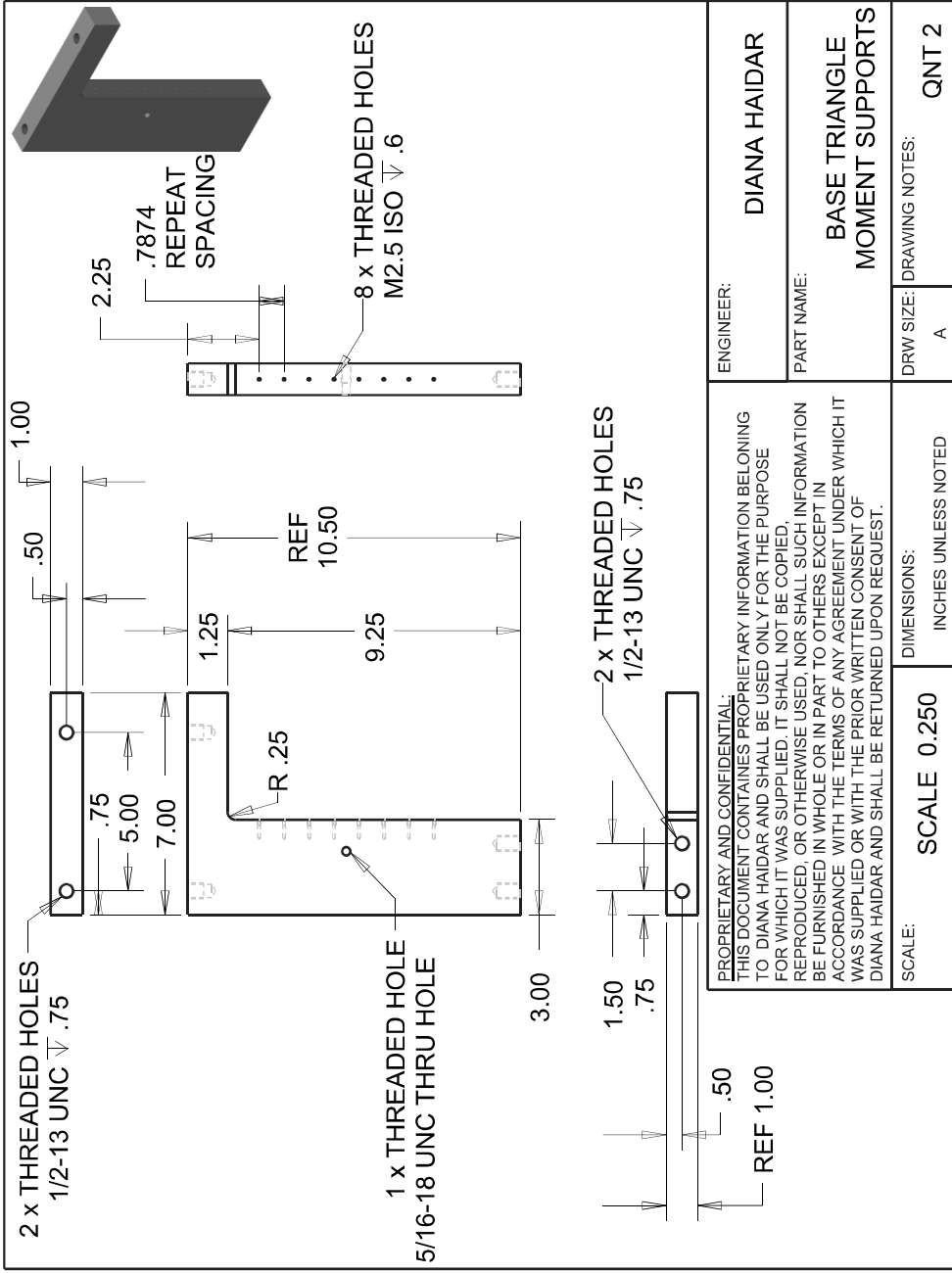


## A.2 Frame Components

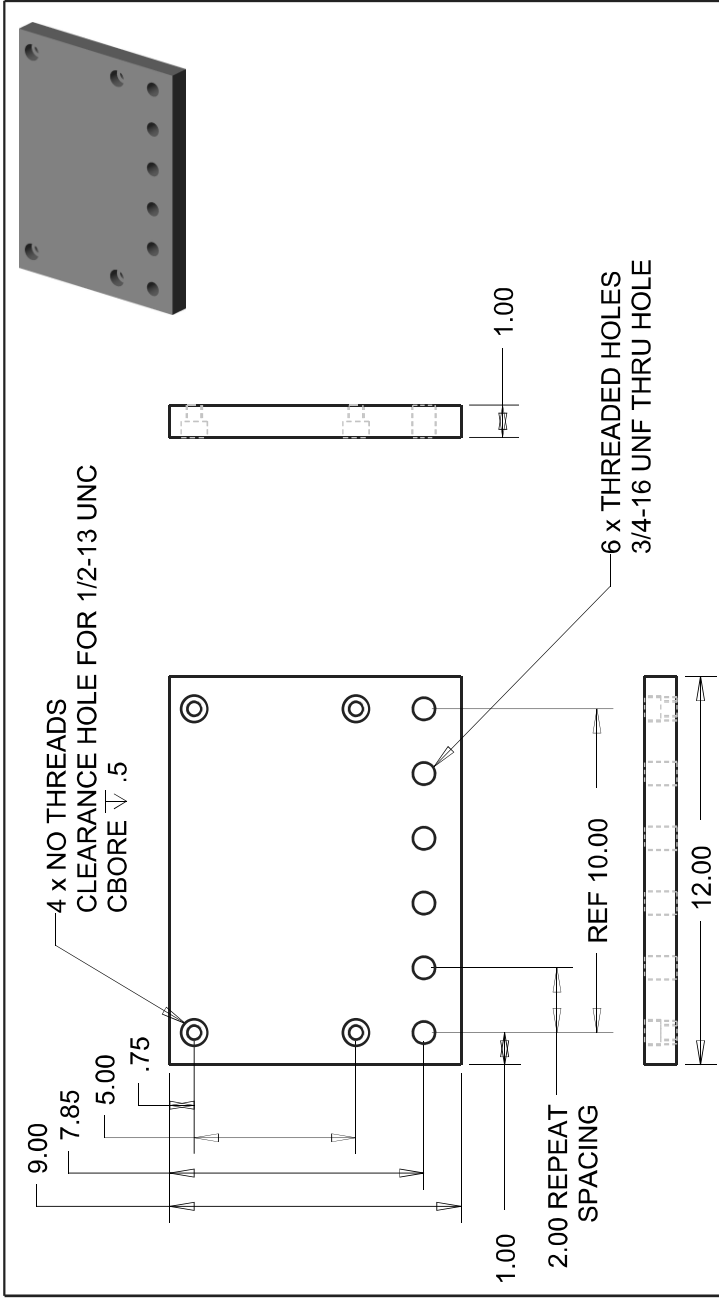




<p><b>PROPRIETARY AND CONFIDENTIAL:</b>          THIS DOCUMENT CONTAINS PROPRIETARY INFORMATION BELONGING TO DIANA HAIDAR AND SHALL BE USED ONLY FOR THE PURPOSE FOR WHICH IT WAS SUPPLIED. IT SHALL NOT BE COPIED, REPRODUCED, OR OTHERWISE USED, NOR SHALL SUCH INFORMATION BE FURNISHED IN WHOLE OR IN PART TO OTHERS EXCEPT IN ACCORDANCE WITH THE TERMS OF ANY AGREEMENT UNDER WHICH IT WAS SUPPLIED OR WITH THE PRIOR WRITTEN CONSENT OF DIANA HAIDAR AND SHALL BE RETURNED UPON REQUEST.</p>		ENGINEER:	DIANA HAIDAR
		PART NAME:	BASE PLATE
SCALE:	SCALE 0.250	DRW SIZE:	A
DIMENSIONS:	INCHES UNLESS NOTED	DRAWING NOTES:	QNT 1



<p><b>PROPRIETARY AND CONFIDENTIAL:</b>          THIS DOCUMENT CONTAINS PROPRIETARY INFORMATION BELONGING TO DIANA HAIDAR AND SHALL BE USED ONLY FOR THE PURPOSE FOR WHICH IT WAS SUPPLIED. IT SHALL NOT BE COPIED, REPRODUCED, OR OTHERWISE USED, NOR SHALL SUCH INFORMATION BE FURNISHED IN WHOLE OR IN PART TO OTHERS EXCEPT IN ACCORDANCE WITH THE TERMS OF ANY AGREEMENT UNDER WHICH IT WAS SUPPLIED OR WITH THE PRIOR WRITTEN CONSENT OF DIANA HAIDAR AND SHALL BE RETURNED UPON REQUEST.</p>		<p>ENGINEER: <b>DIANA HAIDAR</b></p>
<p>SCALE: <b>0.250</b></p>		<p>PART NAME: <b>BASE TRIANGLE MOMENT SUPPORTS</b></p>
<p>DIMENSIONS: INCHES UNLESS NOTED</p>		<p>DRW SIZE: <b>A</b></p>
<p>SCALE: <b>0.250</b></p>		<p>DRAWING NOTES: <b>QNT 2</b></p>



<p><b>PROPRIETARY AND CONFIDENTIAL:</b>          THIS DOCUMENT CONTAINS PROPRIETARY INFORMATION BELONGING TO DIANA HAIDAR AND SHALL BE USED ONLY FOR THE PURPOSE FOR WHICH IT WAS SUPPLIED. IT SHALL NOT BE COPIED, REPRODUCED, OR OTHERWISE USED, NOR SHALL SUCH INFORMATION BE FURNISHED IN WHOLE OR IN PART TO OTHERS EXCEPT IN ACCORDANCE WITH THE TERMS OF ANY AGREEMENT UNDER WHICH IT WAS SUPPLIED OR WITH THE PRIOR WRITTEN CONSENT OF DIANA HAIDAR AND SHALL BE RETURNED UPON REQUEST.</p>		<p>ENGINEER: <b>DIANA HAIDAR</b></p>
<p>SCALE: <b>SCALE 0.250</b></p>		<p>PART NAME: <b>PISTON PLATE</b></p>
<p>DIMENSIONS: INCHES UNLESS NOTED</p>		<p>DRW SIZE: <b>A</b></p>
<p>SCALE: <b>SCALE 0.250</b></p>		<p>DRAWING NOTES: <b>QNT 1</b></p>

# Frame Analysis of a 6-Sample Tribometer

## Problem Statement:

Tribology, the study of friction, lubrication, and wear of interacting surfaces, is an important area of research especially in today's world. The need for new materials that can withstand wear and tear over long periods of time is essential for mechanical processes to continue as smoothly and as long as possible. In the lab, tribometers are instruments used to measure a material's tribological properties (e.g. friction, wear, hardness) through movement of a sample across a counter-sample. By obtaining these properties, engineers can then choose the appropriate materials for their machinery's parts.

In Dr. Burris's lab, each tribometer can only test one sample at a time. Due to the large number of samples needed to be tested, each with their own set of loading and cycling variables, a new tribometer that can handle multiple samples was needed to be created to decrease experiment time. In the country, only a few multi-throughput tribometers have been created and by analyzing the photos of their instruments, we were able to design a six-sample tribometer of our own. One aspect of the design that needed to be analyzed carefully was the frame of the entire tribometer. Due to the constant cycling of the horizontal track and stage and the large force being applied by the pistons, stresses could develop that could loosen the frame's bolts, causing too great of a deflection in the plates and/or cause the frame or bolts to fail prematurely. During the design phase, these variables are needed to be analyzed in order to create the most stable frame possible without over-designing different parts to reduce overcompensation and to decrease spending on materials.

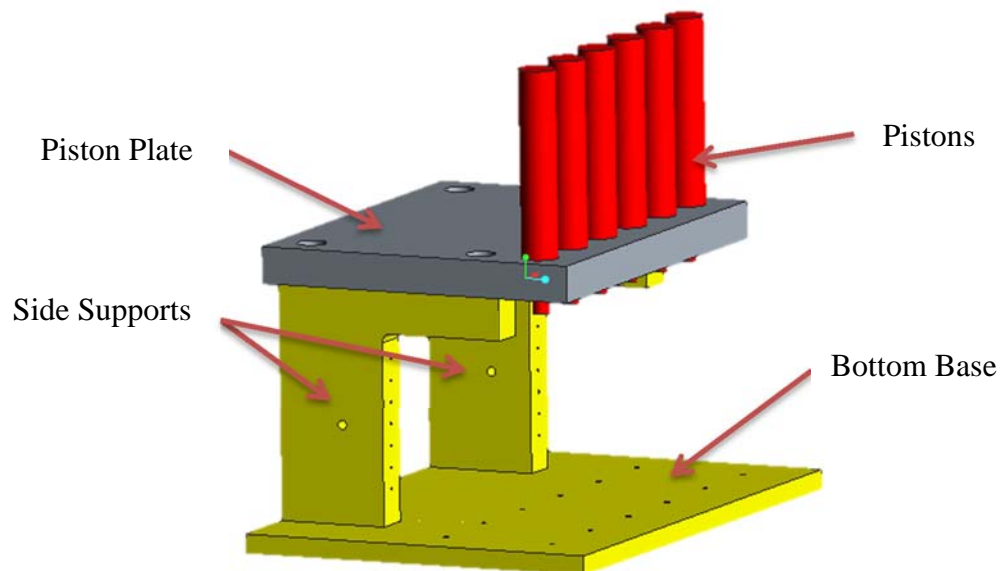
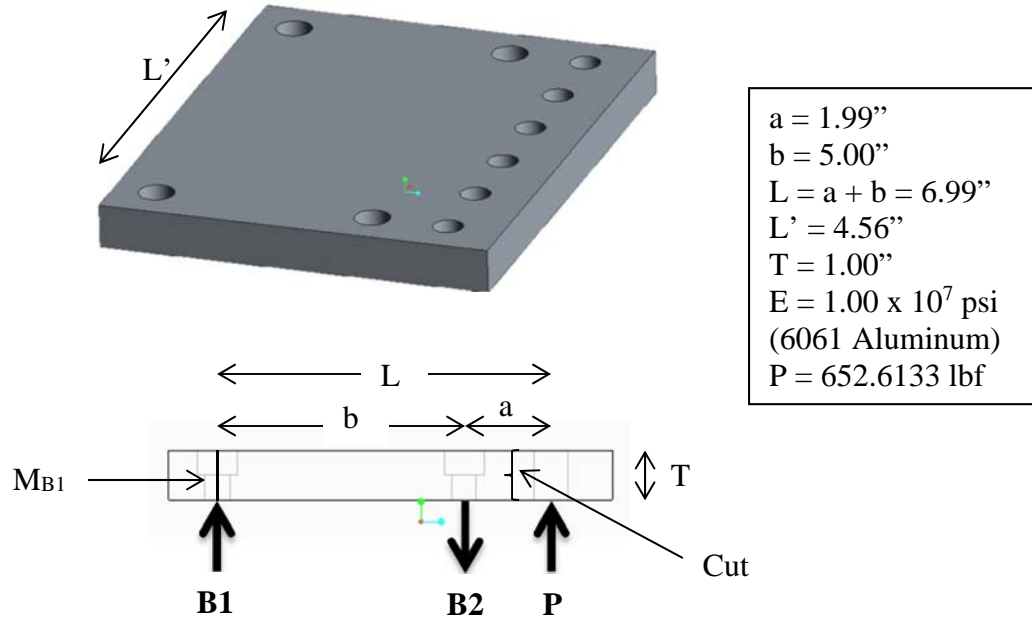


Figure 1: Six-Sample Tribometer frame needed to be analyzed for deflection. The piston plate is supported by two side supports which are attached to the base. The bolts for each interface will also be analyzed.

## Engineering Analysis:

### Piston Plate:



$$P = \text{Area of piston} * \text{Pressure of 3 Pistons} = 0.149987 \text{ in}^2 * 4351.13214 \text{ psi} = 652.6133 \text{ lbf}$$

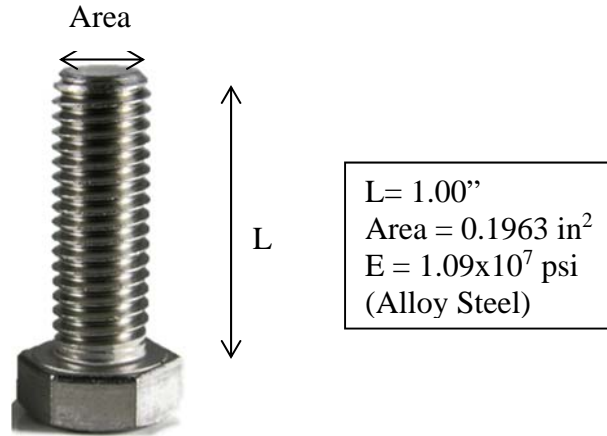
$$\begin{aligned} \Sigma F_y = 0 &= B1 - B2 + P \\ \Sigma M_{B1} = 0 &= B2 * b + P(a + b) \\ B2 &= \frac{P(a + b)}{b} = \frac{652.6133(1.99 + 5.00)}{5.00} = 912.4 \text{ lbf} \\ B1 &= B2 - P = 912.4 - 652.6133 = 259.7 \text{ lbf} \end{aligned}$$

$$\begin{aligned} I &= T * \frac{L'^3}{12} = 0.38 \text{ in}^4 \\ \frac{d^2 y}{d^2 x} &= \frac{M(x)}{EI} \Rightarrow y = \frac{1}{EI} \iint M(x) dx dx + C_1 x + C_2 \\ M(x) &= P(L - x) \Rightarrow \int M(x) dx = P(Lx - \frac{x^2}{2}) \Rightarrow \iint M(x) dx dx = P(\frac{Lx^2}{2} - \frac{x^3}{6}) \\ y &= \frac{1}{EI} (P(\frac{Lx^2}{2} - \frac{x^3}{6}) + C_1 x + C_2) \\ y(x=0) = 0 &= C_2; y(x=b) = 0 = \frac{P}{EI} (\frac{Lb^2}{2} - \frac{xb^3}{6}) + C_1 \\ y &= \frac{P}{EI} (\frac{Lx^2}{2} - \frac{x^3}{6} - \frac{Lbx}{2} + \frac{x^2 b^2}{6}) \end{aligned}$$

Max deflection will occur at  $x = L$ :

$$y(L) = \frac{P}{EI} \left( \frac{L^3}{2} - \frac{L^3}{6} - \frac{L^2 b}{2} + \frac{L^2 b^2}{6} \right) = 0.0035754''$$

**Piston Plate and Side Plate Interface Bolts**



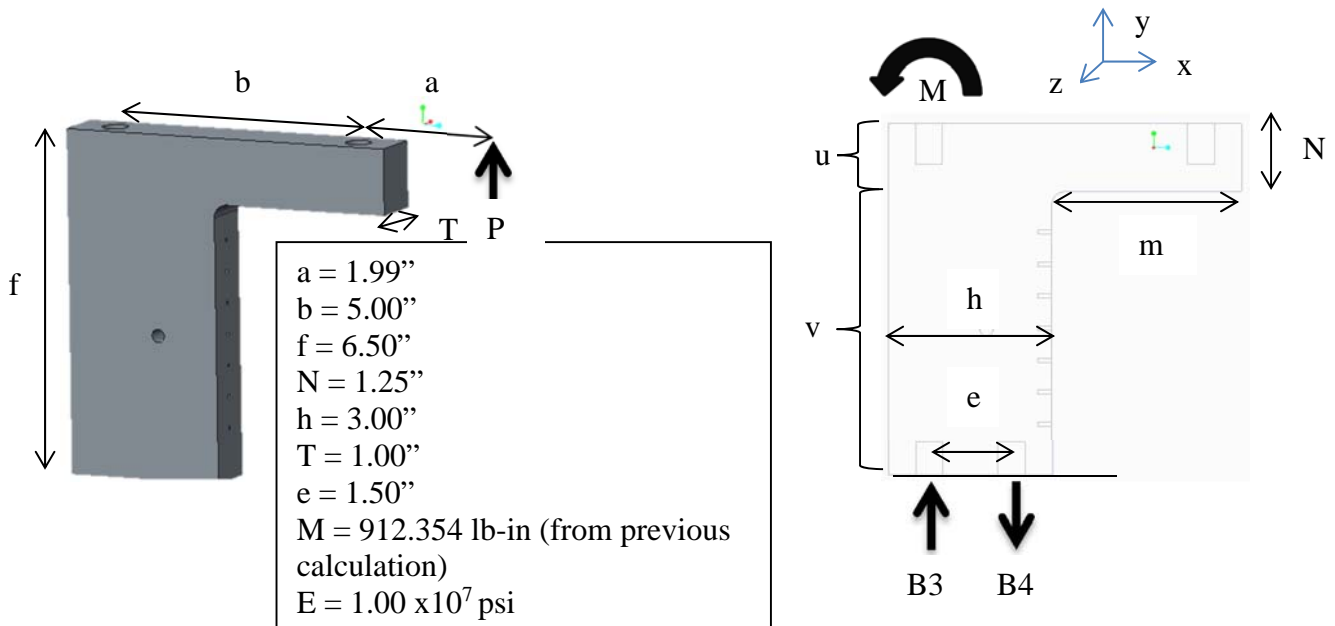
Deflection of B1:

$$y = \frac{L}{E} * (B1 * Area) = 0.000121362''$$

Deflection of B2:

$$y = \frac{L}{E} * (B2 * Area) = 0.000426292''$$

**Side Plate**



Using the equation of a cantilever beam with a couple moment at the free end, we can calculate the max deflection of part “v” in the x-direction and “u” in the y-direction:

$$I_v = \frac{Th^3}{12} = 2.25 \text{ in}^4$$

$$x = \frac{Mf^2}{2EI_v} = 0.0008565984''$$

$$I_u = \frac{TN^3}{12} = 0.16276 \text{ in}^4$$

$$y = \frac{Mm^2}{2EI_u} = 0.003433368''$$

Solving for the Bolt forces, B3 and B4:

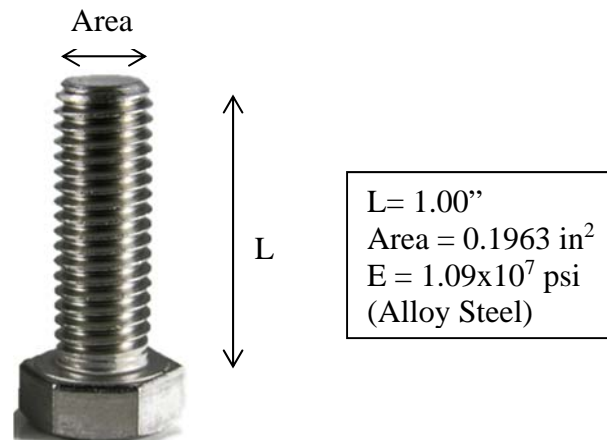
$$\Sigma F_y = 0 = B3 - B4 + P$$

$$\Sigma M_{B3} = M = -B4 * e + P(a + b)$$

$$B4 = \frac{-M + P(a + b)}{e} = 2432.94222 \text{ lbf}$$

$$B3 = B4 - P = 1780.328963 \text{ lbf}$$

### Side Plate and Base Interface Bolts

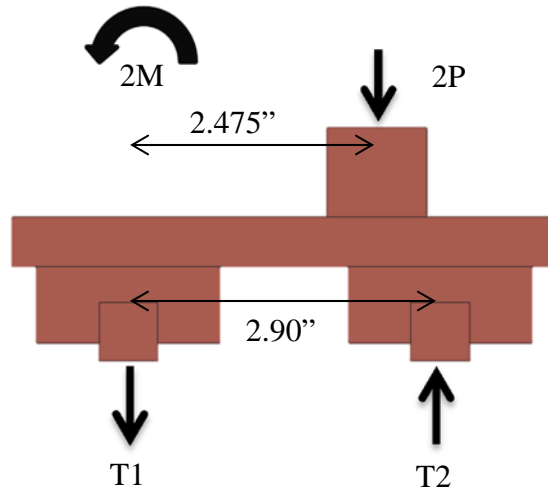
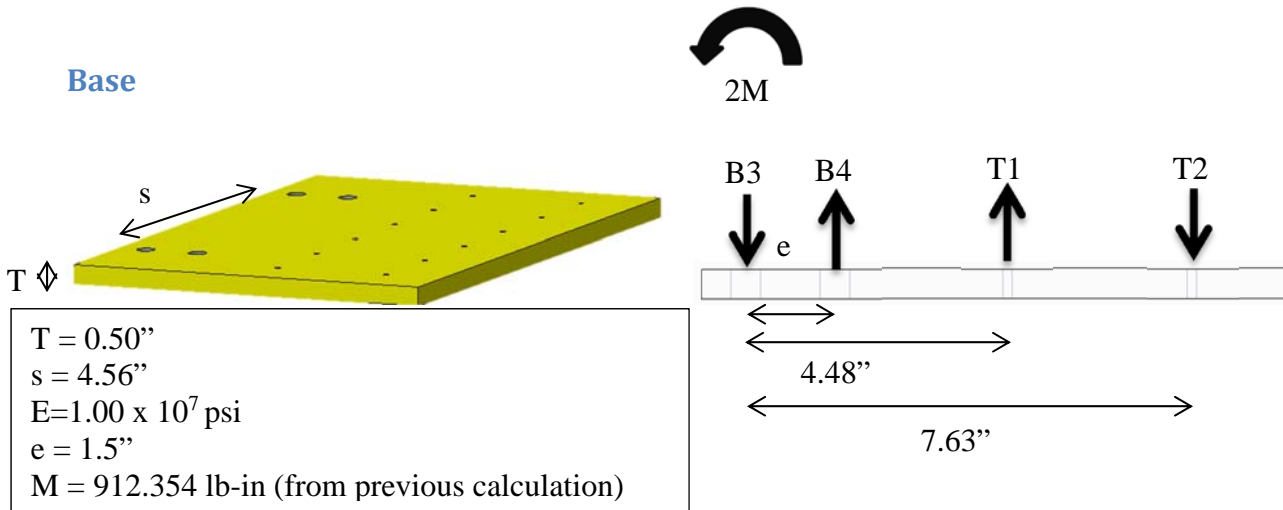


Deflection of B3:

$$y = \frac{L}{E} * (B3 * Area) = 0.000831848''$$

Deflection of B4:

$$y = \frac{L}{E} * (B4 * Area) = 0.001136777''$$



For the horizontal stage, T1 and T2 are:

$$\begin{aligned} \Sigma F_y = 0 &= -T1 + T2 - 2P \\ \Sigma M_{T1} = 2M &= -2P * 2.475 + T2 * 2.90 \\ T2 &= \frac{M + 2P * 2.475}{2.90} = 1587.603099 \text{ lbf} \\ T1 &= T2 + 2P = 282.3765863 \text{ lbf} \end{aligned}$$

To determine the max deflection of the base:

$$\begin{aligned} I &= T * \frac{s^3}{12} = 3.950784 \text{ in}^4 \\ \frac{d^2y}{dx^2} &= \frac{M(x)}{EI} \Rightarrow y = \frac{1}{EI} \iint M(x) dx dx + C_1x + C_2 \\ M(x) &= 2M + \frac{B4x}{e} - B3x \Rightarrow \int M(x) dx = 2Mx + \frac{B4x^2}{2e} - \frac{B3x^2}{2} \Rightarrow \end{aligned}$$

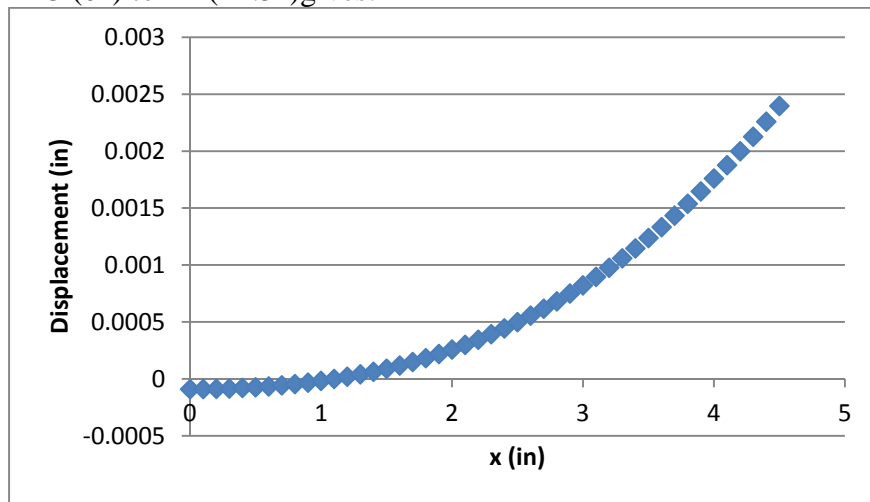
$$\iint M(x) dx dx = \frac{2Mx^2}{2} + \frac{B4x^3}{6e} - \frac{B3x^3}{6}$$

$$y = \frac{1}{EI} \left( \frac{2Mx^2}{2} + \frac{B4x^3}{6e} - \frac{B3x^3}{6} + C_1x + C_2 \right)$$

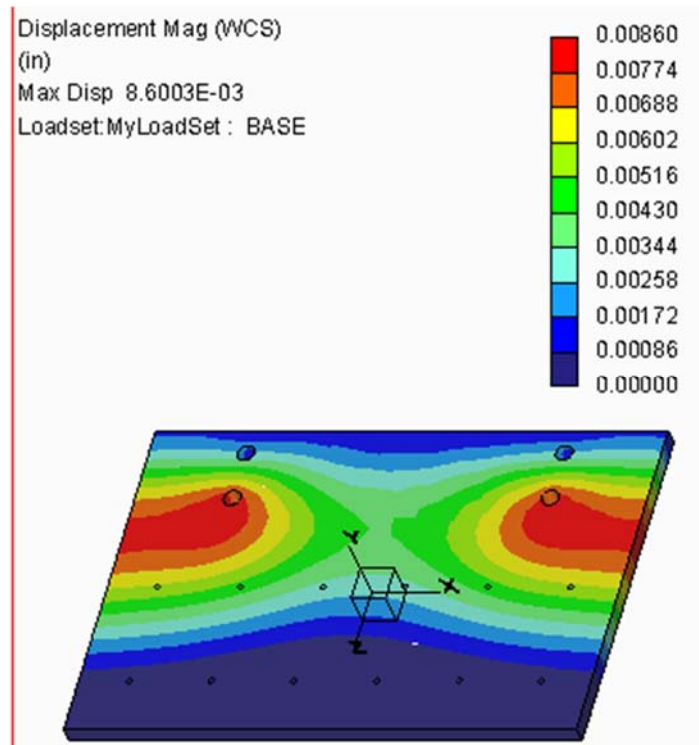
$$y(x=0) = 0 = C_2; y(x=e) = 0 = \frac{1}{EI} \left( \frac{2Me}{2} + \frac{B4e}{6} - \frac{B3e^2}{6} \right) + C_1$$

$$y = \frac{1}{EI} \left( \frac{M2x^2}{2} + \frac{B4x^3}{6e} - \frac{B3x^3}{6} - \frac{2Me}{2} - \frac{B4e}{6} + \frac{B3e^2}{6} \right)$$

Plotting y from B3 (0") to T1 (~4.5") gives:



Using a simplified finite element program installed with the CAD software with constraints on the front and back edges of the plate gives a similar result, but with a greater displacement.

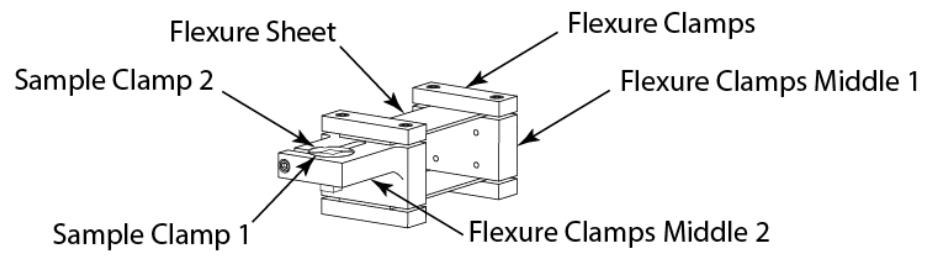
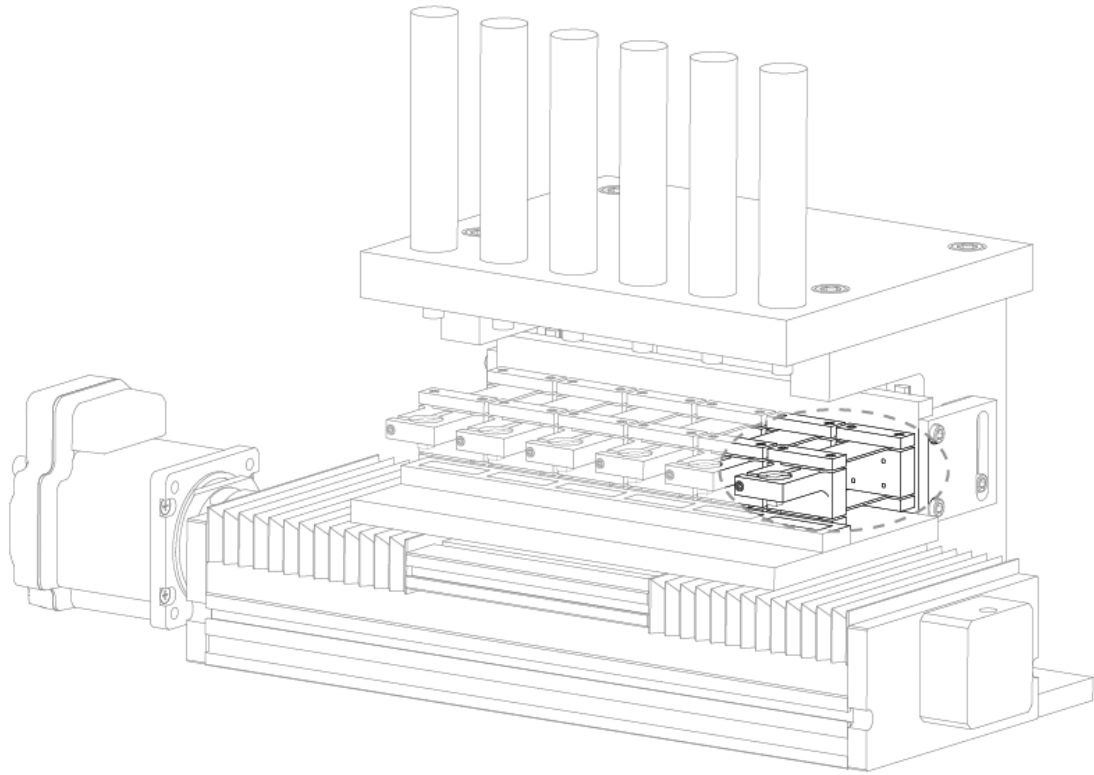


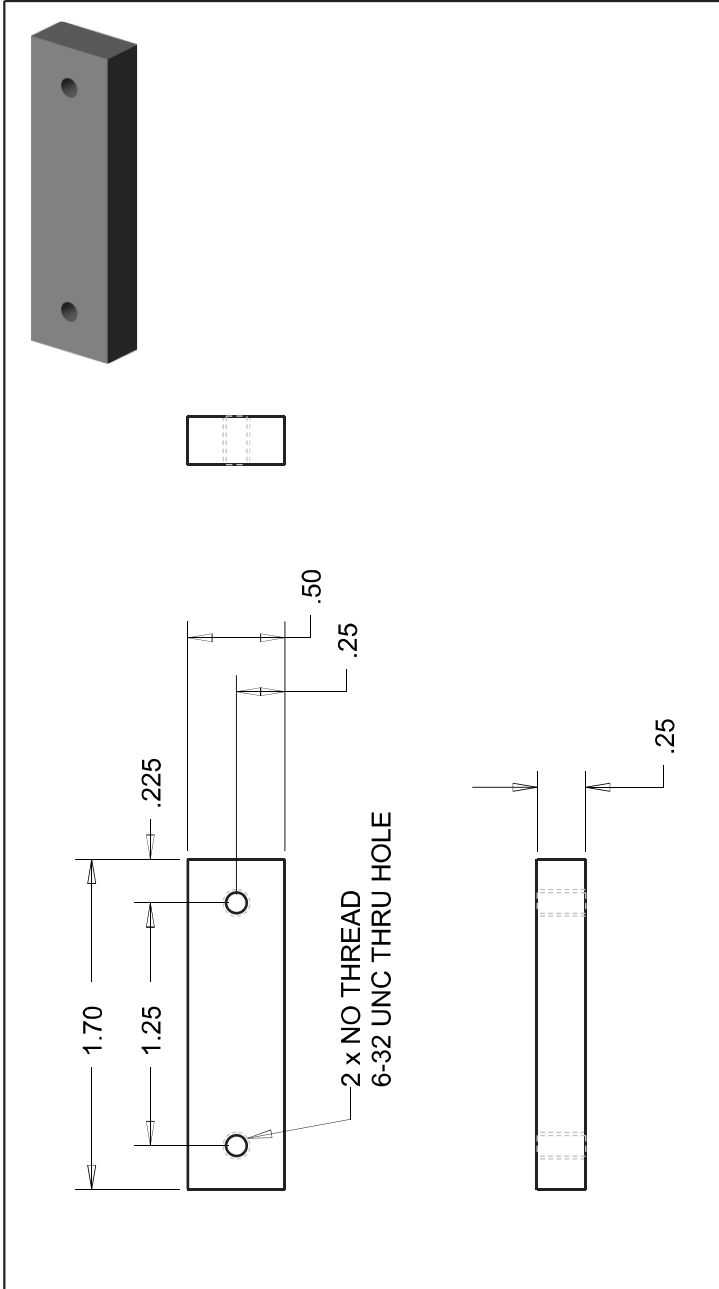
### Recommendations:

From this analysis of the tribometer frame, I can conclude that each part of the frame will not deflect more than 0.005", except for the possibility of the base. In order to help minimize the deflection of the base, the base needs to increase in thickness or add reinforcing struts to the bottom to counteract the large moment applied by the pistons. By adding reinforcing struts, costs can be kept down instead of buying a thicker plate.

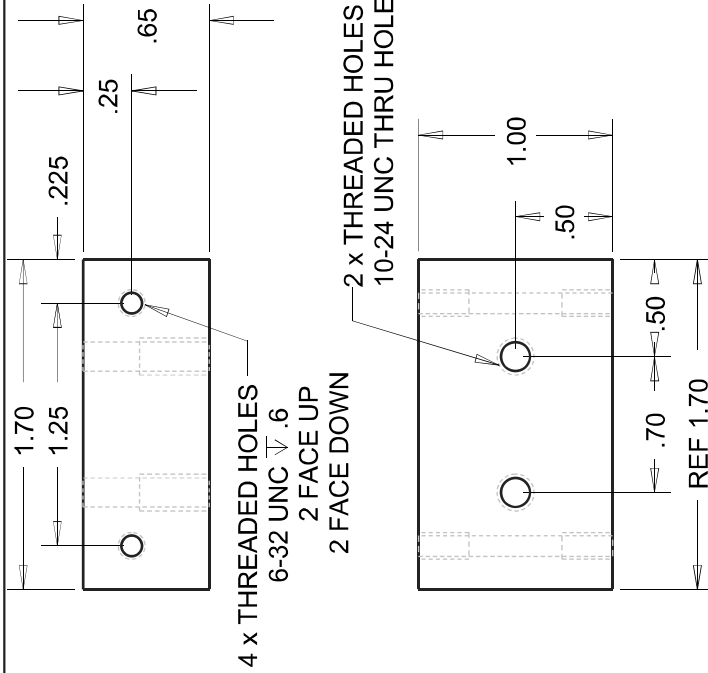
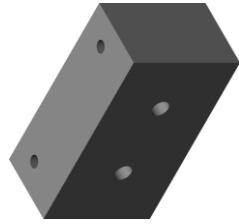
Another recommendation is to decrease the length and/or the radii of the bolts. This would be useful in order to cut costs in the budget. Overall, each part has been simplified enough in order to prevent over-compensation on any one part with the addition of base struts.

### A.3 Flexure Components

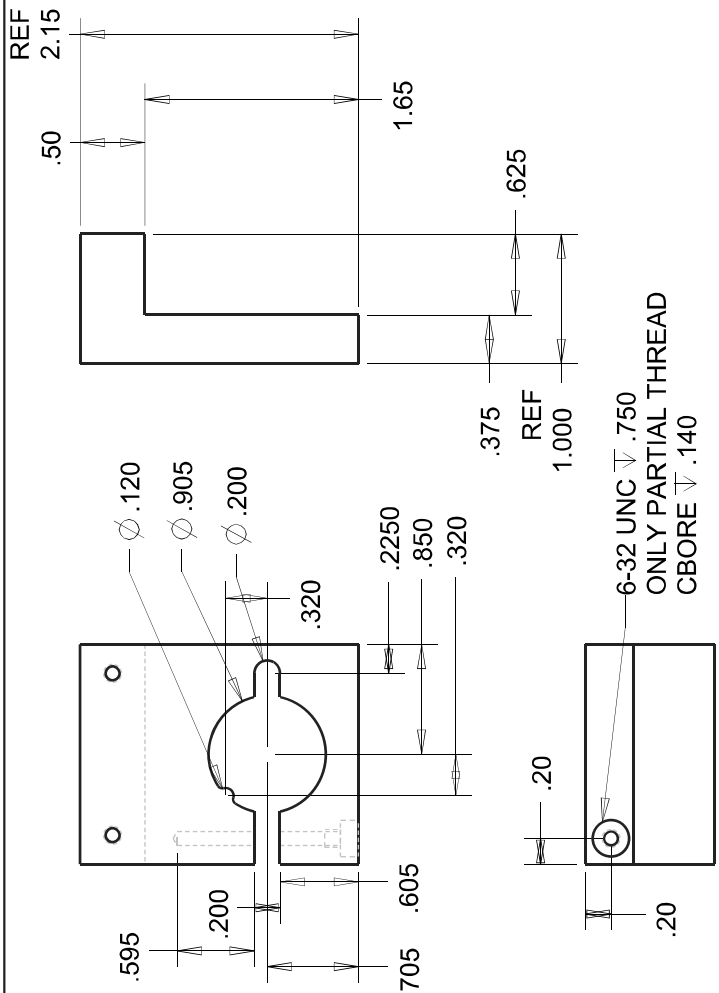
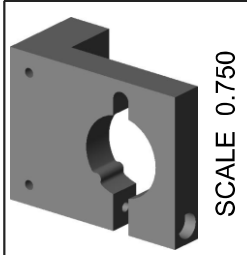




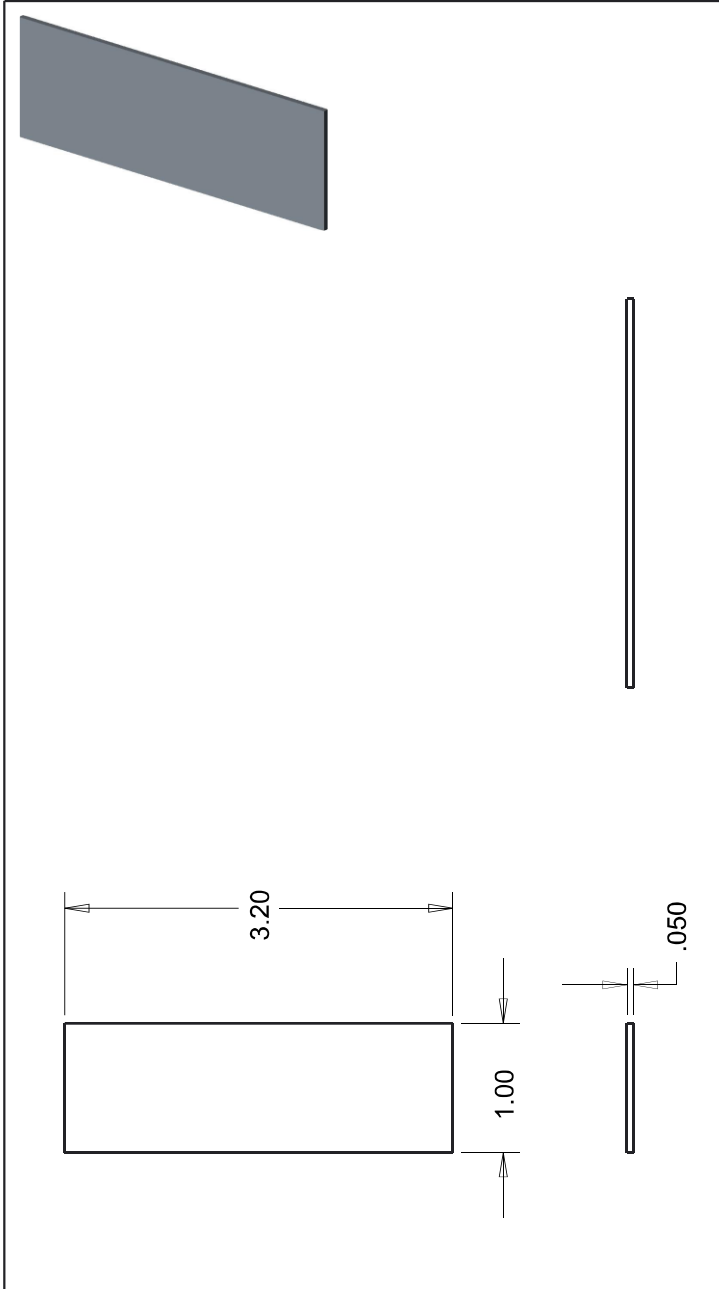
<p><b>PROPRIETARY AND CONFIDENTIAL:</b> THIS DOCUMENT CONTAINS PROPRIETARY INFORMATION BELONGING TO DIANA HAIDAR AND SHALL BE USED ONLY FOR THE PURPOSE FOR WHICH IT WAS SUPPLIED. IT SHALL NOT BE COPIED, REPRODUCED, OR OTHERWISE USED, NOR SHALL SUCH INFORMATION BE FURNISHED IN WHOLE OR IN PART TO OTHERS EXCEPT IN ACCORDANCE WITH THE TERMS OF ANY AGREEMENT UNDER WHICH IT WAS SUPPLIED OR WITH THE PRIOR WRITTEN CONSENT OF DIANA HAIDAR AND SHALL BE RETURNED UPON REQUEST.</p>	ENGINEER:	DIANA HAIDAR
	PART NAME:	FLEXURE CLAMPS
SCALE:	SCALE 1.500	DIMENSIONS: INCHES UNLESS NOTED
DRW SHEET:	A	REVISION NOTES: QNT 24



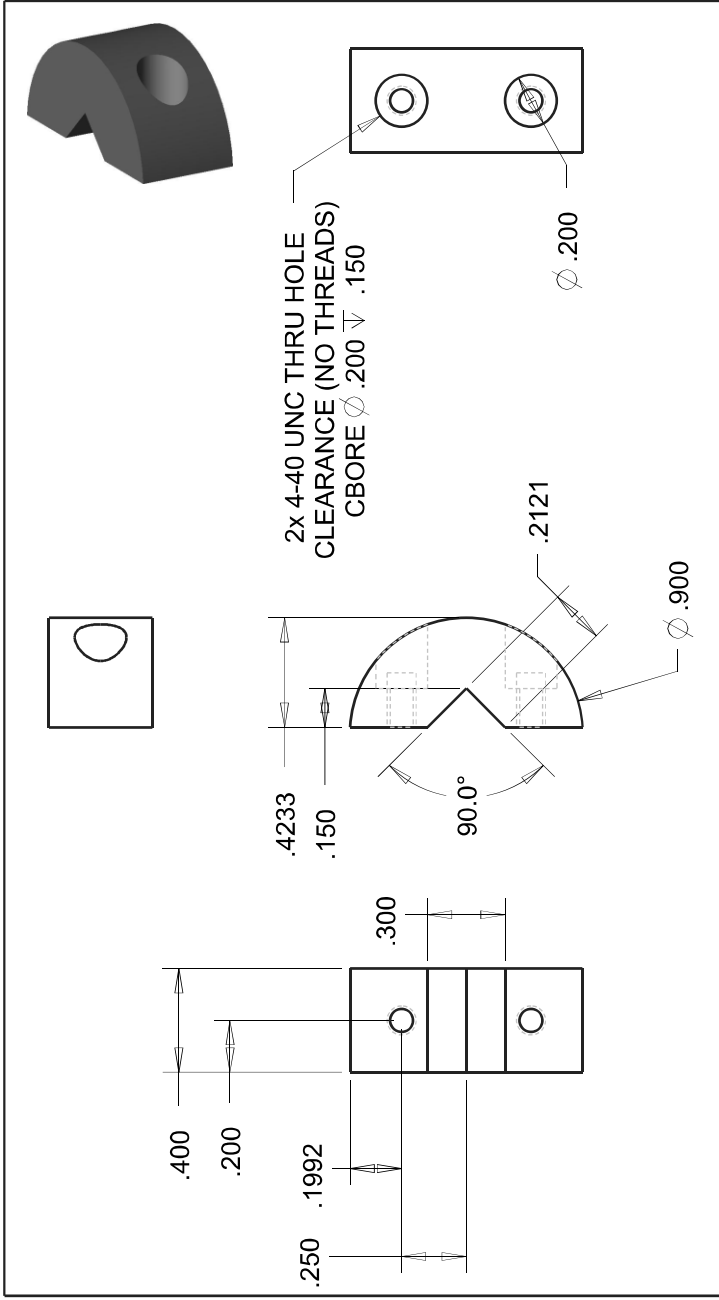
<p><b>PROPRIETARY AND CONFIDENTIAL:</b> THIS DOCUMENT CONTAINS PROPRIETARY INFORMATION BELONGING TO DIANA HAIDAR AND SHALL BE USED ONLY FOR THE PURPOSE FOR WHICH IT WAS SUPPLIED. IT SHALL NOT BE COPIED, REPRODUCED, OR OTHERWISE USED, NOR SHALL SUCH INFORMATION BE FURNISHED IN WHOLE OR IN PART TO OTHERS EXCEPT IN ACCORDANCE WITH THE TERMS OF ANY AGREEMENT UNDER WHICH IT WAS SUPPLIED OR WITH THE PRIOR WRITTEN CONSENT OF DIANA HAIDAR AND SHALL BE RETURNED UPON REQUEST.</p>		<p>ENGINEER: <b>DIANA HAIDAR</b></p>
<p>SCALE: <b>SCALE 1.500</b></p>		<p>PART NAME: <b>FLEXURE CLAMP MIDDLE 1</b></p>
<p>DIMENSIONS: INCHES UNLESS NOTED</p>		<p>DRW SIZE: A</p>
<p>DRAWING NOTES: <b>QNT 6</b></p>		



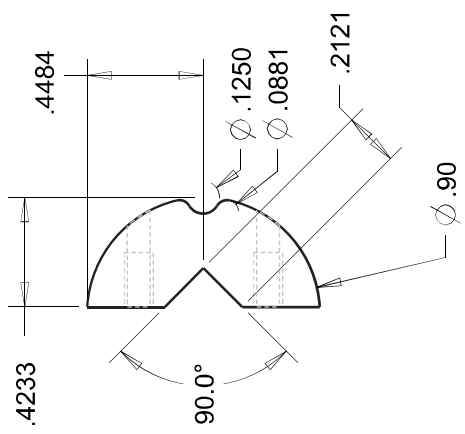
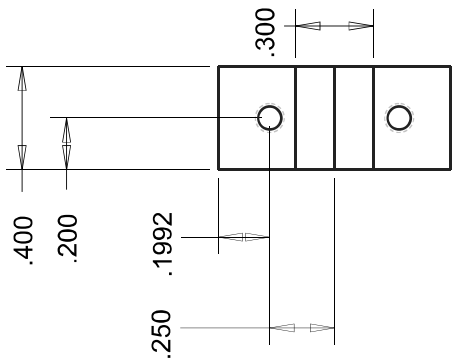
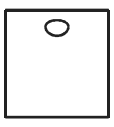
<p><b>PROPRIETARY AND CONFIDENTIAL:</b> THIS DOCUMENT CONTAINS PROPRIETARY INFORMATION BELONGING TO DIANA HAIDAR AND SHALL BE USED ONLY FOR THE PURPOSE FOR WHICH IT WAS SUPPLIED. IT SHALL NOT BE COPIED, REPRODUCED, OR OTHERWISE USED, NOR SHALL SUCH INFORMATION BE FURNISHED IN WHOLE OR IN PART TO OTHERS EXCEPT IN ACCORDANCE WITH THE TERMS OF ANY AGREEMENT UNDER WHICH IT WAS SUPPLIED OR WITH THE PRIOR WRITTEN CONSENT OF DIANA HAIDAR AND SHALL BE RETURNED UPON REQUEST.</p>		<p>ENGINEER: <b>DIANA HAIDAR</b></p>
<p>SCALE: <b>SCALE 1.000</b></p>		<p>PART NAME: <b>FLEXURE CLAMP MIDDLE 2</b></p>
<p>DIMENSIONS: INCHES UNLESS NOTED</p>		<p>DRW SIZE: <b>A</b></p>
<p>SCALE: <b>SCALE 1.000</b></p>		<p>DRAWING NOTES: <b>QNT 6</b></p>



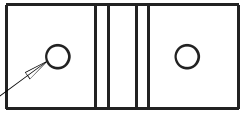
<p><b>PROPRIETARY AND CONFIDENTIAL:</b>          THIS DOCUMENT CONTAINS PROPRIETARY INFORMATION BELONGING TO DIANA HAIDAR AND SHALL BE USED ONLY FOR THE PURPOSE FOR WHICH IT WAS SUPPLIED. IT SHALL NOT BE COPIED, REPRODUCED, OR OTHERWISE USED, NOR SHALL SUCH INFORMATION BE FURNISHED IN WHOLE OR IN PART TO OTHERS EXCEPT IN ACCORDANCE WITH THE TERMS OF ANY AGREEMENT UNDER WHICH IT WAS SUPPLIED OR WITH THE PRIOR WRITTEN CONSENT OF DIANA HAIDAR AND SHALL BE RETURNED UPON REQUEST.</p>		ENGINEER:	DIANA HAIDAR
		PART NAME:	FLEXURE SHEET
SCALE:	SCALE 1.000	DIMENSIONS:	INCHES UNLESS NOTED
DRW SIZE:	A	DRAWING NOTES:	QNT 12



<p><b>PROPRIETARY AND CONFIDENTIAL:</b>          THIS DOCUMENT CONTAINS PROPRIETARY INFORMATION BELONGING TO DIANA HAIDAR AND SHALL BE USED ONLY FOR THE PURPOSE FOR WHICH IT WAS SUPPLIED. IT SHALL NOT BE COPIED, REPRODUCED, OR OTHERWISE USED, NOR SHALL SUCH INFORMATION BE FURNISHED IN WHOLE OR IN PART TO OTHERS EXCEPT IN ACCORDANCE WITH THE TERMS OF ANY AGREEMENT UNDER WHICH IT WAS SUPPLIED OR WITH THE PRIOR WRITTEN CONSENT OF DIANA HAIDAR AND SHALL BE RETURNED UPON REQUEST.</p>	ENGINEER:	DIANA HAIDAR	
	PART NAME:	SAMPLE CLAMP 1	
SCALE:	SCALE	2.000	DIMENSIONS: INCHES UNLESS NOTED
DRW SIZE:	A	DRAWING NOTES: QNT 6	



2x 4-40 UNC  
THREADED  
THRU HOLE



<p><b>PROPRIETARY AND CONFIDENTIAL:</b>          THIS DOCUMENT CONTAINS PROPRIETARY INFORMATION BELONGING TO DIANA HAIDAR AND SHALL BE USED ONLY FOR THE PURPOSE FOR WHICH IT WAS SUPPLIED. IT SHALL NOT BE COPIED, REPRODUCED, OR OTHERWISE USED, NOR SHALL SUCH INFORMATION BE FURNISHED IN WHOLE OR IN PART TO OTHERS EXCEPT IN ACCORDANCE WITH THE TERMS OF ANY AGREEMENT UNDER WHICH IT WAS SUPPLIED OR WITH THE PRIOR WRITTEN CONSENT OF DIANA HAIDAR AND SHALL BE RETURNED UPON REQUEST.</p>	
<p>ENGINEER: <b>DIANA HAIDAR</b></p>	<p>PART NAME: <b>SAMPLE CLAMP 2</b></p>
<p>SCALE: <b>SCALE 2.000</b></p>	<p>DIMENSIONS: <b>INCHES UNLESS NOTED</b></p>
<p>DRW SIZE: <b>A</b></p>	<p>DRAWING NOTES: <b>QNT 6</b></p>

# Flexure Design for high-throughput tribometer

Raja Ganesh

## 1. Problem Statement

The flexure assembly is incorporated into the tribometer to allow flexibility in terms of vertical motion of the specimen while constraining all other degrees of freedom (Figure 1). The optimal design would:

- a) Maximize the torsional/shear stiffness of the flexure assembly
- b) Minimize the bending resistance

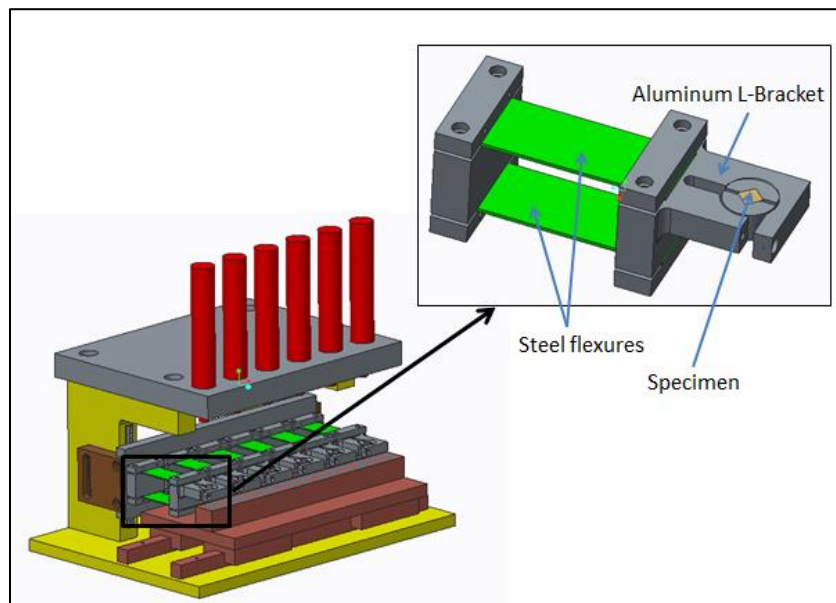


**Figure 1: Flexure assembly in high throughput tribometer**

## 2. Design Goals

- a) For a total wear of  $1 \text{ mm}^3$  in the specimen, the variability in the vertical reaction force should be less than 1 % of the applied load
- b) The maximum horizontal deflection should be less than 50 microns.
- c) The horizontal load on the flexure is cyclic in nature. The stresses in the flexures should be below the endurance limit of the material to avoid fatigue failure.

### 3. Material Properties

The flexures will be made of ASTM A36 Sheet steel with a thickness of 0.05” as it provides sufficient shear stiffness, provides bending flexibility and is easily available. The properties of this material are summarized in Table 1.

**Table 1 : Material Properties of flexure sheets**

Property	Value
Young's Modulus, E	200 GPa
Poisson's ratio, $\nu$	0.32
Shear modulus, G	75 GPa
Sheet thickness, t	1.27 mm

### 4. Initial Design

The Length (L), Width (b), and Spacing (s) of the flexures (Figure 2) were chosen so as to meet the design goals while providing sufficient clearances and ease-of-integration into the overall assembly. The chosen dimensions of the flexure assembly are shown in Table 2.

**Table 2 : Flexure Dimensions**

Property	Value (in)	Value (mm)
Length, L	2.0	50.8
Width, b	1.0	25.4
Spacing, s	1.0	25.4
Sheet thickness, t	0.05	1.27

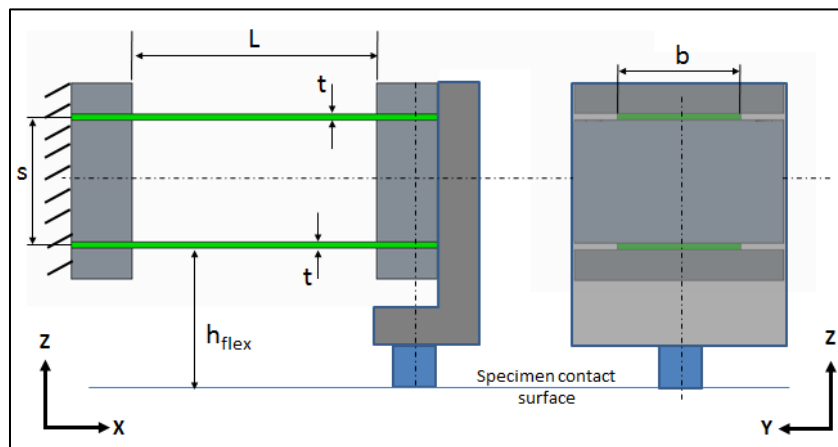


**Figure 2 : Initial flexure design**

## 5. Vertical force variability caused by the flexures

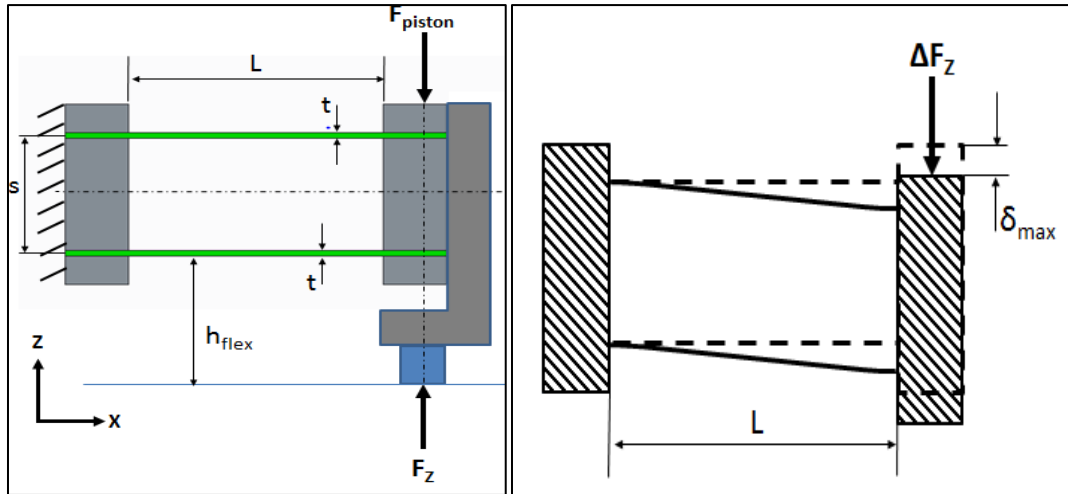


**Figure 3 : Bending of flexures**

As the specimen wears off during the test, the bending resistance offered by the flexure plates will lead to a reduction in the vertical reaction force between the specimen and the counter-surface. The reaction force,  $F_z$ , will no longer be equal to the force applied by the piston,  $F_{piston}$ . The difference between these two forces is given by:

$$\Delta F_z = F_z - F_{piston}$$

The bending stiffness of the flexures needs to be minimized so as to keep  $\Delta F_z$  as small as possible. For this design, we target to keep  $\Delta F_z$  to within 1 % of the load applied by the piston at all times.

Assuming a maximum specimen wear of  $1 \text{ mm}^3$ , the max deflection at the end of the flexures is given by,

$$\delta_{max} = \frac{1 \text{ mm}^3}{6 \text{ mm} \times 6 \text{ mm}} = 0.028 \text{ mm}$$

Considering each flexure to be a thin plate, the bending stiffness of each flexure is,

$$EI = \frac{Ebt^3}{12(1-\nu^2)} = 1.93 \times 10^6 \text{ N.mm}^2$$

Therefore, treating the flexures as thin cantilevered plates, the net reduction in applied force,

$$\Delta F_z = \frac{3\delta_{max}(2EI)}{L^3} = 1.23 \text{ N}$$

As per the design requirements for this tribometer, the minimum contact pressure experienced by the specimen is 4 MPa, which translates to a minimum applied force,

$$F_{Z\_min} = 144 \text{ N}$$

Maximum variability in applied force caused by flexure system =  $\frac{\Delta F_Z}{F_{Z\_min}} \times 100 = 0.85 \%$

## 6. Torsional deflection in the flexures

The frictional force,  $F_Y$ , will cause a torque,  $T_X$ , on the flexures. The spacing between the two flexures,  $s$ , needs to be maximized to minimize displacements due to torsion.

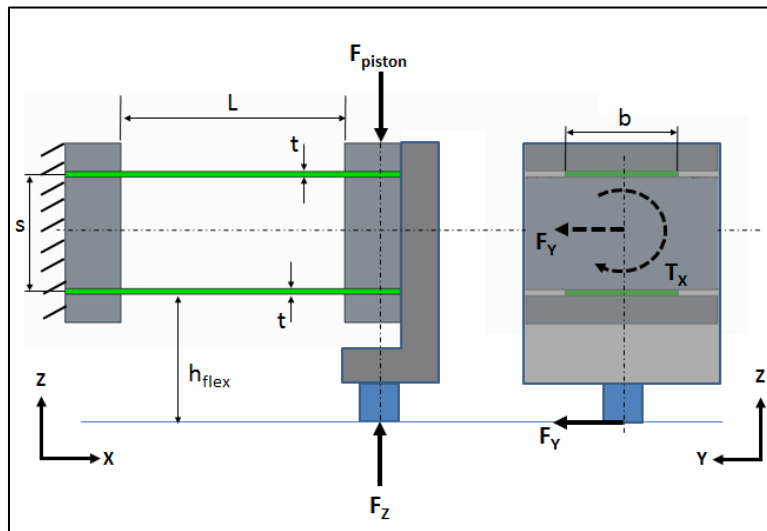


**Figure 4 : Effect of friction forces on the flexure**

Assuming a highly conservative coefficient of friction value of 1, for the maximum contact pressure of 20 MPa, the frictional force,  $F_Y = 720 \text{ N}$

Height of lower flexure from specimen contact surface,  $h_{flex} = 1.5'' = 38.1 \text{ mm}$

Torque on flexures,  $T_X = F_Y \times \left( h_{flex} + \frac{s}{2} \right) = 36.6 \times 10^3 \text{ N.mm}$

Shear stress on the flexure,  $\tau_{xy} = \frac{T_X}{sbt} = 44.5 \text{ MPa}$

Maximum Horizontal displacement,  $v_{max} = \frac{\tau_{xy}}{GL} = 30 \mu\text{m}$

The maximum horizontal displacement is within the limit of 50 microns. However, warping of the thin flexure sheets was ignored in this analysis. Given that the thickness of each flexure is only 0.05'', warping of the flexures is a distinct possibility and, if that occurs, the actual displacements could be much higher than the value of 30 microns predicted by this analysis.

## 7. Design Modification to eliminate torsion

To avoid the uncertainty caused by warping of the flexure sheets, the initial design was modified to eliminate the torque acting on the flexures, and subject them to simple shear instead. This was achieved by moving the specimen contact surface upwards until it is in line with the shear center of the flexure plates.

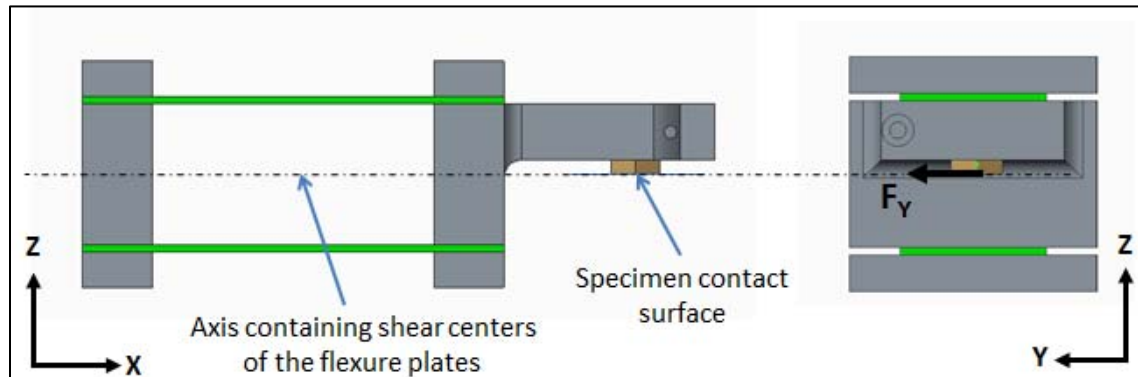


**Figure 5 : Modified design to eliminate Torsion on the flexures**

Now, shear stress in each flexure,  $\tau_{xy} = \frac{F_Y}{2bt} = 11.2 \text{ MPa}$

Maximum Horizontal displacement,  $v_{max} = \frac{\tau_{xy}}{GL} = 8 \mu m$

Thus, the design modification not only removed the uncertainty caused by the possibility of warping of the flexures, but also reduced the maximum horizontal deflection of the flexure assembly to below 10 microns.

Since the dimensions of the flexures are unchanged from the previous design, the variability in the vertical force caused by them remains the same as before.

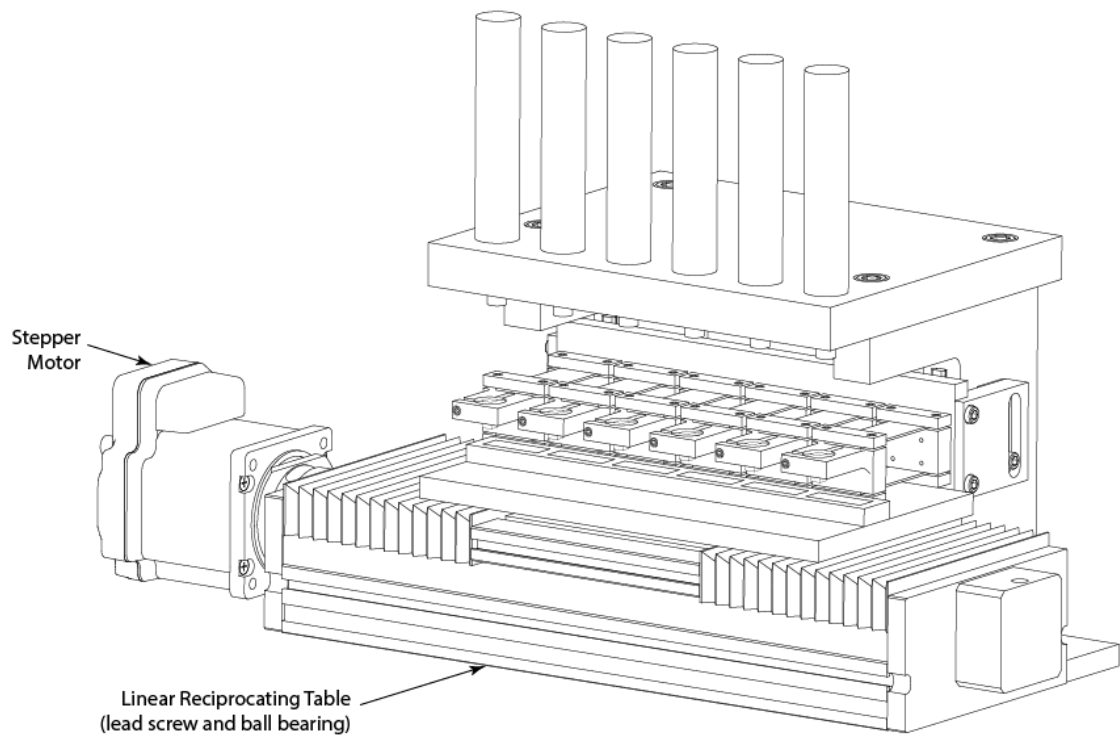
## 8. Stresses in the flexures

The endurance limit for A36 steel is 250 MPa. Assuming that the endurance limit in shear is half of that value, i.e. 125 MPa, the max shear stress in the flexures is only 11.2 MPa which is less than 10 % of the endurance limit. So the flexures will not fail in fatigue.

## 9. Summary

- The chosen flexure dimensions will ensure that the variability in applied force is below 1 %.
- The modified design that completely eliminates the torque on the flexures is preferred as it is difficult to quantify the effects of warping of steel sheets under torsion.
- The maximum horizontal deflection in the flexures is only 8 microns.
- The stresses in the steel sheet are within 10 % of the endurance limit.

## A.4 Reciprocation Components



# An analysis for a lead screw, ball bearing, and motor assembly

Diana R. Haidar

Department of Mechanical Engineering, Doctoral Candidate, University of Delaware  
Address: 130 Academy St., 333 Spencer Lab, Newark, DE, 19716, USA  
Email: [dhaidar@udel.edu](mailto:dhaidar@udel.edu)

## 1. Background Information

Lead screws, also known as power screws, are used in machinery to translate rotary motion into linear motion. In many cases, the rotary motion of a motor shaft turns the lead screw, which is threaded through a ball bearing that is rigidly attached to a table. Here, the screw's rotational motion causes linear translation of that table as it slides along guide rails, as shown in Figure 1. In effect, when the motor shaft rotates in one direction and then reverses it provides the table with reciprocal linear motion.

Many types of industrial equipment use this technology. In these, a program directs the motor to produce a precise amount of rotation so that the table is moved to a desired location at a set speed. A prime example is Computer Numerical Control (CNC) milling machines, in which accurately locating a part mounted on the linear table and setting the material feed rate is of critical importance for cutting prescribed geometries.

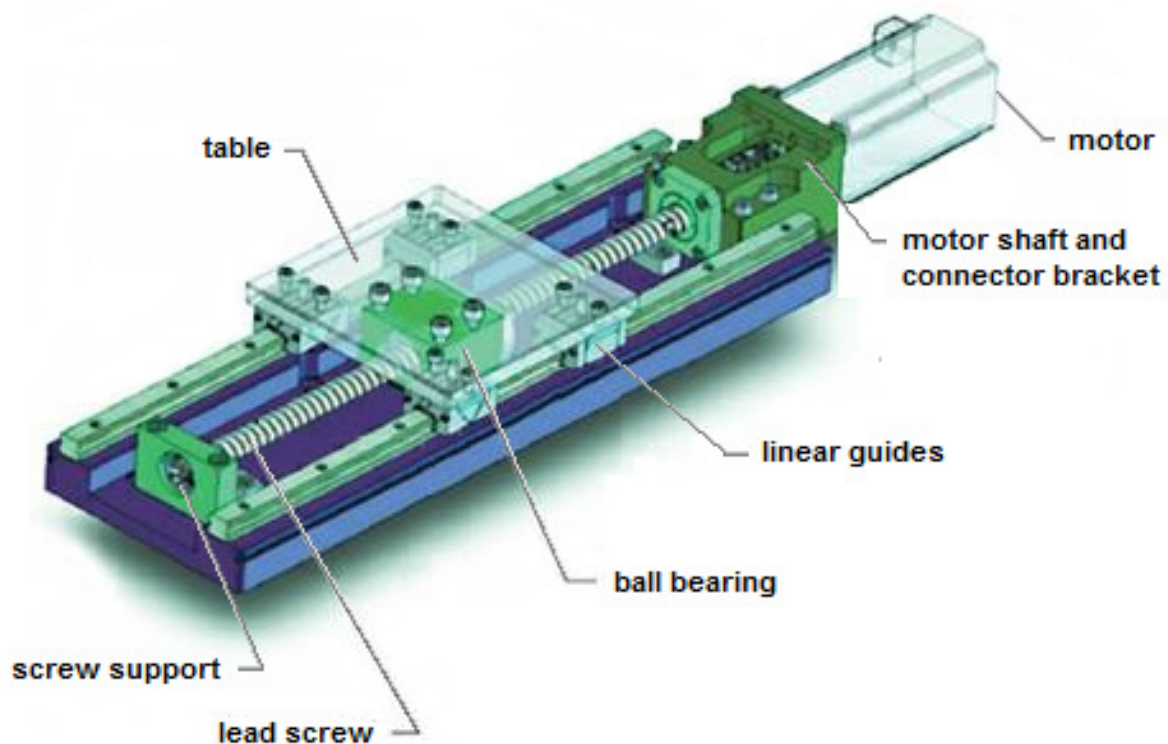


Figure 1: Linearly Reciprocating Table Driven by a Rotating Lead Screw [1]

## 2. Problem Statement

### a. tribometry

A tribometer is an instrument that brings materials into relative sliding contact, so that surface phenomena from wear, friction and adhesion can be quantitatively measured and qualitatively observed. There are a variety of ways to induce relative sliding between two materials. For the case of linear reciprocation a pin-on-flat tribometer can be utilized. Figure 2 displays a common setup, in which the hard flat counterface is mounted to a sliding table and the subject material is compressively load into contact with it.

### b. motivation

Among the materials tested for their tribological properties in this manner is PTFE nanocomposites. These materials are well known to need only trace amounts of nanocomposite reinforcements in order to perform as ultra-low wear rate materials [2]. However, an obstacle in studying these extremely low wear rate materials in conditions with notable material loss is the requirement of lengthy testing times – these experiments can last for weeks or months. Traditionally an entire tribometer, like the one imaged in Figure 3, is occupied by a single sample for the duration of these tests. In order to expedite this process, efforts must be made to develop tribometers capable of testing multiple samples at once.

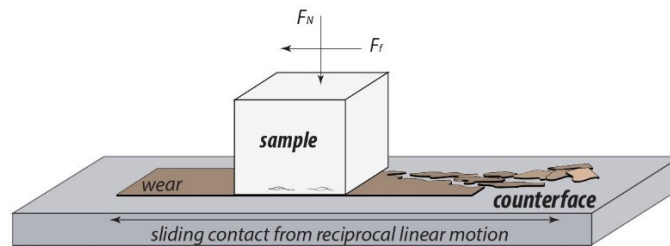


Figure 2: Linear Reciprocating Motion of a Pin-on-Flat

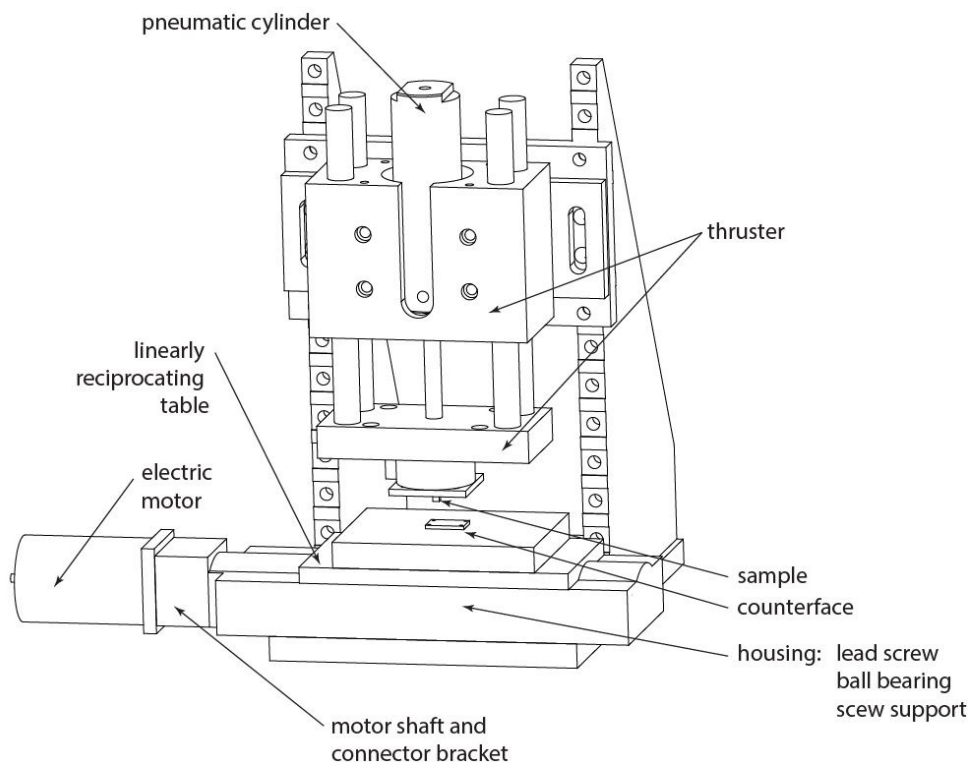


Figure 3: Pin-on-Flat Tribometer

### c. global objective

The overall objective is to design an entirely new tribometer with the following specifications:

- 1) 6 samples for testing, easily removed & returned
- 2) controllable contact pressure, 1-20 [MPa]
- 3) controllable sliding speeds, 1-100 [mm/s]
- 4) normal load feedback, via load cell
- 5) LabVIEW interface, controls & data collection

The foundation of a linearly reciprocating tribometer is the assembly driving the motion, whose design is completely dependent on these ambitious specifications. Therefore, a comprehensive engineering analysis of this region is critical to ensure a long working lifetime with a high level of performance.

### d. report goals

The goal of this report is to provide a complete engineering analysis of a lead screw in order to select an appropriate ball bearing and motor for a linearly reciprocating tribometer.

In order to satisfy the given design specifications, the first step is to calculate the loads induced from frictional sliding. Then an analysis to appropriately size a lead screw and ball bearing is conducted. The ability of the selected lead screw to withstand fatigue and buckling is considered before selecting an appropriate motor that will communicate with LabVIEW.

## 3. Lead Screw Analysis

### a. frictional forces

For the multi-sample pin-on-flat tribometer considered here, frictional forces between the subject pins and their paired counterfaces are the main resistance to sliding. Since the counterfaces, table and ball bearing are all rigidly stacked, one can consider a total sum of frictional forces  $F_{f1}$  to be acting on threads parallel to the axial direction of the lead screw.

Since the balls from the bearing are located between the lead screw threads, the total frictional force  $F_{f1}$  is applied along the screw's mean diameter  $\varnothing_{mean}$ , as depicted by the force body diagram (FBD) in Figure 4. Due to this geometry, a torque  $T$  producing the force  $F_t$  is necessary for overcoming the static condition and inducing motion of the linear table, as shown by the FBD in Figure 7.

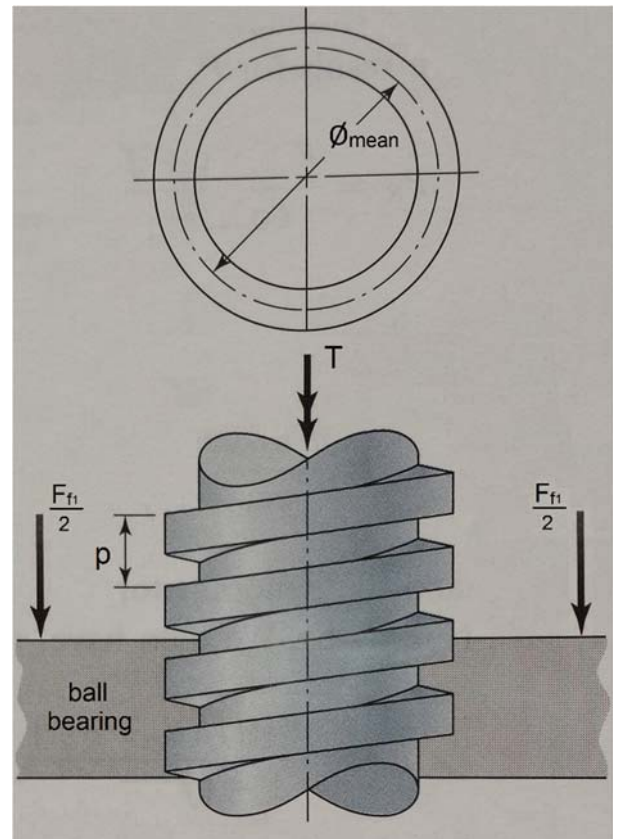


Figure 4: Lead Screw and Ball Bearing, overall FBD

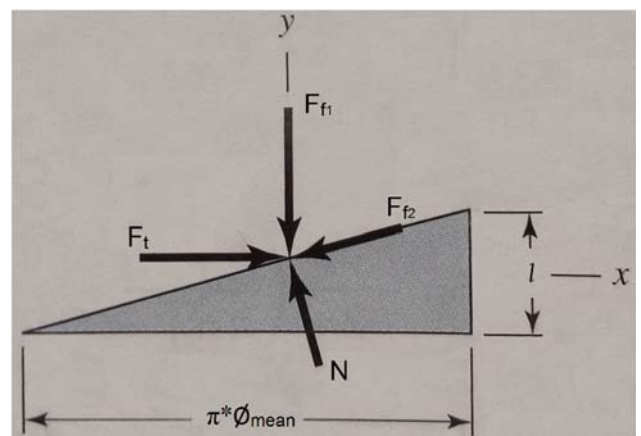


Figure 5: Lead Screw and Ball Bearing, one thread FBD

Normal Force

$$F_n = \frac{P}{A}$$

Frictional Force – total summation

$$F_{f1} = f_1 * F_n * (\# \text{ samples})$$

P - compressive pressure	6.5	[MPa]
A - sample surface area ~6.2x6.2mm <sup>2</sup>	38	[mm <sup>2</sup> ]
<b>F<sub>n</sub> - normal force</b>	<b>250</b>	<b>[N]</b>

Table 1: Example Calculation for Normal Force

F <sub>n</sub> - normal force	250	[N]
f <sub>1</sub> - sample friction coefficient	1	[-]
# of samples	6	[-]
<b>F<sub>f1</sub> - total frictional force</b>	<b>1500</b>	<b>[N]</b>

Table 2: Example Calculation for Total Frictional Force

**b. applied torque**

The force F<sub>t</sub> applied by a torque T on the lead screw is necessary to induce linear motion of the table. To calculate F<sub>t</sub> an analysis of the forces between the balls of the bearing and threads of the lead screw was conducted by summing forces in the x-direction and y-direction of the FBD in Figure 7. Then F<sub>t</sub> was used to calculate the applied torque T based on the lead screw geometry.

Applied Force – on one thread

$$F_t = \frac{F_{f1} \left( \frac{l}{\pi * \phi_{mean}} + f_2 \right)}{1 - \left( \frac{f_2 * l}{\pi * \phi_{mean}} \right)}$$

Applied Torque – distributed by bearing

$$T = \left( \frac{\phi_{mean}}{2} \right) * F_t * (\# \text{ threads})$$

ϕ mean - avg screw diameter	13	[mm]
p - screw pitch	5	[mm]
l - screw lead	5	[mm]
f <sub>2</sub> - friction lubed steel on steel	0.15	[-]
<b>F<sub>t</sub> - applied force on one thread</b>	<b>421</b>	<b>[N]</b>

Table 3: Example Calculation for Applied Force

F <sub>t</sub> - applied force on one thread	421	[N]
d - length of ball bearing	50	[mm]
# of threads contacting = l/d	10	[-]
F - force distributed by bearing = F <sub>t</sub> *(l/d)	27	[N]
<b>T - applied torque distributed by bearing</b>	<b>27</b>	<b>[N*cm]</b>

Table 4: Example Calculation for Applied Torque

**c. selecting variables**

It is clear that the example calculation for the applied torque T on the lead screw in Tables 1-4 contained a variety of assumptions including:

- 1) mid-range contact pressure, 6.5 [MPa]
- 2) mid-range bearing length and contacting threads 50 [mm] and 10 [-]
- 3) mid-range lead screw diameter, 13 [mm]
- 4) over-estimation of sample friction, 1.0 [-]

In order to optimize the selection of variables for the lead screw and ball bearing, it is essential to elucidate the effect of these assumptions on the value of applied torque. This was done over a range of sample contact pressures to observe the broader trends.

First considered is bearing length. The amount of applied torque in response to the addition of contacting threads, in increments of 5, is plotted in Figure 6. It is observed that initially small increases causes a significant reduction in the required torque. This trend is reasonable because the number of threads increasing from 5 to 10 is doubled whereas another doubling requires transitioning from 10 to 20 threads and so on. Hence, there is a diminishing return with regards to elongating the ball bearing. Since utilizing 10 contacting threads makes a significant improvement in load distribution without requiring an oversized ball bearing, the length of 50 [mm] is recommended.

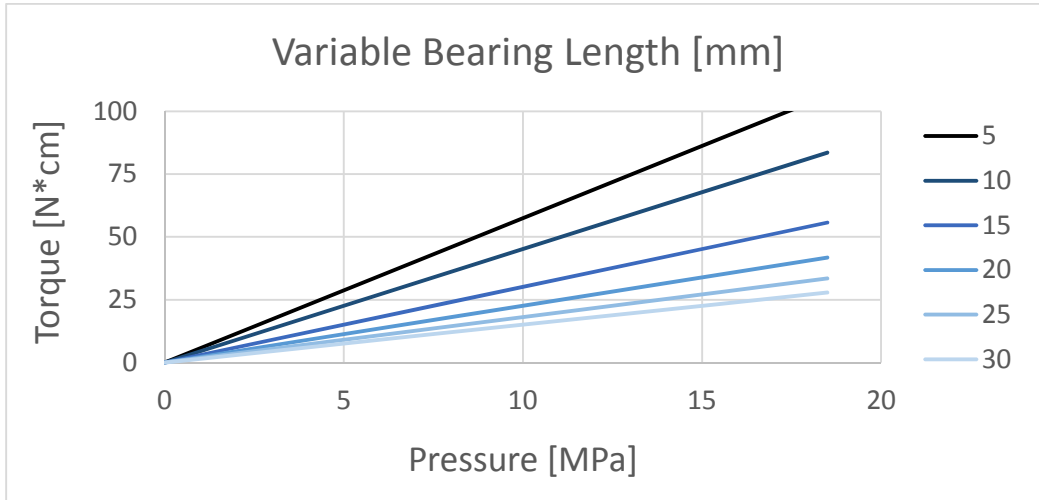


Figure 6: Graph of Torque vs. Pressure as a function of Variable Ball Bearing Length

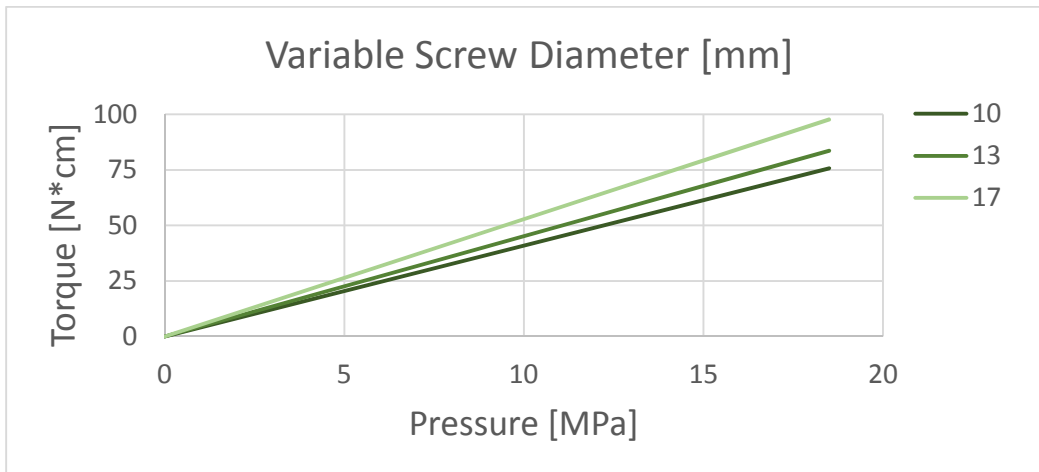


Figure 7: Graph of Torque vs. Pressure as a function of Variable Lead Screw Diameter

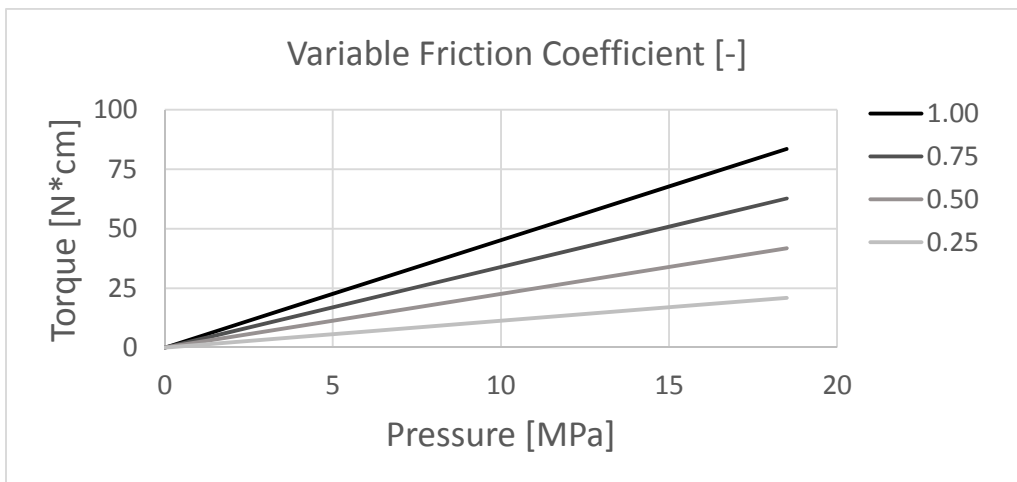


Figure 8: Graph of Torque vs. Pressure as a function of Variable Sample Friction Coefficients

Although larger screws have the ability to support higher load capacities, they also necessitate a larger applied torque. In this scenario, torque is calculated as force times the lead screw radius. The plot in Figure 7 shows variable diameter has a direct effect on torque, though not as significant in total range as with the bearing length because the diameters considered were within 25 [mm]. In order to balance higher loading capacities with lower torque, the mid-range diameter of 13 [mm] is selected.

Finally considered is the effect of friction coefficient of the subject material. The value of 1.0 [-] is considerably higher than most materials tested in a tribometer, especially since most studies aim to observe the behavior of materials that have both relatively low wear and low sliding friction. The plot in Figure 8 shows the value of 1.0 [-] to be a highly conservative estimate, but it is maintained as the value for this analysis as a factor of safety. If any subject materials are expected to be above this friction coefficient, the tribometer's user can compensate by reducing the total number of samples being tested.

**d. failure analysis**

With the lead screw and ball bearing variables selected, an analysis determining whether the screw will prematurely fail due to fatigue and buckling is conducted. In most of these calculations, the primary assumption made is that the distribution of a 1055 hardened steel screw's stress in a threaded hole is reasonably similar to a ball bearing.

First evaluated is the alternating stress of the lead screw. This stress is due to the screw undergoing repeated loading and unloading in torsion, due to the reciprocal motion of the linear table. It is found that the alternating stress  $\sigma$  is far below both the yield strength and the torsional endurance limit for  $10^6$  cycle lifetime. Thus, the assembly of the recommended lead screw and ball bearing are satisfactory for resisting premature torsional fatigue failure.

$\varnothing$ mean - avg screw diameter	13	[mm]
d - length of ball bearing	50	[mm]
A - approximate effective area	756	[mm <sup>2</sup> ]
Ft - total applied force by torsion	421	[N]
K - concentration factor, hardened steel	3	[-]
<b><math>\sigma</math> - alternating stress, thread root stress = (F*K)/A</b>	<b>1.7</b>	<b>[MPa]</b>

Table 5: Alternating Stress of Threaded Screw

<b>Sy - yield strength</b>	<b>560</b>	<b>[MPa]</b>
<b>Su - ultimate tensile strength</b>	<b>660</b>	<b>[MPa]</b>
Sn' - fatigue strength for torsional loads = Su/2	330	[MPa]
CL - load factor, torsion	0.580	[-]
CG - gradient factor, $\varnothing 13$ [mm]	0.900	[-]
CS - surface factor, fine polish hardened steel	0.900	[-]
CT - temperature factor, below 840°F	1.000	[-]
CR - reliability factor, 90%	0.897	[-]
<b>Sn - endurance limit <math>10^6</math> cycles</b>	<b>139</b>	<b>[MPa]</b>

Table 6: Torsional Endurance Limit for  $10^6$  cycle lifetime

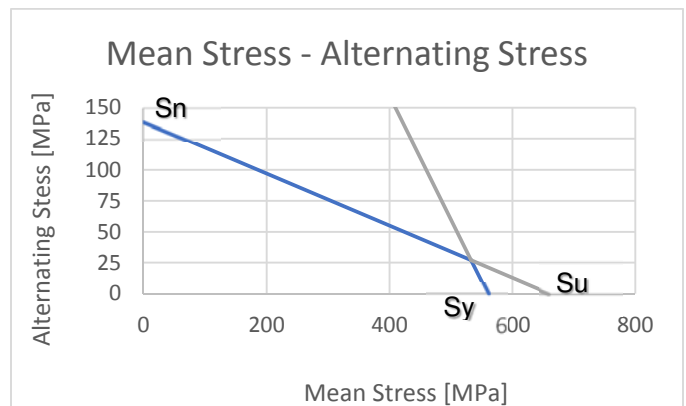


Figure 9: Lead Screw Mean Stress–Alternating Stress

The second calculation is for the critical buckling load of the lead screw. Based on the previous lead screw recommendations, the critical buckling load for the mid-range diameter screw in Table 7 is nearly equal to the total frictional force  $F_{f1}$  and therefore unsatisfactory. Yet due to the area moment of inertia calculation, it is clear that a small increase in diameter will have a large improvement on buckling load. Another calculation for the larger diameter previously under consideration is shown in Table 8 to be satisfactory having a factor of safety of 3. Therefore, the lead screw recommendation has been modified to implement a diameter size of  $\varnothing 17$ [mm].

$\varnothing$ mean - avg screw diameter	13	[mm]
E - Young's Modulus	200,000	[MPa]
I - area moment of inertia = $(\pi * \varnothing^4)/64$	1277	[mm <sup>4</sup> ]
L - screw overall length	400	[mm]
<b>Pc - critical buckling load</b>	<b>15,754</b>	<b>[N]</b>

Table 7: Critical Buckling Load for  $\varnothing 13$ [mm]

$\varnothing$ mean - avg screw diameter	17	[mm]
E - Young's Modulus	200,000	[MPa]
I - area moment of inertia = $(\pi * \varnothing^4)/64$	4100	[mm <sup>4</sup> ]
L - screw overall length	400	[mm]
<b>Pc - critical buckling load</b>	<b>50,580</b>	<b>[N]</b>

Table 8: Critical Buckling Load for  $\varnothing 17$ [mm]

**e. selection for purchase**

Lead Screw – Thompson Linear Motion

<b>Thread Direction</b>	Right Hand
<b>Screw Material</b>	Alloy Steel
<b>Part Number</b>	<b>190-9101</b>

<b>Diameter x Lead (in.)</b>	0.750 x 0.200
<b>Lead Accuracy (in/ft)</b>	$\pm 0.004$
<b>Screw Weight (lbs/ft)</b>	1.4
<b>Screw Root Diameter (in.)</b>	0.66
<b>Nominal Ball Diameter (in.)</b>	0.125
<b>Number of Starts</b>	1

Lead Screw – Thompson Linear Motion

<b>Thread Direction</b>	Right Hand
<b>Nut Material</b>	Alloy Steel
<b>Dynamic Load (lbs)</b>	1,900
<b>Max. Static Load (lbs)</b>	18,800
<b>Torque to raise 1 lb (oz-in.)</b>	0.57
<b>Nut weight (lbs)</b>	0.75
<b>Ball Nut Part Number</b>	<b>8107-448-027</b>

note: the applied force from torque has a safety factor of 22 to ball bearing's dynamic load

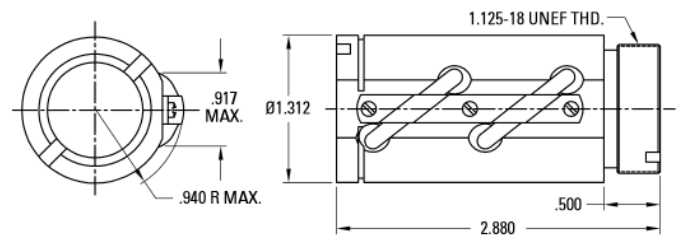


Figure 10: Lead Screw & Ball Bearing Assembly [3]

**4. Motor Selection**

With the lead screw and ball bearing variables selected, the known range of torques necessary for sliding motion can be used to choose a motor that will communicate directly with LabVIEW.

It is industry standard to select motor with at least 2 factors of safety. Therefore in upholding the full range of testing contact pressures from 1-20 [MPa] it is seen that the Lexium MDrive NEMA 34 single stack motor 70 [VDC] is recommended for purchase. Yet selecting a smaller motor remains an option if the common 6.5 [MPa] test with low friction coefficients is satisfactory for regular use.

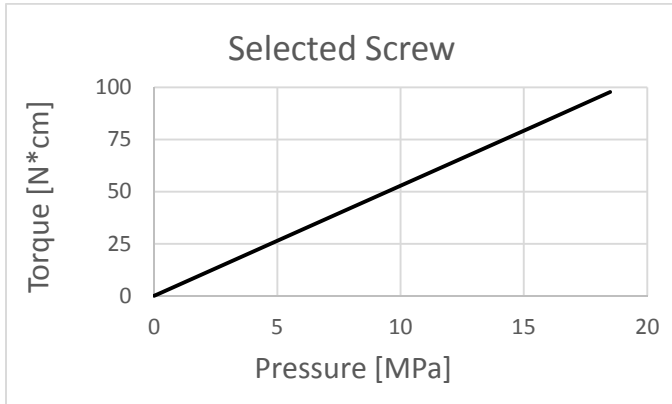


Figure 11: Selected Lead Torques

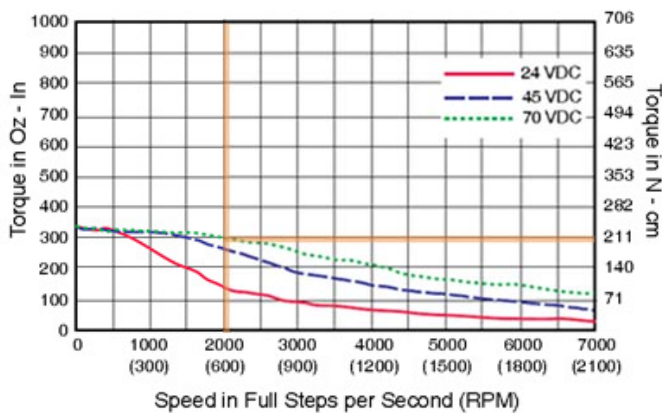


Figure 12: NEMA 34 Motor Torques [4]

## Acknowledgements

Instruments Instructor:

Dr. David Burris, University of Delaware,  
Associate Professor of Mechanical Engineering

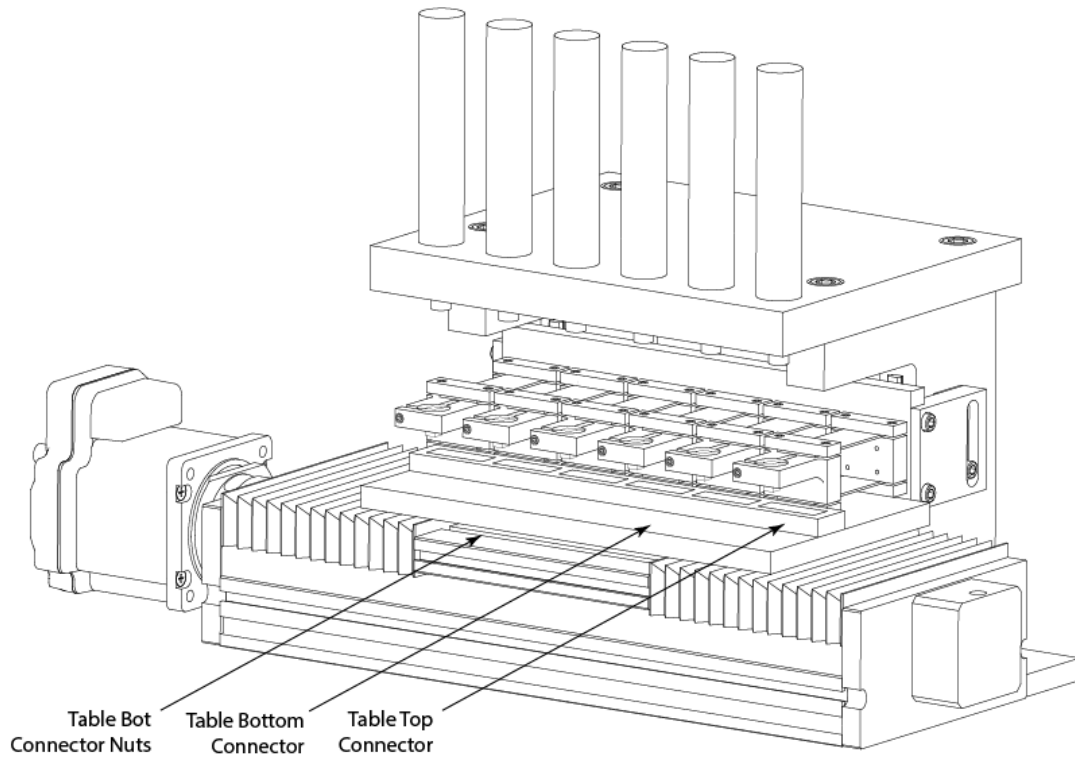
PhD Advisor:

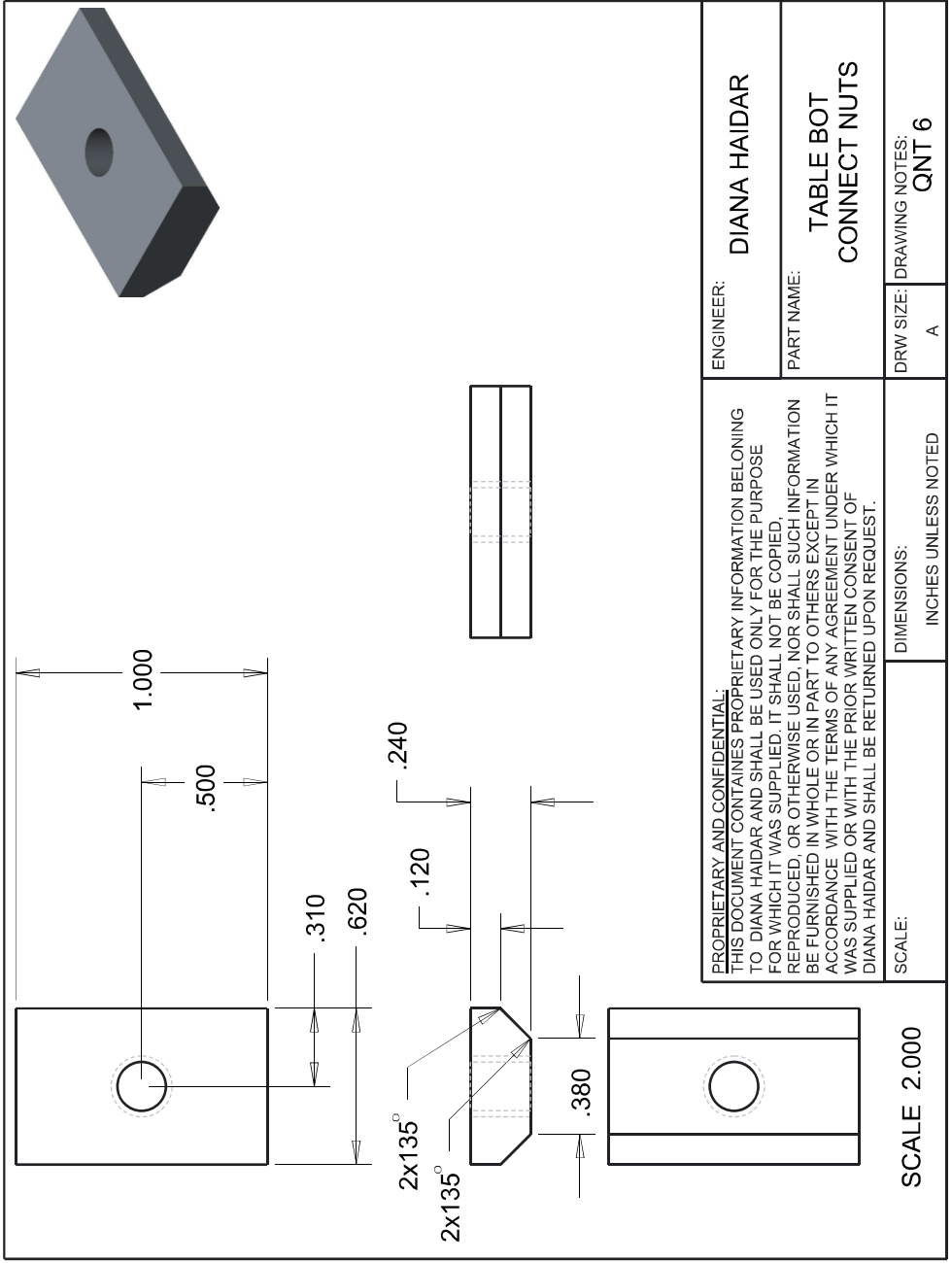
Dr. David Burris, University of Delaware,  
Associate Professor of Mechanical Engineering

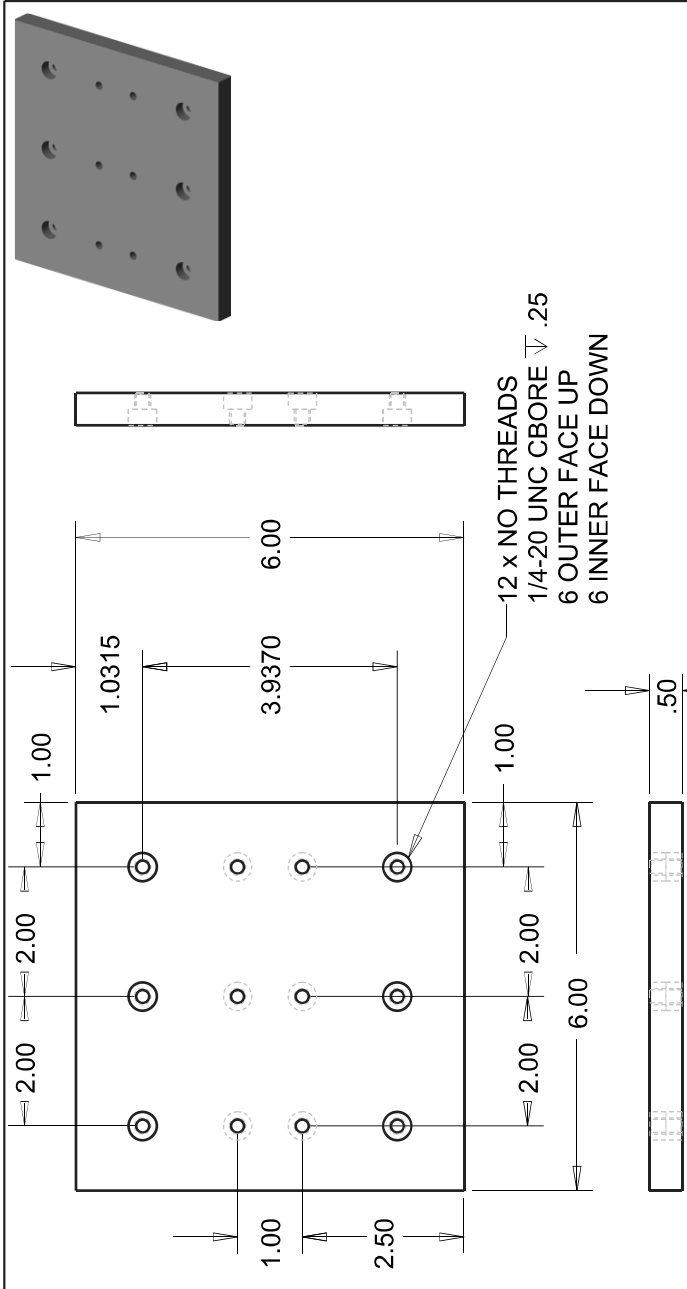
## References

- [1] "Scanning for ideas: Options make ball-screw drive flexible and versatile," *Machine Design*, 21-Nov-2007. [Online]. Available: <http://machinedesign.com/archive/scanning-ideas-options-make-ball-screw-drive-flexible-and-versatile>. [Accessed: 27-May-2015].
- [2] D. L. Burris, S. Zhao, R. Duncan, J. Lowitz, S. S. Perry, L. S. Schadler, and W. G. Sawyer, "A route to wear resistant PTFE via trace loadings of functionalized nanofillers," *Wear*, vol. 267, no. 1-4, pp. 653-660, Jun. 2009.
- [3] "Thomson Linear Motion Ball Screws (Inch)." [Online]. Available: [http://www.thomsonlinear.com/website/com/eng/products/ball\\_screws\\_and\\_lead\\_screws/ball\\_screws/precision\\_plus\\_ground.php](http://www.thomsonlinear.com/website/com/eng/products/ball_screws_and_lead_screws/ball_screws/precision_plus_ground.php). [Accessed: 28-May-2015].
- [4] "Lexium MDrive Motor ...: Schneider Electric Motion USA." [Online]. Available: <http://motion.schneider-electric.com/lmd/lexium-mdrive-pulse-direction.php?nema=34>. [Accessed: 28-May-2015].

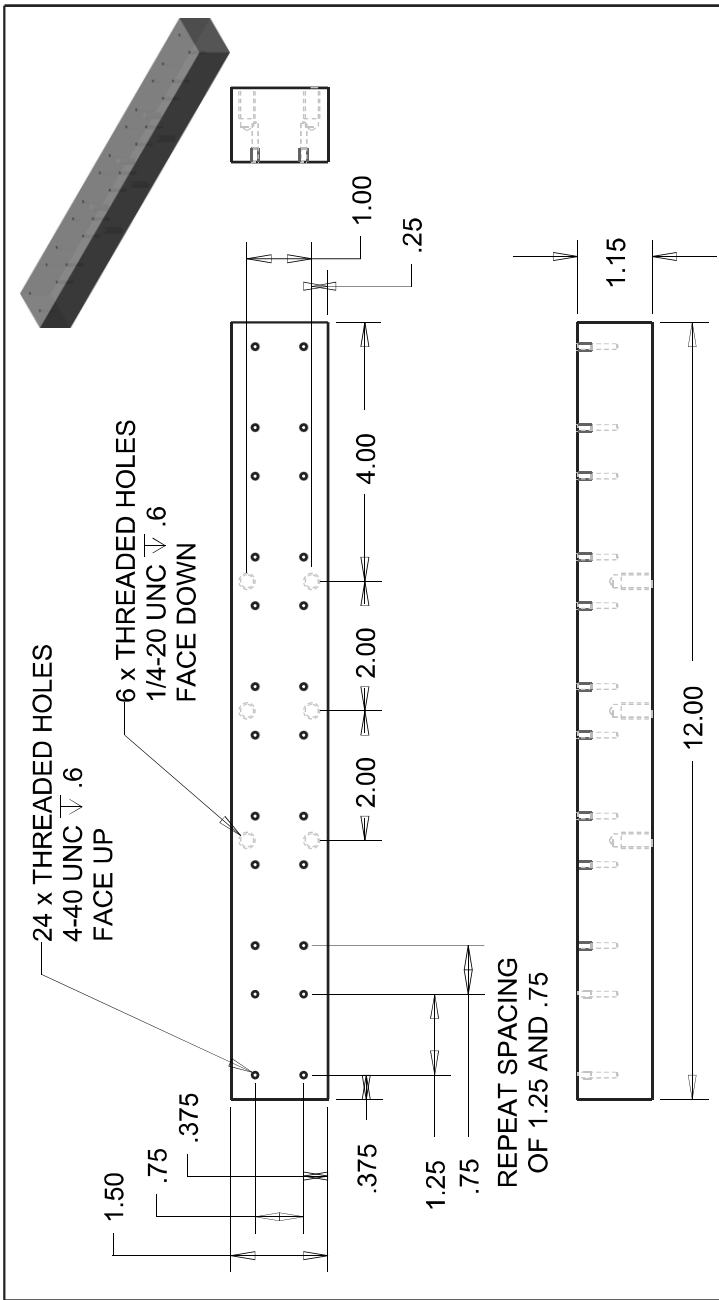
## A.5 Table Components





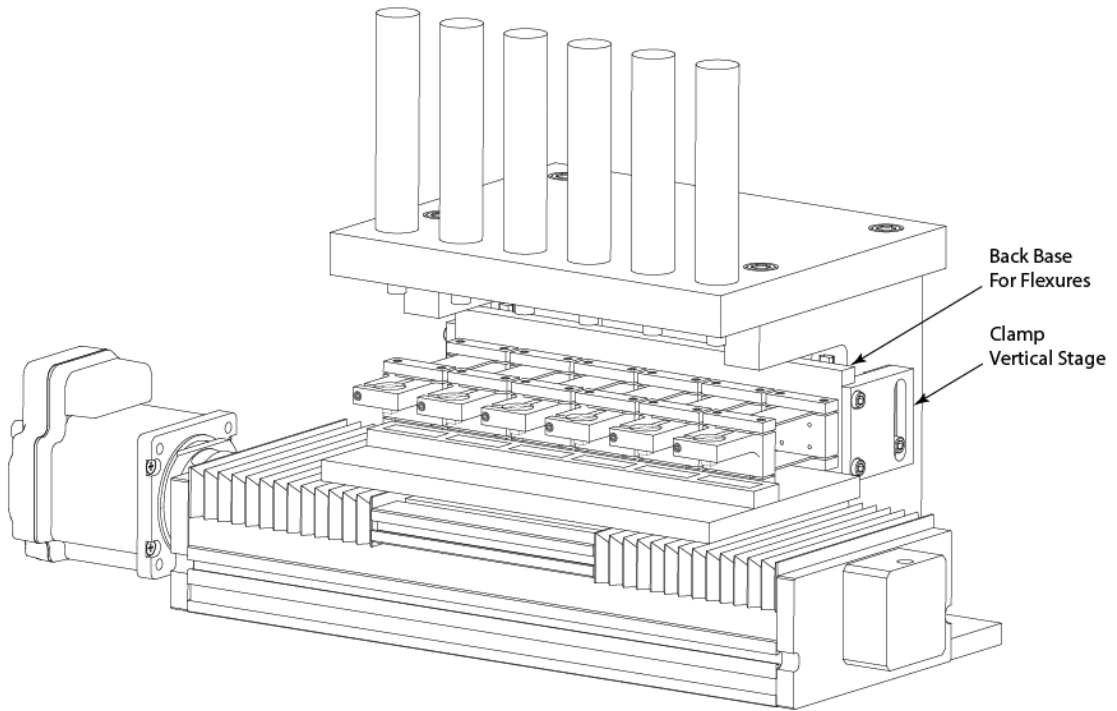


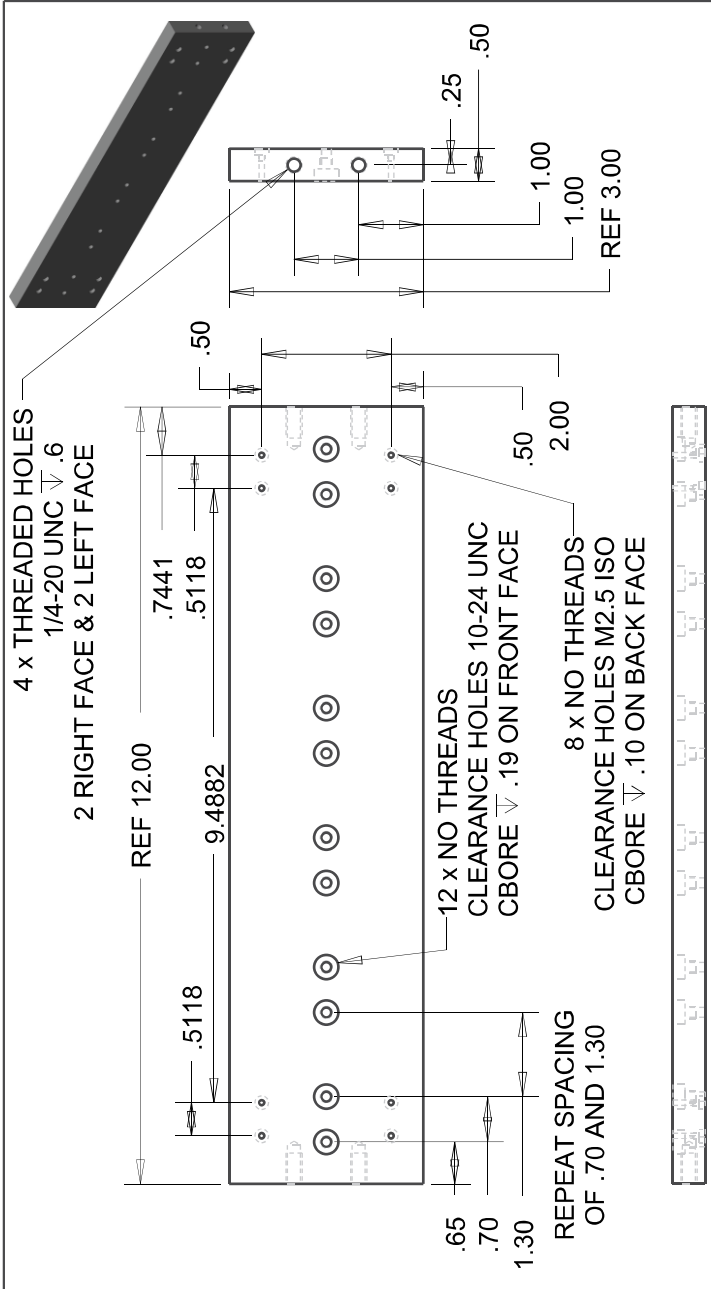
<p><b>PROPRIETARY AND CONFIDENTIAL:</b>          THIS DOCUMENT CONTAINS PROPRIETARY INFORMATION BELONGING TO DIANA HAIDAR AND SHALL BE USED ONLY FOR THE PURPOSE FOR WHICH IT WAS SUPPLIED. IT SHALL NOT BE COPIED, REPRODUCED, OR OTHERWISE USED, NOR SHALL SUCH INFORMATION BE FURNISHED IN WHOLE OR IN PART TO OTHERS EXCEPT IN ACCORDANCE WITH THE TERMS OF ANY AGREEMENT UNDER WHICH IT WAS SUPPLIED OR WITH THE PRIOR WRITTEN CONSENT OF DIANA HAIDAR AND SHALL BE RETURNED UPON REQUEST.</p>	<p>ENGINEER: <b>DIANA HAIDAR</b></p>	
	<p>PART NAME: <b>TABLE BOTTOM CONNECTOR</b></p>	
<p>SCALE: <b>SCALE 0.500</b></p>	<p>DIMENSIONS: <b>INCHES UNLESS NOTED</b></p>	<p>DRW SHEET: <b>A</b></p>
<p>SCALE: <b>0.500</b></p>		<p>DRAWING NOTES: <b>QNT 1</b></p>



<p><b>PROPRIETARY AND CONFIDENTIAL:</b> THIS DOCUMENT CONTAINS PROPRIETARY INFORMATION BELONGING TO DIANA HAIDAR AND SHALL BE USED ONLY FOR THE PURPOSE FOR WHICH IT WAS SUPPLIED. IT SHALL NOT BE COPIED, REPRODUCED, OR OTHERWISE USED, NOR SHALL SUCH INFORMATION BE FURNISHED IN WHOLE OR IN PART TO OTHERS EXCEPT IN ACCORDANCE WITH THE TERMS OF ANY AGREEMENT UNDER WHICH IT WAS SUPPLIED OR WITH THE PRIOR WRITTEN CONSENT OF DIANA HAIDAR AND SHALL BE RETURNED UPON REQUEST.</p>	ENGINEER:	DIANA HAIDAR
	PART NAME:	TABLE TOP CONNECTOR
SCALE: <b>SCALE 0.500</b>	DIMENSIONS: INCHES UNLESS NOTED	DRW SIZE: A
		DRAWING NOTES: QNT 1

## A.6 Carriage Components

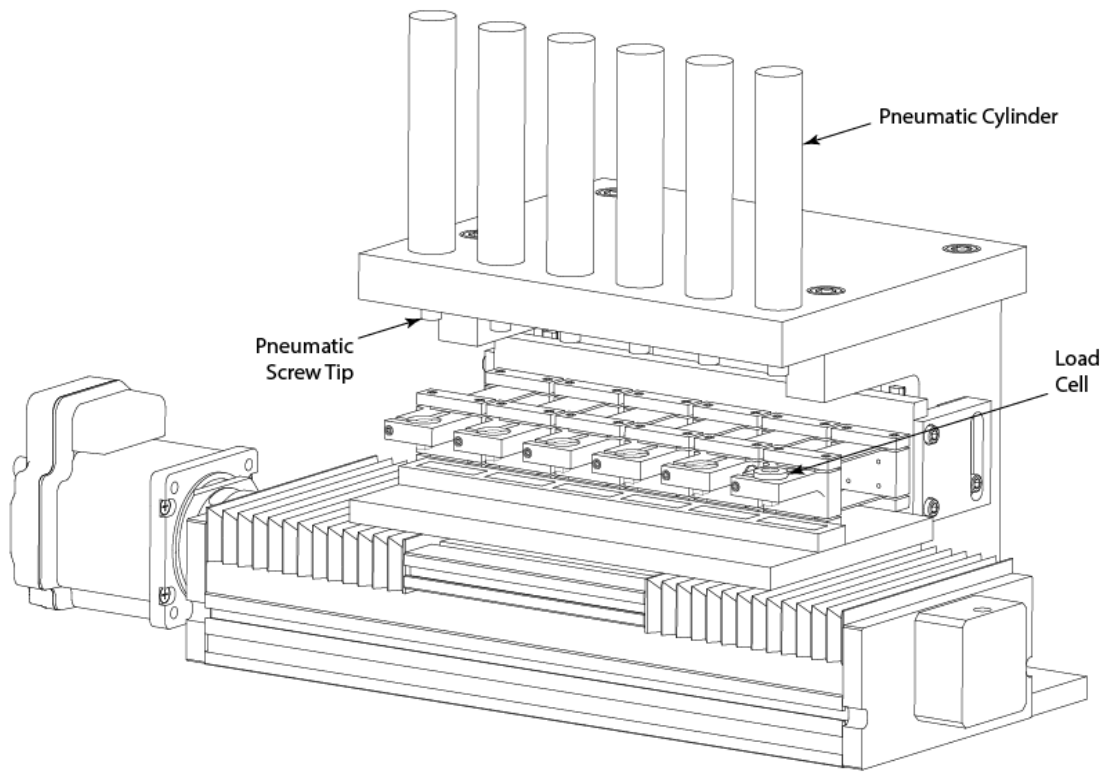


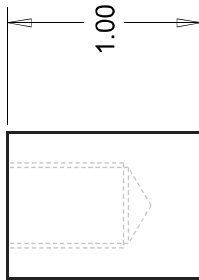
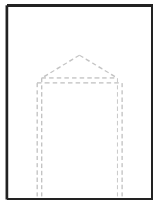
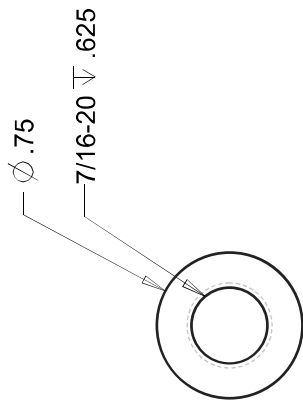


<p><b>PROPRIETARY AND CONFIDENTIAL:</b> THIS DOCUMENT CONTAINS PROPRIETARY INFORMATION BELONGING TO DIANA HAIDAR AND SHALL BE USED ONLY FOR THE PURPOSE FOR WHICH IT WAS SUPPLIED. IT SHALL NOT BE COPIED, REPRODUCED, OR OTHERWISE USED, NOR SHALL SUCH INFORMATION BE FURNISHED IN WHOLE OR IN PART TO OTHERS EXCEPT IN ACCORDANCE WITH THE TERMS OF ANY AGREEMENT UNDER WHICH IT WAS SUPPLIED OR WITH THE PRIOR WRITTEN CONSENT OF DIANA HAIDAR AND SHALL BE RETURNED UPON REQUEST.</p>		<p>ENGINEER: <b>DIANA HAIDAR</b></p>
<p>SCALE: <b>SCALE 0.500</b></p>		<p>PART NAME: <b>BACK BASE FOR FLEXURES</b></p>
<p>DIMENSIONS: INCHES UNLESS NOTED</p>		<p>DRW SIZE: DRAWING NOTES: A QNT 1</p>



## A.7 Pneumatics





<b>NOTE:</b> -MATERIAL HDPE	<b>PROPRIETARY AND CONFIDENTIAL:</b> THIS DOCUMENT CONTAINS PROPRIETARY INFORMATION BELONGING TO DIANA HAIDAR AND SHALL BE USED ONLY FOR THE PURPOSE FOR WHICH IT WAS SUPPLIED. IT SHALL NOT BE COPIED, REPRODUCED, OR OTHERWISE USED, NOR SHALL SUCH INFORMATION BE FURNISHED IN WHOLE OR IN PART TO OTHERS EXCEPT IN ACCORDANCE WITH THE TERMS OF ANY AGREEMENT UNDER WHICH IT WAS SUPPLIED OR WITH THE PRIOR WRITTEN CONSENT OF DIANA HAIDAR AND SHALL BE RETURNED UPON REQUEST.		ENGINEER: <b>DIANA HAIDAR</b>
	SCALE: <b>SCALE 1.500</b>	DIMENSIONS: INCHES UNLESS NOTED	PART NAME: <b>PNEUMATIC SCREW TIP</b>
SCALE: <b>SCALE 1.500</b>		DIMENSIONS: INCHES UNLESS NOTED	DRW SIZE: <b>A</b>
		DRAWING NOTES: <b>QNT 6</b>	

## Appendix B

### DATA FROM PEEK-PTFE ENVIRONMENTAL MOISTURE STUDY

Table B-1 Average surface roughness ( $R_a$ ) of each 304 stainless steel counterface used for wear tests conducted in dry nitrogen environment (<0.05% RH). The roughness value reported for each counterface was measured in 3 regions within the area designated for the polymer sample's wear track to form during testing. Measurements were taken using a Veeco Wyko NT9100 scanning white light interferometer at 5.5x zoom with a viewing window of 0.86 mm x 1.10 mm (N=3).

PEEK Filler (wt%)	PTFE Matrix (wt%)	Dry Nitrogen Environment 304 Stainless Steel Counterface Average Surface Roughness, $R_a$ (nm)
0	100	36.00
5	95	29.78
10	90	31.82
20	80	29.44
30	70	21.99
40	60	35.32
50	50	13.17
60	40	13.84
70	30	15.78
90	10	18.64
100	0	15.27

Table B-2 Average surface roughness ( $R_a$ ) of each 304 stainless steel counterface used for wear tests conducted in humid air environment (30% RH). The roughness value reported for each counterface was measured in 3 regions within the area designated for the polymer sample's wear track to form during testing. Measurements were taken using a Veeco Wyko NT9100 scanning white light interferometer at 5.5x zoom with a viewing window of 0.86 mm x 1.10 mm (N=3).

PEEK Filler (wt%)	PTFE Matrix (wt%)	Humid Air Environment 304 Stainless Steel Counterface Average Surface Roughness, $R_a$ (nm)
0	100	33.20
5	95	18.71
10	90	17.24
20	80	17.95
30	70	22.78
40	60	21.34
50	50	23.60
100	0	16.96

Table B-3 Density ( $\rho$ ) of each polymer sample subject to wear tests conducted in both dry nitrogen environment (<0.05% RH) and humid air environment (30% RH). The density value reported for each counterface was determined by measuring volume using a Starrett outside micrometer and mass using a Mettler Toledo XP105 DeltaRange™ balance (N=1).

PEEK Filler (wt%)	PTFE Matrix (wt%)	Polymer Sample Density, $\rho$ ( $10^{-3}$ g/mm <sup>3</sup> )
0	100	2.15
5	95	2.07
10	90	2.01
20	80	1.87
30	70	1.71
40	60	1.70
50	50	1.60
60	40	1.51
70	30	1.46
90	10	1.29
100	0	1.29

Table B-4 A collection of mass ( $m$ ) values measured for a ~10 g calibration ‘weight’ as a function of date using a Mettler Toledo XP105 DeltaRange™ balance. The mass values for this reference object were gathered in the same sessions as mass values for polymer samples, which was conducted each time a wear test was interrupted. Data in this table displays the long-term variability in the mass balance, which could have influenced polymer volume loss and polymer wear rate. The mass reported for each session is an average of 3 measurements (N=3).

<b>Date (mm/dd/yy)</b>	<b>Mass of ~10 g Calibration ‘Weight’, <math>m</math> (g)</b>
12/14/2016	9.99860
12/14/2016	9.99862
12/14/2016	9.99863
12/14/2016	9.99858
12/14/2016	9.99861
12/14/2016	9.99871
12/14/2016	9.99868
12/15/2016	9.99872
12/16/2016	9.99865
12/17/2016	9.99870
12/17/2016	9.99869
12/17/2016	9.99864
12/18/2016	9.99866
12/18/2016	9.99867
12/21/2016	9.99870
12/22/2016	9.99871
12/22/2016	9.99872
12/22/2016	9.99877
12/23/2016	9.99871
12/23/2016	9.99866
12/23/2016	9.99865
12/27/2016	9.99866
12/27/2016	9.99867
12/27/2016	9.99868
12/28/2016	9.99867
12/28/2016	9.99868
01/02/2017	9.99867
01/03/2017	9.99865
01/04/2017	9.99866
01/05/2017	9.99866

<b>Date (mm/dd/yy)</b>	<b>Mass of ~10 g Calibration ‘Weight’, <i>m</i> (g)</b>
01/08/2017	9.99865
01/09/2017	9.99868
01/11/2017	9.99868
01/13/2017	9.99864
01/14/2017	9.99869
01/15/2017	9.99866
05/03/2017	9.99856
05/03/2017	9.99855
05/04/2017	9.99858
05/05/2017	9.99865
05/06/2017	9.99857
05/08/2017	9.99860
05/10/2017	9.99858
05/12/2017	9.99857
05/15/2017	9.99854
05/18/2017	9.99856
05/19/2017	9.99858
05/22/2017	9.99860
05/24/2017	9.99860
05/25/2017	9.99859
05/29/2017	9.99860
05/29/2017	9.99860
05/29/2017	9.99861
05/29/2017	9.99863
05/29/2017	9.99860
05/29/2017	9.99861
05/30/2017	9.99861
05/31/2017	9.99860
06/01/2017	9.99859
06/02/2017	9.99861
06/03/2017	9.99860
06/05/2017	9.99862
06/07/2017	9.99859
06/09/2017	9.99859
06/11/2017	9.99862
06/13/2017	9.99859
06/17/2017	9.99861
06/21/2017	9.99859

Table B-5 The complete dataset of polymer wear rates and running film FTIR-ATR spectra comparing the peak-to-peak signal intensity of 1650/1150  $\text{cm}^{-1}$  / $\text{cm}^{-1}$  in this study. The wear test was conducted in a dry nitrogen environment unless indicated by the \* symbol as a humid environment. All metric values are reported as the mean  $\pm$  95% confidence interval (N=5).

<b>material</b>	<b>wear rate, <i>k</i> (<math>10^{-6}</math> mm<sup>3</sup>/(Nm))</b>	<b>I<sub>1655</sub>/I<sub>1150</sub>, unworn (-)</b>	<b>I<sub>1655</sub>/I<sub>1150</sub>, running film (-)</b>
100 wt% PTFE	340 $\pm$ 21	0.008	0.015
* 100 wt% PTFE	610 $\pm$ 83	0.008	0.354
5 wt% PEEK-PTFE	0.13 $\pm$ 0.007	0.017	0.073
* 5 wt% PEEK-PTFE	1.9 $\pm$ 0.07	0.017	0.093
10 wt% PEEK-PTFE	0.068 $\pm$ 0.005	0.031	0.062
* 10 wt% PEEK-PTFE	0.37 $\pm$ 0.04	0.031	0.052
20 wt% PEEK-PTFE	0.073 $\pm$ 0.005	0.050	0.135
* 20 wt% PEEK-PTFE	0.089 $\pm$ 0.006	0.050	0.274
30 wt% PEEK-PTFE	0.14 $\pm$ 0.008	0.136	0.184
* 30 wt% PEEK-PTFE	0.13 $\pm$ 0.005	0.136	0.312
40 wt% PEEK-PTFE	0.21 $\pm$ 0.011	0.054	0.177
* 40 wt% PEEK-PTFE	0.16 $\pm$ 0.007	0.054	0.280
50 wt% PEEK-PTFE	0.91 $\pm$ 0.027	0.430	0.252
* 50 wt% PEEK-PTFE	0.11 $\pm$ 0.006	0.430	0.550
60 wt% PEEK-PTFE	1.6 $\pm$ 0.06	0.268	0.230
70 wt% PEEK-PTFE	1.1 $\pm$ 0.03	0.268	0.378
90 wt% PEEK-PTFE	9.0 $\pm$ 0.41	0.481	0.350
100 wt% PEEK	7.8 $\pm$ 0.44	0.529	0.555
* 100 wt% PEEK	11 $\pm$ 0.7	0.529	0.304

Table B-6 The complete dataset of polymer wear rates and running film FTIR-ATR spectra comparing the peak-to-peak signal intensity of 1490/1150  $\text{cm}^{-1}$  / $\text{cm}^{-1}$  in this study. The wear test was conducted in a dry nitrogen environment unless indicated by the \* symbol as a humid environment. All metric values are reported as the mean  $\pm$  95% confidence interval (N=5).

<b>material</b>	<b>wear rate, <math>k</math> (<math>10^{-6} \text{ mm}^3/(\text{Nm})</math>)</b>	<b><math>I_{1490}/I_{1150}</math>, unworn (-)</b>	<b><math>I_{1490}/I_{1150}</math>, running film (-)</b>
100 wt% PTFE	340 $\pm$ 21	0.004	0.007
* 100 wt% PTFE	610 $\pm$ 83	0.004	0.079
5 wt% PEEK-PTFE	0.13 $\pm$ 0.007	0.036	0.169
* 5 wt% PEEK-PTFE	1.9 $\pm$ 0.07	0.036	0.208
10 wt% PEEK-PTFE	0.068 $\pm$ 0.005	0.084	0.125
* 10 wt% PEEK-PTFE	0.37 $\pm$ 0.04	0.084	0.142
20 wt% PEEK-PTFE	0.073 $\pm$ 0.005	0.126	0.257
* 20 wt% PEEK-PTFE	0.089 $\pm$ 0.006	0.126	0.551
30 wt% PEEK-PTFE	0.14 $\pm$ 0.008	0.410	0.515
* 30 wt% PEEK-PTFE	0.13 $\pm$ 0.005	0.410	0.726
40 wt% PEEK-PTFE	0.21 $\pm$ 0.011	0.142	0.506
* 40 wt% PEEK-PTFE	0.16 $\pm$ 0.007	0.142	0.690
50 wt% PEEK-PTFE	0.91 $\pm$ 0.027	0.657	0.646
* 50 wt% PEEK-PTFE	0.11 $\pm$ 0.006	0.657	1.066
60 wt% PEEK-PTFE	1.6 $\pm$ 0.06	0.633	0.660
70 wt% PEEK-PTFE	1.1 $\pm$ 0.03	0.917	0.958
90 wt% PEEK-PTFE	9.0 $\pm$ 0.41	1.115	1.073
100 wt% PEEK	7.8 $\pm$ 0.44	1.200	1.220
* 100 wt% PEEK	11 $\pm$ 0.7	1.200	0.877

Table B-7 The complete dataset of polymer wear rates and running film FTIR-ATR spectra comparing the peak-to-peak signal intensity of 1280/1150  $\text{cm}^{-1}$  / $\text{cm}^{-1}$  in this study. The wear test was conducted in a dry nitrogen environment unless indicated by the \* symbol as a humid environment. All metric values are reported as the mean  $\pm$  95% confidence interval (N=5).

<b>material</b>	<b>wear rate, <math>k</math> (<math>10^{-6} \text{ mm}^3/(\text{Nm})</math>)</b>	<b><math>I_{1280}/I_{1150}</math>, unworn (-)</b>	<b><math>I_{1280}/I_{1150}</math>, running film (-)</b>
100 wt% PTFE	340 $\pm$ 21	0.020	0.018
* 100 wt% PTFE	610 $\pm$ 83	0.020	0.087
5 wt% PEEK-PTFE	0.13 $\pm$ 0.007	0.037	0.075
* 5 wt% PEEK-PTFE	1.9 $\pm$ 0.07	0.037	0.082
10 wt% PEEK-PTFE	0.068 $\pm$ 0.005	0.057	0.080
* 10 wt% PEEK-PTFE	0.37 $\pm$ 0.04	0.057	0.079
20 wt% PEEK-PTFE	0.073 $\pm$ 0.005	0.073	0.128
* 20 wt% PEEK-PTFE	0.089 $\pm$ 0.006	0.073	0.200
30 wt% PEEK-PTFE	0.14 $\pm$ 0.008	0.160	0.194
* 30 wt% PEEK-PTFE	0.13 $\pm$ 0.005	0.160	0.280
40 wt% PEEK-PTFE	0.21 $\pm$ 0.011	0.074	0.185
* 40 wt% PEEK-PTFE	0.16 $\pm$ 0.007	0.074	0.250
50 wt% PEEK-PTFE	0.91 $\pm$ 0.027	0.205	0.221
* 50 wt% PEEK-PTFE	0.11 $\pm$ 0.006	0.205	0.455
60 wt% PEEK-PTFE	1.6 $\pm$ 0.06	0.268	0.218
70 wt% PEEK-PTFE	1.1 $\pm$ 0.03	0.365	0.393
90 wt% PEEK-PTFE	9.0 $\pm$ 0.41	0.460	0.367
100 wt% PEEK	7.8 $\pm$ 0.44	0.484	0.500
* 100 wt% PEEK	11 $\pm$ 0.7	0.484	0.957

## Appendix C

### EVALUATION OF TRANSFER FILMS METRICS USING MATLAB CODE

#### C.1 Transfer Film Characterization Code

The MATLAB ® software used in this work was provided by the University of Delaware from Mathworks under the license number 129273, which was usable on UD-owned computers. The code used in this study to evaluate transfer film free-space length and area fraction was developed for this purpose by Dr. Jiaxin Ye [106]. The following code can be obtained from the Materials Tribology Lab at <http://research.me.udel.edu/~dlburris/publicationsOther.html>

```
function [af,ll] = distribution()
clear
clc
close all

% V5 %
% April, 2014, modified by Jiaxin based on dispersion code by Harman
%

fprintf('TRANSFER FILM DISTRIBUTION CHARACTERIZATION CODE \nMaterials
Tribology Laboratory\nUniversity of Delaware\n\n')

fprintf('Please refer to accompanying document for further
instructions \n\tand illustrations on using this code.\n\n')

syms logil y n;

% Version check for SORT function
logil = input('Is the version of MATLAB 7.0 or later? (Y/N): ', 's');

if strcmpi(logil, 'y') ==1;
    vzn = 1;
else
    vzn = 0;
end
```

```

syms logi2 y n;

logi2 = input('Is the transfer film image converted to black and
white already? (Y/N) : ' , 's');

if strcmpi(logi2, 'y') ==1;
    vzn2 = 1;
else
    vzn2 = 0;
end

%%%%%%%%%%%%%%%%%%%%%%%%%%%%%%%%%%%%%%%%%%%%%%%%%%%%%%%%%%%%%%%%%%%%%%%%
%%%%%%%%
%%%%%%%%%% Read image of b/w bitmap and generate pixel matrix 'A'
%%%%%%%%%%
%%%%%%%%%%%%%%%%%%%%%%%%%%%%%%%%%%%%%%%%%%%%%%%%%%%%%%%%%%%%%%%%%%%%%%%%
%%%%%%%%%%
if vzn2 == 1

    [filename,PathName] = uigetfile('*.bmp','Select the .BMP image');
    A = imread([PathName,filename], 'bmp');
    offx=ceil(size(A,1)/2); %Offset for periodic boundary
    offy=ceil(size(A,2)/2); %Offset for periodic boundary

%%%%%%%%%%%%%%%%%%%%%%%%%%%%%%%%%%%%%%%%%%%%%%%%%%%%%%%%%%%%%%%%%%%%%%%%
%%%%%%%%%%
%%%%%%%%%% Read image of RGB bitmap and generate pixel matrix 'A'
%%%%%%%%%%
%%%%%%%%%%%%%%%%%%%%%%%%%%%%%%%%%%%%%%%%%%%%%%%%%%%%%%%%%%%%%%%%%%%%%%%%
%%%%%%%%%%
else if vzn2 == 0

    [filename,PathName] = uigetfile('*.bmp','Select the .BMP image');
    AA = imread([PathName,filename], 'bmp');
    nox = input('Enter number of counterface reference points for
image conversion:');
    imshow(filename)
    [fx,fy]=ginput(nox);

    syms logi3 y n;

    logi3 = input('Is the transfer film brighter than substrate?
(Y/N): ' , 's');

    if strcmpi(logi3, 'y') == 1;
        vzn1 = 1;
    else
        vzn1 = 0;
    end

```

```

end

syms logi22 itr n
    logi22 = 'y';
while strcmpi(logi22, 'y') == 1;

    bwd = input('Enter # of STDEVS to use for defining lower or
upper bounds of color threshold (Suggested = 3 to 5): ');
    for i=1:nox
        Rffx(i)=AA(round(fy(i)),round(fx(i)),1);
        Rfx(i)=double(Rffx(i));
        Bffx(i)=AA(round(fy(i)),round(fx(i)),3);
        Bfx(i)=double(Bffx(i));
        Gffx(i)=AA(round(fy(i)),round(fx(i)),2);
        Gfx(i)=double(Gffx(i));
    end

    %%%%%%%%% Rth, Bth, Gth define RGB thresholds %%%%%%%%%
    Rth=mean(Rfx)-bwd*std(Rfx);
    Bth=mean(Bfx)-bwd*std(Bfx);
    Gth=mean(Gfx)-bwd*std(Gfx);

    Rth2=mean(Rfx)+bwd*std(Rfx);
    Bth2=mean(Bfx)+bwd*std(Bfx);
    Gth2=mean(Gfx)+bwd*std(Gfx);

    rzz=size(AA,1);
    clm=size(AA,2);
    A=[];

    for i=1:rzz
        for j=1:clm
            A(i,j)=255;
        end
    end

    if vnz1 == 0
        for i=1:rzz
            for j=1:clm
                if AA(i,j,1)<Rth
                    A(i,j)=0;
                else if AA(i,j,3)<Bth
                    A(i,j)=0;
                else if AA(i,j,2)<Gth
                    A(i,j)=0;
                end
            end
        end
    end
else if vnz1 == 1

```

```

        for i=1:rzz
            for j=1:clm
                if AA(i,j,1)>Rth2
                    A(i,j)=0;
                else if AA(i,j,3)>Bth2
                    A(i,j)=0;
                else if AA(i,j,2)>Gth2
                    A(i,j)=0;
                end
            end
        end
    end
end
end
end
end
end
imwrite(A, 'converted BW image.bmp', 'bmp')
imshow(A)
offx=ceil(size(A,1)/2); %Offset for periodic boundary
offy=ceil(size(A,2)/2); %Offset for periodic boundary
logi22 = input('Tweak #STDEV further? (Y/N):','s');
end
end
end
%%%%%%%%%%%%%%%%%%%%%%%%%%%%%%%%%%%%%%%%%%%%%%%%%%%%%%%%%%%%%%%%%%%%%%%%%%
%%%%%%%%%%%%%%%%%%%%%%%%%%%%%%%%%%%%%%%%%%%%%%%%%%%%%%%%%%%%%%%%%%%%%%%%%%
%%%%%%%%%%%%%%%%%%%%%%%%%%%%%%%%%%%%%%%%%%%%%%%%%%%%%%%%%%%%%%%%%%%%%%%%%% Area fraction calculation
%%%%%%%%%%%%%%%%%%%%%%%%%%%%%%%%%%%%%%%%%%%%%%%%%%%%%%%%%%%%%%%%%%%%%%%%%%
%%%%%%%%%%%%%%%%%%%%%%%%%%%%%%%%%%%%%%%%%%%%%%%%%%%%%%%%%%%%%%%%%%%%%%%%%%
%%%%%%%%%%%%%%%%%%%%%%%%%%%%%%%%%%%%%%%%%%%%%%%%%%%%%%%%%%%%%%%%%%%%%%%%%%

filledcells=0;
totalcells=0;

for i=1:size(A,1);
    for j=1:size(A,2);
        totalcells=totalcells+1;
        if A(i,j)<150;
            filledcells = filledcells+1;
        end
    end
end
af=filledcells/totalcells;

%%%%%%%%%%%%%%%%%%%%%%%%%%%%%%%%%%%%%%%%%%%%%%%%%%%%%%%%%%%%%%%%%%%%%%%%%%
%%%%%%%%%%%%%%%%%%%%%%%%%%%%%%%%%%%%%%%%%%%%%%%%%%%%%%%%%%%%%%%%%%%%%%%%%%
%%%%%%%%%%%%%%%%%%%%%%%%%%%%%%%%%%%%%%%%%%%%%%%%%%%%%%%%%%%%%%%%%%%%%%%%%% Create data matrix which contains periodic boundary condition
%%%%%%%%%%%%%%%%%%%%%%%%%%%%%%%%%%%%%%%%%%%%%%%%%%%%%%%%%%%%%%%%%%%%%%%%%%
%%%%%%%%%%%%%%%%%%%%%%%%%%%%%%%%%%%%%%%%%%%%%%%%%%%%%%%%%%%%%%%%%%%%%%%%%%
%%%%%%%%%%%%%%%%%%%%%%%%%%%%%%%%%%%%%%%%%%%%%%%%%%%%%%%%%%%%%%%%%%%%%%%%%%

```

```

%%%%%%%% Top layer: Top quarter of the data matrix
for i = 1:offx;
    for j = 1:offy;
        Matrix(i,j)=A(offx+i, (offy+j));
    end
end

for i = 1:size(A,1);
    for j = 1:offy;
        Matrix(i+offx,j)=A(i,j+offy);
    end
end

for i = 1:offx;
    for j = 1:offy;
        Matrix(i+offx+size(A,1),j)=A(i,j+offy);
    end
end

%%%%%%%% Middle layer: Middle two-rows of data matrix
for i = 1:offx;
    for j = 1:size(A,2);
        Matrix(i,j+offy)=A(i+offx,j);
    end
end

for i = 1:size(A,1);
    for j = 1:size(A,2);
        Matrix(i+offx,j+offy)=A(i,j);
    end
end

for i = 1:offx;
    for j = 1:size(A,2);
        Matrix(i+offx+size(A,1),j+offy)=A(i,j);
    end
end

%%%%%%%% Bottom layer: Bottom quarter of data matrix
for i = 1:offx;
    for j = 1:offy;
        Matrix(i,j+offy+size(A,2))=A(i+offx,j);
    end
end

for i = 1:size(A,1);
    for j = 1:offy;
        Matrix(i+offx,j+offy+size(A,2))=A(i,j);
    end
end

```

```

for i = 1:offx;
    for j = 1:offy;
        Matrix(i+offx+size(A,1),j+offy+size(A,2))=A(i,j);
    end
end

syms logi y n;

%%%%%%%%%%%%%%%%%%%%%%%%%%%%%%%%%%%%%%%%%%%%%%%%%%%%%%%%%%%%%%%%%%%%%%%%
%%%%%%%%
%%%%%%%% Define initial square parameters
%%%%%%%%
%%%%%%%%%%%%%%%%%%%%%%%%%%%%%%%%%%%%%%%%%%%%%%%%%%%%%%%%%%%%%%%%%%%%%%%%
%%%%%%%%

scale1= input('Enter approximate width of transfer film image in
micrometers: ');
scale= scale1/size(A,2);
xf1 = input('Enter initial guess of characteristic square width in
micrometers: ');
xf = xf1/scale1;
Nsquares = input('Enter number of random squares to use for analysis:
');

fprintf('\n\n')
fprintf('Computation may take several seconds to a few minutes,
depending on input parameters\n Press Ctrl+C any time to terminate
computation\n\n')

s2=size(A,1)*size(A,1);

%%%%%%%%%%%%%%%%%%%%%%%%%%%%%%%%%%%%%%%%%%%%%%%%%%%%%%%%%%%%%%%%%%%%%%%%
%%%%%%%%
%%%%%%%% First count to Nsquares (corresponding to manual input of
'xf') %%%
%%%%%%%%%%%%%%%%%%%%%%%%%%%%%%%%%%%%%%%%%%%%%%%%%%%%%%%%%%%%%%%%%%%%%%%%
%%%%%%%%

length = ceil(xf*size(A,2));
for i = 1:Nsquares;
    x=ceil(rand*size(A,1))+offx;
    y=ceil(rand*size(A,2))+offy;
    counter=0;

```

```

    for s = 1:length;
        for t = 1:length;
            mx=x-floor(length/2)+s;
            my=y-floor(length/2)+t;
            if Matrix(mx,my)<150;
                counter=counter+1;
            end
        end
    end
    P(i)=counter;
end
data=P';
bimreal=mode(data);

h1=hist(P,2500);
[m,n1]=max(h1);
l=xf;

boxar=length^2;

if boxar==bimreal
    isbimo=1;
    h1(1,2500)=0;
    [m,n1]=max(h1);
else
    isbimo=0;
end

if n1~=1

%%%%%%%%%%%%%%%%%%%%%%%%%%%%%%%%%%%%%%%%%%%%%%%%%%%%%%%%%%%%%%%%%%%%%%%%%%%%%%
%%
%%%%%%%%%%%%%%%%%%%%%%%%%%%%%%%%%%%%%%%%%%%%%%%%%%%%%%%%%%%%%%%%%%%%%%%%%%%%%%
Automatic iteration to obtain Free Space Length
%%%%%%%%%%%%%%%%%%%%%%%%%%%%%%%%%%%%%%%%%%%%%%%%%%%%%%%%%%%%%%%%%%%%%%%%%%%%%%
%%

margin=1;
while margin > .05

    while n1~=1
        xfnew=xf/2;
        l=xf-xfnew; %==xf/2
    end
end

```

```

length = ceil(1*size(A,2));
for i = 1:Nsquares;
    x=ceil(rand*size(A,1))+offx;
    y=ceil(rand*size(A,2))+offy;
    counter=0;
    for s = 1:length;
        for t = 1:length;
            mx=x-floor(length/2)+s;
            my=y-floor(length/2)+t;
            if Matrix(mx,my)<150;
                counter=counter+1;
            end
        end
    end
    P(i)=counter;
end
data=P';
bimreal=mode(data);
boxar=length^2;

h2=hist(P,2500);

if boxar==bimreal
    isbimo=1;
    h2(1,2500)=0;
    [m,n1]=max(h2);
else
    isbimo=0;
    [m,n1]=max(h2);
end

xf=xfnew;

end

if n1==1
    if vzn == 1;
        SRT=sort(h2, 'descend');
    else
        SRT=fliplr(sort((h2)));
    end

margin=1-(SRT(2)/SRT(1));

if margin > 0.05
    xfjumpup=2.5*xf;
    xf=xfjumpup;

    xfnew=xf/2;
    l=xf-xfnew; %==xf/2

```

```

length = ceil(1*size(A,2));
for i = 1:Nsquares;
    x=ceil(rand*size(A,1))+offx;
    y=ceil(rand*size(A,2))+offy;
    counter=0;
    for s = 1:length;
        for t = 1:length;
            mx=x-floor(length/2)+s;
            my=y-floor(length/2)+t;
            if Matrix(mx,my)<150;
                counter=counter+1;
            end
        end
    end
    P(i)=counter;
end
data=P';
bimreal=mode(data);
boxar=length^2;

h2=hist(P,2500);

if boxar==bimreal
    isbimo=1;
    h2(1,2500)=0;
    [m,n1]=max(h2);
else
    isbimo=0;
    [m,n1]=max(h2);
end

xf=xfnew;

else
end
else
continue

end

end
end

```

```
%%%%%%%%%%%%%%%%%%%%%%%%%%%%%%%%%%%%%%%%%%%%%%%%%%%%%%%%%%%%%%%%%%%%%%%%
%%%%%%%%%%%%%%%%%%%%%%%%%%%%%%%%%%%%%%%%%%%%%%%%%%%%%%%%%%%%%%%%%%%%%%%% Display results %%%%%%%%%%%%%%%%%%%%%%%%%%%%%%%%%%%%%%%%%%%%%%%%%%%%%%%%%%%%%%%%%%%%%%%%%
%%%%%%%%%%%%%%%%%%%%%%%%%%%%%%%%%%%%%%%%%%%%%%%%%%%%%%%%%%%%%%%%%%%%%%%%
```

```
l1=1*size(A,2)*scale;
disp('Value of free space length is (in micrometers): ')
disp(ceil(l1))
```

```
disp('Film area fraction (where film is represented by black pixels):
')
disp(af)
```

```
hist(P,2500), xlabel('# of film pixels in a box'), ylabel('# of
occurrences')
```

```
%%%%%%%%%%%%%%%%%%%%%%%%%%%%%%%%%%%%%%%%%%%%%%%%%%%%%%%%%%%%%%%%%%%%%%%%
%%%%%%%%%%%%%%%%%%%%%%%%%%%%%%%%%%%%%%%%%%%%%%%%%%%%%%%%%%%%%%%%%%%%%%%% Manual Mode %%%%%%%%%%%%%%%%%%%%%%%%%%%%%%%%%%%%%%%%%%%%%%%%%%%%%%%%%%%%%%%%%%%%%%%%%
%%%%%%%%%%%%%%%%%%%%%%%%%%%%%%%%%%%%%%%%%%%%%%%%%%%%%%%%%%%%%%%%%%%%%%%%
```

```
logi = input('Automatic iteration completed. Continue to manual
mode? (Y/N) :', 's');
```

```
while strcmpi(logi, 'y') == 1;
    xf1 = input('Enter desired square width in micrometers: ');
    xf = xf1/scale1;
    Nsquares = input('Enter number of random squares to use for
analysis: ');
```

```
    %s2=size(A,1)*size(A,1);
```

```

%%%%%%%%%%%%%%%%%%%%%%%%%%%%%%%%%%%%%%%%%%%%%%%%%%%%%%%%%%%%%%%%%%%%%%%%
%%%%%%%%
%%%%%%%% Calculate box size for manual input
%%%%%%%%%%%%%%%%%%%%%%%%%%%%%%%%%%%%%%%%%%%%%%%%%%%%%%%%%%%%%%%%%%%%%%%%

%%%%%%%%%%%%%%%%%%%%%%%%%%%%%%%%%%%%%%%%%%%%%%%%%%%%%%%%%%%%%%%%%%%%%%%%
%%%%%%%%

```

```

length = ceil(xf*size(A,2));
for i = 1:Nsquares;
x=ceil(rand*size(A,1))+offx;
y=ceil(rand*size(A,2))+offy;
counter=0;
for s = 1:length;
for t = 1:length;
mx=x-floor(length/2)+s;
my=y-floor(length/2)+t;
if Matrix(mx,my)<150;
counter=counter+1;
end
end
end
P(i)=counter;
end
data=P';
bimreal=mode(data);
boxar=length^2;

```

```

h1=hist(P,2500);

if boxar==bimreal
isbimo=1;
h1(1,2500)=0;
[m,n1]=max(h1);
else
isbimo=0;
[m,n1]=max(h1);
end

```

```

zerocount=0;
for j=1:size(P,2);
if P(j)==0;
zerocount=zerocount+1;
end
end
end

```

```

%%%%%%%%%%%%%%%%%%%%%%%%%%%%%%%%%%%%%%%%%%%%%%%%%%%%%%%%%%%%%%%%%%%%%%%%
%%%%%%%%%%%%%%%%%%%%%%%%%%%%%%%%%%%%%%%%%%%%%%%%%%%%%%%%%%%%%%%%%%%%%%%% Display results %%%%%%%%%%%%%%%%%%%%%%%%%%%%%%%%%%%%%%%%%%%%%%%%%%%%%%%%%%%%%%%%%%%%%%%%%
%%%%%%%%%%%%%%%%%%%%%%%%%%%%%%%%%%%%%%%%%%%%%%%%%%%%%%%%%%%%%%%%%%%%%%%%

```

```

    hist(P,2500), xlabel('# of film pixels in a box'), ylabel('# of
occurrences')
    disp('Number of boxes with a zero black-pixel count: ')
    disp(zeroCount)

```

```

    logi = input('Enter parameters again? (Y/N) :', 's');

```

```

end

```

```

end

```

```

function [result,percents]=mode(x)
%MODE
% Finds the mode of a 2d matrix.
% [result percents]=mode(matrix)
% where result is the mode of the matrix
% and percents is the amount of difference within the mode
% ORIGINALLY TABULATE.m by B.A. Jones
% Changes by David Li, UCSB updated: 4-8-2004

[Mo,No]=size(x);
x=reshape(x,Mo*No,1);

y = x(find(~isnan(x)))+1;

maxlevels = max(y(:));
minlevels = min(y(:));
[counts values] = hist(y,(minlevels:maxlevels));
total = sum(counts);

result=-1;
index=1;
while(counts(index) ~= max(counts))
    index=index+1;
end
result=values(index)-1; %disp(result);

percents =counts(index)/total;

end

```

## C.2 Tutorial for Transfer Film Characterization Code

The instructional document for the MATLAB® code used in this study to evaluate transfer film free-space length and area fraction was developed for this purpose by Dr. Jiaxin Ye [106]. The following manual can be obtained from the Materials Tribology Lab at <http://research.me.udel.edu/~dlburris/publicationsOther.html>.

I	Using the code	162
II	Choosing representative transfer film images for analysis	165
III	Selecting counterface reference points for image conversion	166
IV	Selecting number of standard deviations	168
V	Selecting the size of the initial box	169
VI	Selecting the number of boxes	171
VII	Manual Mode	172
VIII	Illustrations	173
IX	Overview of code algorithm	177

## I. Using the code:

The following is a step-by-step instruction on using the dispersion code.

### Step 1

Upon execution, the code will prompt for a bitmap of the transfer film image to be analyzed. This could be an optical, profilometric or electron microscopic image. Note that the format of this file should be **.bmp**. The image size (in pixels, or otherwise) or the aspect ratio is not important, however, **pixel values should be even** (for example, 231px x 422px will need to be cropped to 230px x 422px, etc.). The image *should* be in RGB scale (grey scale image need to be converted to RGB scale) and have a good contrast between film and substrate. If a converted black and white image is already available, answer 'Y' to the following question and skip to step 6.

```
Is the transfer film image converted to black and white  
already? (Y/N):
```

### Step 2

In the next step, you are required to manually pick up reference points at area of counterface in the transfer film image. Color intensities of selected points will be used as reference to distinguish counterface from film. Enter the number of reference points you wish to use at the following prompt (recommended: 20):

```
Enter number of counterface reference points for image  
conversion:
```

### Step 3

In the next step, you are asked about if the transfer film appears brighter or darker than the counterface in the provided image. This will help the code to determine the right thresholding direction. Answer 'Y' or 'N' at the following prompt:

```
Is the transfer film brighter than substrate? (Y/N):
```

### Step 4

In the next step, you are asked to choose the number of standard deviations to use for defining color intensity bound for image thresholding (see Section II for more details). 3 to 5 is suggested as illustrated in author's paper.

```
Enter # of STDEVS to use for defining lower or upper bounds of  
color threshold (Suggested = 3 to 5):
```

### Step 5

In the next step, you are prompted with a converted black and white image based on previous selected reference points and number of standard deviations. Answer 'Y' if you feel the intensity bound need to be tweaked and you will be redirected to step 4, answer 'N' if you are comfortable with the converted image and will proceed to step 6:

```
Tweak #STDEV further? (Y/N):
```

### Step 6

Now you are required to provide the physical width of the transfer film image selected in step 1. The width may be ascertained from the scale bar. This input is required for the code to work. Enter the width of the transfer film image in micrometers at the following prompt:

```
Enter approximate width of transfer film image in micrometers:
```

### Step 7

A starting estimate of the characteristic free space length needs to be provided next. This 'starter' value is determined visually from the transfer film image- looking at the image, what is the approximate length scale of the film-free space in micrometers? Enter this value at the following prompt:

```
Enter initial guess of characteristic square width in micrometers:
```

Remember, this value will always be approximate based on individual perception of the transfer film image. The value you enter will only affect how long it takes for the solution to converge to the 'actual' value, and not the value itself. For suggestions on selecting the initial value, please refer to section II below.

### Step 8

In order to generate histograms of pixel distribution within the chosen box size, you next need to specify how many of the boxes are to be used for gathering data for the histograms. Do this at the following prompt:

```
Enter number of random squares to use for analysis:
```

A higher number of boxes ensures statistical robustness of your answer, but might take a longer time to complete due to lengthier computations. A smaller number of boxes ensures quicker computation, albeit a slightly inaccurate result, and can be used for non-rigorous analyses.

*Typically, this number may vary between 100 and 1000 for an acceptable accuracy + speed combination.* For suggestions on selecting the appropriate number of boxes, see section III

### Step 9

After the automatic iteration to the characteristic box size is completed, the code prompts if you wish to proceed to the 'Manual Mode'. The manual mode is an optional extension of the code that allows you to gather statistical information such as scatter in the value of the characteristic box size. If you wish you use the value generated by the automatic iteration, and not enter the manual mode, enter 'n' at the following prompt:

```
Automatic iteration completed. Continue to manual mode? (Y/N)
```

More information on the Manual Mode is given in Section IV

### Results:

The final value of transfer film free space length ( $L_f$ ) after iteration is displayed:

```
Value of free space length is (in micrometers):
```

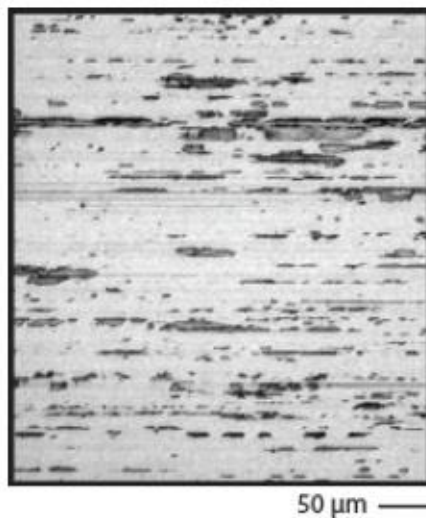
Further, the area fraction of the image occupied by transfer film (identified as black pixels) is also displayed:

```
Film area fraction (where film is represented by black pixels):
```

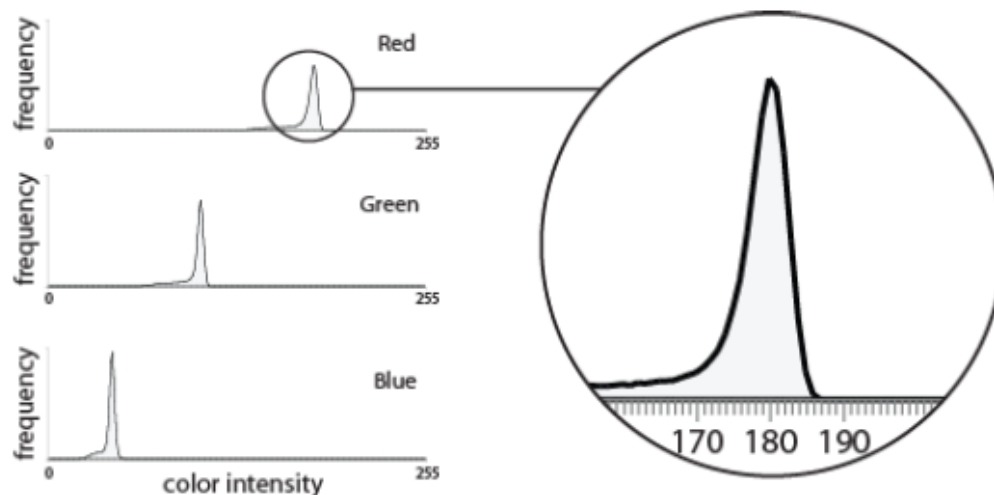
A histogram is generated showing the zero-mode corresponding to the free space length displayed above.

## II. Choosing representative transfer film images for analysis (step 1)

Before applying the code, you need to choose appropriate transfer film images used for analysis. Our code can be used on optical micrographs, electron micrographs and profilometric maps depending on what you have access to. Image should be **representative** of a certain transfer film morphology and also provide **good contrast** between transfer film and counterface. Below is an example image of transfer film that we use to demonstrate the method in this document.

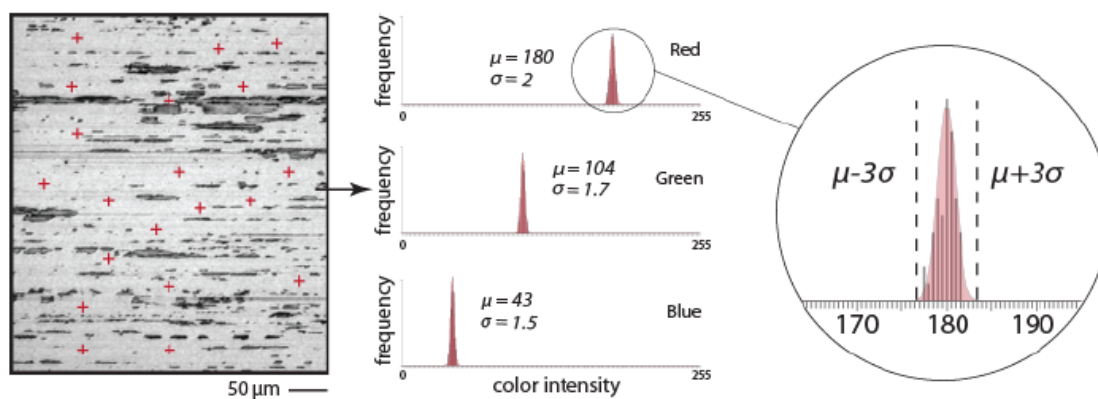


This image is an optical micrograph of a low wear alumina-PTFE nanocomposite transfer film taken with a bright field, reflected light microscope (Nikon MM-400/S). Counterface was pre-polished to 10 nm Ra and therefore reflects light much stronger than transfer film and has a brighter appearance than film. Dimension of the image is 440 (W)  $\times$  498(H) pixel. Below is the color intensity histogram of all pixels within the image. Notice the long tail at the left of each plot which represents the transfer film covered regions.



### III. Selecting counterface reference points for image conversion (step 2)

In step 2, you are prompted to manually pick up a statistically significant number of random pixels where transfer film is known to be absent. The rationale is to distinguish the film free counterface area by calculating the channel mean and standard deviation of all pixels within this region.



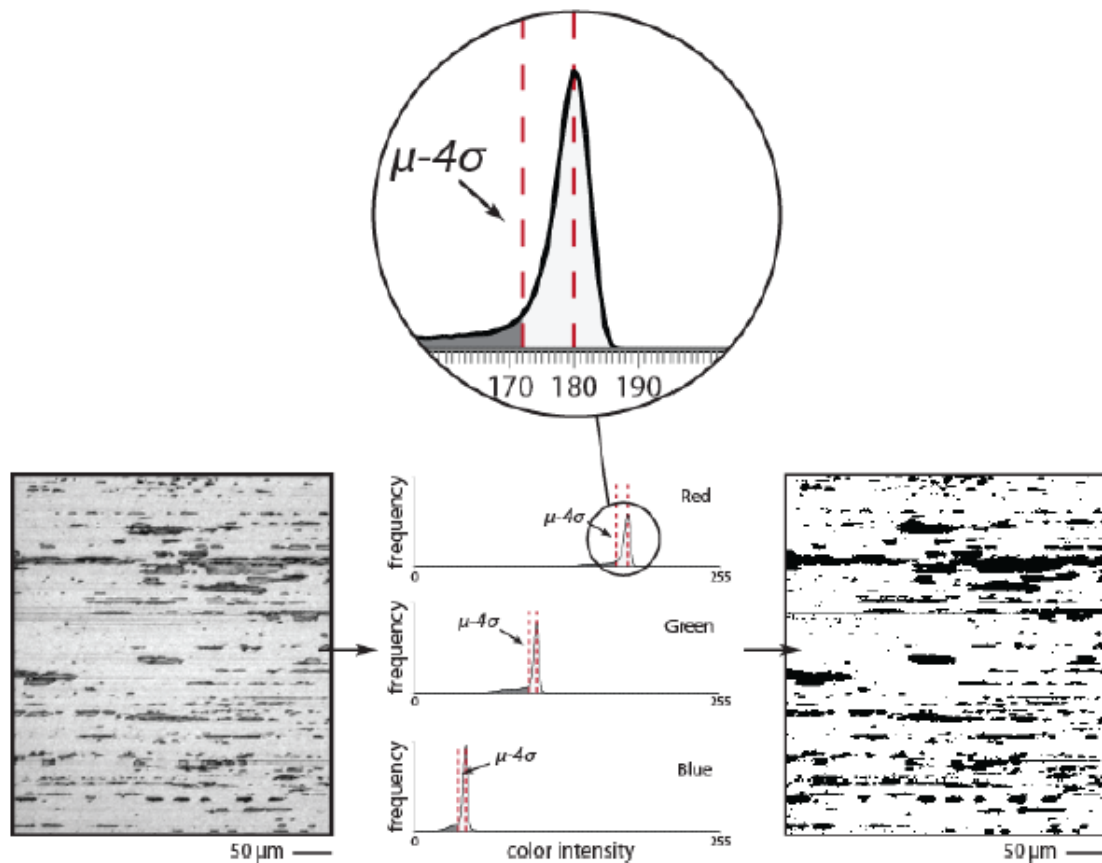
In example image shown above, we manually select 50 points as reference. Histograms of the color intensities of selected points were shown. It can be seen that each distribution can be satisfactorily described using Normal Distribution:

$$f(x, \mu, \sigma) = \frac{1}{\sigma\sqrt{2\pi}} e^{-\frac{(x-\mu)^2}{2\sigma^2}}$$

Where the mean ( $\mu$ ) and standard deviation ( $\sigma$ ) of the distribution can be estimated from sampled dataset. The simulated full distribution curve (shadowed) were overlaid on top of the sampled data as shown above. In addition, such simulated histograms of color intensity closely resembled the high peaks in the histograms of the overall image (see figure in previous page). This provides the necessary condition for thresholding the image based on pixel intensities.

#### IV. Selecting number of standard deviations (step 4)

In step 4, user are prompted to choose number of standard deviations ( $n\sigma$ ) used for defining the RGB color threshold during image conversion ( $\mu \pm n\sigma$ ). As seen in previous section, pixels of counterface are known to be within  $\mu \pm 3\sigma$  range with a 99.7% confidence. By declaring any pixel with intensity outside this range to be covered with transfer film will provide a reasonable conversion of the original RGB image into a binary matrix. In our experience, we find that 3-5 $\sigma$  consistently provides optimal detection. In example image shown below,  $n = 4$  results in a binary matrix that closely resembles the appearance of its parent image. Here, **black** represents film and **white** represents uncovered counterface.



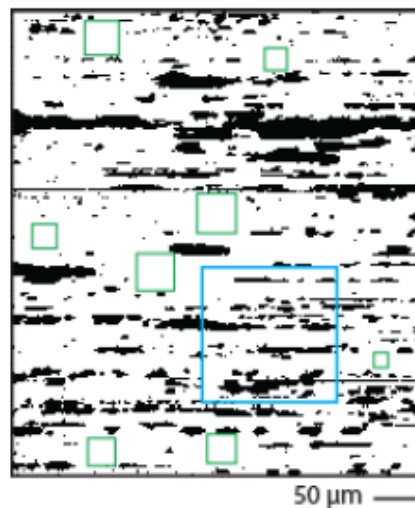
#### Note:

Depending on the image histogram, ' $\mu - n\sigma$ ' (when transfer film is darker than counterface) or ' $\mu + n\sigma$ ' (when transfer film is brighter than counterface) will be set as the threshold value.

## V. Selecting size of initial box (step 7)

At step 7, you are prompted to enter an ‘initial guess of characteristic square width in micrometers’.

When using this code to calculate the size of the free space length, we are interested in finding the (largest) square size that, when thrown over the image at random locations a given number of times, would be most likely to have no film pixel contained within it. The code uses an initial user-input, and iterates to the actual value by generating these boxes, and placing them over across the transfer film image. A good analogy is to compare it to throwing a fishing net at different points in a lake, with the hope of *not* catching any fish. Of course, you will need to keep reducing the size of your net, until you reach a ‘critical’ dimension where you’re more probable to drop the net at different locations, and still not catch anything. The largest net for which this happens is what is analogous to the free space length. Looking at the transfer film image then, we need a subjective measure of what *seems* like the free space length. The green boxes in the following image could all very well be this starting size:



Note that a box size similar to the blue box would never be completely particle-free, regardless of where you position it. We seek to identify which among the green boxes is the truest representation of the free space length.

For this purpose, you may use a numeric value slightly larger than what seems like the free space length (green boxes in this case), and let the code iteratively reach the ‘optimal’ box size (work its way down). Alternatively, you may use a value which *seems* like the free space length (or even slightly smaller) and if

you're too small, you can always start again with a marginally increased value (a good way to tell if you're too small is if the value the code outputs is the same as the value you entered for the box size). The disadvantage in using the former is wastage of computational time/effort. Since the code will be trying to work its way down from your starting value, depending how overestimated this starting value is, the code might take a prohibitively longer time simply as an artifact of the starting choice. For this purpose then, a size slightly smaller than the perceived free space length is preferred because if it's too small, the code will "tell" us, and we can always restart with a slightly incremented starting value.

For the illustration shown above, then, the width of the transfer film image were 406 micrometers, the size of our initial guess (which should be definitely less than the size of the blue box), would be about a fourth of the image width (or maybe smaller still), or roughly 100 micrometers. If your initial size is too small (say, the same size as one of the smaller green boxes), you can restart with a larger initial guess.

## VI. Selecting the number of boxes (step 8)

In order for a given sized square to be indicative of the free space length, it is imperative that the given square is representative of the film spatial statistics across the entire image. As a result, it is not difficult to realize that for a more accurate and statistically robust measurement of the characteristic box, a larger number of squares need to be overlaid at random locations on the image. While an increase in number of boxes overlaid (for any box size) increases accuracy (how close the number you're getting is to the actual free space length) of the eventual 'solution', increasing the number of boxes may increase computational effort.

It is observed that, usually, the same computational effort is required for a larger number of smaller sized squares (say, an order of magnitude smaller than the image size), as is for a smaller number of large-sized squares (say, comparable or of the same order of magnitude as the image size). The relative importance of computational speed and accuracy of result is the choice of the user.

For images where a larger starting box size is necessitated by nature of transfer film distribution, it is advisable to limit the number of squares in the initial stages. Thereafter, depending on the convergence speed, the user may subsequently increase the number of squares to obtain a more accurate solution.

Always bear in mind, however, that smaller sampling will always give you numbers which will be off substantially from the actual characteristic box. If the code is run multiple times on the same image (say, in manual mode), with the same parameters, changing only the number of boxes, a large scatter in your free space value will be seen for a smaller 'number of boxes' value. This is largely mitigated at higher 'number of boxes' values.

Ideally, a user may initially wish to experiment with box numbers between 100 and 1000, to obtain the required accuracy coupled with desired convergence speed. As mentioned earlier, if the square size is large relative to the image size, one may start with box numbers as few as 50, and work their way upwards till computational time becomes prohibitive. Once an accurate-enough value for characteristic box is obtained (reduced scatter between successive runs), 'fine tuning' to get the exact value may be done in the manual mode.

## VII. Manual Mode (step 9)

After the code iterates to the value of the characteristic box size, an option is provided by which the user can enter a 'manual' mode. Using the value provided by the automatic mode, the user can, without having to reselect the image, input only the new characteristic size and number of boxes he or she wishes to simulate, and obtain results for those parameters.

The manual mode only provides the film pixel distribution for the given box size and box numbers- it does not attempt to iterate on its own to an 'optimal' value. This feature is helpful for those users who wish to 'fine tune' the value provided by the automatic iteration, or those who wish to gather information on how changing an individual parameter changes the output (for instance, how changing the number of boxes for the same box size changes the shape of the histogram).

'Fine tuning' may be performed by using as a reference the final value outputted by the automatic iteration (provided care was taken to use an adequate sampling size to reduce scatter). Using this value, the user may manually increment or decrement in the box size and observe the generated histogram to ascertain the value of the characteristic box size. Further, since no step-wise iteration is performed, a single 'manual-mode' measurement is significantly faster than the automatic mode, which means that a higher sampling size (number of boxes) may be used to truly iron out the real characteristic box size.

As an illustration, one may use 200 boxes for a given rough starting box size, work up to 500 boxes till computation time becomes prohibitive. Then, using the value the code gives you at 500 boxes, and incrementing/decrementing that value with a much higher number of boxes (say, even 3000, etc.) one can find the size of the characteristic box to a resolution of a single nanometer (this, of course, would be a function of statistical error derived from your sampling size).

It may be mentioned here that the only data that 'carries over' from the automatic mode to the manual mode is the image pixel matrix, and the image size in nanometers. Aside from these, values you obtained from the automatic mode (box size, histogram, etc.) do not influence your results in the manual mode. The auto mode can be thought of as merely something to give a reference point for starting the manual tuning.

## VIII. Illustrations

In this section, a walk-through is provided for measuring the free space length of two transfer film images: the first is an optical image of a low wear alumina-PTFE nanocomposite transfer film taken with a bright field, reflected light microscope (Nikon MM-400/S). The second is a profilometry image of transfer film of the same material system taken with a scanning white light interferometer (Wyko NT9100).

### *Optical Image of Transfer Film*

In the illustrative, the example optical image was shown on the right, we notice that transfer film is composed of many streak-like debris spreading across the view field and has slightly darker appearance. They are distributed rather uniformly despite most of the area is still uncovered and is transfer film free.

Our aim in this example is to measure the free space length of such transfer film distribution. It is assumed that such metric is important to the wear reduction induced by any transfer film at sliding surfaces.

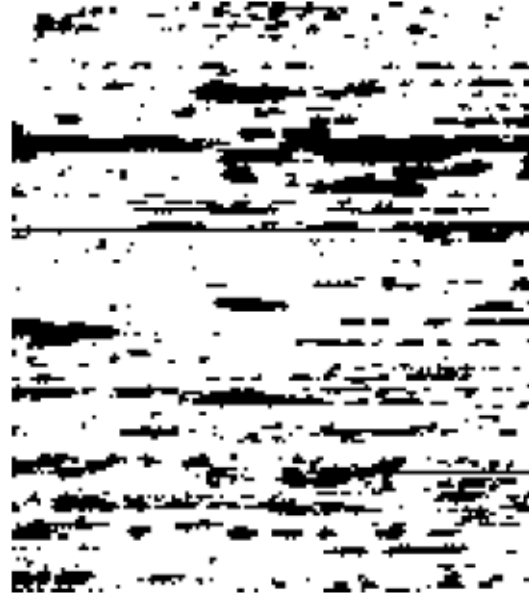


50  $\mu\text{m}$  —

First, let us establish some parameters. The width of the image, as we can calculate from the scale bar given, is about 406  $\mu\text{m}$ . In an actual transfer film micrograph (as we shall see in the next example), the size of the image is often known. The steps involved in evaluating the free space length ( $L_f$ ) are as listed below:

1. Executing the .m file, at the prompt: `Is the version of MATLAB 7.0 or later? (Y/N) : we enter: Y`
2. At the following prompt: `Is the transfer film image converted to black and white already? (Y/N) : as we don't have a converted image already, we enter: N` and select the sample image 'Optical.bmp'

3. The following prompt asks us to `Enter number of counterface reference points for image conversion:` we enter 20 in order to save some labor and still be able to pick up the statistics of pixel intensity distribution. A window will pop out displaying the raw image, waiting for mouse input. We go ahead and select 20 points at transfer film free area across the whole view field
4. The code now asks a question: `Is the transfer film brighter than substrate? (Y/N):` we enter N as the transfer film appears darker than the substrate in our case
5. At the following prompt, we are asked to `Enter # of STDEVS to use for defining lower or upper bounds of color threshold (Suggested = 3 to 5):` we enter 4 as we discussed earlier in section III. It takes a few seconds before MATLAB finish the image conversion and pop out the converted binary image (shown below)
6. At the following prompt: `Tweak #STDEV further? (Y/N):` we enter N as this converted image is closely representative of the original image, if the you are not satisfied with the conversion, enter Y and you will be able to choose a different number of standard deviation used for thresholding in previous step
7. The following prompt asks us to `Enter approximate width of transfer film image in micrometers:` We enter 406 as we calculated from the scale bar earlier
8. The following prompt asks us to `Enter initial guess of characteristic square width in micrometers:` Observing that the image width is 406  $\mu\text{m}$ , and as per the discussion is section V, the pockets of filler-free space seem to be about a fourth of the image width, we enter 100  $\mu\text{m}$  as our initial guess (underestimate the one-fourth value).

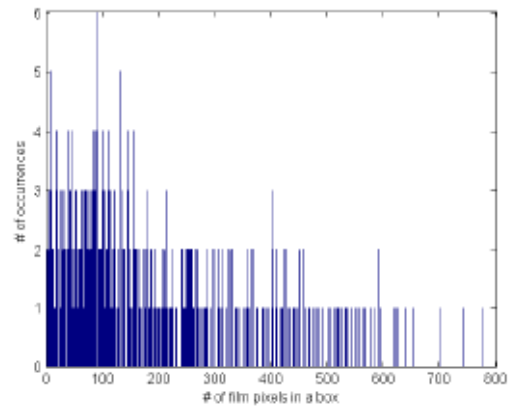


9. Next, we are asked to Enter number of random squares to use for analysis: Since we are unsure of how computationally intensive our selection of 100  $\mu\text{m}$  is going to be, we choose to use 500 squares (which is about halfway between the recommended 100 and 1000)
10. After allowing the computation to finish (in this case, the simulation ran for less than 5 seconds, while this may vary from one run to another even with same parameters), we obtain the following results:

```
Value of free space  
length is (in  
micrometers):  
27
```

```
Film area fraction (where  
film is represented by  
black pixels): 0.2163
```

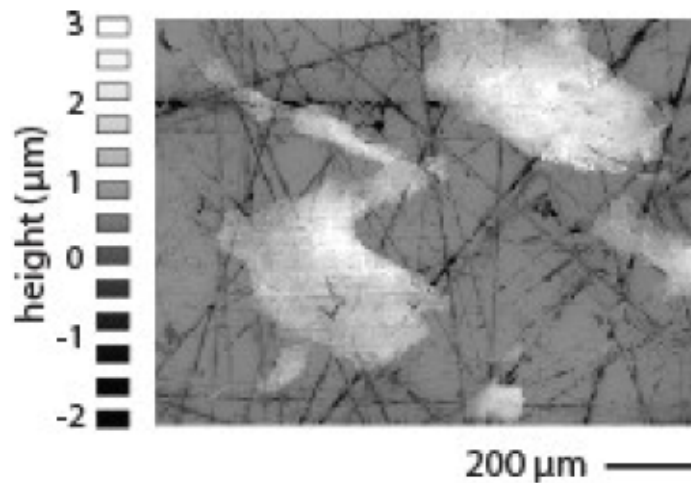
```
Further, the adjoining  
histogram is generated.  
Clearly then (and as was  
discussed in section II), our  
starting guess of 400  $\mu\text{m}$  was a
```



```
large overestimate of the actual 27  $\mu\text{m}$ . In hindsight, we might have  
saved some computation time by selecting an initial starting value of,  
say, 250  $\mu\text{m}$ , or 300  $\mu\text{m}$ . While not illustrated in this example, the value  
of 27  $\mu\text{m}$  may be further tuned in manual mode.
```

### *Profilometry Image of Transfer Film*

In this example, we will use a profilometry image of transfer film shown in the right. Notice that transfer film is composed of two large, discrete pieces of debris and a few other smaller debris in the view field.



Our aim in this example is to demonstrate measuring the free space

length using a profilometry image of transfer film. More importantly, the use of profilometry image provide an unique advantage of distinguishing film from rough counterface as counterface scratches can become indistinguishable from the film under optical mircoscopy. While in a profilometry map, scratches will always be less intensive than the film and can be thresholded easily.

First, the image width, as can be calculated from the scale bar, is about 1.15 mm, or 1150  $\mu\text{m}$ . This can also be obtained from the interferometry software used for taking the image. The steps involved in evaluating the free space length ( $L_f$ ) are as listed below:

1. Executing the .m file, at the prompt: `Is the version of MATLAB 7.0 or later? (Y/N) :` we enter: `Y`
2. At the following prompt: `Is the transfer film image converted to black and white already? (Y/N) :` as we don't have a converted image already, we enter: `N` and select the sample image 'HeightMap.bmp'

3. The following prompt asks us to `Enter number of counterface reference points for image conversion:` we enter `20` in order to save some labor and still be able to pick up the statistics of pixel intensity distribution. A window will pop out displaying the raw image, waiting for mouse input. We go ahead and select 20 points at transfer film free area across the whole view field, pay attention not to select points at those dark lines which are deep scratches as they only comprise a small portion of the counterface and are not representative to the whole transfer film free domain
4. The code now asks a question: `Is the transfer film brighter than substrate? (Y/N):` we enter `Y` as the transfer film does appear brighter than the substrate in this case
5. At the following prompt, we are asked to `Enter # of STDEVS to use for defining lower or upper bounds of color threshold (Suggested = 3 to 5):` we enter `4` as we discussed earlier in section III. It takes less than half minute before MATLAB finish the image conversion and pop out the converted binary image (shown below)



6. At the following prompt: `Tweak #STDEV further? (Y/N):` we enter `N` as this converted image is closely representative of the original image, if the you are not satisfied with the conversion, enter `Y` and you will be able to choose a different number of

standard deviation used for thresholding in previous step

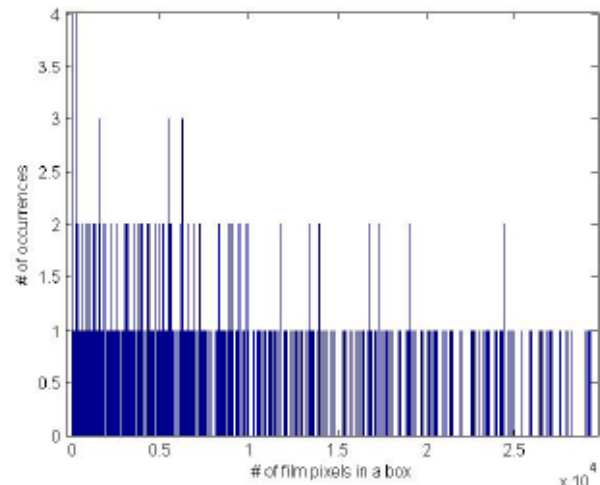
7. The following prompt asks us to `Enter approximate width of transfer film image in micrometers:` we enter `1150` as we estimated earlier

8. The following prompt asks us to Enter initial guess of characteristic square width in micrometers: Observing that the image width is 1150  $\mu\text{m}$ , and as per the discussion in section V, the pockets of filler-free space seem to be about half of the image width, we enter 550  $\mu\text{m}$  as our initial guess (underestimate the one half value).
9. Next, we are asked to Enter number of random squares to use for analysis: Since we are unsure of how computationally intensive our selection of 100  $\mu\text{m}$  is going to be, we choose to use 500 squares (which is about halfway between the recommended 100 and 1000)
10. After allowing the computation to finish (in this case, the simulation ran for less than a minute, while this may vary from one run to another even with same parameters), we obtain the following results:

```
Value of free
space length is
(in micrometers):
263
Film area fraction
(where film is
represented by
black pixels):
0.2559
```

Further, the adjoining histogram is generated. Clearly then (and as was discussed in section II), our starting guess of 550  $\mu\text{m}$  was a little

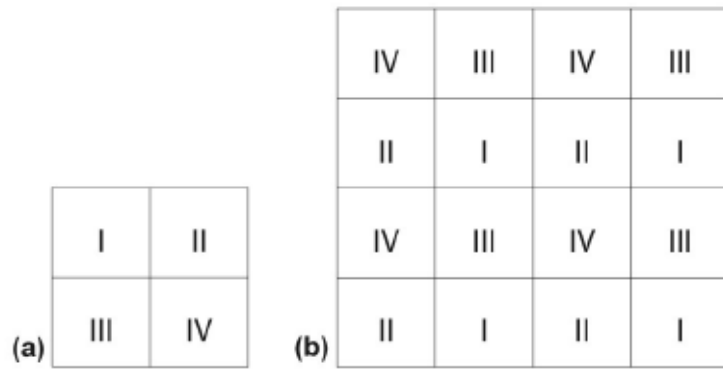
overestimate of the actual 263  $\mu\text{m}$ . While not illustrated in this example, the value of 263  $\mu\text{m}$  may be further tuned in manual mode



## IX. Overview of code algorithm:

The general algorithm of the code is as outlined:

1. A bitmap (.bmp) transfer film image (RGB mode, any pixel size, any aspect ratio) is imported to MATLAB<sup>TM</sup>, and stored as matrix 'AA', it's elements being the R,G,B values associated with the pixels in the image.
2. After user manually picked the reference points at counterface area, mean ( $\mu$ ) and standard deviation ( $\sigma$ ) of pixel values at selected positions were calculated for R, G and B channels.
3. With a threshold pixel value of  $(\mu \pm n\sigma)$  to distinguish film from substrate, pixel with an intensity value outside this range will be declared as transfer film free and stored in a new matrix 'A' with pixel value '0', while pixel at transfer film covered region will be given a pixel value '255', the resulting matrix A will be solely composed of 0 and 255 and can be displayed as a binary image
4. With a threshold grayscale value of 150 to distinguish film from the substrate, transfer film area fraction ('af') is evaluated.
5. A 'data' matrix is next generated, which has periodic boundary conditions. In other words, the data matrix is composed of the 'A' pixel matrix at the core, adjoined by portions of the 'A' matrix such that a periodic boundary is obtained at the edge of the 'data' matrix. This is illustrated in figure A1, where I, II, III, IV indicate the quadrants of the original 'A' matrix.
6. An initial value of box size is inputted from the user, together with the number of random boxes that the user wishes to analyze the image with and the size of the TEM image in nanometers.
7. The code converges on the characteristic box size, thereafter performing incremental 'jump ups' and 'trim downs' to converge to the actual characteristic box size. If the distribution is bimodal, the 'false' mode is suppressed in order to obtain the correct value of 'l'.
8. Results are displayed, together with a histogram of particle occurrences for the given 'Nsquare' boxes.
9. A Manual mode is provided at the end of the code, which in essence has the similar algorithm as the computation above, except for the automatic box-size adjustments (jump up/trim down) which cause the code to iterate to the characteristic value. Instead, the manual mode just provides the histogram for the value of box size and sampling size selected by the user.



(a) The image pixel-matrix 'A', with its four quadrants indicated by numerals. (b) The 'data' matrix, with 'A' at its core, and periodic boundaries along the edges. Note that if 'A' is of order 500x500 (say), the 'data' matrix is of order 1000x1000.

Appendix D

**REPRINT PERMISSION LETTERS**



# RightsLink®

Home

Create Account

Help



**Title:** Mechanistic Studies in Friction and Wear of Bulk Materials

**Author:** W. Gregory Sawyer, Nicolas Argibay, David L. Burris, et al

**Publication:** Annual Review of Materials Research

**Publisher:** Annual Reviews

**Date:** Jul 1, 2014

Copyright © 2014, Annual Reviews

**LOGIN**

If you're a **copyright.com user**, you can login to RightsLink using your copyright.com credentials. Already a **RightsLink user** or want to [learn more?](#)

### Permission Not Required

Material may be republished in a thesis / dissertation without obtaining additional permission from Annual Reviews, providing that the author and the original source of publication are fully acknowledged.

BACK

CLOSE WINDOW

Copyright © 2017 [Copyright Clearance Center, Inc.](#) All Rights Reserved. [Privacy statement.](#) [Terms and Conditions.](#) Comments? We would like to hear from you. E-mail us at [customer@copyright.com](mailto:customer@copyright.com)



# RightsLink®

[Home](#)
[Account Info](#)
[Help](#)


**Title:** Transfer Film Tenacity: A Case Study Using Ultra-Low-Wear Alumina-PTFE

Logged in as:

Diana Haidar

Account #:  
3001046690

**Author:** J. Ye

**Publication:** Tribology Letters

**Publisher:** Springer

**Date:** Jan 1, 2015

Copyright © 2015, Springer Science+Business Media  
New York

[LOGOUT](#)

## Order Completed

Thank you for your order.

This Agreement between Diana R Haidar ("You") and Springer ("Springer") consists of your license details and the terms and conditions provided by Springer and Copyright Clearance Center.

Your confirmation email will contain your order number for future reference.

### Printable details.

License Number	4146751312809
License date	Jul 12, 2017
Licensed Content Publisher	Springer
Licensed Content Publication	Tribology Letters
Licensed Content Title	Transfer Film Tenacity: A Case Study Using Ultra-Low-Wear Alumina-PTFE
Licensed Content Author	J. Ye
Licensed Content Date	Jan 1, 2015
Licensed Content Volume	59
Licensed Content Issue	3
Type of Use	Thesis/Dissertation
Portion	Figures/tables/illustrations
Number of figures/tables/illustrations	1
Author of this Springer article	No
Order reference number	
Original figure numbers	Figure 8
Title of your thesis / dissertation	A NEW SOLUTION TO AN OLD PROBLEM: DESIGNING AN ULTRALOW WEAR POLYMERIC SOLID LUBRICANT FOR BEARING APPLICATIONS IN CHALLENGING ENVIRONMENTS
Expected completion date	Aug 2017
Estimated size(pages)	200
Requestor Location	Diana R Haidar 130 Academy Street Room 126  NEWARK, DE 19716 United States Attn: Diana R Haidar
Billing Type	Invoice
Billing address	Diana R Haidar 130 Academy Street Room 126  NEWARK, DE 19716 United States Attn: Diana R Haidar
Total	0.00 USD

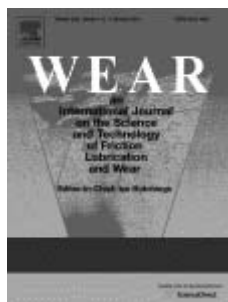
**ORDER MORE**

**CLOSE WINDOW**

Copyright © 2017 [Copyright Clearance Center, Inc.](#) All Rights Reserved. [Privacy statement.](#) [Terms and Conditions.](#)  
Comments? We would like to hear from you. E-mail us at [customer care@copyright.com](mailto:customer care@copyright.com)



# RightsLink®

[Home](#)
[Account Info](#)
[Help](#)


**Title:** Improved wear resistance in alumina-PTFE nanocomposites with irregular shaped nanoparticles

**Author:** David L. Burris, W. Gregory Sawyer

**Publication:** Wear

**Publisher:** Elsevier

**Date:** 7 April 2006

Copyright © 2005 Published by Elsevier B.V.

Logged in as:

Diana Haidar

Account #:  
3001046690

[LOGOUT](#)

## Order Completed

Thank you for your order.

This Agreement between Diana R Haidar ("You") and Elsevier ("Elsevier") consists of your license details and the terms and conditions provided by Elsevier and Copyright Clearance Center.

Your confirmation email will contain your order number for future reference.

### Printable details.

License Number	4146760182459
License date	Jul 12, 2017
Licensed Content Publisher	Elsevier
Licensed Content Publication	Wear
Licensed Content Title	Improved wear resistance in alumina-PTFE nanocomposites with irregular shaped nanoparticles
Licensed Content Author	David L. Burris, W. Gregory Sawyer
Licensed Content Date	Apr 7, 2006
Licensed Content Volume	260
Licensed Content Issue	7-8
Licensed Content Pages	4
Type of Use	reuse in a thesis/dissertation
Portion	figures/tables/illustrations
Number of figures/tables/illustrations	1
Format	both print and electronic
Are you the author of this Elsevier article?	No
Will you be translating?	No
Order reference number	
Original figure numbers	Figure 1
Title of your thesis/dissertation	A NEW SOLUTION TO AN OLD PROBLEM: DESIGNING AN ULTRALOW WEAR POLYMERIC SOLID LUBRICANT FOR BEARING APPLICATIONS IN CHALLENGING ENVIRONMENTS
Expected completion date	Aug 2017
Estimated size (number of pages)	200
Elsevier VAT number	GB 494 6272 12
Requestor Location	Diana R Haidar 130 Academy Street Room 126  NEWARK, DE 19716 United States Attn: Diana R Haidar
Publisher Tax ID	98-0397604
Total	0.00 USD

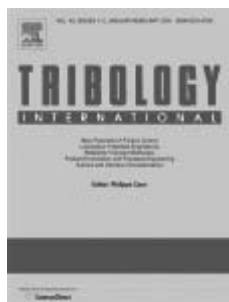
[ORDER MORE](#)

[CLOSE WINDOW](#)

Copyright © 2017 [Copyright Clearance Center, Inc.](#) All Rights Reserved. [Privacy statement](#). [Terms and Conditions](#).  
Comments? We would like to hear from you. E-mail us at [customercare@copyright.com](mailto:customercare@copyright.com)



# RightsLink®

[Home](#)
[Account Info](#)
[Help](#)


**Title:** Ultralow wear fluoropolymer composites: Nanoscale functionality from microscale fillers

**Author:** Brandon A. Krick, Angela A. Pitenis, Kathryn L. Harris, Christopher P. Junk, W. Gregory Sawyer, Scott C. Brown, H. David Rosenfeld, Daniel J. Kasprzak, Ross S. Johnson, Christopher D. Chan, Gregory S. Blackman

**Publication:** Tribology International

**Publisher:** Elsevier

**Date:** March 2016

Copyright © 2015 The Authors and E.I. DuPont de Nemours and Company. Published by Elsevier Ltd. All rights reserved.

Logged in as:

Diana Haidar

Account #:  
3001046690

[LOGOUT](#)

## Order Completed

Thank you for your order.

This Agreement between Diana R Haidar ("You") and Elsevier ("Elsevier") consists of your license details and the terms and conditions provided by Elsevier and Copyright Clearance Center.

Your confirmation email will contain your order number for future reference.

### Printable details.

License Number	4146760372272
License date	Jul 12, 2017
Licensed Content Publisher	Elsevier
Licensed Content Publication	Tribology International
Licensed Content Title	Ultralow wear fluoropolymer composites: Nanoscale functionality from microscale fillers
Licensed Content Author	Brandon A. Krick, Angela A. Pitenis, Kathryn L. Harris, Christopher P. Junk, W. Gregory Sawyer, Scott C. Brown, H. David Rosenfeld, Daniel J. Kasprzak, Ross S. Johnson, Christopher D. Chan, Gregory S. Blackman
Licensed Content Date	Mar 1, 2016
Licensed Content Volume	95
Licensed Content Issue	n/a
Licensed Content Pages	11
Type of Use	reuse in a thesis/dissertation
Portion	figures/tables/illustrations
Number of figures/tables/illustrations	4
Format	both print and electronic
Are you the author of this Elsevier article?	No
Will you be translating?	No
Order reference number	
Original figure numbers	Figure 1, 2, 4, 5
Title of your thesis/dissertation	A NEW SOLUTION TO AN OLD PROBLEM: DESIGNING AN ULTRALOW WEAR POLYMERIC SOLID LUBRICANT FOR BEARING APPLICATIONS IN CHALLENGING ENVIRONMENTS
Expected completion date	Aug 2017
Estimated size (number	200

of pages)

Elsevier VAT number GB 494 6272 12  
Requestor Location Diana R Haidar  
130 Academy Street  
Room 126

NEWARK, DE 19716  
United States  
Attn: Diana R Haidar

Publisher Tax ID 98-0397604

Total 0.00 USD

[ORDER MORE](#)

[CLOSE WINDOW](#)

Copyright © 2017 [Copyright Clearance Center, Inc.](#) All Rights Reserved. [Privacy statement.](#) [Terms and Conditions.](#)  
Comments? We would like to hear from you. E-mail us at [customercare@copyright.com](mailto:customercare@copyright.com)



# RightsLink®

[Home](#)
[Account Info](#)
[Help](#)


**Title:** In Vacuo Tribological Behavior of Polytetrafluoroethylene (PTFE) and Alumina Nanocomposites: The Importance of Water for Ultralow Wear

Logged in as:  
Diana Haidar  
Account #:  
3001046690

[LOGOUT](#)

**Author:** Angela A. Pitenis

**Publication:** Tribology Letters

**Publisher:** Springer

**Date:** Jan 1, 2013

Copyright © 2013, Springer Science+Business Media  
New York

## Order Completed

Thank you for your order.

This Agreement between Diana R Haidar ("You") and Springer ("Springer") consists of your license details and the terms and conditions provided by Springer and Copyright Clearance Center.

Your confirmation email will contain your order number for future reference.

### Printable details.

License Number	4146760539494
License date	Jul 12, 2017
Licensed Content Publisher	Springer
Licensed Content Publication	Tribology Letters
Licensed Content Title	In Vacuo Tribological Behavior of Polytetrafluoroethylene (PTFE) and Alumina Nanocomposites: The Importance of Water for Ultralow Wear
Licensed Content Author	Angela A. Pitenis
Licensed Content Date	Jan 1, 2013
Licensed Content Volume	53
Licensed Content Issue	1
Type of Use	Thesis/Dissertation
Portion	Figures/tables/illustrations
Number of figures/tables/illustrations	2
Author of this Springer article	No
Order reference number	
Original figure numbers	Figure 2, 4
Title of your thesis / dissertation	A NEW SOLUTION TO AN OLD PROBLEM: DESIGNING AN ULTRALOW WEAR POLYMERIC SOLID LUBRICANT FOR BEARING APPLICATIONS IN CHALLENGING ENVIRONMENTS
Expected completion date	Aug 2017
Estimated size(pages)	200
Requestor Location	Diana R Haidar 130 Academy Street Room 126  NEWARK, DE 19716 United States Attn: Diana R Haidar
Billing Type	Invoice
Billing address	Diana R Haidar 130 Academy Street Room 126

7/12/2017

Rightslink® by Copyright Clearance Center

NEWARK, DE 19716  
United States  
Attn: Diana R Haidar

Total

0.00 USD

[ORDER MORE](#)

[CLOSE WINDOW](#)

Copyright © 2017 [Copyright Clearance Center, Inc.](#) All Rights Reserved. [Privacy statement.](#) [Terms and Conditions.](#)  
Comments? We would like to hear from you. E-mail us at [customercare@copyright.com](mailto:customercare@copyright.com)



# RightsLink®

[Home](#)
[Account Info](#)
[Help](#)


**Title:** Ultralow Wear PTFE and Alumina Composites: It is All About Tribochemistry

Logged in as:

Diana Haidar

Account #:  
3001046690

**Author:** Angela A. Pitenis

**Publication:** Tribology Letters

**Publisher:** Springer

**Date:** Jan 1, 2014

Copyright © 2014, Springer Science+Business Media  
New York

[LOGOUT](#)

## Order Completed

Thank you for your order.

This Agreement between Diana R Haidar ("You") and Springer ("Springer") consists of your license details and the terms and conditions provided by Springer and Copyright Clearance Center.

Your confirmation email will contain your order number for future reference.

### Printable details.

License Number	4146760813945
License date	Jul 12, 2017
Licensed Content Publisher	Springer
Licensed Content Publication	Tribology Letters
Licensed Content Title	Ultralow Wear PTFE and Alumina Composites: It is All About Tribochemistry
Licensed Content Author	Angela A. Pitenis
Licensed Content Date	Jan 1, 2014
Licensed Content Volume	57
Licensed Content Issue	1
Type of Use	Thesis/Dissertation
Portion	Figures/tables/illustrations
Number of figures/tables/illustrations	1
Author of this Springer article	No
Order reference number	
Original figure numbers	Figure 3
Title of your thesis / dissertation	A NEW SOLUTION TO AN OLD PROBLEM: DESIGNING AN ULTRALOW WEAR POLYMERIC SOLID LUBRICANT FOR BEARING APPLICATIONS IN CHALLENGING ENVIRONMENTS
Expected completion date	Aug 2017
Estimated size(pages)	200
Requestor Location	Diana R Haidar 130 Academy Street Room 126  NEWARK, DE 19716 United States Attn: Diana R Haidar
Billing Type	Invoice
Billing address	Diana R Haidar 130 Academy Street Room 126  NEWARK, DE 19716 United States Attn: Diana R Haidar
Total	0.00 USD

[ORDER MORE](#)

[CLOSE WINDOW](#)

Copyright © 2017 [Copyright Clearance Center, Inc.](#) All Rights Reserved. [Privacy statement.](#) [Terms and Conditions.](#)  
Comments? We would like to hear from you. E-mail us at [customer care@copyright.com](mailto:customer care@copyright.com)

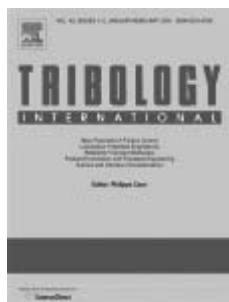


RightsLink®

Home

Account  
Info

Help



**Title:** Environmental dependence of ultra-low wear behavior of polytetrafluoroethylene (PTFE) and alumina composites suggests tribochemical mechanisms

**Author:** Brandon A. Krick, Jeffrey J. Ewin, Gregory S. Blackman, Christopher P. Junk, W. Gregory Sawyer

**Publication:** Tribology International

**Publisher:** Elsevier

**Date:** July 2012

Copyright © 2012 Elsevier Ltd. All rights reserved.

Logged in as:

Diana Haidar

Account #:  
3001046690

LOGOUT

## Order Completed

Thank you for your order.

This Agreement between Diana R Haidar ("You") and Elsevier ("Elsevier") consists of your license details and the terms and conditions provided by Elsevier and Copyright Clearance Center.

Your confirmation email will contain your order number for future reference.

### Printable details.

License Number	4146760685919
License date	Jul 12, 2017
Licensed Content Publisher	Elsevier
Licensed Content Publication	Tribology International
Licensed Content Title	Environmental dependence of ultra-low wear behavior of polytetrafluoroethylene (PTFE) and alumina composites suggests tribochemical mechanisms
Licensed Content Author	Brandon A. Krick, Jeffrey J. Ewin, Gregory S. Blackman, Christopher P. Junk, W. Gregory Sawyer
Licensed Content Date	Jul 1, 2012
Licensed Content Volume	51
Licensed Content Issue	n/a
Licensed Content Pages	5
Type of Use	reuse in a thesis/dissertation
Portion	figures/tables/illustrations
Number of figures/tables/illustrations	2
Format	both print and electronic
Are you the author of this Elsevier article?	No
Will you be translating?	No
Order reference number	
Original figure numbers	Figure 1, 2
Title of your thesis/dissertation	A NEW SOLUTION TO AN OLD PROBLEM: DESIGNING AN ULTRALOW WEAR POLYMERIC SOLID LUBRICANT FOR BEARING APPLICATIONS IN CHALLENGING ENVIRONMENTS
Expected completion date	Aug 2017
Estimated size (number of pages)	200
Elsevier VAT number	GB 494 6272 12
Requestor Location	Diana R Haidar 130 Academy Street Room 126

7/12/2017

Rightslink® by Copyright Clearance Center

NEWARK, DE 19716  
United States  
Attn: Diana R Haidar

Publisher Tax ID 98-0397604  
Total 0.00 USD

[ORDER MORE](#)

[CLOSE WINDOW](#)

Copyright © 2017 [Copyright Clearance Center, Inc.](#) All Rights Reserved. [Privacy statement.](#) [Terms and Conditions.](#)  
Comments? We would like to hear from you. E-mail us at [customercare@copyright.com](mailto:customercare@copyright.com)



RightsLink®

Home

Account  
Info

Help

ACS Publications  
Most Trusted. Most Cited. Most Read.

**Title:** Interrelated Effects of  
Temperature and Environment  
on Wear and Tribochemistry of  
an Ultralow Wear PTFE  
Composite

Logged in as:

Diana Haidar

Account #:  
3001046690

LOGOUT

**Author:** H. S. Khare, A. C. Moore, D. R.  
Haidar, et al

**Publication:** The Journal of Physical  
Chemistry C

**Publisher:** American Chemical Society

**Date:** Jul 1, 2015

Copyright © 2015, American Chemical Society

### PERMISSION/LICENSE IS GRANTED FOR YOUR ORDER AT NO CHARGE

This type of permission/license, instead of the standard Terms & Conditions, is sent to you because no fee is being charged for your order. Please note the following:

- Permission is granted for your request in both print and electronic formats, and translations.
- If figures and/or tables were requested, they may be adapted or used in part.
- Please print this page for your records and send a copy of it to your publisher/graduate school.
- Appropriate credit for the requested material should be given as follows: "Reprinted (adapted) with permission from (COMPLETE REFERENCE CITATION). Copyright (YEAR) American Chemical Society." Insert appropriate information in place of the capitalized words.
- One-time permission is granted only for the use specified in your request. No additional uses are granted (such as derivative works or other editions). For any other uses, please submit a new request.

If credit is given to another source for the material you requested, permission must be obtained from that source.

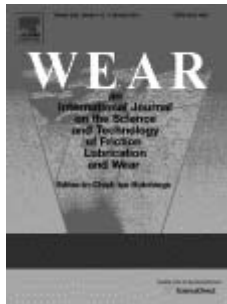
BACK

CLOSE WINDOW

Copyright © 2017 [Copyright Clearance Center, Inc.](#) All Rights Reserved. [Privacy statement.](#) [Terms and Conditions.](#)  
Comments? We would like to hear from you. E-mail us at [customer@copyright.com](mailto:customer@copyright.com)



# RightsLink®

[Home](#)
[Account Info](#)
[Help](#)


**Title:** Transfer film evolution and its role in promoting ultra-low wear of a PTFE nanocomposite

**Author:** J. Ye,H.S. Khare,D.L. Burriss

**Publication:** Wear

**Publisher:** Elsevier

**Date:** 15 January 2013

Logged in as:  
Diana Haidar  
Account #:  
3001046690

[LOGOUT](#)

Copyright © 2012 Elsevier B.V. All rights reserved.

## Order Completed

Thank you for your order.

This Agreement between Diana R Haidar ("You") and Elsevier ("Elsevier") consists of your license details and the terms and conditions provided by Elsevier and Copyright Clearance Center.

Your confirmation email will contain your order number for future reference.

### Printable details.

License Number	4146761213391
License date	Jul 12, 2017
Licensed Content Publisher	Elsevier
Licensed Content Publication	Wear
Licensed Content Title	Transfer film evolution and its role in promoting ultra-low wear of a PTFE nanocomposite
Licensed Content Author	J. Ye,H.S. Khare,D.L. Burriss
Licensed Content Date	Jan 15, 2013
Licensed Content Volume	297
Licensed Content Issue	1-2
Licensed Content Pages	8
Type of Use	reuse in a thesis/dissertation
Portion	figures/tables/illustrations
Number of figures/tables/illustrations	1
Format	both print and electronic
Are you the author of this Elsevier article?	No
Will you be translating?	No
Order reference number	
Original figure numbers	Figure 1
Title of your thesis/dissertation	A NEW SOLUTION TO AN OLD PROBLEM: DESIGNING AN ULTRALOW WEAR POLYMERIC SOLID LUBRICANT FOR BEARING APPLICATIONS IN CHALLENGING ENVIRONMENTS
Expected completion date	Aug 2017
Estimated size (number of pages)	200
Elsevier VAT number	GB 494 6272 12
Requestor Location	Diana R Haidar 130 Academy Street Room 126  NEWARK, DE 19716 United States Attn: Diana R Haidar
Publisher Tax ID	98-0397604
Total	0.00 USD

[ORDER MORE](#)
[CLOSE WINDOW](#)

Copyright © 2017 [Copyright Clearance Center, Inc.](#) All Rights Reserved. [Privacy statement.](#) [Terms and Conditions.](#)  
Comments? We would like to hear from you. E-mail us at [customercare@copyright.com](mailto:customercare@copyright.com)



# RightsLink®

Home

Account Info

Help



**Title:** Quantitative characterization of solid lubricant transfer film quality

**Author:** J. Ye,H.S. Khare,D.L. Burris

**Publication:** Wear

**Publisher:** Elsevier

**Date:** 15 August 2014

Copyright © 2014 Elsevier B.V. All rights reserved.

Logged in as:  
Diana Haidar  
Account #:  
3001046690

LOGOUT

## Order Completed

Thank you for your order.

This Agreement between Diana R Haidar ("You") and Elsevier ("Elsevier") consists of your license details and the terms and conditions provided by Elsevier and Copyright Clearance Center.

Your confirmation email will contain your order number for future reference.

### Printable details.

License Number	4146761390009
License date	Jul 12, 2017
Licensed Content Publisher	Elsevier
Licensed Content Publication	Wear
Licensed Content Title	Quantitative characterization of solid lubricant transfer film quality
Licensed Content Author	J. Ye,H.S. Khare,D.L. Burris
Licensed Content Date	Aug 15, 2014
Licensed Content Volume	316
Licensed Content Issue	1-2
Licensed Content Pages	11
Type of Use	reuse in a thesis/dissertation
Portion	figures/tables/illustrations
Number of figures/tables/illustrations	2
Format	both print and electronic
Are you the author of this Elsevier article?	No
Will you be translating?	No
Order reference number	
Original figure numbers	Figure 2, 4
Title of your thesis/dissertation	A NEW SOLUTION TO AN OLD PROBLEM: DESIGNING AN ULTRALOW WEAR POLYMERIC SOLID LUBRICANT FOR BEARING APPLICATIONS IN CHALLENGING ENVIRONMENTS
Expected completion date	Aug 2017
Estimated size (number of pages)	200
Elsevier VAT number	GB 494 6272 12
Requestor Location	Diana R Haidar 130 Academy Street Room 126  NEWARK, DE 19716 United States Attn: Diana R Haidar
Publisher Tax ID	98-0397604
Total	0.00 USD

ORDER MORE

CLOSE WINDOW

Copyright © 2017 [Copyright Clearance Center, Inc.](#) All Rights Reserved. [Privacy statement.](#) [Terms and Conditions.](#)  
Comments? We would like to hear from you. E-mail us at [customercare@copyright.com](mailto:customercare@copyright.com)

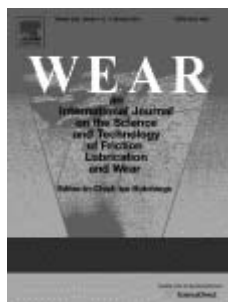


RightsLink®

Home

Account  
Info

Help



**Title:** Assessing quantitative metrics of transfer film quality as indicators of polymer wear performance

**Author:** D.R. Haidar, J. Ye, A.C. Moore, D.L. Burriss

**Publication:** Wear

**Publisher:** Elsevier

**Date:** 15 June 2017

© 2017 Elsevier B.V. All rights reserved.

Logged in as:  
Diana Haidar  
Account #:  
3001046690

LOGOUT

## Order Completed

Thank you for your order.

This Agreement between Diana R Haidar ("You") and Elsevier ("Elsevier") consists of your license details and the terms and conditions provided by Elsevier and Copyright Clearance Center.

Your confirmation email will contain your order number for future reference.

### Printable details.

License Number	4146770039818
License date	Jul 12, 2017
Licensed Content Publisher	Elsevier
Licensed Content Publication	Wear
Licensed Content Title	Assessing quantitative metrics of transfer film quality as indicators of polymer wear performance
Licensed Content Author	D.R. Haidar, J. Ye, A.C. Moore, D.L. Burriss
Licensed Content Date	Jun 15, 2017
Licensed Content Volume	380
Licensed Content Issue	n/a
Licensed Content Pages	8
Type of Use	reuse in a thesis/dissertation
Portion	figures/tables/illustrations
Number of figures/tables/illustrations	5
Format	both print and electronic
Are you the author of this Elsevier article?	Yes
Will you be translating?	No
Order reference number	
Original figure numbers	Figure 1, 2, 3, 4, 5
Title of your thesis/dissertation	A NEW SOLUTION TO AN OLD PROBLEM: DESIGNING AN ULTRALOW WEAR POLYMERIC SOLID LUBRICANT FOR BEARING APPLICATIONS IN CHALLENGING ENVIRONMENTS
Expected completion date	Aug 2017
Estimated size (number of pages)	200
Elsevier VAT number	GB 494 6272 12
Requestor Location	Diana R Haidar 130 Academy Street Room 126  NEWARK, DE 19716 United States Attn: Diana R Haidar
Publisher Tax ID	98-0397604

Total 0.00 USD

[ORDER MORE](#)

[CLOSE WINDOW](#)

Copyright © 2017 [Copyright Clearance Center, Inc.](#) All Rights Reserved. [Privacy statement.](#) [Terms and Conditions.](#)  
Comments? We would like to hear from you. E-mail us at [customercare@copyright.com](mailto:customercare@copyright.com)



RightsLink®

Home

Account  
Info

Help



**Title:** Tribological results of PEEK nanocomposites in dry sliding against 440C in various gas environments

**Author:** N.L. McCook, M.A. Hamilton, D.L. Burris, W.G. Sawyer

Logged in as:  
Diana Haidar  
Account #:  
3001046690

LOGOUT

**Publication:** Wear  
**Publisher:** Elsevier  
**Date:** 10 May 2007

Copyright © 2007 Published by Elsevier B.V.

## Order Completed

Thank you for your order.

This Agreement between Diana R Haidar ("You") and Elsevier ("Elsevier") consists of your license details and the terms and conditions provided by Elsevier and Copyright Clearance Center.

Your confirmation email will contain your order number for future reference.

### Printable details.

License Number	4146770182561
License date	Jul 12, 2017
Licensed Content Publisher	Elsevier
Licensed Content Publication	Wear
Licensed Content Title	Tribological results of PEEK nanocomposites in dry sliding against 440C in various gas environments
Licensed Content Author	N.L. McCook, M.A. Hamilton, D.L. Burris, W.G. Sawyer
Licensed Content Date	May 10, 2007
Licensed Content Volume	262
Licensed Content Issue	11-12
Licensed Content Pages	5
Type of Use	reuse in a thesis/dissertation
Portion	figures/tables/illustrations
Number of figures/tables/illustrations	1
Format	both print and electronic
Are you the author of this Elsevier article?	No
Will you be translating?	No
Order reference number	
Original figure numbers	Figure 3
Title of your thesis/dissertation	A NEW SOLUTION TO AN OLD PROBLEM: DESIGNING AN ULTRALOW WEAR POLYMERIC SOLID LUBRICANT FOR BEARING APPLICATIONS IN CHALLENGING ENVIRONMENTS
Expected completion date	Aug 2017
Estimated size (number of pages)	200
Elsevier VAT number	GB 494 6272 12
Requestor Location	Diana R Haidar 130 Academy Street Room 126  NEWARK, DE 19716 United States Attn: Diana R Haidar
Publisher Tax ID	98-0397604

Total 0.00 USD

[ORDER MORE](#)

[CLOSE WINDOW](#)

Copyright © 2017 [Copyright Clearance Center, Inc.](#) All Rights Reserved. [Privacy statement.](#) [Terms and Conditions.](#)  
Comments? We would like to hear from you. E-mail us at [customercare@copyright.com](mailto:customercare@copyright.com)



RightsLink®

Home

Account  
Info

Help

ACS Publications  
Most Trusted. Most Cited. Most Read.

**Title:** Tribological Insensitivity of an  
Ultralow-Wear  
Poly(etheretherketone)–  
Polytetrafluoroethylene Polymer  
Blend to Changes in  
Environmental Moisture

Logged in as:  
Diana Haidar  
Account #:  
3001046690

LOGOUT

**Author:** Diana R. Haidar, K. Istiaque  
Alam, David L. Burris

**Publication:** The Journal of Physical  
Chemistry C

**Publisher:** American Chemical Society

**Date:** Mar 1, 2018

Copyright © 2018, American Chemical Society

### PERMISSION/LICENSE IS GRANTED FOR YOUR ORDER AT NO CHARGE

This type of permission/license, instead of the standard Terms & Conditions, is sent to you because no fee is being charged for your order. Please note the following:

- Permission is granted for your request in both print and electronic formats, and translations.
- If figures and/or tables were requested, they may be adapted or used in part.
- Please print this page for your records and send a copy of it to your publisher/graduate school.
- Appropriate credit for the requested material should be given as follows: "Reprinted (adapted) with permission from (COMPLETE REFERENCE CITATION). Copyright (YEAR) American Chemical Society." Insert appropriate information in place of the capitalized words.
- One-time permission is granted only for the use specified in your request. No additional uses are granted (such as derivative works or other editions). For any other uses, please submit a new request.

If credit is given to another source for the material you requested, permission must be obtained from that source.

BACK

CLOSE WINDOW

Copyright © 2018 Copyright Clearance Center, Inc. All Rights Reserved. [Privacy statement](#). [Terms and Conditions](#).  
Comments? We would like to hear from you. E-mail us at [customercare@copyright.com](mailto:customercare@copyright.com)